Selective introduction of nitrogen into bulk chemicals via homogeneously catalyzed reactions

Zur Erlangung des akademischen Grades eines

Dr.rer.nat.

von der Fakultät Bio- und Chemieingenieurwesen
der Technischen Universität Dortmund
genehmigte Dissertation

vorgelegt von
M.Sc. Kevin Hares

aus

Wickede an der Ruhr

Tag der mündlichen Prüfung: 28.06.2024

1. Gutachter/-in: Prof. Dr. Dieter Vogt

2. Gutachter/-in: Prof. Dr. Jörg Tiller

Dortmund 2024

“It's sort of a mental attitude about critical thinking and curiosity.
It's about mindset of looking at the world in a playful and curious and creative way.”

– Adam Savage

Acknowledgements

Finishing this Dissertation would not have been possible without the help and encouragement of many whom I would like to thank.

First of all, I would like to express my deepest gratitude to Prof. Dieter Vogt for giving me the opportunity to work in the Laboratory for Industrial Chemistry at TU Dortmund. Your guidance, especially in the intricate details of catalyst synthesis and connecting me with the Kamer Group, has been invaluable. I am truly grateful for all the insightful discussions and the constant support you've provided throughout this journey.

I would also like to extend my sincere thanks to Prof. Jörg Tiller for graciously agreeing to be the second reviewer for this thesis, and to Prof. Freund for your role in moderating the examination — your contributions have been greatly appreciated.

Many thanks as well to Dr. Thomas Seidensticker for the countless fruitful discussions and your never-ending flow of ideas, which often opened new perspectives and inspired me to think beyond the obvious. Your creativity and support made a significant difference throughout the process.

I had a truly wonderful time at TC, and it's largely thanks to all my companions who made the journey so memorable. A special mention goes out to my fellow corner office residents, Christian, Johanna, and Hannes, whose company and support made even the toughest days more enjoyable. I also want to express my gratitude to the climbing gang — Alex, Maxi, Thomas, and Tim — for not only being great friends but for providing the perfect escape from work when needed. For keeping things running smoothly in the lab, I owe a big thanks to Iris, Justin, and Andi. Your help and patience were invaluable.

I would like to thank all the students who contributed to this work: Malte Menk, Charlotte-Sophie Wernsdörfer, Lilia Milius, Niklas Kost, Annika Schmidt, Bernd Rienhoff, Georg Beckmann, Hannes Wegener und Renè Reichert.

I would like to extend my heartfelt thanks to my family for their unwavering support throughout my entire studies. Your constant encouragement and belief in me have been the foundation that helped me stay focused and motivated, even during the most challenging moments.

Finally, a special thanks goes to Rey, whose persistent motivation and encouragement in the final stages of writing gave me the extra push I needed to see this thesis through to completion. Your support made all the difference in bringing this journey to a successful conclusion.

Table of Contents

1. Abstract

Nitrogen-containing chemical compounds are used everywhere in our day-to-day lives, from high-performance polymers to pharmaceuticals and crop protection. Despite being produced on very large scale, many of their production lines lack efficiency and have a significant impact on the environment.

Amides are often synthesized by highly activated coupling agents with an inherently low E-factor. Therefore, developing a catalytic reaction that can produce amides directly from bulk chemicals is highly desired. Primary amines are essential intermediates in the chemical industry, and their selective synthesis is challenging due to their reactive properties. Although they are also produced from bulk feedstock, they require many steps when a renewable substrate is used.

This dissertation addresses these challenges by developing and optimizing homogeneous transition metal catalysts. The work is structured into three main parts, each addressing different types of reactions to introduce nitrogen into bulk chemicals:

1. Carbonylative telomerization is a complex chemical reaction that synthesizes amides from simple feedstock molecules, but its high catalyst loading presents a challenge, as well as a limited scope. Both were addressed by optimizing the reaction conditions and adding new dienes and nucleophiles to the reaction portfolio of carbonylative telomerization.
2. Converting fatty esters directly into amines in a one-pot reaction is sought to streamline chemical production, requiring the development of a new catalyst to facilitate the process and improve resource and energy efficiency. Therefore, modified triphos ligands were synthesized and combined with ester amination.
3. The conversion of aldoximes into primary amines, offers a possible alternative to the highly desired hydroamination of alkenes. This is achieved through the combination with hydroformylation, which enables the conversion of alkenes into primary.

These contributions offer new efficient ways of introducing nitrogen into bulk feedstock to synthesize more complex amides and primary amines through homogeneous transition metal catalysts.

2. Introduction

2.1. Nitrogen is everywhere

Nitrogen is a highly abundant element in our everyday life. It is essential for life as it is an integral part of amino acids, enabling life and playing a key role in the origin of life on Earth.[1] Not as essential, however making our life easier and more enjoyable are all the products containing nitrogen, form paints over fertilizer to 3D printing filament. In the chemical industries amines are used as solvents (*e.g.* quinoline and tributylamine), to purify gases (*e.g.* monoethanolamine), as curing agents for epoxides (*e.g.* triethylenetetramine), and as intermediates for chemical processes (e.g. aniline or morpholine). Widely used plastics like polyamide 6 (PA 6), PA 6,6, PA 12, and PA 12,12 contain nitrogen in their structure (Figure 1). Since, nitrogen is found in amino acids and therefore peptides, many nitrogen containing compound also show bioactivity. They are used for active ingredients in pharmaceuticals (*e.g.* paracetamol) or crop protection in the form of pesticides and herbicides (*e.g.* glyphosate). The active groups are often amine and amide functionalities.

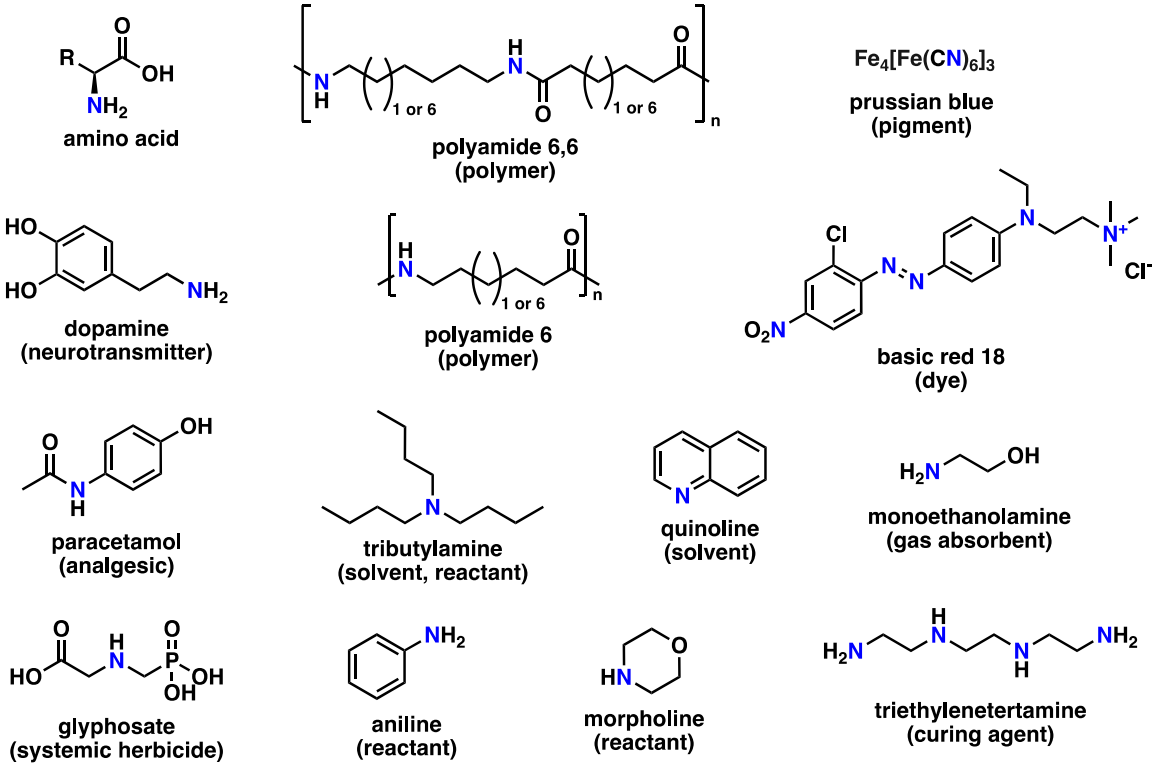

Figure 1: Example nitrogen containing compounds.

Although most of the air around us is made of nitrogen, it is not easy to utilize it. The N_2 molecule is relatively inert due to its N-N-triple bond. It has to be activated to be used for chemical reactions. That is why the HABER-BOSCH process is one of the most essential chemical processes in the industry today and makes nitrogen readily available in the form of ammonia. The yearly ammonia production is estimated to be 150 million metric tons and is responsible for up to 2 % of global energy consumption.[2] Most of the ammonia is used for fertilizer production. Due to readily available fertilizer, global food production rose and enabled our population to elevate from 1.9 billion to the about 8 billion[3] people there are today.[4] Therefore, the Haber-Bosch process is at the core of the chemical value chain and was awarded the Nobel Prize twice. In 1918, HABER received the prize for successfully synthesizing ammonia form directly from nitrogen and hydrogen.[5] Later 1931, BOSCH was awarded the Nobel Prize for overcoming the challenges

associated with the high pressure of the reaction and making large-scale ammonia production possible.[6]

Ammonia is a reactive form of nitrogen readily available for chemical reactions. The most efficient way of introducing nitrogen into chemical compounds is using ammonia since derivatization is unnecessary. However, the selectivity of such reactions is often difficult to control because the reaction products are more reactive than ammonia in many cases and lead to unwanted consecutive reactions (Figure 2).

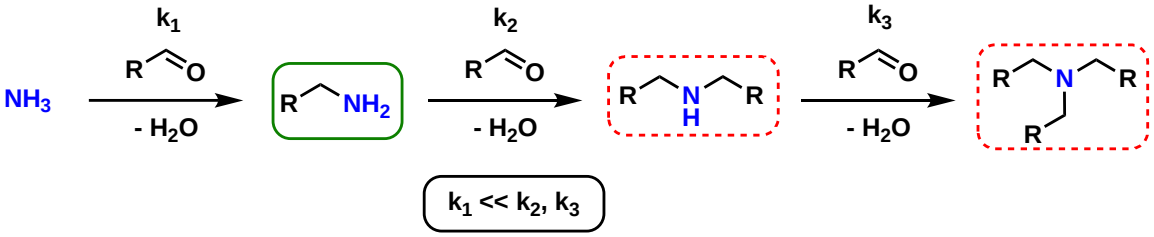

Figure 2: Reactivity trend of ammonia and its consecutive products.

Finely tuned catalysts are a solution to this problem, as they can be used to control the selectivity of a reaction towards the desired molecules. Due to the lack of such catalysts, reactions that require a different kind of activated nitrogen compound are still widely used. Compounds such as hydrogen cyanide, azides, nitric acid, or hydroxylamine can be used to synthesize many nitrogen-containing target molecules, but they require additional reaction steps for their own synthesis.

2.2.Amides, Amines and why they are so interesting

2.2.1. Amides – Pharmaceuticals, crop protection and more

Amides are one of the most important chemical functional groups in our modern society and the most prominent example for nitrogen containing compounds. As depicted above amides can be found in polymers and are produced on very large scale. There is also high demand for amides in smaller scale reactions for pesticides and pharmaceuticals. Due to their unique properties, amides are found more than one third of the 200 best selling drugs in 2022.[7]

> *"Furthermore, the favorable properties of amides, such as high polarity, stability and conformational diversity, make it one of the most popular and reliable functional groups in all branches of organic chemistry."* (PATTABIRAMAN *et al. 2011*)[8]

Therefore, amide formation is the most abundant used chemical transformation according to two literature review papers in the journal of medicinal chemistry: In 2011 ROUGHLEY *et al.*, analyzed a total of 139 publications by three large pharmaceutical companies[99] and five years later in 2016 BROWN *et al.* compared 125 publications from 1984 and 125 manuscripts from 2014. Their study includes work from academia and industry.[10] The trend is increasing and in 2014 amide bond formation occurred in about 50 % of the dataset. Despite the abundance of amide bond formation, many synthesis routs are waste intensive and suffer from poor atom economy.

Amides can be typically synthesized either *via* C-N bond formation or *via* C-O bond formation. These can in each case be carried out with stoichiometric reagents or catalytically (Figure 3).

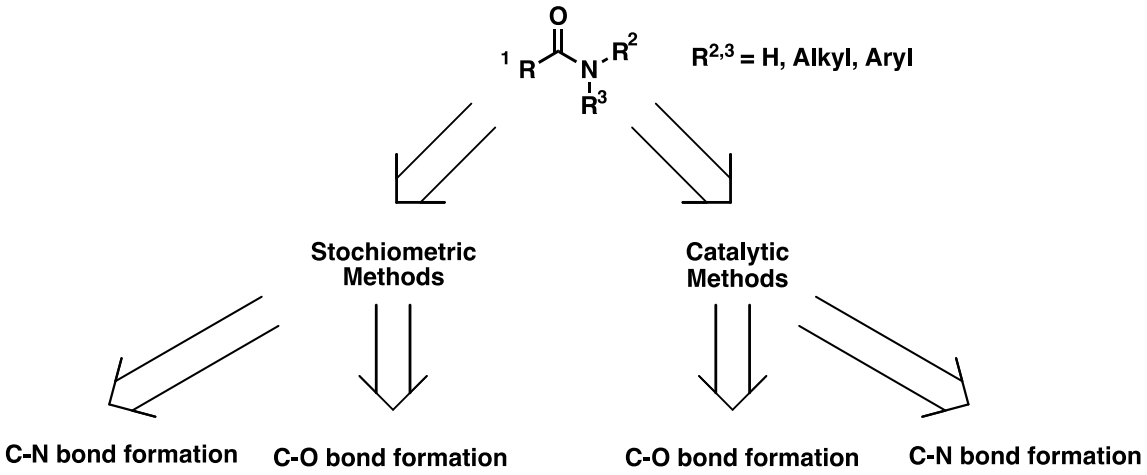

Figure 3: Possible amide synthesis methods.

Stoichiometric methods – Coupling reagents

The majority of methods employed in these processes rely on nucleophilic acyl substitution. This approach is known for its simplicity and high yield. However, it comes with certain drawbacks – it often involves toxic reagents, exhibits low atom economy, and involves high costs. Typically, these procedures involve the activation of carboxylic acids, *e.g. via* the formation of acid chlorides, anhydrides, or the use of coupling reagents.[8] In the study by ROUGHLEY in 2011 the activation of carboxylic acids accounts for 16 % of all reaction analyzed in this study, emphasizing the popularity of coupling reagents.[9]

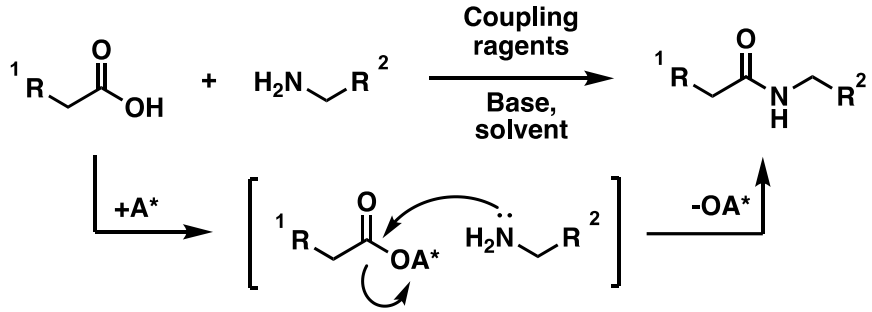

Figure 4: Schematic Amide bond formation via coupling reagents.[8]

More recent examples for developments in the field of amide synthesis can be categorized in the following:

C–N Bond formation:

In 2019, DE LUCA used visible light and trichloroisocyanuric acid (TCCA) without a photo-catalyst to activate an aldehyde and form an acid chloride. The acid chloride reacts readily with various primary or secondary amines in a 68-83 % yield.[11] The scope seems limited to aryl, and *tert*-butyl (*t*-Bu) rests on the aldehyde.

An electrochemical approach was developed by VANNUCCI and coworkers in 2019.[12] In their so-called anion pool synthesis, the group produced a broad variety of aryl amides alongside benzylic esters under mild conditions. For this approach, anhydrides and benzylbromides are required.

Additionally, transamidation reactions have been widespread. For example, the SZOSTAK group has investigated the destabilization of *tert*-butyloxycarbonyl (Boc) protecting groups on amides, which enables base-promoted transamidation.[13] Until then, this transformation required transition metal catalysts. Nonetheless, Boc-activated amides produce more significant amounts of waste.

C–O Bond formation:

A formation of amides *via* C–O bond linkage can be achieved either by oxidation or hydration reaction. In 2017, SALLES and coworkers identified optimized parameters for the transformation of a benzylic amine into the corresponding unsymmetrical amide. This conversion was achieved in the presence of NaOCl through an oxygen donor partner-mediated attack, as documented in their research.[14]

The LI group developed a continuous-flow conversion of nitriles into primary amides with hydrogen-peroxide in 2018.[15] This example yields more simple primary amides; however, it has a comparably high atom efficiency since water is the only byproduct.

A basic feedstock is seldom used in amide synthesis because the target molecules for pharmaceuticals are often complex. LOUKRAKPAM and PHUKAN investigated the synthesis of primary amides from alkenes and alkynes with aqueous ammonia.[16] The transformation proceeds *via* a tricyclic bromide species from the reaction with *N,N*-dibromo-p-toluene sulfonamide. Additionally, iodine is required to form another intermediate before ammonia can attack to form the desired amide. Despite starting from relatively simple starting materials, this reaction requires many reagents and has low atom efficiency.

However, substantially higher atom efficiencies can be achieved by using a catalyst to activate the starting materials.

Catalytic methods – Beyond classic coupling

As the name suggests, sub-stoichiometric amounts of activation agents are used in catalytic amidation reactions, which are primarily direct amidation between carboxylic acids and amines.

However, as stated by MASSOLO:

> *"Catalytic methods are not widely adopted often due to scarce efficacy, or the need of large quantities of solvents, also during the workup."* (MASSOLO *et al.* 2020)[17]

Water removal or high catalyst loading is often required, and substrate generality is limited. On the positive side, waste production is reduced, resulting in significantly better E-factors for catalytic syntheses.[18] Again, the catalytic amide bond formation reaction can be divided into two groups.

C–N Bond formation:

Popular catalysts for the C–N bond formation are arylboronic acids, which have been used for this type of reaction since 1996.[19] More recently, 5-methoxy-2-iodophenylboronic acid (MIBA) was used as an effective catalyst with reduced use of dehydrating agent.[20] Also often used catalysts consist of group IV metals. Hafnium (IV) bis(cyclopentadienyl)dichloride was discovered to be active at room temperature with 4 Å mole sieves as the dehydrating agent.[21] Since the mole sieves can be regenerated, the total amount of waste per product is drastically reduced. The group of MILSTEIN was able to perform an acceptor less oxidative amidation with a ruthenium PNN pincer catalyst.[22] This type of reaction is especially interesting because alcohols can be coupled directly with amines, liberating hydrogen as the only byproduct. Amidocarbonylation reactions couple at least three molecules to form amides directly and the carbonyl group is formed by the insertion of carbon monoxide.[23]

C–O Bond formation:

Amines are selectively oxidized to form amides in C–O bond formation type reactions. In 2017, ADIMURTHY and coworkers developed an iodine-catalyzed reaction in combination with tertbutylhydroperoxide.[24] More efficient is the direct use of oxygen, which can be enabled by photoredox-catalysts.

Noteworthy, most amide synthesis procedures require amine substrates, which come with their own challenges.

2.2.2. Amines – Intermediates, solvents and more

Amines are crucial in the synthesis of amides but are not limited to this use. They are a focal point of scientific research in the vast field of organic chemistry and are essential components in

creating molecular diversity. Amines have a wide range of chemical behaviors, from being intermediates in biochemical processes to being critical components in the synthesis of pharmaceuticals, agrochemicals, and materials.

Amines are appealing because of their presence in nature and their synthetic adaptability, which provides chemists with various options for customizing molecular architectures. The use of amines extends beyond traditional organic synthesis and encompasses diverse fields such as medicinal chemistry, materials science, and catalysis. Understanding the underlying principles governing amine reactivity and their multifaceted roles in various chemical contexts is essential.

While amines hold immense promise for their diverse applications, their synthesis is not without challenges, presenting researchers with intriguing puzzles that demand creative solutions. Amine synthesis still presents several challenges, which are among others:

1. **Selectivity and Functional Group Tolerance:** Achieving high selectivity in amine synthesis remains a formidable challenge, especially in the presence of multiple functional groups. Many synthetic methodologies struggle to discriminate between different reactive sites, leading to undesired byproducts and complicating the isolation of the target amines.[25,26]
2. **Reductive Amination Challenges:** Reductive amination, a widely employed method for amine synthesis, faces obstacles related to chemoselectivity and the compatibility of reducing agents. Overcoming these challenges is essential for the efficient and clean conversion of carbonyl compounds to amines. Especially, the selectivity with direct use of ammonia is difficult to control.[27–29]
3. **Sustainable and Green Synthesis:** Developing environmentally friendly amine synthesis methods is a pressing challenge due to the increasing emphasis on sustainable chemistry. It is essential to minimize the use of hazardous reagents, reduce waste generation, and improve energy efficiency for the future of amine synthesis. The growing interest in replacing fossil feedstock with renewable starting materials presents challenges, as traditional synthesis routes may no longer be applicable.[30,31]
4. **Transition Metal-Catalyzed Amination:** While transition metal-catalyzed amination reactions have emerged as powerful tools for amine synthesis, challenges persist regarding catalyst stability, substrate scope, and the requirement for expensive metal catalysts. Addressing these limitations is pivotal for advancing the efficiency and applicability of these transformations.[27]

Navigating the challenges of amine synthesis deepens our understanding of fundamental chemical processes and paves the way for developing more efficient, selective, and sustainable methodologies with broader utility across various scientific disciplines. Overcoming these obstacles promises to unlock new frontiers in the synthesis of amines and expand the horizons of their applications in diverse fields.

3. Goals

Although amides and amines play a major role in the chemical and pharmaceutical industries, their production methods are often waste-intensive or energy-demanding. This is mainly due to stoichiometric reagents and multistep reactions. Catalytic reactions could lead to an improvement since they are inherently more efficient.

To take a step towards a more sustainable industry, implementing resource-effective reactions for such significant products is of great value. These play a major role in protecting the environment by reducing waste and using fewer resources, especially in large-scale processes.

This work investigates the potential for improving the synthesis process of amides and amines using homogeneous transition metal catalysts. The objective is to develop or improve three distinct methods to enhance the efficiency of amide and amine synthesis and discover novel methods for incorporating nitrogen into the desired product:

1. **Carbonylative telomerization** is an outstanding chemical reaction combining four simple feedstock molecules into one significantly more complex molecule. Amides are obtained if amines are used as the nucleophile in the reaction. The objective is to **expand the scope to highly branched amides**. A drawback of this reaction is its high catalyst loading, making it costly. Therefore, this work aims to reduce the required amount of catalyst.
2. Fatty esters are popular bio-based feedstock materials for many production lines and are the base of the chemical value chain. However, several reaction steps are required for transforming them into primary amines. The goal of this work is the **direct introduction of ammonia to esters to form primary amines** in a one-pot reaction. For this novel reaction, a new catalyst must be developed to combine the necessary sub-reactions. This procedure could lead to increased resources and energy efficiency.
3. Controlling selectivity in present syntheses for primary amines is difficult due to reactive imine intermediates. A promising group of intermediates are aldoximes. By reduction, they can be transformed into primary amines, which has been done only with heterogeneous catalysts so far. This work aims to combine aldoxime reduction with a homogeneous catalyst to further improve the promising reaction route. Finally, this method is applied to **synthesize primary amines from alkenes,** by combining it with hydroformylation and an oximation step. This reaction setup presents a promising alternative to the highly desired hydroamination of alkenes.

By addressing these milestones, this work significantly contributes to the development of a more environmentally friendly synthesis of amides and amines.

4. Carbonylative telomerization

4.1. Abstract

Carbonylative telomerization is a powerful tool for efficiently converting basic building blocks such as butadiene and β-myrcene into highly functionalized products in only one reaction step. In this chapter, the synthesis tool is expanded to the production of highly branched amides. For the first time, β-myrcene was combined with amines to yield highly branched amides with up to 97 %. Afterward, an entirely new product class was added to the synthesis spectrum of carbonylative telomerization by adding mixed carboxylic anhydrides, which are highly reactive intermediates. A catalytic reaction path was described, and a quantification protocol was developed. The yields of the reactive anhydrides could be determined by derivatization into amides. Finally, a new reaction protocol was developed to improve the atomic efficiency of the reaction *via* sub-stoichiometricstoichiometric use of the acid in the combined carbonylative telomerization amidation approach.

This chapter is in parts based on the following works which were adopted in parts, extended and modified:

Bachelothesis:

a) Malte Menk (2019): Palladiumkatalysierte Carboxytelomerisation von β-Myrcen mit Diethylamin zu ungesättigten C21-Amiden, TU Dortmund
b) Charlotte Wernsdörfer (2019): Expansion of the Synthesis-Tool of Carboxytelomerization for the Two-Step Synthesis of Amides via Anhydrides
c) Arno Windisch (2019): Accessing New Products via the Synthesis Tool Carboxytelomerization – Utilizing Highly Reactive Anhydride Intermediates

Masterthesis:

d) Lilia Milius (2020): Tandem-Catalysed Conversion of 1,3-Dienes with Amine Nucleophiles via Acid-Assisted Carboxytelomerisation in a One-Step Reaction System, Master Thesis, TU Dortmund

Publications:

e) Hares, K.; Vogelsang, D.; Wernsdörfer, C. S.; Panke, D.; Vogt, D.; Seidensticker, T. Palladium-catalyzed synthesis of mixed anhydrides via carbonylative telomerization. *Catal. Sci. Technol*. **2022**, DOI: 10.1039/D2CY00486K

4.2. Carbonylative telomerization – An underestimated reaction?

The carbonylative telomerization was discovered by BILLUPS *et al.* in 1971 at UNION CARBIDE CORP during their work on carbonylation of dienes.[32] They discovered that the absence of chloride ions in the palladium precursor led to a new product class. Additionally, to the desired carbonylation a dimerization of the diene occurs. For the first time, direct formation of ethyl nona-3,8-denoate from ethanol and butadiene in the presence of CO was reported, with up to 38 % yield (Figure 5). They confirmed that the reaction was not a combination of telomerization with a consecutive carbonylation of the resulting unsaturated alcohol. Instead, the halide free catalyst combines five molecules to form the product ester in one reaction, theoretically 100 % atom economic.

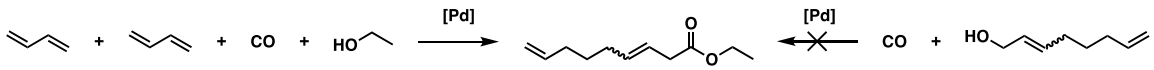

Figure 5: Carbonylative telomerization with 1,3-butadiene and ethanol published by ROMANELLI et al..

Shortly after TSUJI[3333] published a more detailed study on the influence of halides on the reaction and ROMANELLI[3434] patented the first industrial application (Figure 6). In 1979, KNIFTON conducted an extensive study on the carbonylative telomerization.[35] The research paper focused on the influence of solvents and phosphine. KNIFTON proposed a catalytic mechanism (Figure 7, left cycle) and thereby refined the work of BILLUPS. With the new findings the yield could be improved up to 64 %.[35] The interest in the reaction faded until several publications in 2018.

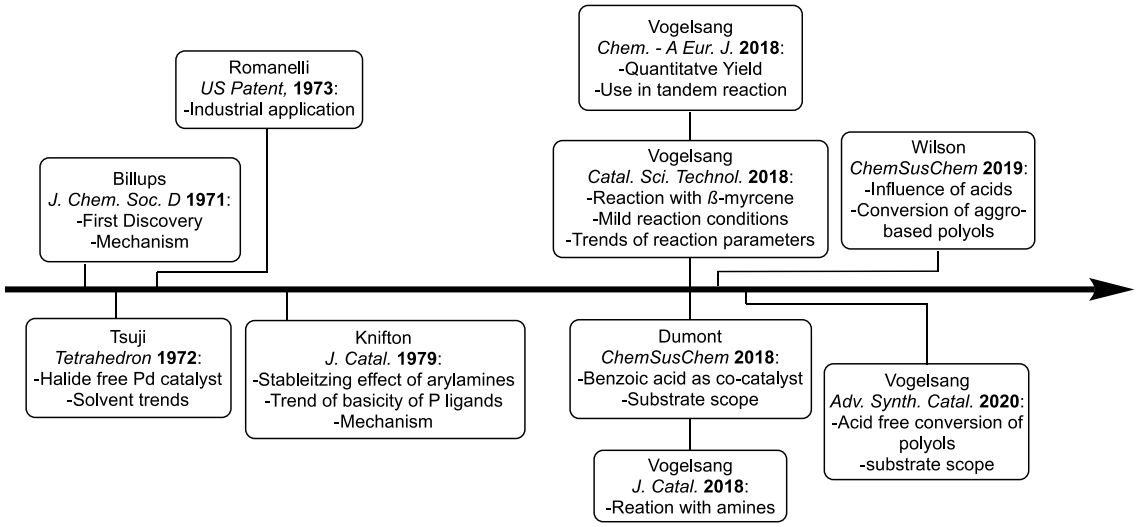

Figure 6: History of the carbonylative telomerization.[32–42]

VOGELSANG *et al.* investigated the synthesis of diesters through a tandem catalytic reaction, by combining the carbonylative telomerization with an additional carbonylation of the terminal double bond of the unsaturated ester.[40] The first quantitative yield could be achieved, highlighting the efficiency of their catalytic system. Moreover, they adapted the reaction conditions and could convert β-myrcene, under mild reaction conditions compared to the reaction with butadiene.[39] This development underscores their ability to expand the substrate scope of the reaction, revealing intriguing trends in reaction parameters that can be leveraged for further advancements.

The incorporation of amines as nucleophiles introduces possibilities for diversifying the scope of reactions and enhancing the overall synthetic utility of carbonylative telomerization and was also published by them in the same year.[38]

Parallelly, in the same year, DUMONT *et al.* investigated the conversion of otherwise recalcitrant nucleophiles, such as phenols.[36] Their key was the utilization of benzoic acid as a co-catalyst, which supposedly leads to a cationic catalyst cycle (Figure 7, right).

So far, two different reaction mechanisms have been proposed for the carbonylative telomerization.[35,36]

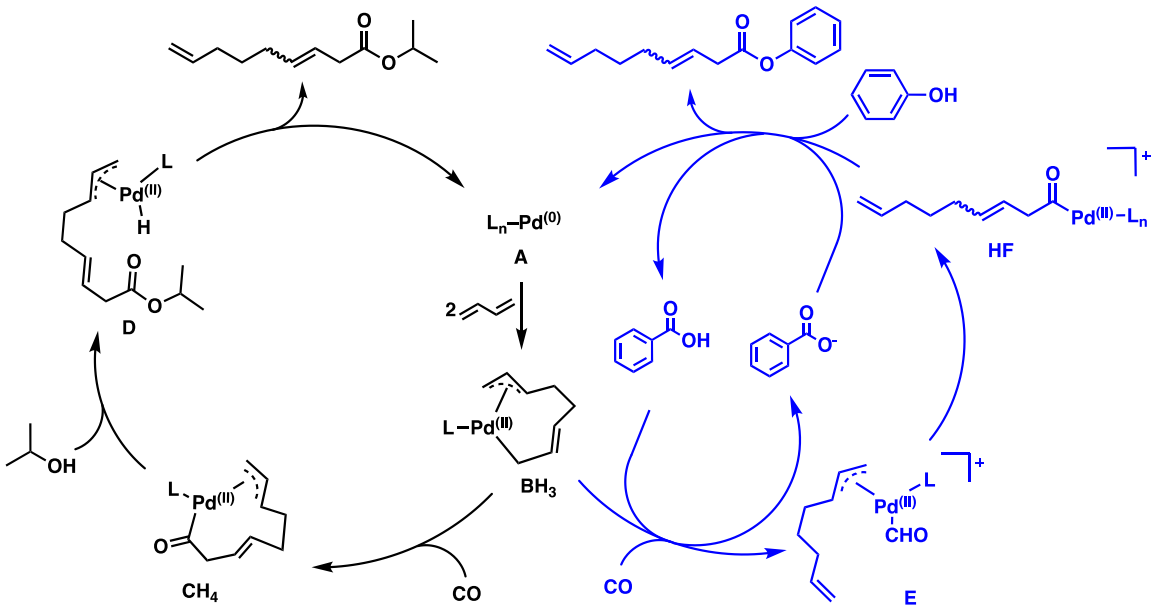

Figure 7: Catalytic cycles proposed for the carboxytelomerization proposed by KNIFTON (left)[35] *and SAUTHIER (right).*[36]

Similar to the mechanism of a "simple" telomerization reaction, the first step represents an oxidative coupling of two 1,3-butadiene molecules forming the allyl complex **B** (Figure 7, **A** to **B**). Insertion of CO into the σ-allyl C–Pd bond forms the acyl complex **C**. This species is then attacked by the alcohol nucleophile to form the intermediate **D**, which collapses *via* a reductive elimination into the desired ester product and the active catalyst complex **A** (Figure 7, left).[35]

SAUTHIER and coworkers proposed a different mechanism for the carbonylative telomerization of phenols (Figure 7, right cycle).[36] Phenols result in low yields under common carbonylative telomerization conditions. The key for this improvement was the addition of benzoic acid, resulting in a proposed cationic Pd-complex. Due to its positive charge, the complex supposedly becomes more electrophilic increasing the interaction with the phenol nucleophile. In their mechanism, the complex **B** is protonated by the acid and forms the cationic complex **E** upon coordination of CO. The CO then undergoes a migratory insertion into the η^3-allyl C–Pd bond forming **F**. In the last step, the phenol cleaves the ester from the Pd-complex, while restoring the active catalyst **A** as well as a proton (Figure 7, right).[36]

One year later the same group published the conversion of agro-based alcohols with their acid co-catalyzed system, further expanding the scope of the carbonylative telomerization by polyols. In 2020 VOGELSANG *et al.* found reaction conditions which allowed the same conversion of polyols without an additional acid. Such polyols yield multi-unsaturated polyesters which can potentially be used as linker molecules, e.g., for coatings or polymers.

The carbonylative telomerization is, as the name suggest closely related to the more commonly known telomerization reaction without the addition of CO. Ethers instead of esters and amines instead of amides are the result (Table 1).

Table 1: Scope of the telomerization compared with the scope of carbonylative telomerization. Tiles in blue representing established products and green the objective of this work.

Diene	Nucleophile	Telomerization	Carbonylative telomerization
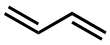		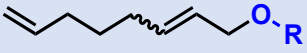 SMUTNY 1967[43]	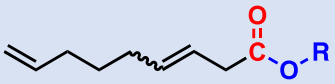 BILLUPS 1971[32]
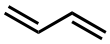	 R' = H, Alkyl, Aryl	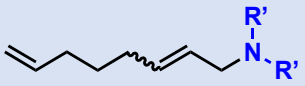 WALKER 1970[44]	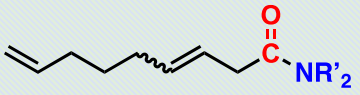 VOGELSANG 2018[38] This work
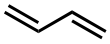	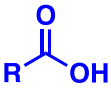	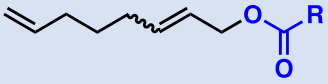 TAKAHASHI 1967[45]	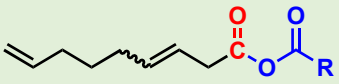 This work
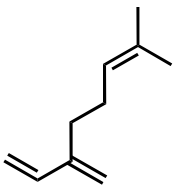		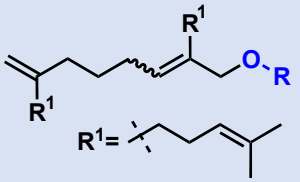 LOPES 2011[46]	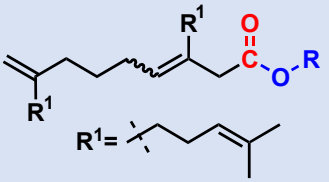 VOGELSANG 2018[39]
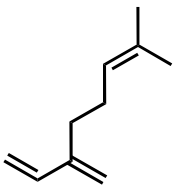	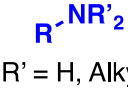 R' = H, Alkyl, Aryl	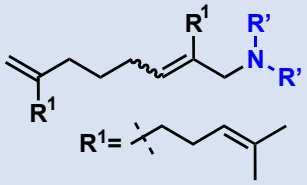 BEHR 2010[47]	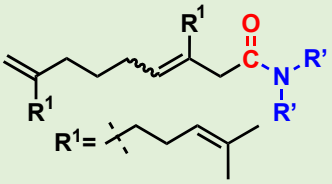 This work

Since both reactions are related and, in many cases, the same nucleophiles and dienes have been reported for both reactions, this trend should also be feasible to continue. For instance, amines have been used as nucleophiles in both reactions and β-myrcene as the diene respectively. However, highly branched amides form the carbonylative telomerization of β-myrcene with amines was not reported so far. A noteworthy limitation of the reported amidotelomerization is the high catalyst loading of 5 mol% Pd necessary for a sufficient conversion. This limitation could be one explanation why such a combination was not attempted so far. Another interesting combination would be the carbonylative telomerization of carboxylic acids, because the products are highly reactive mixed carboxylic anhydrides which would be interesting intermediates.

4.3.Goals

In response to the growing challenge of resource scarcity, there is an increasing need to adopt more atom-efficient synthetic pathways to convert bulk feedstock materials. Carboxytelomerization stands out as a promising reaction in this regard, demonstrating its capacity to generate complex molecules exclusively from readily available dienes, nucleophiles, and carbon monoxide. Due to its 100% atom-economic nature, this reaction is particularly interesting for expanding its applicability to a wider range of products. A comparison with related telomerization reactions reveals untapped potential, especially concerning nitrogen nucleophiles. In 2018, our group demonstrated the successful conversion of butadiene with amines;[38] however, the use of other dienes like β-myrcene was not investigated.

Given that an example of telomerization using amines was already documented in 2010[47], it is reasonable to explore the possibility of expanding this approach to carbonylative telomerization. **The first goal is to include highly branched amides into the list of possible products by combining β-myrcene with amines under carbonylative telomerization conditions.** These amides would require complex multistep synthesis routes and could be used as lubricants.

Further comparison of the two reactions reveals that carboxylic acids have been used in telomerization for a long time but not in carbonylative telomerization. **The second goal is the utilization of carboxylic acids in carbonylative telomerization, which would lead to highly reactive mixed anhydrides.** Due to their outstanding reactivity, mixed carboxylic anhydrides are popular reagents in organic synthesis. Usually, their production requires a multistep synthesis with stoichiometric amounts of reagents, resulting in large waste quantities. In this case, carbonylative telomerization would be the first highly atom-economic synthesis of mixed anhydrides. Combining the anhydrides with a large variety of nucleophiles would open access to a wide range of products. When carboxylic anhydrides are combined with a nucleophile, a carboxylic acid is released from the reaction. With a tuned reaction, this is the same acid used to form the anhydride via carbonylative telomerization. Therefore, a catalytic use of the acid might be possible. **The third goal is the sub-stoichiometric use of a carboxylic acid to promote the formation in a tandem catalytic reaction**. Especially this could be useful for the formation of amides, which are less easily accessible through amidotelomerization, due to the high catalyst loading necessary.[38]

4.4.Highly branched amides from a single reaction with β-myrcene

Highly branched amides are potential lubricants, tenside precursors and bioactive compounds. Carbonylative telomerization with β-myrcene and amines would yield such compounds. β-Myrcene, which comes from the pyrolysis of β-pinene, a waste product from the paper industry, is a renewable feedstock and offers an alternative to otherwise petrochemical starting material. Due to its unsaturated hydrocarbon backbone with a diene unit β-myrcene is similar to the hydrocarbons derived from the petrochemical value chain and has gained popularity in the recent decade. While β-myrcene has been used in carboxytelomerization, its combination with amines, *i.e.* Amidotelomerization, is unexplored. This process poses challenges related to achieving selectivity, with numerous side reactions to consider (Figure 8).

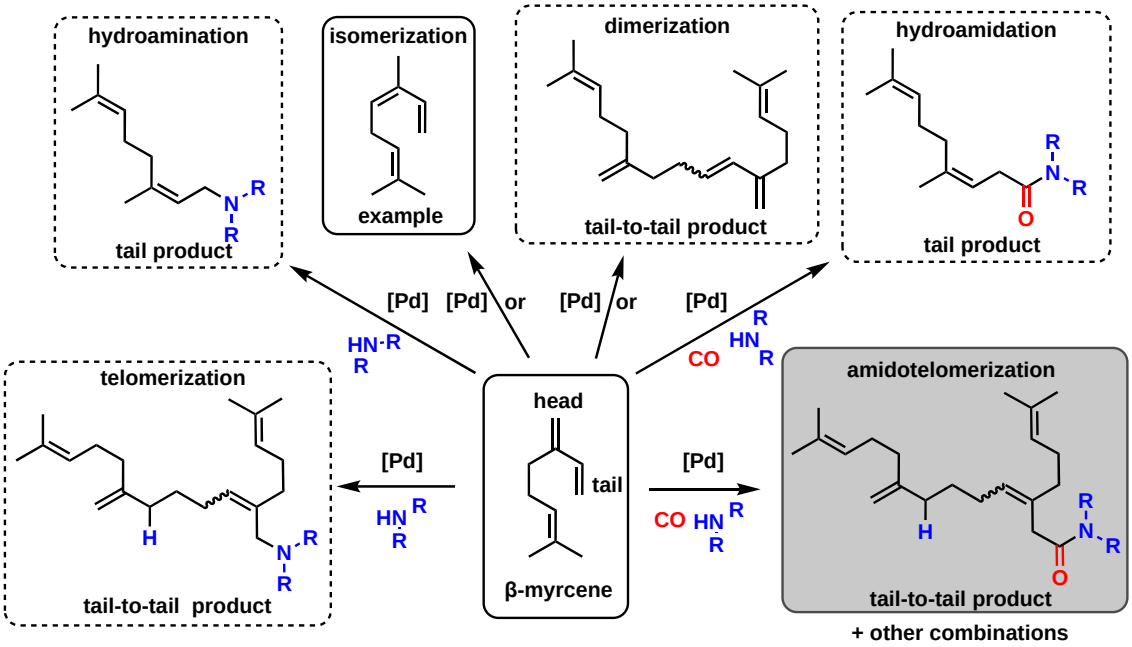

Figure 8: Possible side reaction in the amidotelomerization of β-myrcene. With examples of the resulting isomers.

Myrcene, a non-symmetrical molecule, possesses a highly reactive diene moiety that can undergo isomerization induced by heat or catalyzed by palladium. Dimerization of β-myrcene can generate multiple possible isomers, including tail-to-tail, tail-to-head, head-to-tail, and head-to-head configurations. These dimers contain several double bounds and a conjugated diene moiety, which, combined with β-myrcene's low stability at elevated temperatures, often leads to oligomerization or polymerization. For this reason, commercially available β-myrcene often contains stabilizers to prevent polymerization.

This reactivity leads to many different reaction outcomes for functionalization as well, producing combinations of tail and head product isomers. For simplicity, Figure 8 shows only the tail and tail-to-tail products; however, a mixture of tail and head products is expected and, where applicable, also tail-to-head and head-to-head combinations.

β-Myrcene can react directly with an amine, leading to amine formation, i.e., **hydroamination**. It can undergo an additional CO insertion, known as **hydroamidation**, resulting in the production of amides. The **telomerization** process involves dimerization and the attack of a Brønsted acidic nucleophile, resulting in several possible isomers. For a comprehensive understanding of telomerization, BEHR published an extensive review paper on the reaction.[48,49]

To produce amides in **amidotelomerization**, the introduction of a carbonyl function is crucial. This carbonyl function is inserted during the catalytic cycle, combining two β-myrcene molecules, one CO molecule, and one amine, ultimately forming highly branched unsaturated amides. This unique process is aptly termed amidotelomerization like the carboxytelomerization yielding esters.

The catalyst system was adapted from that work since the reaction had already been carried out with butadiene.[38] In the carboxytelomerization of β-myrcene, low CO pressure under neat conditions was crucial. Therefore, no additional solvent was used at 5 bar CO (Figure 9).[39]

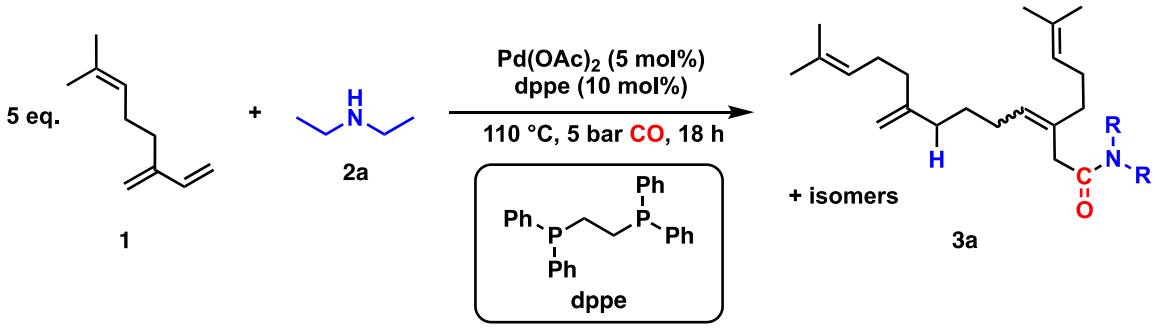

Figure 9: Starting conditions adapted from previous work for the carbonylative telomerization of amines with β-myrcene.

The initial results of the experiment indicated that only traces of the amidotelomerization product were produced, while the main product was the amine from telomerization, with a yield of 48 %, followed by the hydroamination product with a yield of 31 %. In contrast to previous research on amidotelomerization[38], no hydroamidation product was detected. This initial experiment demonstrates that the reaction is possible, however further optimization is necessary to increase its efficiency. It is important to note that this initial experiment was conducted without an inert atmosphere in the reactor during the preparation of the experiment. Despite being purged with CO prior to the reaction, oxygen might have been present in the reaction solution during the reaction, potentially leading to the oxidation of the phosphine ligand, *i.e.* 1,2-bis(diphenylphosphino)ethane (dppe), and inhibiting the reaction.

4.4.1. Pd-complex stabilizers – Solvents and ligands

When conducted under an argon atmosphere, an increase in conversion and the hydroamination reaction were observed. The amidotelomerization product **3** was also increased to 5 %. To reduce costs, it is economically beneficial to use no solvent, if the reaction performance is not reduced. However, in some cases, the performance of the reaction can be significantly enhanced by dilution or the stabilization effects of the solvent on the catalyst. Additionally, previous research has shown that the ligand used has a significant influence on the reaction performance. Therefore, the more basic and sterically demanding ligand PCy_2Ph, was compared in the three tested solvents to the previously used dppe ligand (Figure 10).

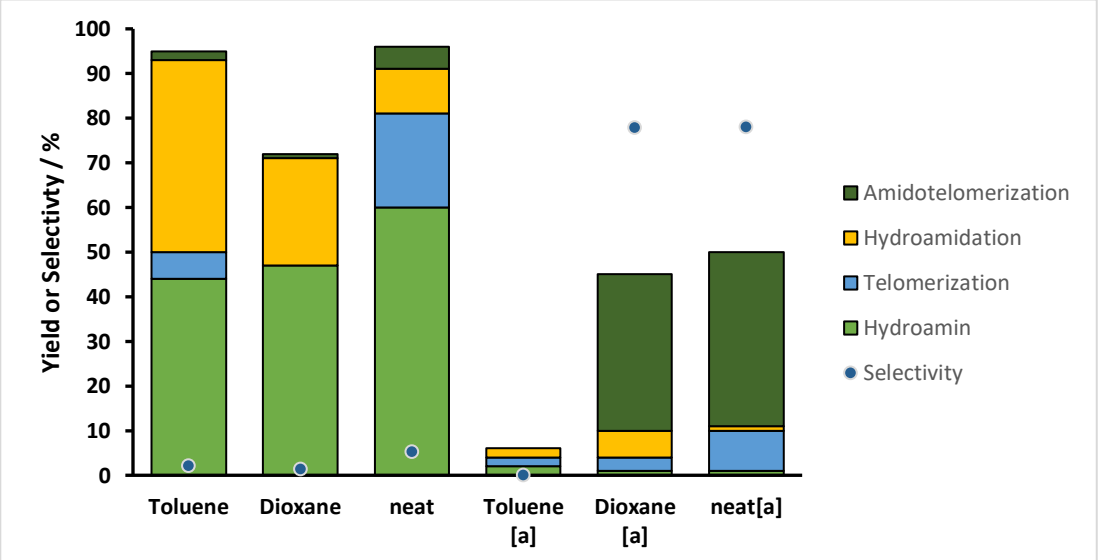

*Figure 10: Influence of additional solvent on the amidotelomerization of β-myrcene **1**. Conditions: 1.73 mmol diethylamine **2a**, 5 mol% $Pd(OAc)_2$, 10 mol% dppe, 5 bar CO, 110 °C, 18 h, 600 rpm. [a]: 10 mol% PCy_2Ph*

With the bidentate ligand dppe the reaction reaches a high conversion of the nucleophile of up to 96 %, yet only a small fraction of 1-5 % of the products was related to the amidotelomerization. Hydroamination was the main reaction and in the presence of a solvent the second most reaction became hydroamidation. The conversion of >90 % indicates a high activity of the catalyst, but the active centrum seems to be crowded by the bidentate ligand as the reaction requiring a dimerization of the diene are performing poorly.

In contrast, the monodentate ligand promotes dimerization and amidotelomerization is the main reaction. This drastic improvement in selectivity is traded with a lower overall activity of the system since the conversion is limited to about 50 %. Again, without a solvent the amidotelomerization yield was the highest with 39 %.

4.4.2. Butadiene – Shifting from monomeric to dimeric products

An excess of the diene had a significant influence in previous work on carbonylative telomerization and was investigated next (Figure 11).

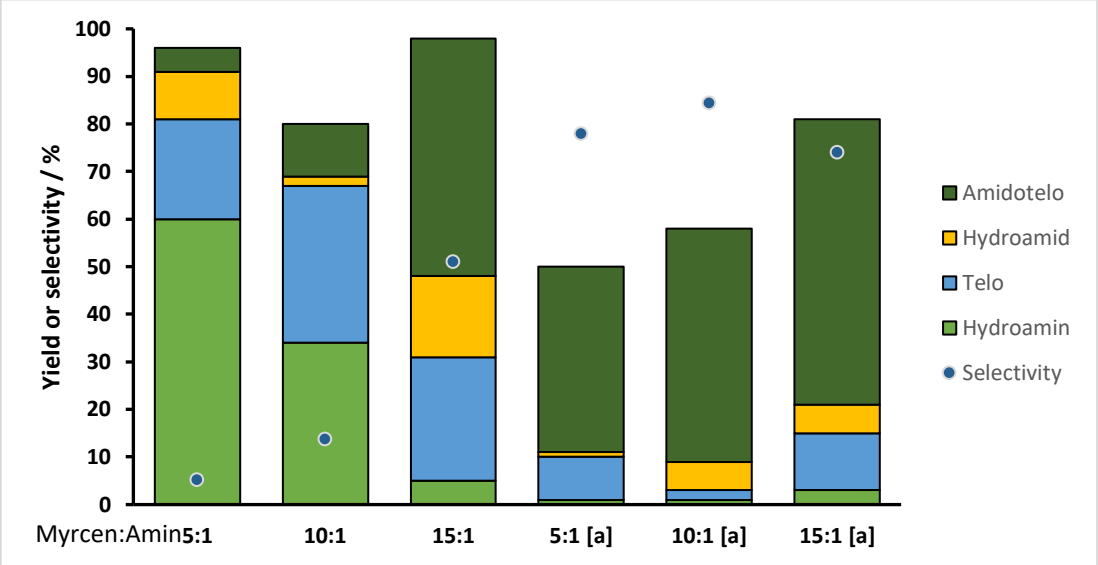

*Figure 11: Influence of an excess of β-myrcene **1**. Conditions: 1.73 mmol diethylamine **2a**, 5 mol% $Pd(OAc)_2$, 10 mol% dppe, 5 bar CO, 110 °C, 18 h, 600 rpm. [a]: PCy_2Ph.*

The β-myrcene:amine ratio plays a critical role in the yield distribution of the reaction. With a β-myrcene:amine ratio of 5:1, the total yield was already at 96 %, while at 15:1, the yield increased to 98 % with 50 % amidotelomerization. The results are in line with previous findings, indicating that a large excess of diene is beneficial for amidotelomerization. Hydroamination is preferred at lower diene concentrations, while dimerization takes over when more diene is present. The conversion of the reaction goes down at a β-myrcene:amine ratio of 10:1, suggesting a transition between the two types of reactions.

The selectivity towards amidotelomerization was significantly increased by using a more basic monodentate ligand. Negligible hydroamination and hydroamidation products were found in the product solution. The higher content of β-myrcene **1** (at a ratio of 15:1 of β-myrcene:amine) also proved to be beneficial, increasing selectivity from 39 % to 60 %. The highest selectivity was observed at a ratio of 10:1, with fewer side products detected despite lower conversion.

4.4.3. CO pressure

The monodentate ligand performed the best, as it promoted dimerization and favored amidotelomerization. In addition to the diene concentration, the concentration of carbon monoxide in the reaction solution can influence the reaction according to Le Chatelier's principle.

The concentration in the solution is correlated to the CO pressure in the reactor following Henry's law for ideal behavior:

$$H_s^{cp} = \frac{c_a}{p} \quad (1)$$

Hence, the influence of the CO pressure on the reaction performance was investigated next.

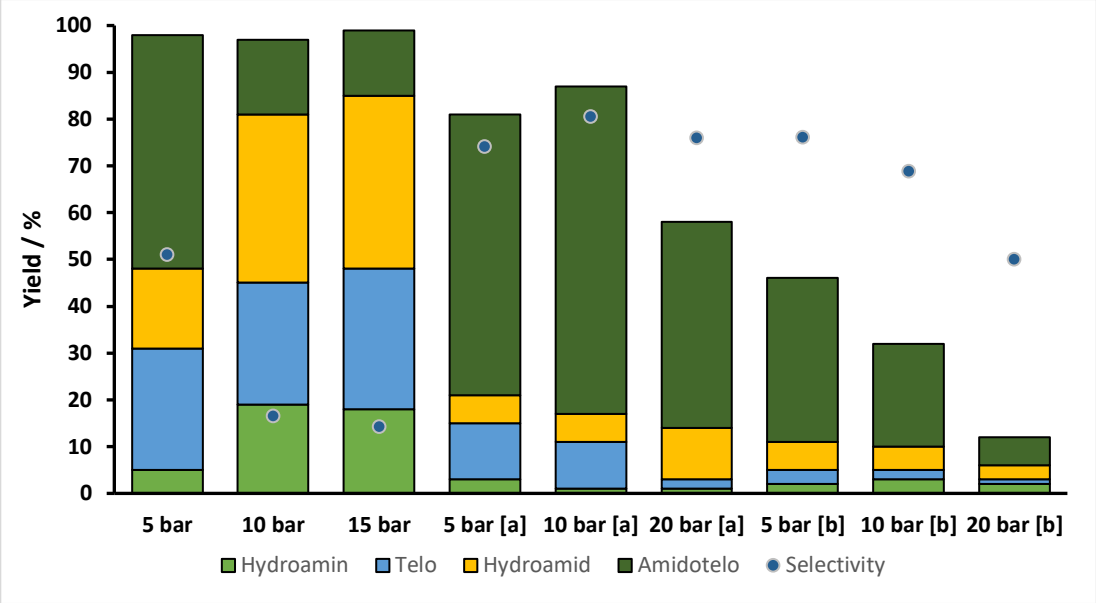

*Figure 12: Influence of CO pressure on the amidotelomerization with β-myrcene **1**. Conditions: 1.73 mmol diethylamine **2a**, butadiene:amine 15:1, 5 mol% Pd(OAc)₂, 10 mol% dppe, 5 bar CO, 110 °C, 18 h, 600 rpm. [a]: PCy_2Ph [b]: PCy_2Ph and 2 mL of dioxane.*

For the bidentate ligand the amidotelomerization behaves anti-proportional to the CO pressure in the reactor and the best results were achieved at 5 bar CO. Higher pressures in the reactor seem to inhibit the dimerization, hence more hydroamination and hydroamination can be observed.

Using the monodentate ligand the performance could be improved applying 10 bar of CO to 70 % amidotelomerization products **3**. At higher pressure of 20 bar, the performance decreases significantly, due to CO crowding the catalyst center. Additionally, the influence of CO on the reaction was investigated using dioxane as an additional solvent. The results show the same trend as the bidentate ligand; however, the conversion is lower at below 60 %, hence the amount of amidotelomerization is less. The combined optimized conditions are summarized in Figure 13.

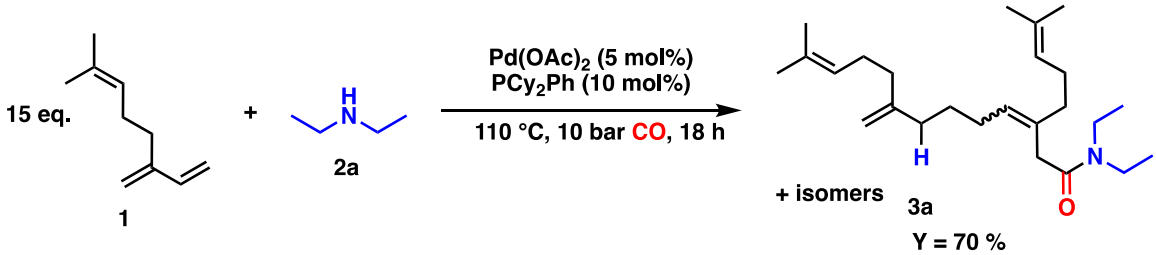

Figure 13: Optimized reaction condition for the amidotelomerization of β-myrcene **1** *with diethylamine **2a**.*

As a result of the optimization, the reaction performance could be increased from the starting yield of 3 % to a yield of 70 % (Figure 13). A conversion of 87 % was reached after 18 h reaction time, resulting in a selectivity of the reaction of 80 %. Since the activity of the nucleophile can also have an impact on the reaction's performance the scope of the reaction was investigated next.

4.4.4. Scope of the reaction

The optimized conditions were applied to various types of amines. During the optimization diethylamine **2a** was the nucleophile used and in the short investigation of the scope the longer chain dibutylamine, the very sterically demanding dicyclohexylamine and the cyclic piperidine were tested (Table 2).

Table 2: Investigation of the scope in the amidotelomerization of β-myrcene.

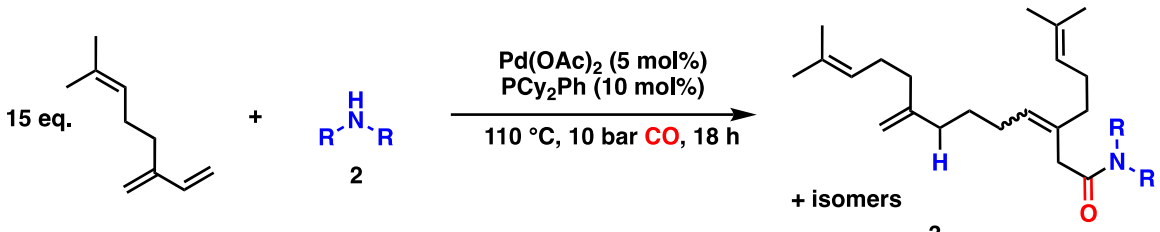

Entry	Substrate	Product	Y [%]	S [%]
1	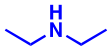 **2a**	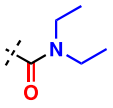 **3a**	70	80
2	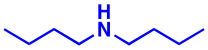 **2b**	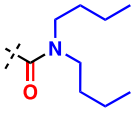 **3b**	80	99
3	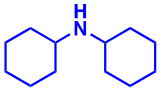 **2c**	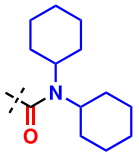 **3c**	94	99
4	 **2d**	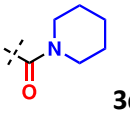 **3d**	97	99

Conditions: 1.73 mmol amine, butadiene:amine 15:1, 5 mol% $Pd(OAc)_2$, 10 mol% PCy_2Ph, 10 bar CO, 110 °C, 18 h, 600 rpm.

With the reaction parameters presented, good to excellent yields can be obtained with outstanding selectivities. In the case of dibutylamine **2b**, the yield of 80 % is higher compared to diethylamine **2a**. The sterically demand does not have a strong impact on the amidotelomerization. On the contrary the data hints to a positive correlation, since the extremely sterically demanding dicyclohexylamine **2c** has results in an even higher yield with 94 %. The remaining factors could be either the basicity or the nucleophilicity of the reagents. Yields of 97 % can be achieved with piperidine **2d**, which is known to be a strong nucleophile due to its cyclic structure.[50] Finally, from these results, another relevant influence is the basicity of the amine used, which seems to compete with the increasing steric demand of the substituents in terms of product yield.

4.4.5. Conclusions

After the optimization, adding highly branched amides to the accessible products for carbonylative telomerization was possible for the first time. With the optimized reaction parameters (Figure 13), yields of up to 70 % of the desired target products could be generated using diethylamine **2a** as a model substrate. β-myrcene **1** is directly converted in a single reaction

step. However, for this reaction an inert atmosphere is more crucial than with other nucleophile diene combinations in carbonylative telomerization.

It was found that the selectivity, and hence the efficiency of the reaction in terms of yield, increases significantly with the use of the monodentate ligand PCy_2Ph over bidentate ligands such as dppe. The catalyst loading, the choice of CO pressure, the β-myrcene **1** to amine ratio, and the absence of additional solvents were identified as crucial reaction parameters.

Furthermore, the optimized reaction conditions could be extended to additional amines with different basicity and steric properties. These amines reached higher selectivities and excellent yields of up to about 97 % of the desired target products in the case of piperidine **2d**.

Further research should focus on reducing the high amount of catalyst necessary for the reaction. Palladium is a costly precious metal, and reducing its amount in the reaction would render the whole process more viable for larger-scale reactions.

4.4.6. Experimental

General

Solvents and Chemicals: All Solvents and chemicals were purchased from ABCR, Acros Organics, TCI, Sigma Aldrich, VWR or UMICORE. All precursors and ligands were stored in Schlenk flasks under an argon atmosphere.

Autoclaves: The catalytic experiments were performed in 25 mL stainless steel autoclaves (Figure 14). The autoclaves were equipped with a quick-fit adapter for a simple and safe connection to the pressure station.

Figure 14: 25 mL autoclave for high-pressure catalytic experiments.

Catalytic experiments: The internal standard *n*-octane (75 mg, 0.66 mmol) and the substrate diethylamine **2a** (128 mg, 1.73 mmol, 1 eq.) were transferred *via* syringe into a 20 mL crimp-cap vial, which was previously sealed with a septum. The mixture was then cooled with liquid nitrogen and inertized by the freeze-pump-thaw method. Then β-myrcene **1** (4.9 mL, 26 mmol, 15 eq.) was added in argon countercurrent. The catalyst $Pd(OAc)_2$ (19.4 mg, 0.087 mmol, 5 mol%) and the ligand PCy_2Ph (50 mg, 0.17 mmol, 10 mol%) were weighed into the vessel of a self-made 25 mL stainless steel autoclave, the reactor was then sealed and flushed with argon. The solution from the crimp-cap vial was added to the reactor in an argon countercurrent. The reactor was pressurized with 5 bar CO and reaction solution was left to stir overnight at 110 °C. After

completion of the desired reaction time the mixture was cooled in an ice bath. Then the reactor was vented carefully and reaction mixture was analyzed using GC.

GC-Analysis and parameter

For GC analysis, 0.5 mL of the reaction solution and 0.5 mL of toluene were added to a standard crimp-cap GC vial. The samples were measured with an AGILENT 7890B, a gas chromatograph from AGILENT with a flame ionization detector and a mass detector. The device is equipped with an HP-5 column (length = 30 m, diameter = 0.25 mm, film thickness = 25 µm) and an autosampler. Nitrogen was used as the carrier gas (v = 1.2 mL/min, 30 cm/s). Each measurement was performed with an injection volume of 1 µL and a split ratio of 75:1.

Table 3: Parameters of the acquisition method.

	Heating rate [°C /min]	Endpoint [°C]	Hold [min]
Start	-	50	5
Ramp 1	15	290	1
Ramp 2	40	320	5

Sternberg response factors were used to calculate the yields. These are listed below.

Table 4: Response factors calculated according to STERNBERG.

Compound	Response factor
Diethylamine **2a**	1,58
C_{21}-Amide **3a**	1,12
Hydroamidation product	1,23
Telomerization product	1,04
Hydroamination product	1,09
Dicyclohexylamine **2c**	2,43
C_{33}-Amide **3c**	1,13
Dioctylamine	1,11
C_{37}-Amide	1,08
Piperidine **2c**	1,41
C_{26}-Amid **3c**	1,11

4.4.7. Analytics

Highly branched C_{21}-Amide (N,N-diethyl-4,8-bis(4-methyl-3-pentenyl)3,8-nonadienamide) 3a

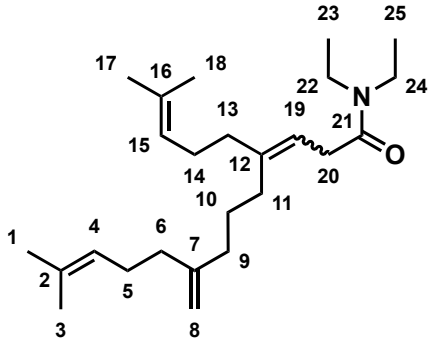

^{1}H-NMR (400 MHz, $CDCl_3$): **δ** = 1.01 – 1.18 (**23, 25**; m; 6H), 1.41 – 1.55 (**10**; m; 2H), 1.57 - 1.61 (**1, 18**; s; 6H), 1.64 – 1.69 (**3,17**; s; 6H), 1.94 – 2.16 (**5, 6, 9, 11, 13, 14**; m; 12H), 2.98 – 3.15 (**20**; d; 2H), 3.2 – 3.43 (**22, 24**; m; 4H), 4.66 – 4.76 (**8**; s; 2H), 5.02 – 5.12 (**4, 15**; s; 2H), 5.23 – 5.42 (**19**; m; 1H) ppm.

^{13}C {^{1}H}-NMR (100 MHz, $CDCl_3$): δ = 13.24 (**C23, C25**; s), 17.81 (**C3, C18**; s), 25.8 (**C1**, **C17**; s), 26.84 (**C5**, **C14**; s), 27.72 (**C10**; s), 30.81 (**C11**; s), 35.87 (**C20**; s), 37.03 (**C9**; s), 42.24 (**C22, C24**; s), 108.96 (**C8**; s), 118.31 (**C19**; s), 124.11 (**C4, C15**; s), 127.62 (**C2, C16**; s), 131.95 (**C12**; s), 133.75 (**C7**; s), 170.21 (**C21**; s) ppm.

LR-MS: m/z (%) = 373 (5), 304 (26), 234 (5), 189 (8), 168 (5), 115 (26), 109 (6), 100 (100), 91 (11), 72 (77)

FTIR: ν = 2929 (C-H_3, alkane vibrate), 1641 (RC=ONR_2, amide vibration), 1429 (C-H, alkane deformation), 969 (C=C, mono substituted alkene bend), 704 (C=C, disubstituted alkene bend) cm^{-1}.

N,N-diethyl-4,8-dimethyl-3,7nonadienylamide

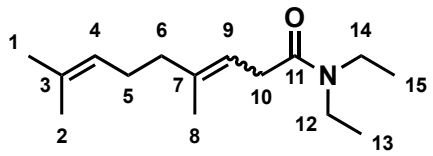

^{1}H-NMR (400 MHz, $CDCl_3$): **δ** = 1.05 – 1.71 (**13, 15**; m; 6H), 1.52 – 1.68 (**1, 2, 8**; m; 9H), 1.94 – 2.11 (**5, 6**; m; 4H), 2.96 – 3.07 (**10**; d; 2H), 3.19 – 3.39 (**12**, **14**; td; 4H), 5 – 5.15 (**4**; t, 1H), 5.28 – 5.38 (**9**; t; 1H) ppm.

LR-MS: m/z (%) = 237 (5), 194 (5), 168 (46), 126 (5), 115 (23), 100 (100), 95 (10), 86 (7), 81 (6), 74 (4)

Telomerization product C_{20}-Amine ((N,N-diethyl-3,7-bis(4-methyl-3-pentenyl)2,7-octadineamine)

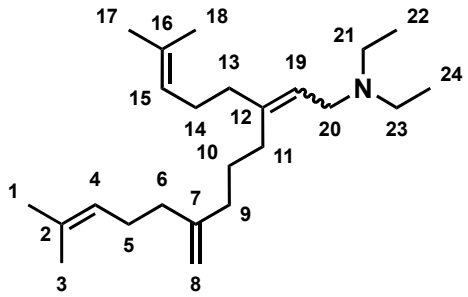

^{1}H-NMR (400 MHz, $CDCl_3$): **δ** = 0.86 – 0.97 (**22, 24**; t; 6H), 1.37 – 1.5 (**10**; m; 2H), 1.48 - 1.68 (**1, 3, 5, 6, 13, 14, 3, 17**; d; 20H); 1.87 – 1.95 (**9, 11**; m; 4H), 2.29 – 2.42 (**21, 23**; q; 4H), 2.8 – 2.88 (**20**; d; 2H); 4.62 – 4.7 (**8**; s; 2H), 5.01 – 5.08 (**4, 15**; m; 2H), 5.18 - 5.27 (**19**; t; 1H) ppm.

LR-MS: m/z (%) = 345 (2), 276 (16), 194 (100), 166 (3), 138 (9), 121 (7), 107 (7), 95 (6), 86 (59), 82 (5)

N,N-diethyl-3,7-dimethyl-2,6-octadieneamine

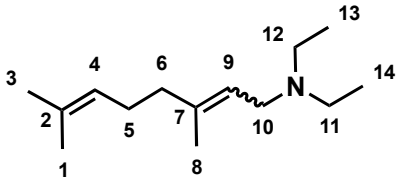

^{1}H-NMR (400 MHz, $CDCl_3$): **δ** = 0.92 – 1.00 (11, 13; m; 6H), 1.56 – 1.65 (1, 3, 8; d; 9H), 2.03 – 2.1 (5, 6; s; 4H), 2.35 – 2.44 (10, 12; q; 4H), 4.98 – 5.18 (4; m; 1H), 5.27 – 5.46 (9; m; 1H) ppm.

LR-MS: m/z (%) = 209 (19), 194 (52), 140 (20), 138 (54), 124 (22), 110 (30), 95 (22), 91 (10), 82 (16), 79 (12)

4.5. Expanding the scope to carboxylic acids – A direct route to anhydrides

After successfully adding highly branched amides to the list of possible products, the next goal was to expand the tool of carbonylative telomerization to the synthesis of carboxylic anhydrides. As stated above, carboxylic acids have already been used in the telomerization reaction years ago. Since both reactions are related, the additional insertion of CO should also be possible for carboxylic acids. The resulting anhydrides would open broad application in consecutive reaction, as they are potent reactants in combination with many nucleophiles, such as alcohols and amines.

The experiments were initially carried out employing 1,3-butadiene in combination with glacial acetic acid **1a** as model substrates, as the latter is a well-known nucleophile in the related telomerization reaction.[43,44,51] Carbonylative telomerization conditions (Figure 15) were adapted from our previous studies,[40] and applied using a 20 mL stainless steel autoclave with magnetic stirring. The catalyst was *in situ* generated from $Pd(OAc)_2$ as the precursor and the ligand tri-*n*-butyl phosphine.

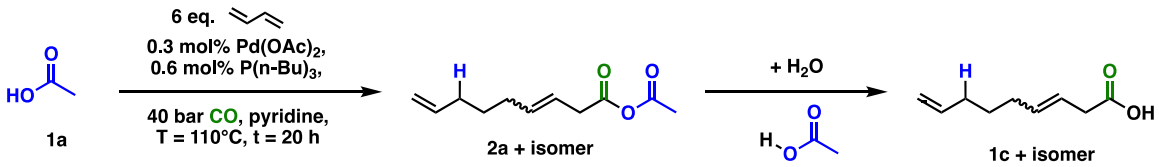

Figure 15: Initial reaction conditions for carbonylative telomerization of 1,3-butadiene with acetic acid.

The reaction was examined *via* GC-MS (see in Analytics of this chapter). The analysis of the spectra indicated the presence of the desired mixed anhydride **2a** beside one main isomer, presumably its branched isomer. Additionally, two derivatives of 3,8-nonadienoic acid (**1c**+isomer) were detected, which may have formed by hydrolysis of the mixed anhydrides, underlining the expected high reactivity of the formed product. Consequently, isolation of **2a** *via* standard purification methods such as chromatography is rather tricky and complicates its precise quantification.

However, this high reactivity allows easy derivatization into more stable compounds, quantified with higher accuracy. Hence, carbonylative telomerization was repeated with acetic acid, but after depressurizing the reactor, butyl alcohol **3a** was added as the nucleophile (Figure 16) before the analysis. The corresponding esters could be readily detected via GC-MS and were quantified by GC-FID.

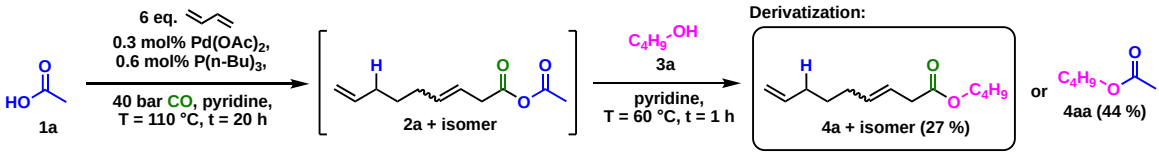

*Figure 16: Synthesis of butyl nona-3,8-dienoate **4a** by carbonylation telomerization of 1,3-butadiene with acetic acid and subsequent derivatization.*

Under these non-optimized conditions, yields were not satisfactory yet. The corresponding acetate **4aa**, resulting from a nucleophilic attack of the alcohol on the acetate side of the anhydride, was the main product. Since more straightforward and effective acylating agents are available, it is not favorable to transfer the acetic acid side of the mixed anhydride to the nucleophile. Instead, transfer of the 3,8-nonadienoic acid part of the anhydride to the nucleophile is desired. In this way, it is possible to produce valuable unsaturated products that can be readily functionalized further due to their terminal double bond. Moreover, if the transfer of the 3,8-nonadienoic acid part of the anhydride to the nucleophile is selective, the initial acid **1a** is reformed, offering potential reuse.

The relatively low selectivity can be explained by the nature of the formed mixed anhydride **2a**: The acid functionalities in acetic acid and nonadienoic acid have a similar pK_a-value and

nucleophilicity since both are aliphatic acids. High selectivity may be achieved if one of the acid groups is a significantly better leaving group. For instance, acids having a lower pK_a-value are usually better leaving groups. Another option would be the use of resonance-stabilized acids such as benzylic acid derivatives. A well-known reaction making use of this concept is the Yamaguchi esterification.[52] The reaction results in rapid and highly selective formation of esters from carboxylic acids by activation through a mixed anhydride. In this case, electron-poor benzoic acid derivatives are used to increase the reactivity and selectivity drastically. Benzoates are resonance-stabilized; therefore, they are better leaving groups than non-aromatic acid anions. Hence, benzoic acid (**1b**) was used, providing a more stable leaving group, aiming for higher selectivity.

4.5.1. Improvement and validation of the system with benzoic acid (1b)

Benzoic acid (**1b**) was chosen as the nucleophile and was tested under carbonylative telomerization conditions (Figure 17).

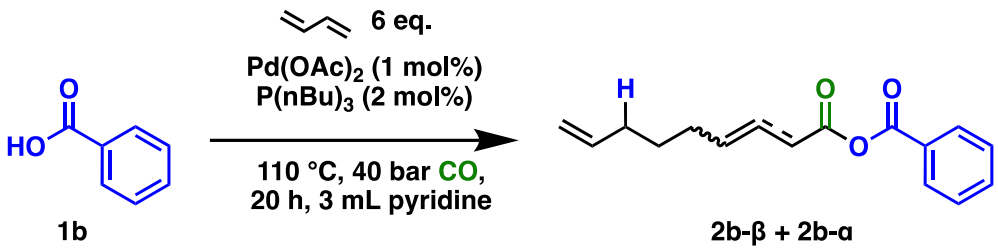

Figure 17: Carbonylative telomerization of 1,3-butadiene with benzoic acid

GC-MS analysis revealed the presence of the mixed carboxylic anhydride. A small amount of the product could be separated *via* chromatography with an isolated yield of 6% using dry solvents. The presence of anhydrides was confirmed by FT-IR (see in Analytics of this chapter), indicating the success of the reaction. NMR spectra of the product revealed the isomerization of the β-unsaturated product **2b-*β*** to the α-unsaturated isomer of **2b-α** (see in Analytics of this chapter). This isomer seems to be more stable, presumably due to the conjugated double-bond and therefore could be isolated. The formation of the conjugated isomer of **2b** could be promoted by the acidic reaction environment, which can lead to Pd-hydride species. These species are known for their isomerization activity.[53–55]

The corresponding symmetrical anhydrides, *i.e.,* benzoic acid anhydride and nonadienoic acid anhydride, respectively, were detected during GC-analysis. Presumably, the highly reactive mixed anhydrides undergo disproportionation reactions under the high temperatures in the GC injecting block, yielding an equilibrium of the two symmetrical and the mixed anhydride (Figure 18).[56–58] Symmetrical anhydrides should not be formed during carbonylation telomerization. However, this must be excluded for precise quantification, and a different analysis protocol must be developed.

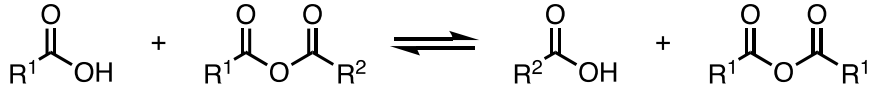

Figure 18: Disproportionation reaction of a mixed anhydride to the corresponding symmetrical anhydrides.[56]

For quantitative analysis of mixed anhydrides formed *via* carbonylative telomerization under the initial conditions, a nucleophile was added to the reaction mixture after stopping (ice bath and depressurization) (Figure 19). Next, amines were added for derivatization, which are more nucleophilic compared to the initially applied alcohols.

For the most precise data the derivatization must be quantitative. Therefore, the carbonylative telomerization was carried out and in the derivatization step, different conditions were compared. Triethylamine, tributylamine and piperidine were tested at low to moderate temperatures at reaction times of 2 h or 22 h (Table 5).

Table 5: Screening of the derivatization conditions.

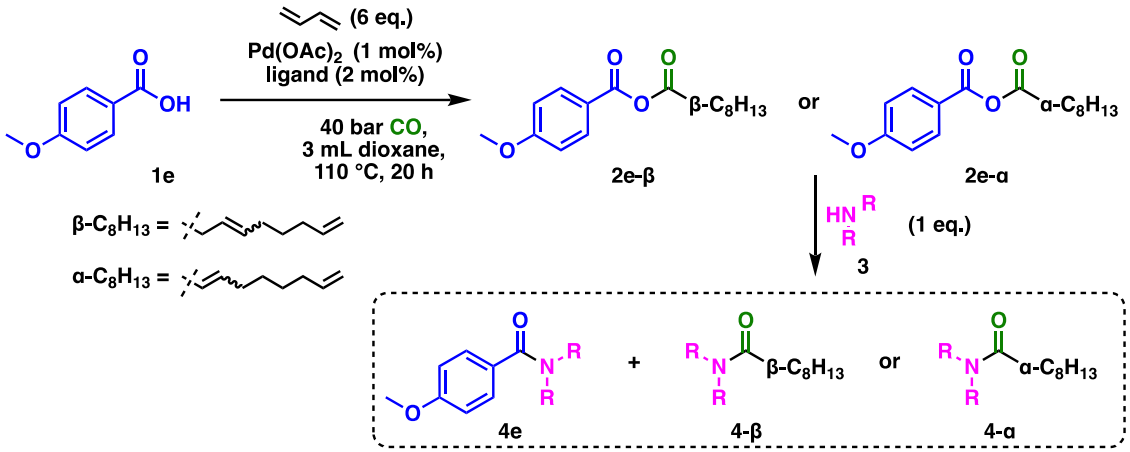

Entry	Amine	T [°C]	t [h]	Combined Amide Yield [%]
1	diethylamine **3c**	50	22	58
2	diethylamine **3c**	25	22	53
3	diethylamine **3c**	25	2	51
4	di-*n*-butylamine **3d**	50	22	59
5	di-*n*-butylamine **3d**	25	22	57
6	di-*n*-butylamine **3d**	25	2	57
7[a]	di-*n*-butylamine **3d**	50	22	56
8[a]	di-*n*-butylamine **3d**	25	23	55
9[a]	di-*n*-butylamine **3d**	25	3	55
10	piperidine **3b**	50	22	68
11	piperidine **3b**	25	22	67
12	piperidine **3b**	25	2	65

Conditions: carbonylative telomerization: 3 mmol anisic acid, 18 mmol 1,3-butadiene, 1 mol% $Pd(OAc)_2$, 2 mol% $P(n\text{-}Bu)_3$, 3 mL dioxane, 40 bar CO, 110 °C, 20 h, 600 rpm, internal standard: 75 mg n-decane. Derivatization: 3 mmol amine, 600 rpm. a = 1 eq. pyridine added. Yield related to acid determined via GC-FID analysis.

Highest yields were achieved after 22 h using piperidine at 50 °C. To compensate for a shorter reaction time of 5 h an excess of 4 equivalents of **3b** was applied to ensure a complete amidation of the mixed anhydrides. Additionally, dioxane was adapted as the solvent from SAUTHIER and coworkers since it already had proven to be beneficial for carbonylative telomerization in the presence of acids and will avoid pyridinium salt formation.[36] This sequential reaction set up was used in the following to optimize the carbonylative telomerization of benzoic acid **1b** regarding the amount of 1,3-butadiene, the ligand, the CO pressure and the temperature (Figure 19).

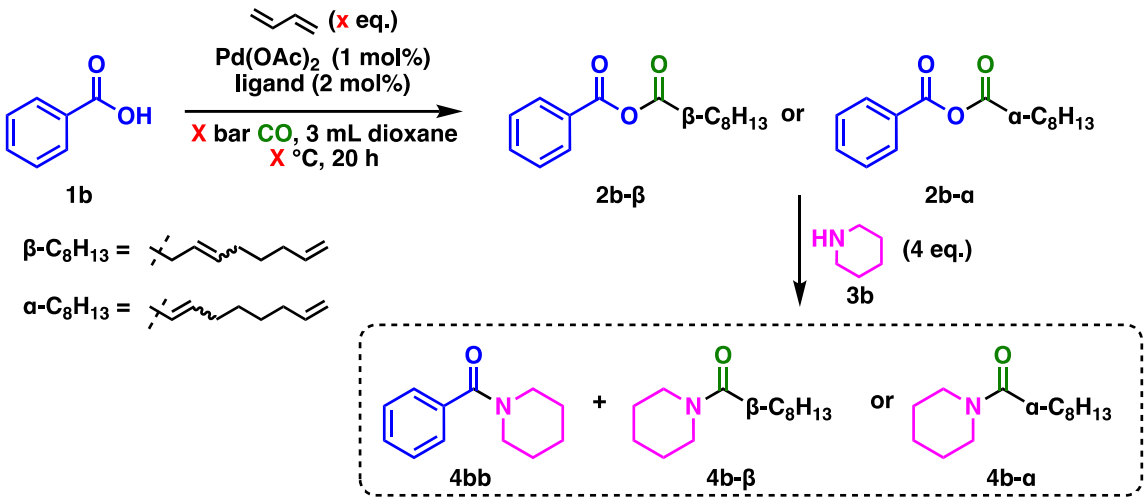

*Figure 19: Carbonylative telomerization of 1,3-butadiene with benzoic acid (**1b**) for the synthesis of mixed anhydrides **2b** prior to optimization and subsequent derivatization yielding amides for quantification.*

It is important to exclude other reaction pathways towards the analyzed amides, as this would lead to false quantification of the mixed anhydrides. We tested whether amides **4b** and **4bb** may be formed by direct reactions between the acid and the amine (Figure 20) to validate the chosen analysis method consisting of derivatization and quantification of the resulting amides. 3,8-Nonadienoic acid **1c** was included since it can be a by-product of the side reaction towards **4bb**.

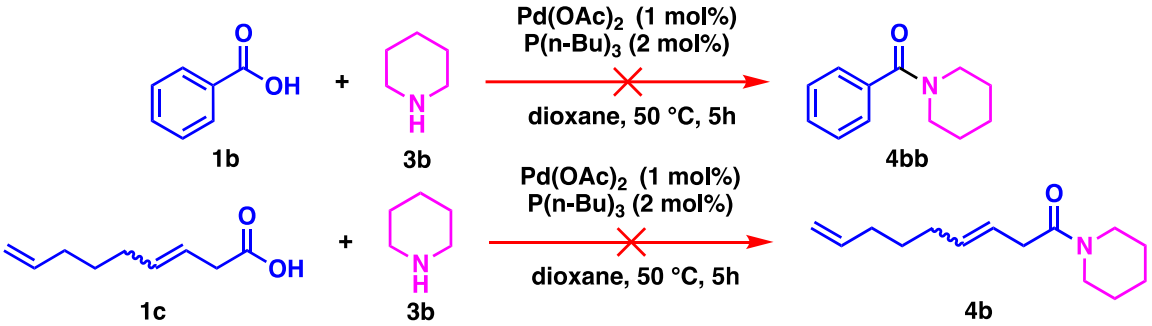

*Figure 20: Exclusion experiments with benzoic acid **1b** and 3,8-nonadienoic acid **1c**.*

In both cases, no amides were detected. Hence, all amides from the derivatization step result from the reaction of the mixed anhydride and the amine. Their combined yield can thus give precise information about the yield of the mixed anhydride formed *via* carbonylative telomerization.

4.5.2. How a "Design of Experiments" speeds up research and improves insight

The Design of Experiments (DoE) concept is a statistical approach that enables the reduction of experimental trials, associated time and costs while providing maximum information from collected data to enhance process insight. This approach adopts a systematic and objective investigation methodology to determine crucial parameters and interactive relationships based on statistical principles. By simultaneously varying all relevant factors and connecting the results with a mathematical model, the design space can be identified, interpreted, predicted, and optimized. DoE can be an efficient and powerful method to identify optimal system conditions.

However, the accuracy of numerical results obtained from DoE can be affected by various factors such as the algorithm, implementation method, software, and hardware used. Therefore, prior knowledge of the examined reaction system is crucial to avoid misinterpretation of the gained analysis data.

MODDE® is a widely used software that can be employed to design a statistical experimental setup to determine significant reaction parameters and predict optimal settings to maximize given parameters such as product yield and selectivity.

The most commonly used statistical experiment designs are the two-level factorial designs, where each experimental factor has two level of settings, namely the lower and upper levels. This design can be executed as a full factorial design or a fractional factorial design. The full factorial design requires 2^n runs, where n denotes the number of factors, and the number of runs increases exponentially for a growing number of factors. However, the fractional factorial design can significantly reduce the number of experiments to 2^{n-k}, where k represents the number of fractions specified by the full factorial design without compromising essential information. However, confounding effects in the fractional design can result in information loss and difficulty in attributing the effect to the main effect of one factor or the interaction of several factors. The Therefore, the prediction results must be validated with experiments to confirm their accuracy and should be carried out in duplicates to increase statistical relevance.

4.5.3. Optimization *via* DoE

Having an established protocol for quantifying carbonylative telomerization in hand (Figure 19), this set-up was used to optimize the reaction conditions *via* a Design of Experiments (DoE) towards an increased anhydride yield.

Previous investigations on carbonylative telomerization reactions have revealed significant parameters, such as temperature, CO pressure and the excess of 1,3-butadiene. These factors were varied in the ranges stated in Table 6, taking other research on these reactions into account. Additionally, the ligand plays a crucial role regarding reaction yield. KNIFTON has initially shown that basic monodentate phosphines resulted in good to excellent yields, and VOGELSANG *et al.* have shown the positive effects of large Tolman angles.[35] Therefore, P(*n*-Bu)$_3$, PPh_3 and PCy_2Ph were chosen for this investigation; all other parameters were kept constant (see Figure 19.)

Table 6: Factor settings for the DoE

Factor	Temperature [°C]	CO pressure [bar]	1,3-butadiene eq. [-]	Ligand (Tolman angle)
Minimum	80	20	4	P(*n*-Bu)$_3$ (132°)
Middle	100	30	6	PPh_3 (148°)
Maximum	120	40	9	PCy_2Ph (164°)
Optimized	93	20	7.9	PCy_2Ph (164°)

The sum of the detected amides after derivatization was considered the anhydride yield, hence the output for the DoE. A central composite face-centered design was chosen using the optimization software MODDE©, which resulted in a total of 27 experiments, each carried out as duplicates (see in experimental section). The data was evaluated, and the model had to be changed for better results to enhance the accuracy of the prediction. One option is the exclusion of insignificant parameters, which add more complexity to the system without adding more value for the analytics. The confidence plot reveals such data points (Figure 21).

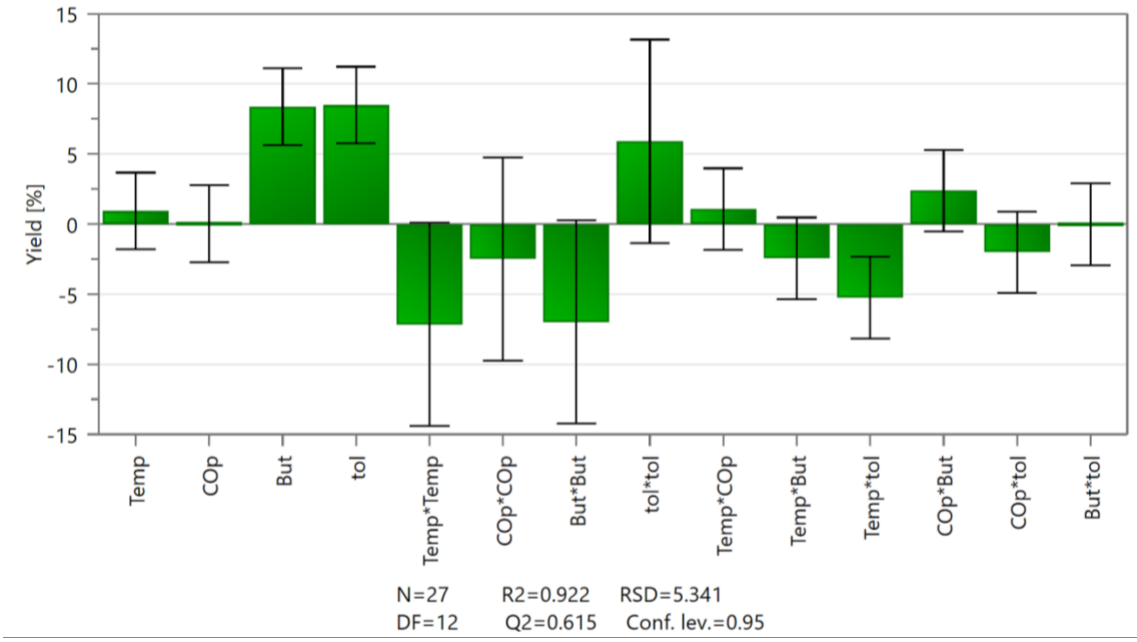

Figure 21: Coefficient plot (scaled and centered) Temp: temperature; COp: carbon monoxide pressure; But: equivalents of butadiene; tol: Tolman angle.(from Wernsdörfer 2019[59])

The green bars depict the influence, negative or positive, on the yield by the given parameter or a combination of two parameters. A tall positive or negative bar represents a higher impact and significant parameters additionally have an uncertainty mark not crossing the x-axis.

For "COp" (carbon monoxide pressure), and all cross-parameters resemble insignificant parameters. Hence, the CO pressure was excluded from the predictions and set to 20 bar for further optimization.

After the exclusion of the parameters containing the CO pressure the resulting confidence plot is more conclusive (Figure 22).

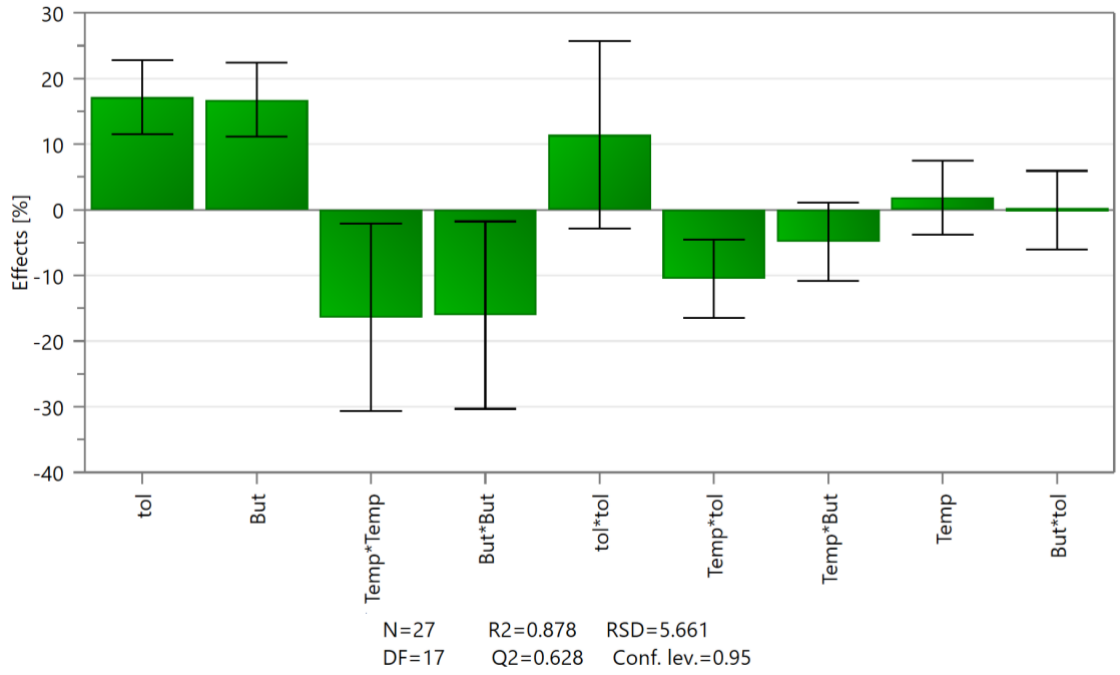

Figure 22: Effect plot after exclusion of non-significant model terms. Temp: temperature; But: equivalents of butadiene; tol: Tolman angle.(from Wernsdörfer 2019[59])

The results indicate a significant effect on the reaction by the ligand and the excess of butadiene, with an increase in the value of these factors leading to a positive effect on the response and consequently higher yields. This could be attributed to the importance of the catalyst complex suitable for the reaction. It can be hypothesized that with a larger Tolman angle, the coordination sites on the catalyst are mostly blocked due to the steric demands of the ligand. As a result, only small molecules such as carbon monoxide or 1,3-butadiene can coordinate to the free coordination sites at the catalyst center, which might lead to a faster release of the product.

Furthermore, two order effects and interactions were observed (Figure 22). The equivalents of 1,3-butadiene were found to have a negative two order effect on the anhydride yield. This implies that up to an optimal value, an excess of 1,3-butadiene has a positive effect on the anhydride yield, and after that point, a further increase in the equivalents of 1,3-butadiene leads to a decrease in the desired yield. The positive main effect of 1,3-butadiene excess is assumed to be necessary to ensure the coordination of two molecules at the catalyst center. A higher amount of 1,3-butadiene than the optimal value could result in more frequent formation of byproducts such as dimers or blocking of coordination sites at the catalyst.

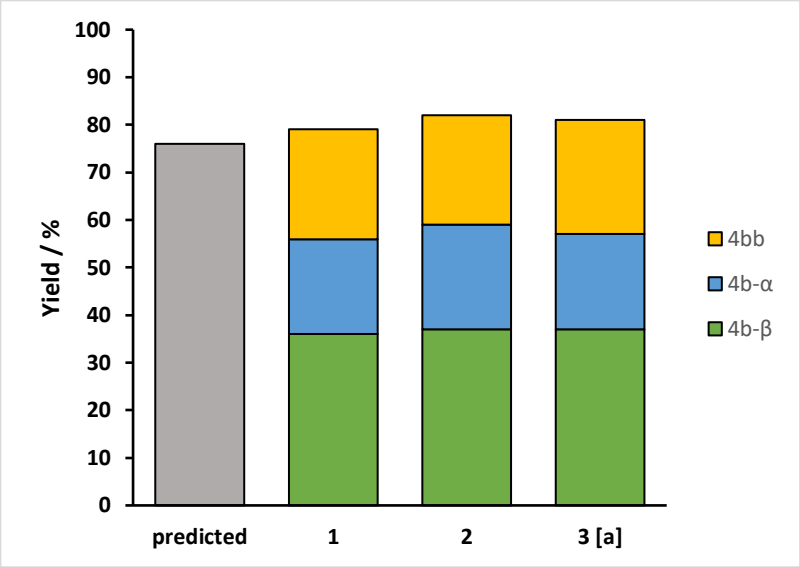

Figure 23: Anhydride yield under optimized conditions compared to predicted yield. Conditions: carbonylative telomerization: 3 mmol benzoic acid, 23.7 mmol (7.9 eq.) 1,3-butadiene, 1 mol% $Pd(OAc)_2$, 2 mol% PCy_2Ph, 3 mL dioxane, 20 bar CO, 93 °C, 20 h, 600 rpm. Internal standard 75 mg decane; Derivatization: 12 mmol piperidine, 50 °C, 5 h, 600 rpm. Yields (Y) were determined via GC-FID analysis using n-decane as an internal standard and calculated with respect to the carboxylic acid. ***α****: Isolated yield. (adapted from Wernsdörfer 2019*[59])

The calculations made by MODDE© applied to the resulting dataset suggested a reaction temperature of 93 °C, and excess of 7.9 eq. 1,3-butadiene and PCy_2Ph as the ligand for the optimized reaction conditions. The predicted yield was 76% of the anhydride. These results were verified by the corresponding experiments using the optimized reaction conditions, which resulted in good reproducibility since the duplicates show high similarity (Figure 23 , bars 1 and 2). The yield distribution of the derivatized products under optimized reaction conditions showed good reproducibility (Figure 23). The sum of amides, equals the yield for the desired mixed anhydride intermediates **2b**-β and **2b**-*α*, showing an average yield of the mixed anhydride of 80%, which is 4% higher than predicted. Moreover, the desired amides **4b**-β and **4b**-*α* account for over 70% of the total amide yield. Consequently, the mixed anhydride favors the transfer of the aliphatic acyl rest (i.e. 3,8-nonadienyl) to the amide yielding linear and branched C_9-amides. The optimization was carried out using calculated response factors using an established estimation method.[60] Afterwards, calculated yields were confirmed by isolation of the product amides (Figure 23, bar 3).

4.5.4. Implementation of optimized conditions

Afterwards, the optimized conditions were applied to a small scope investigation (Table 7). Since the electronic nature of benzoic acid derivatives is mainly influenced by substituents on the aromatic ring, different electron-withdrawing and donating groups were tested (Table 7). In this investigation, two effects must be considered. First, the nucleophilicity of the acid influences the reactivity in carbonylative telomerization. And second, the reactivity of the resulting anhydride is again influenced by the nature of the benzoic acid. An electron-deficient acid is an excellent leaving group. If the anhydride consists of two very different acid groups in pK_a, it becomes more reactive. The electron-rich acid is transferred preferentially in a consecutive reaction, as seen in Yamaguchi esterification.[52] Since the requirements for both reaction parts are opposing, a trade-off has to be found with high reactivity in carbonylative telomerization and satisfactory selectivity of the consecutive reaction.

Table 7: Yield distribution for different substituted acids

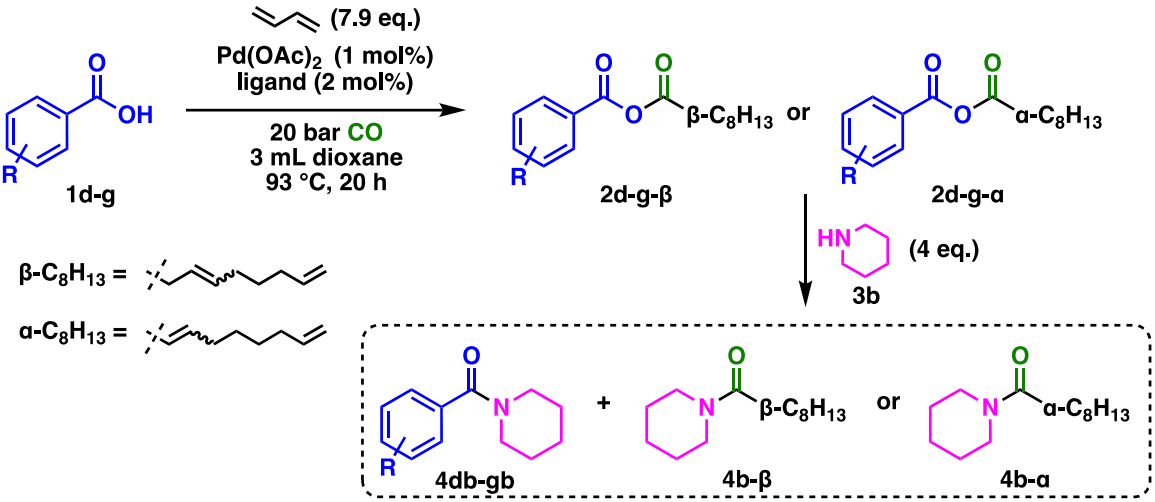

Entry	R (acid)	pK_a[6061]	∑ Yield [%]	Y(4b-*β*) [%]	Y(4b-*α*) [%]	Y(4db-gb) [%]
1	***m*-Me (1d)**	4.28	85	39	22	24
2	***p*-OMe (1e)**	4.49	91	40	26	25
3	***p*-OMe[a] (1e)**	4.49	71	36	17	18
4	***p*-Cl (1f)**	3.98	74	36	37	traces[b]
5	***p*-NO_2 (1g)**	3.42	-	traces[b]	traces[b]	-

Conditions: carbonylative telomerization: 3 mmol acid, 24 mmol 1,3-butadiene, 1 mol% $Pd(OAc)_2$, 2 mol% PCy_2Ph, 3 mL dioxane, 20 bar CO, 93 °C, 20 h, 600 rpm. Internal standard 75 mg decane. a: 0.5 mol% $Pd(OAc)_2$, 1 mol% PCy_2Ph; Derivatization: 12 mmol piperidine, 50 °C, 5 h, 600 rpm. Isolated yield (Y) related to acid. b: not isolated

The highest yield of 91% can be achieved using anisic acid **1e**. Due to the +-M-effect, anisic acid is electron-rich acid and therefore has a higher pK_a value. More electron-rich acids appear to be more reactive in carbonylative telomerization, showing higher overall anhydride yield. The anhydride yield is reduced with a lower pK_a value. In contrast, the selectivity of **4b** increases with a lower pK_a value. As mentioned before, electron-poor acids are better leaving groups and are more stable in their anionic form. All tested acids have a lower pK_a value than 3,8-nonadienoic acid **1c**, which should be similar to nonanoic acid, *i.e.* 4.96.[61] Hence, the 3,8-nonadienoic rest is

preferably transferred to the nucleophile. This effect increases with larger differences in pK_a values and results in higher selectivity with a lower pK_a. For **1f,** it was impossible to isolate the arylamide **4fb**, resulting in the highest selectivity for **4b**. Although the overall activity of **1f** is lower compared to the more electron rich acids, the selectivity towards the unsaturated C9-amides is high. This offers a way to selective pass the newly formed unsaturated C9-chain along to the consecutive product (Table 7, entry 4), since *p*-Cl-benzoate is the better leaving group. In comparison with the anhydride **2e** a selectivity of only 72% was achieved in the amidation reaction. For **1g,** only traces of the products could be observed, indicating low activity in carbonylative telomerization. These results can be explained with the lower nucleophilicity of electron poor carboxylic acids. MAYR *et al.* reported a nucleophilicity scale, showing *p*-nitro benzoate to be significant less nucleophilic than the benzoate ion.[62] The lower nucleophilicity renders the acid les reactive for the carbonylative telomerization, thus forming less of the corresponding anhydride. This shows a compromise has to be found, between a high reactivity in carbonylative telomerization resulting from electron rich carboxylic acids and an ideal anhydride for consecutive reaction built with electron poor carboxylic acids.[52] Additionally, the electronic properties of the acid have an influence on the formation of the *α*-unsaturated isomer **4b**-*α* and **2d-g-4b**-*α*, respectively. More electron-withdrawing groups in *para*-position of the acid result in a higher degree of isomerization and result in equal amounts of **4b**-*α* and **4b**-β (Table 7, Entry 4), which is in contrast to more electron-rich acids, which result in 2:1 ratio of **4b**-*α* and **4b**-β. This aligns with the results found by SAUTHIER *et al.* for the carbonylative telomerization of phenols in the presence of catalytic amounts of benzoic acid.[36] This effect could also be emphasized, by the higher acidity of the *p*-Cl substituted benzoic acid, which could also lead to more Pd–H species forming and thus more isomerization.

4.5.5. Proposed reaction mechanism

The best results in the carbonylative telomerization with carboxylic acids were achieved with the bulky, basic phosphine PCy_2Ph. Such donor ligands are reported to push the equilibrium of the η^3-allyl into a σ-allyl complex (**B**)[63] and an insertion of CO is preferred in this position, thus the carbonyl Pd complex **C** is formed, analogous to the proposed mechanism by KNIFTON (Figure 24).

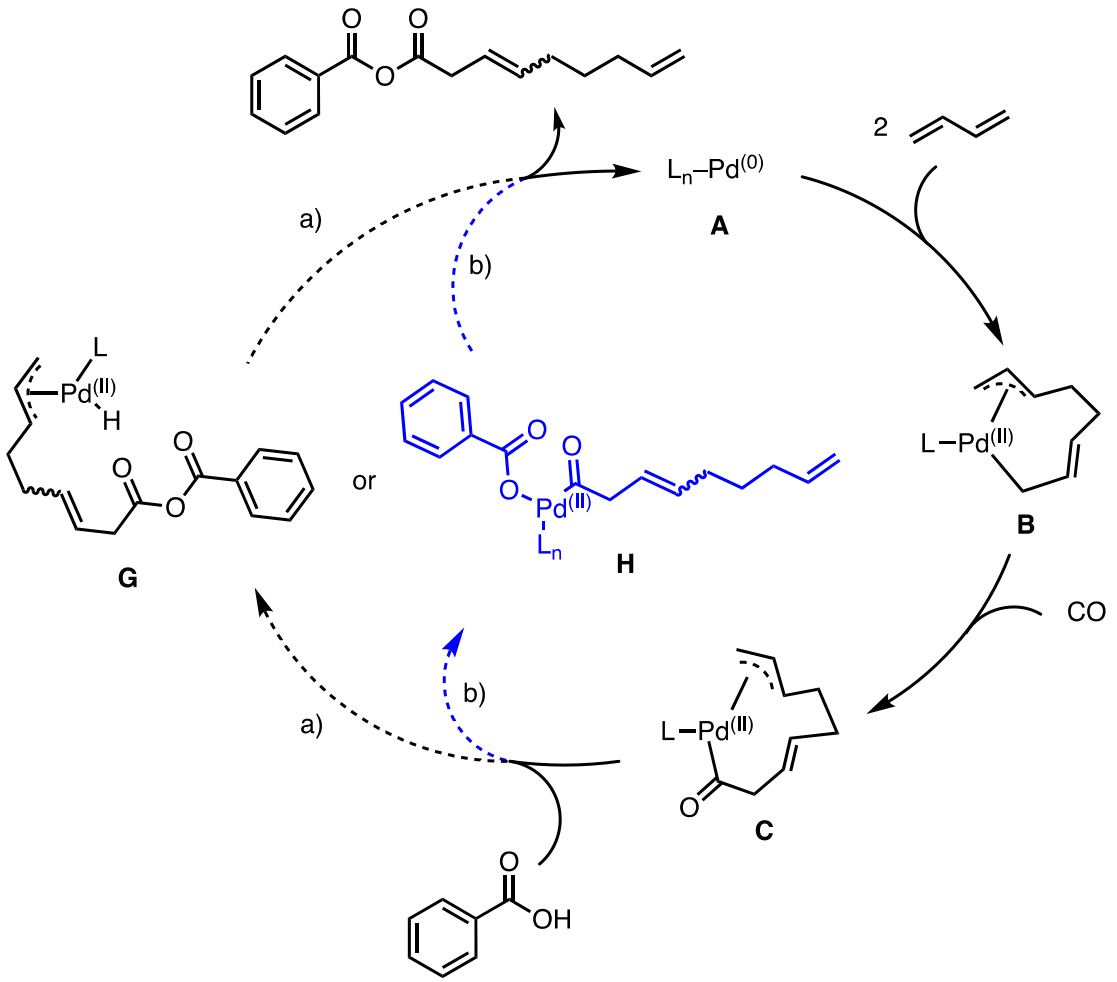

Figure 24: Possible reaction mechanisms for carbonylative telomerization of 1,3-butadiene with benzoic acid.

Two pathways for the interaction of the carboxylic acid are feasible pathways. On the one hand, the reaction continues the mechanism proposed by KNIFTON and forms a Pd–H while the carboxylate inserts in the Pd carbonyl bond (Figure 24, path a))[35], resulting in complex **G**. A reductive elimination of the allyl and the hydride forms the product and closes the catalytic cycle by releasing **A**. On the other hand, the acid could first protonate the remaining Pd-allyl and the resulting carboxylate could coordinate to the complex replacing the former allyl (Figure 24, path b)). Again, a reductive elimination of the product forms the desired anhydride product and **A**. Both proposed pathways would proceed without a cationic catalyst species, since the insertion of CO into the σ-allyl-Pd bond is more likely compared to the migratory-insertion into a η^3-allyl-Pd bond.

4.5.6. Conclusions and outlook

A novel, palladium-catalyzed synthesis for mixed carboxylic acid anhydrides was developed. For the first time, generating mixed anhydrides catalytically from bulk chemicals, namely 1,3-butadiene, CO, and benzoic acid derivatives was possible. In addition, a quantification protocol was developed using amines for quantitative derivatization in combination with standard GC analysis. It was possible to optimize the conditions for the anhydride synthesis using this protocol, and yields up to 82 % were achieved.

A small investigation of the scope of the reaction was carried out, including different benzoic acid derivatives. The experiments have shown the importance of the nature of the acid, as more electron-rich benzoic acid derivatives achieved higher total yields of up to 94 % due to their higher nucleophilicity. In contrast, *p*-Cl-benzoic acid, which is less electron-rich, resulted in only a 74 %

yield in carbonylative telomerization. Still, the consecutive amidation was highly selective due to the better leaving group *p*-Cl-benzoate. Further investigations of the scope, including different dienes and other applications of the resulting anhydrides, are currently in progress. Additionally, the mechanism must be studied in more detail, as the currently accepted proposed mechanism must be updated for carboxylic acid conversion.

Regarding the scope, a variation of the diene component of carbonylative telomerization would be of interest. As presented in chapter 2.3, highly branched products would be possible with β-myrcene. Less complicated, methyl-branched products could be achieved using isoprene or piperylene. Since mixed anhydrides cannot be readily stored, a direct conversion is necessary in many cases. The presented amidation yields the starting carboxylic acid as a byproduct, and a sub-stoichiometric reaction could be possible with the right conditions. The latter is investigated in the following chapter.

4.5.7. Experimental

General

Solvents and Chemicals: All Solvents and chemicals were purchased from ABCR, Acros Organics, TCI, Sigma Aldrich, VWR or UMICORE. Dioxane was dried over 3 Å molecular sieve for at least 24 h and distilled before use. All precursors and ligands were stored in Schlenk flasks under an argon atmosphere.

Autoclaves: The catalytic experiments were performed in 25 mL stainless steel autoclaves (Figure 25). The autoclaves were equipped with a quick-fit adapter for a simple and safe connection to the pressure station.

Figure 25: 25 mL autoclave for high-pressure catalytic experiments.

Carbonylative telomerization (DoE): First, the acid (nucleophile) was weighed into the 25 mL stainless steel vessel of the autoclave containing a stirring bar. The reactor was closed and then evacuated and purged with argon. $Pd(OAc)_2$ (6.74 mg, 0.03 mmol, 1 mol%) and PCy_2Ph (17.3 mg, 0.06 mmol, 2 mol%) were weighed in a 20 mL headspace vial. The vial was sealed with a crimp cap, then alternately evacuated and purged with argon using a needle connected to the Schlenk-line. 3 mL of dioxane and the internal standard *n*-decane (75 mg, 0.527 mmol) were added *via* syringe through the septum of the crimp cap. The mixture was placed in an ultrasonic bath until a homogeneous solution was observed and then transferred to the reactor *via* syringe under argon

counter flow. Liquid 1,3-butadiene was added to the reactor from the cylinder *via* a pressure resistant and transparent pipe. The exact amount was determined by differential weighing. The reactor was pressurized with carbon monoxide to the desired temperature and placed in a pre-heated heating block, magnetically stirred for 20 h.

Derivatization: After 20 h, the reactor was cooled using a water/ice bath, carefully depressurized and purged with argon. Piperidine (1032 mg, 12 mmol, 4 eq.) was added to the reaction mixture *via* syringe under argon counter flow. The solution was stirred for another 5 h at 50 °C in a heating block. Finally, the autoclave was cooled again and an aliquot was taken for GC-FID analysis.

Carbonylative telomerization (isolated yield amides): The reaction was performed as described above without the addition of the internal standard. After completion of the derivatization step, the reaction mixture was concentrated in reduced pressure and dissolved in 10 mL dichloromethane (DCM). This solution was extracted with 15 mL of aqueous sulfuric acid solution (5 wt%). The aqueous phase was extracted two more times with 10 mL DCM. Afterwards, the organic phases were combined and extracted with a 0.1 M NaOH (3x 20 mL) solution. The organic phase was dried with $MgSO_4$ and concentrated under reduced pressure. The residue was adsorbed to celite and further purified by column chromatography using a 40 g silica gel cartridge (ethyl acetate: cyclohexane, 1 % to 10 % in 2 CV, 10 % until eluted).

Carbonylative telomerization (isolated yield anhydrides): The reaction was carried out as described above without the addition of an internal standard and no amine was added for derivatization. The reaction solution was concentrated under reduced pressure. The crude product was then purified by "Dry Column Vacuum Chromatography" using a gradient of 1% to 10 % of dry ethyl acetate in dry cyclohexane.[64]

Synthesis of 3,8-Nonadienoic acid 1c: First methyl 3,8-nonadienoate was synthesized as previously reported.[65] Then 30 mL of a 1 M NaOH solution were added to a flask equipped with a Teflon-coated stirring bar. To the solution methyl 3,8-nonadienoate (2.00 g, 11.9 mmol) was added. The mixture was heated to 90 °C and stirred for 3 h. During the reaction the turbid reaction mixture turned clear, and no phase separation could be observed. The mixture was neutralized with a 5 wt% H_2SO_4. Afterwards the aqueous phase was extracted with diethyl ether (3 x 20 mL). Removing the solvent under reduced pressure yielded 3,8-Nonadienoic acid (1.76 g, 96 %) as a light-yellow liquid.

Exclusion of alternative pathways: 3,8-nonadienoic acid (467 mg, 3 mmol, 1 eq.) was weighed into a 25 mL stainless steel reactor containing a stirring bar. The reactor was closed, then evacuated and purged with argon. The palladium precursor $Pd(OAc)_2$ (6.74 mg, 0.03 mmol, 1 mol%) and PCy_2Ph (17.3 mg, 0.06 mmol, 2 mol%) were weighed into a 20 mL headspace vial and sealed with a crimp cap. The vial was then alternately evacuated and purged with argon. The corresponding amount of dioxane (3 mL) was added to the vial via syringe. The mixture was placed in an ultrasonic bath until a homogeneous solution was obtained and then transferred to the reactor *via* syringe under argon counter flow. Piperidine (1032 mg, 3 mmol, 4 eq.) and 75 mg of the internal standard *n*-decane were also added to the reactor *via* syringe and argon counter flow. The reactor was stirred for 5 h at 50 °C. Afterwards the reaction was stopped by a water/ice bath and the reaction mixture analyzed *via* GC.

Optimization of Anhydride Formation via DoE

The reaction parameters and results are displayed below (Table 8), and the experiments were carried out as stated above. The yield is an average value resulting from two separate runs.

Table 8: Series of performed experiments for the DoE.

Entry	Temperature [°C]	CO pressure [bar]	1,3-Butadiene eq. [-]	TOLMAN angle [°]	Yield [%]
1	80	40	9	163.5	71
2	100	30	6.5	163.5	77
3	120	20	4	163.5	50
4	120	20	4	132	41
5	80	30	6.5	147.75	62
6	100	30	6.5	147.75	57
7	80	20	4	132	20
8	80	20	4	163.5	56
9	80	40	9	132	45
10	120	40	4	163.5	45
11	100	30	6.5	147.75	60
12	120	40	9	132	59
13	80	40	4	132	23
14	120	40	9	163.5	61
15	80	20	9	163.5	69
16	100	30	6.5	132	55
17	100	30	4	147.75	43
18	120	40	4	132	41
19	80	40	4	163.5	41
20	100	20	6.5	147.75	59
21	120	20	9	163.5	57
22	80	20	9	132	40
23	120	20	9	132	48
24	100	30	6.5	147.75	57
25	120	30	6.5	147.75	42
26	100	30	9	147.75	62
27	100	40	6.5	147.75	55

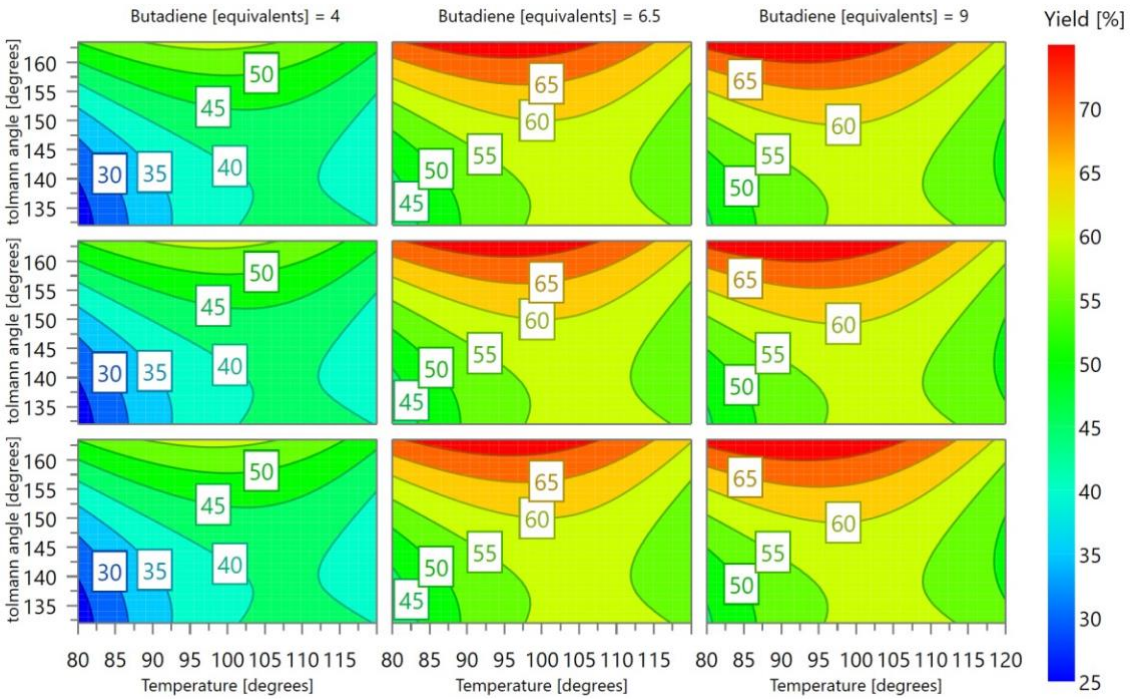

Figure 26: Visualization of the DoE results in contour plot.

4.5.8. Analytics

NMR-Spectroscopy: ^{1}H- and ^{13}C-NMR-spectra were recorded using Bruker Avance III HD NanoBay – 400 MHz, Bruker Avance NEO – 500 MHz or Bruker Avance III HD – 600 MHz spectrometers at ambient temperature with the frequency and solvent noted. Chemical shifts δ are given in ppm relative to tetramethylsilane (0 ppm) and were referenced to residual solvent signals (^{1}H: $CDCl_3$ 7.26 ppm, ^{13}C: $CDCl_3$ 77.16 ppm).

Gas chromatography (GC): Conversion and yield of the reactions were determined *via* GC on an Agilent Technologies INC. chromatograph of the type 7890B with a flame ionization detector (FID). A HP-5 column was used (30 m long, 0.32 mm diameter, 0.25 µm thickness of the layer, 5 min at 50 °C, heating rate 15 °C/min to 290 °C, heating rate 40 °C/min to 320 °C, holding for 10 min). The split was set to 1:75. *n*-Dodecane was chosen as internal standard and response factors of the substrates and products were obtained experimentally by analyzing known quantities of the substances (calibration) or were calculated form literature known methods.[60]

Mass Spectrometry (MS): Qualitative mass analysis was performed *via* GC. A HP-5MS UI (30 m long, 0.25 mm diameter, 0.25 µm thickness of the layer) column was used. The carrier gas was Helium, and the detector was of the Type 5977A MSD of Agilent Technologies INC.

High Resolution Mass Spectrometry (HR-MS): Samples for HRMS were diluted with acetonitrile or methanol to a concentration of 100 µg/mL and measured with an LTQ-Orbitrap (Thermo Scientific).

IR Spectroscopy: All IR-Spectra were acquired using a Bruker Alpha FT-IR with Diamond-ATR.

Flash Chromatography: For isolation of individual substances, a Büchi Flash Pure C-815 was used with cyclohexane and ethyl acetate as eluents. Cartridge size and solvent gradient were used as stated.

GC-MS determination of 3,8-nonadienoic acetic anhydride 2a

Carbonylative telomerization of acetic acid yields 3,8-nonadienoic acetic anhydride **2a**. Figure 27 shows an example chromatogram of the reaction and below it shows the mass-spectrum of the chromatographic peak.

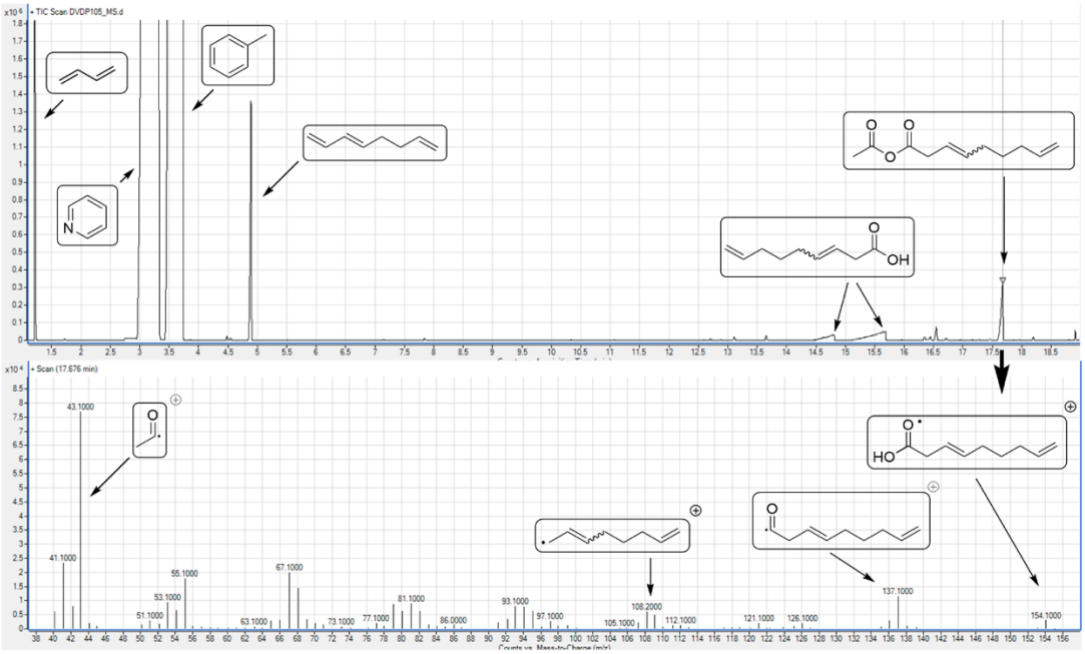

Figure 27: Exemplary chromatogram of the carbonylative telomerization of acetic acid.

The molecule-ion of the anhydride could not be observed, however the mass-spectrum contains a large signal at a m/z of 43.1 which can be assigned to the acetyl-cation resulting from the cleavage of the one of the anhydride bonds. The anhydride can also be cleaved at the opposite side of the anhydride oxygen and yield the 3,8-nonadienal ion with a corresponding m/z value of 137.1. These signals strongly indicate the presence of 3,8-nonadienoic acetic anhydride **2a** as they include the main fragments of the compound, and the chromatographic peak elutes later compared to the single parts.

2,8-Nonadienoic benzoic anhydride (2b)

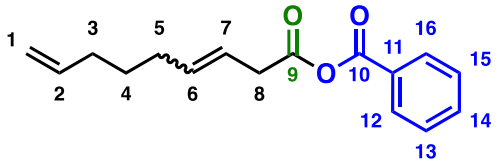

^{1}H NMR (400 MHz, $CDCl_3$): δ = 8.20 – 8.05 (12/16, m, 2H), 7.71 – 7.60 (14, m, 1H), 7.52 (13/15, m, 2H), 7.25 – 6.99 (7, m, 1H), 6.08 – 5.95 (8, m, 1H), 5.85 – 5.74 (2, m, 2H), 5.05 – 4.94 (1, m, 2H), 2.38 – 2.21 (6, m, 2H), 2.14 – 1.99 (3m, 2H), 1.57 – 1.40 (4/5, m, 4H) ppm.

^{13}C {^{1}H} NMR (101 MHz, $CDCl_3$): δ = 162.48 (9, q), 161.98 (10, q), 154.72 (7, t), 138.46 (2, t), 134.67 (14, t), 134.44 (11, q), 130.71 (12/16, t), 129.01 (13/15, t), 120.66(8, t), 114.96 (1, s), 33.34 (3, s), 32.58 (6, s), 28.52 (4, s), 28.48 (5, s) ppm.

FTIR: ν = 2928 (C-H, alkane stretch), 1787 (C=O, anhydride stretch), 1728 (C=O, conjugated anhydride stretch), 1641 (C=C, disubstituted (cis) or mono substituted alkene stretch), 1452 (C-H, bending), 1038 (OC-O-CO, anhydride stretch), 993 (C=C, mono substituted alkene bend), 909 (C=C, mono substituted alkene bend), 704 (C=C, disubstituted(cis) alkene bend) cm^{-1}.

LR-MS: m/z (%) = 153(1), 138(1), 137(13), 119(1), 109(6), 108(4), 106(8), 105(100), 95(6), 81(6), 77(23).

2,8-Nonadienoic 4-methoxybenzoic anhydride (2e)

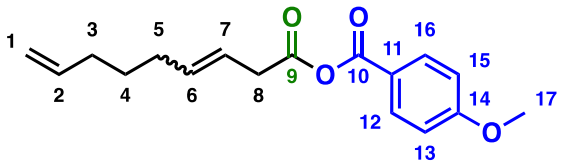

^{1}H NMR (400 MHz, $CDCl_3$): $\boldsymbol{\delta}$ = 8.15 – 7.92 (12/16, m, 2H), 7.23 – 7.04 (7, m, 1H), 6.99 – 6.89 (13/15, m, 2H), 6.00 – 5.83 (8, m, 1H), 5.83 – 5.72 (2, m, 1H), 5.03 – 4.97 (1, m, 1H), 4.97 – 4.92 (1, m, 1H), 3.91 – 3.82 (17, m, 3H), 2.33 – 2.21 (6, m, 2H), 2.10 – 2.02 (3 ,m, 2H), 1.54 – 1.39 (4/5, m, 4H) ppm.

^{13}C {^{1}H} NMR (101 MHz, $CDCl_3$): $\boldsymbol{\delta}$ = 164.59 (9, q), 162.26 (14, q) 162.19 (10, q), 154.18 (7, t), 138.39(2, t), 132.79 (12/16, t), 121.13 (11, q), 120.70 (8, t), 114.84 (1, s), 114.11 (13/15, t), 55.62 (17, p), 33.45 (3, s), 32.43 (6, s), 28.38 (4, s), 27.23 (5, s) ppm.

LR-MS: m/z (%) = 288(1), 244(1), 214(1), 187(1), 152(6), 136(10), 135(100), 119(1), 109(2), 108(1), 107(7), 95(3), 93(3), 92(12), 81(4), 77(12), 74(1).

1-(Piperidin-1-yl) nona-3,8-dien-1-one (4b)

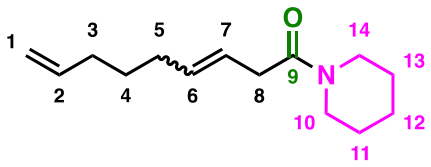

^{1}H NMR (400 MHz, $CDCl_3$): δ = 5.85 – 5.70 (2, m, 1H), 5.60 – 5.44 (6/7, m, 2H), 5.06 – 4.87 (1, m, 2H), 3.59 – 3.46 (10, m, 2H), 3.46 – 3.29 (14, m, 2H), 3.07 (8, d, J = 4.8 Hz, 2H), 2.09 – 1.98 (3/5, m, 4H), 1.65 – 1.57 (4, m, 2H), 1.57 – 1.49 (m, 4H), 1.49 – 1.40 (m, 2H) ppm.

^{13}C {^{1}H} NMR (101 MHz, $CDCl_3$): δ = 169.90 (9, q), 138.79 (2, t), 133.47 (7, t), 123.41 (6, t), 114.63 (1, s), 47.01 (10, s), 42.81 (14, s), 38.03 (8, s), 33.31 (5, s), 32.07 (3, s), 28.57(4, s), 26.59 (10/14, s), 25.65 (11/13, s), 24.62 (12, s) ppm

HR-MS (APCI): calcd. $[M+H]^+$ = 222.1852, found $[M+H]^+$ = 222.18546.

Degree of isomerization: The degree of isomerization was determined via NMR. Both isomers were isolated in the same fraction and the degree of isomerization was determined via integration of specific signals as the example shows (Figure 28, marked with *). In this example the molar ratio of the isomers 4b-β:4b-α = 2.68.

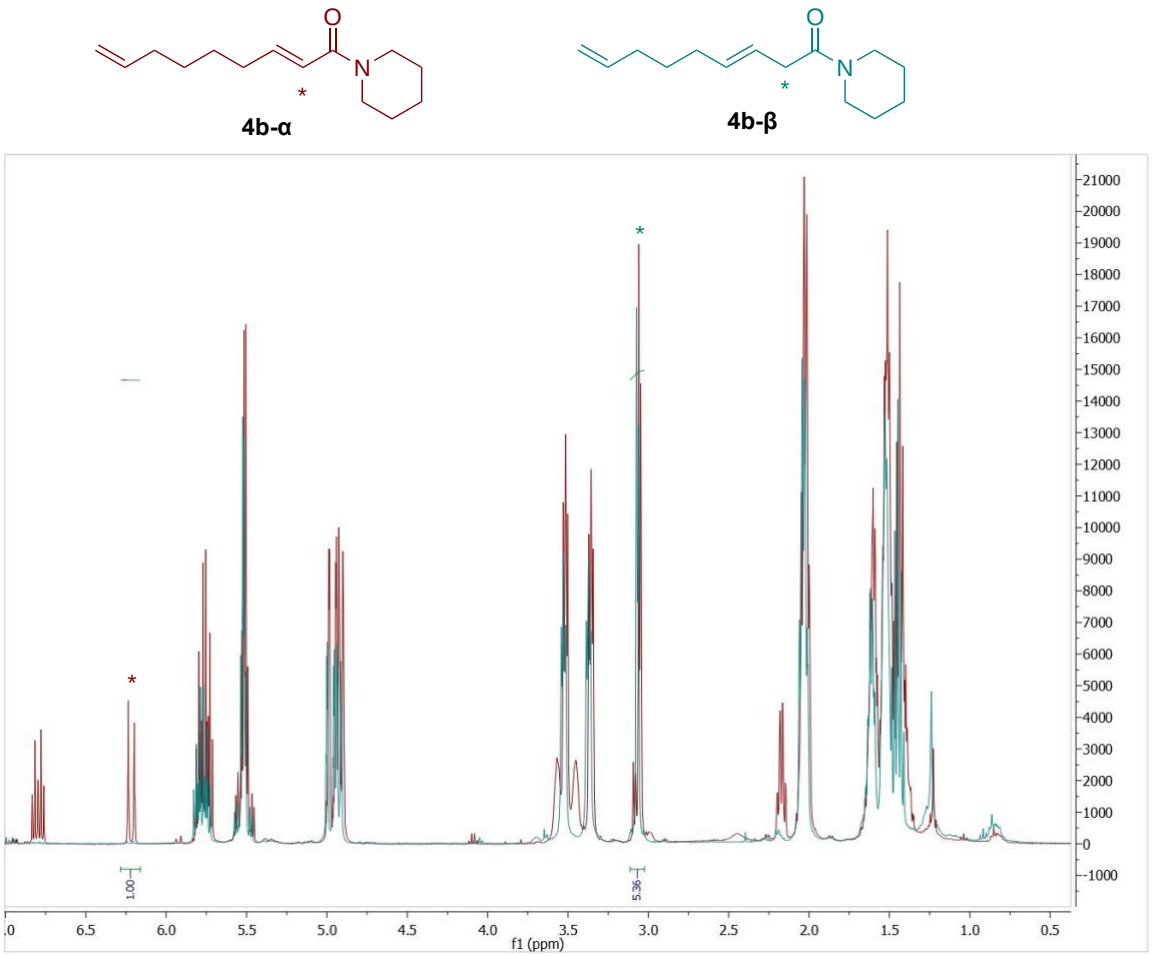

Figure 28: Determination of isomerization via NMR. (Red: ^{1}H (400MHz, $CDCl_3$) Spectrum of a mixture of isomers **4b** and **4'b**; teal: ^{1}H (400MHz, $CDCl_3$) Spectrum of **4b** for comparison.

Di-*n*-butylnona-3,8-dienamide (3d)

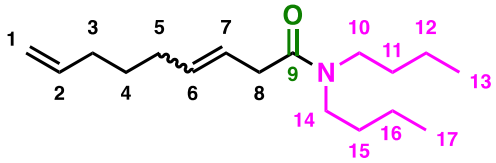

^{1}H NMR (500 MHz, $CDCl_3$): δ = 5.81 – 5.72 (2, m, 1H), 5.62 – 5.44 (6/7, m, 2H), 5.01 – 4.94 (1, m, 1H), 4.94 – 4.90 (1, m, 1H), 3.32 – 3.24 (10, m, 2H), 3.22 – 3.15 (14, m, 2H), 3.10 – 3.01 (8, m, 2H), 2.07 – 1.96 (3/5, m, 4H), 1.57 – 1.39 (4/10/14, m, 6H), 1.35 – 1.22 (12/16, m, 4H), 0.97 – 0.85 (13/17, m, 6H).

^{13}C {^{1}H} NMR (126 MHz, $CDCl_3$): δ = 171.23 (9, q), 138.80 (2, t), 133.27 (7, t), 123.78 (6, t), 114.58 (1, s), 47.91 (10, s), 45.73 (14, s), 37.70 (8, s), 33.29 (5, s), 32.03 (3, s), 31.30 (10/14, s), 29.92 (11/15, s), 28.51 (4, s), 20.34 (12, s), 20.20 (16, s), 13.99 (13, p), 13.94 (17, p) ppm.

LR-MS m/z (%): 265 (35), 224 (22), 210 (15), 182 (23), 156 (95), 137 (2), 128 (30), 109 (7), 86 (100)

3,8-Nonadienoic acid (1c)

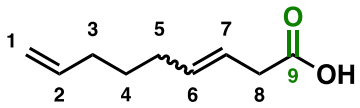

^{1}H NMR (600 MHz, $CDCl_3$): δ = 10.78 (OH, s, 1H), 5.84 – 5.72 (m, 1H), 5.63 – 5.47 (m, 2H), 5.03 – 4.97 (m, 1H), 4.96 – 4.91 (m, 1H), 3.09 (m, 2H), 2.10 – 2.01 (m, 4H), 1.52 – 1.42 (m, 2H).
^{13}C {^{1}H} NMR (151 MHz, $CDCl_3$): δ = 178.75 (9, q), 138.72 (2, t), 135.15 (7, t), 121.3 (6, t), 114.88 (1, s), 38 (8, s), 33.3 (5, s), 31.96 (3, s), 28.52 (4, s) ppm.
HR-MS (ESI): calcd. $[M+H]^+$ = 155.1072, found $[M+H]^+$ = 155.1067.
LR-MS m/z (%): 154 (1), 137 (3), 136 (21), 126 (4), 125 (6), 118 (6), 113 (16), 112 (100), 109 (9), 108 (36).

N-benzoyl-piperidine (4bb)

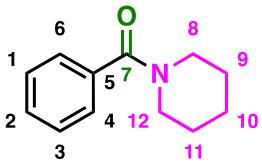

^{1}H NMR (400 MHz, $CDCl_3$): δ = 7.38 (1/2/3/4/6, s, 5H), 3.70 (8, br s, 2H), 3.33 (12, bs s, 2H), 1.67 (9/11, br s, 4H), 1.51 (10, br s, 3H)
^{13}C {^{1}H} NMR (101 MHz, $CDCl_3$): δ = 170.44 (7), 136.61 (5), 129.45 (2), 128.50 (4/6), 126.89 (1/3), 48.86 (8), 43.25 (12), 26.62 (9), 25.68 (11), 24.70 (10).
HR-MS (APCI): calcd. $[M+H]^+$ = 190.1226, found $[M+H]^+$ = 190.12279.

N-*3*-methylbenzoly-piperidine (4db)

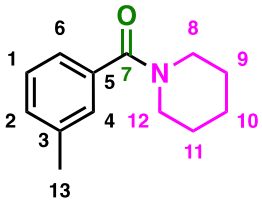

Was isolated as a mixture with **4b.**
^{1}H NMR (600 MHz, $CDCl_3$): δ = 7.27 – 7.23 (m, 1H), 7.19 – 7.17 (m, 2H), 7.15 – 7.12 (m, 1H), 3.68 (br s, 2H), 3.32 (br s, 2H), 2.35 (s, 3H), 1.69 – 1.64 (m, overlapping with **4b**), 1.64 – 1.59 (m, overlapping with **4b**) ppm.
^{13}C {^{1}H} NMR (151 MHz, $CDCl_3$): δ = 170.64 (7, q), 138.34 (3, q), 136.47 (5, q), 130.14 (2, t), 128.28 (1, t), 127.48 (4, t), 123.75(6, t), 48.85 (12, s), 43.20 (8, s), 26.63 (11, s), 25.70 (9, s), 24.70 (10, s), 21.45 (13, p) ppm.
HR-MS (APCI): calcd. $[M+H]^+$ = 204.1383, found $[M+H]^+$ = 204.13847.

N-*p*-methoxybenzoyl-piperidine (4eb)

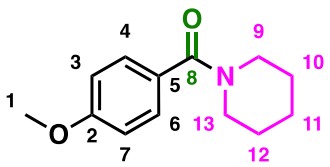

^{1}H NMR (600 MHz, $CDCl_3$): δ = 7.35 (4/6, d, *J* = 8.8 Hz, 2H), 6.88 (3/7, d, *J* = 8.8 Hz, 2H), 3.80 (1, s, 3H), 3.53 (9/13s, 4H), 1.65 (11, d, *J* = 4.2 Hz, 2H), 1.57 (10/12, s, 4H).

$^{13}C\{^{1}H\}$ NMR (151 MHz, $CDCl_3$): δ = 170.44 (8), 160.61 (2), 128.92 (4/6), 128.21 (5), 113.66 (3/7), 55.33 (9/13), 48.94 (9, broad), 43.72 (13, broad), 26.17 (10/12), 24.60 (11, broad).

HR-MS (APCI): calcd. $[M+H]^+$ = 220.1332, found $[M+H]^+$ = 220.13340.

Broad signals were received for the ^{1}H and ^{13}C signals of the piperidinyl ring due to rotation of the amide bond, which aligns with other literature reports of the compound.[66]

4.6. Acid as a co-catalyst – Anhydrides as the key?

The anhydrides from carbonylative telomerization of acids can be combined with a broad spectrum of nucleophiles such as amines and alcohols, which makes this reaction an interesting synthetic tool unsaturated ester and amide production. However, a drawback of this reaction is the lower overall atom economy compared with direct carboxytelomerization or amidotelomerization respectively. The atom economy (AE) first mentioned by TROST, describes the mass of desired product per the total amount of products of a reaction.[67]

$$AE = \frac{molecular\ weight\ desired\ product}{molecular\ weight\ of all\ products} \bullet\ 100\ \% \qquad (2)$$

To reach high AE values, a high selectivity is key, but the use of quantitative reactants has to be avoided as well. High AE values are characteristic for green reactions with a reduced negative impact on the environment, since less waste is produced by the reaction. Additionally, a high AE usually is also positive for the profitability of the resulting process, as a high AE also results in an easier up stream process and less waste treatment necessary.

Homogenous catalyzed reactions are among the highest AE values up to perfect atom economy. Carboxytelomerization of methanol (Figure 29) is such an example where no side or coupled products are formed.

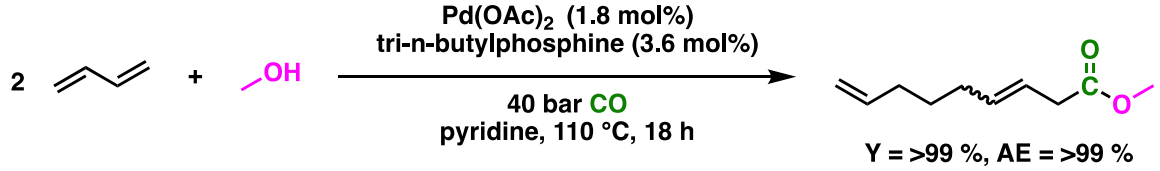

Figure 29: Carboxytelomerization of methanol with butadiene.[40]

The reaction is remarkably atom economic since all atoms from the substrate are rearranged to form the product without any side reactions. Therefore, the AE is >99% for this reaction and emphasizes the importance of using catalysis for a more efficient reaction (Figure 29).

In contrast, the use of stoichiometric reagents in nucleophilic substitution reactions results in an inherently lower AE, due to equimolar side products being formed.

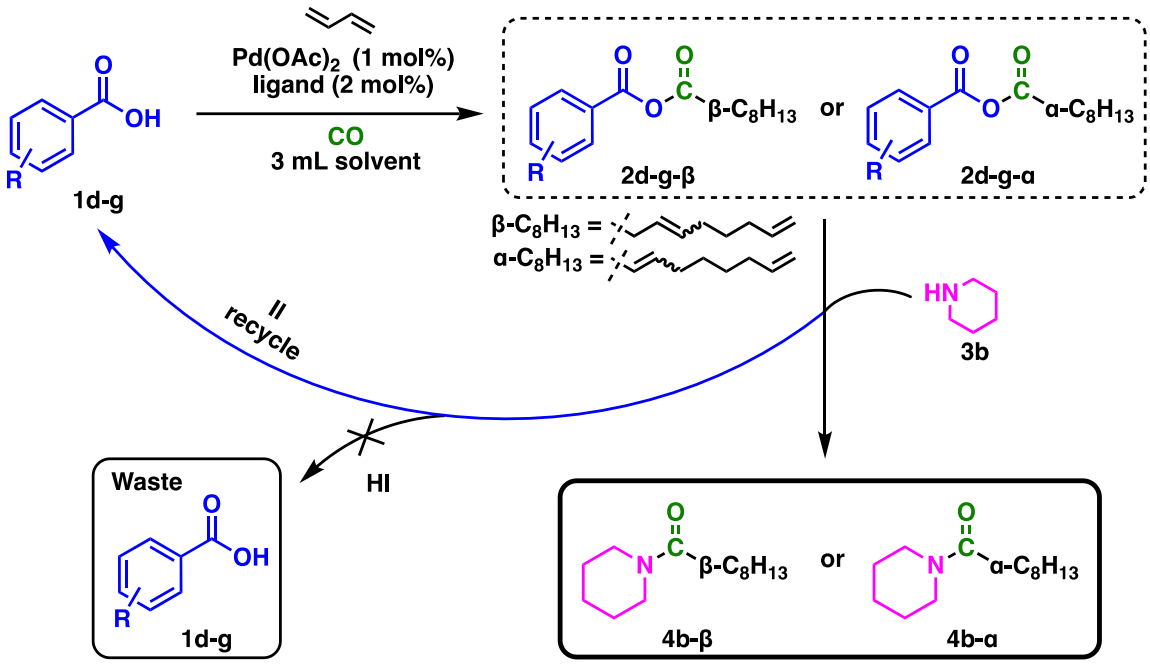

Figure 30: Comparison of the current reaction setup (I) with the new approach (II).

The AE of the reaction is 66 % using benzoic acid and 59 % for anisic acid, which is significant lower due to the waste formed in the second step of the reaction. However, the acid released in the nucleophilic attack of the amine is the same that was used to produce the anhydride in the first place. Therefore, a sub-stoichiometricstoichiometric use of the acid should be possible and a catalytic behavior is possible since the acid is not consumed in the overall reaction. For this reason, the new approach would be in theory 100% atom economic since the acid remains in the reaction system. However, an additional component in the reaction system will also increase its complexity, as depicted in (Figure 31)

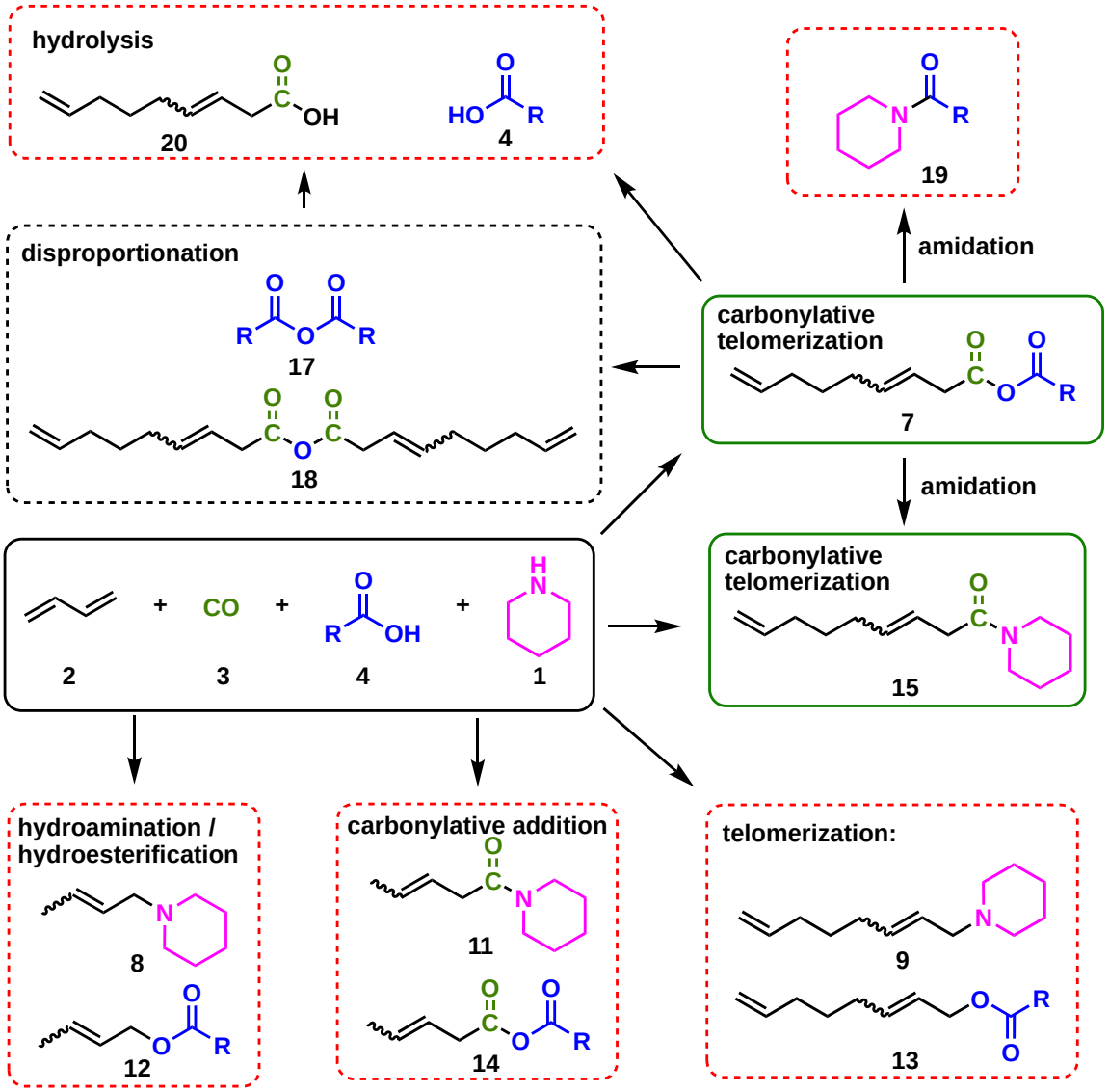

Figure 31: The updated reaction network with the new one-pot approach.

While the formation of the unsaturated amide **15** and its branched isomer (Figure 31) is the intended reaction, the potential direct amido-telomerization has to be considered, as it can be carried out under similar conditions. The presence of an additional nucleophile can contribute to unwanted side reactions, such as hydroesterification and telomerization of the acid with butadiene. This fact significantly amplifies the importance of optimizing the reaction conditions for selectivity in this one-pot process. Particularly, telomerization of the additional carboxylic acid must be inhibited to prevent the loss of the co-catalyst nucleophile. Building on prior research that underscores the substantial influence of ligands on the reaction's outcome, the initial step is the optimization, and several ligands are tested.

4.6.1. Ligand Screening

As described above (chapter 0), more basic ligands are beneficial for carbonylative telomerization and for amidotelomerization the bidentate ligands reached the best results. Therefore, monodentate and bidentate phosphines were teste, as well as a NHC (N-heterocyclic carbene) ligand, due to their performance in the related telomerization reaction.

Table 9: Results of the ligand screening.

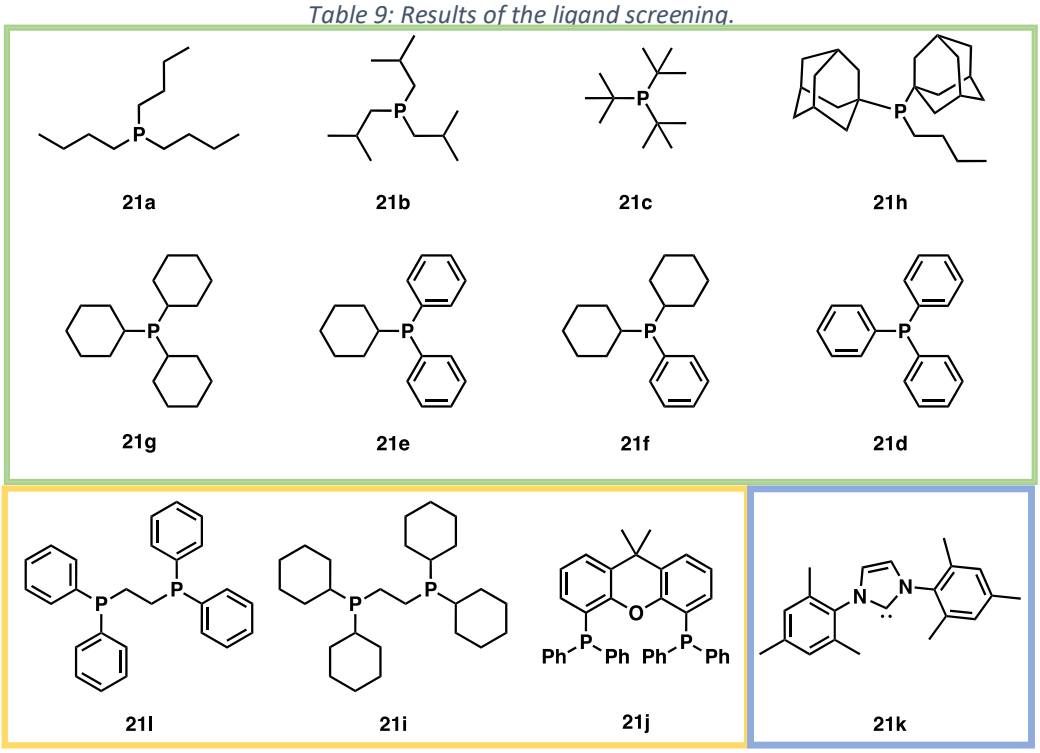

Entry	Ligand No.	$Y_{C9\text{-amides}}$ [%]	$Y_{C8\text{-amines}}$ [%]	Y_8 [%]	Y_{11} [%]	Y_{19} [%]	$S_{C9\text{-amides}}$ [%]	θ [°]	ν_{CO} [cm^{-1}]	pK_a
2.3	21c	**2**	0	0	0	0	2	182[68]	2056.1 [68]	12.2[69]
2.8	21h	**12**	3	0	1	1	14	176[70]	2054.4 [39]	
2.7	21g	***35***	*7*	0	0	1	*35*	170 [68]	2056.4 [68]	11.26[71]
2.6	21f	***38***	*12*	0	0	2	*38*	163[39] [39]	2060.6 [68]	8.46[69]
2.5	21e	**8**	4	0	1	1	10	151[39] [39]	2064.8 [68]	5.87[69]
2.4	21d	**13**	18	0	0	1	14	145 [68]	2068.9 [68]	3.28[69]
2.2	21b	**32**	9	0	2	1	32	143[72]	2059.7 [68]	7.97[71]
2.9	21i	**7**	3	34	1	1	7	142 [68]	2058.6 [73]	
2.1	21a	**25**	20	0	0	1	25	132[67] [68]	2060.3 [68]	8.43[7071]
2.12	21l	**4**	37	2	0	0	5	125 [68]	2076.1 [73]	
2.10	21j	**1**	5	1	0	0	1	111 [74]	2065[73]	
2.11	21k	**1**	5	0	0	0	2	–	2050.7 [75]	

Conditions: 3 mmol piperidine 1, 24 mmol butadiene 2, 0.9 mmol benzoic acid 4i, 0.03 mmol $Pd(OAc)_2$, 0.06 mmol ligand, 3 mL 1,4-dioxane, pCO = 20 bar, tR = 20 h, TR = 93 °C and 600 rpm. Yield determined via GC-analysis with n-decane as internal standard, Selectivity = Yi/X1 (adapted from Milius 2020[76]).

The NHC ligand is known to be an effective telomerization ligand and has the lowest ν_{CO} with a value of 2050.7 cm^{-1}. Under the given condition the overall performance is low wit only 5 % of telomerization product and traces of the C9-amides from amidotelomerization. The poor performance can be traced back to the low stability of the catalyst complex as significant amounts of palladium black was observed after the reaction (Figure 32) and the insertion of CO was not promoted by the catalyst system.

Bidentate ligands did not perform well in carbonylative telomerization, although dppe was best for the direct amidotelomerization, it underperformed in the presence of an additional acid.[38] After the reaction was stopped, large quantities of palladium black were observed (Figure 32). This may be due to an unsaturated coordination sphere, resulting in a poorly stabilized catalyst complex. An interesting note is the activity of ligand **21i** towards the amination of butadiene. The reaction resulted in 34 % of the C5-unsaturated amine, which could be an interesting reaction for the synthesis of amines form butadiene and should be investigated in a new study.

The best results were achieved using monodentate phosphine ligands, which all had less Pd black precipitate in the reactor (Figure 32). Therefore, the reaction system was better suited to keep the Pd in solution and catalyzing the reaction.

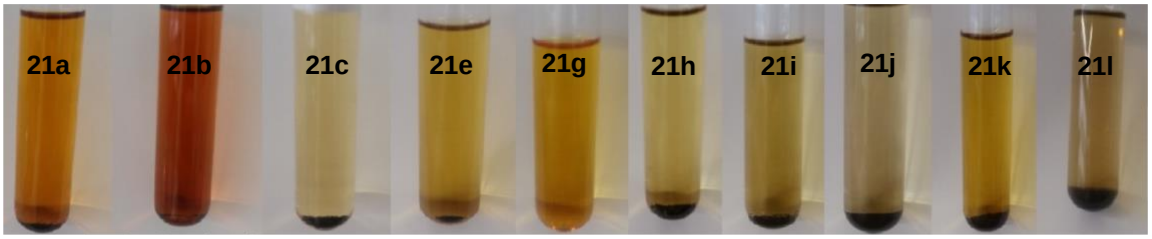

Figure 32:Reaction solution after carbonylative telomerization in the presence of m-toluic acid (adapted from Milius 2020[76]).

Regarding carbonylative telomerization, ligand **21f** and **21g** performed best. The monodentate ligands did not show signs of elemental palladium after the reaction was stopped, which makes the catalyst complex available for the reaction over the whole reaction time. The number of coordinating ligands to the metal center could be limited by the large cone angle, but the position of each ligand is less constrained compared to the bidentate ligands. A larger cone angle hints to a bulkier ligand, which claims more space around the metal center of the catalyst complex, thus limiting the free space around it.

Another reason for the high performance of ligand **21f** and **21g** could be traced back to their basicity, which is comparably high. Ligands **21a** and **21b**, despite having a significantly smaller cone angle, performed well in the reaction, most likely due to their high basicity. The catalyst complex appears to be stabilized by the high basicity, as evidenced by the small amount of Pd black in the reactor (Figure 32). The ligand **21g** was chosen for further experiments due to lower content of telomerization product and similar main product amount. As discovered in the previous work the acid has a significant influence on the reaction, since a different anhydride intermediate is formed during the reaction. Acid base reactions with the catalyst and substrate are possible, since they are equilibrium reactions the strength of the acid is crucial for content of the reaction solution.

4.6.2. Acid Screening

In the two-step process described in the previous chapter, the reaction system is less complicated because the two nucleophiles are added sequentially in two steps. This more sophisticated approach involves the amine nucleophile being present in the same reaction step that forms the acid anhydride, resulting in the formation of ammonium carboxylate salts in the reaction mixture. The reaction outcome is influenced by the pKa of the acid as well was the

structure, because both can influence the equilibrium of the acid-base-reaction. A variety of aromatic and alkyl carboxylic acids were investigated in this study (Figure 33).

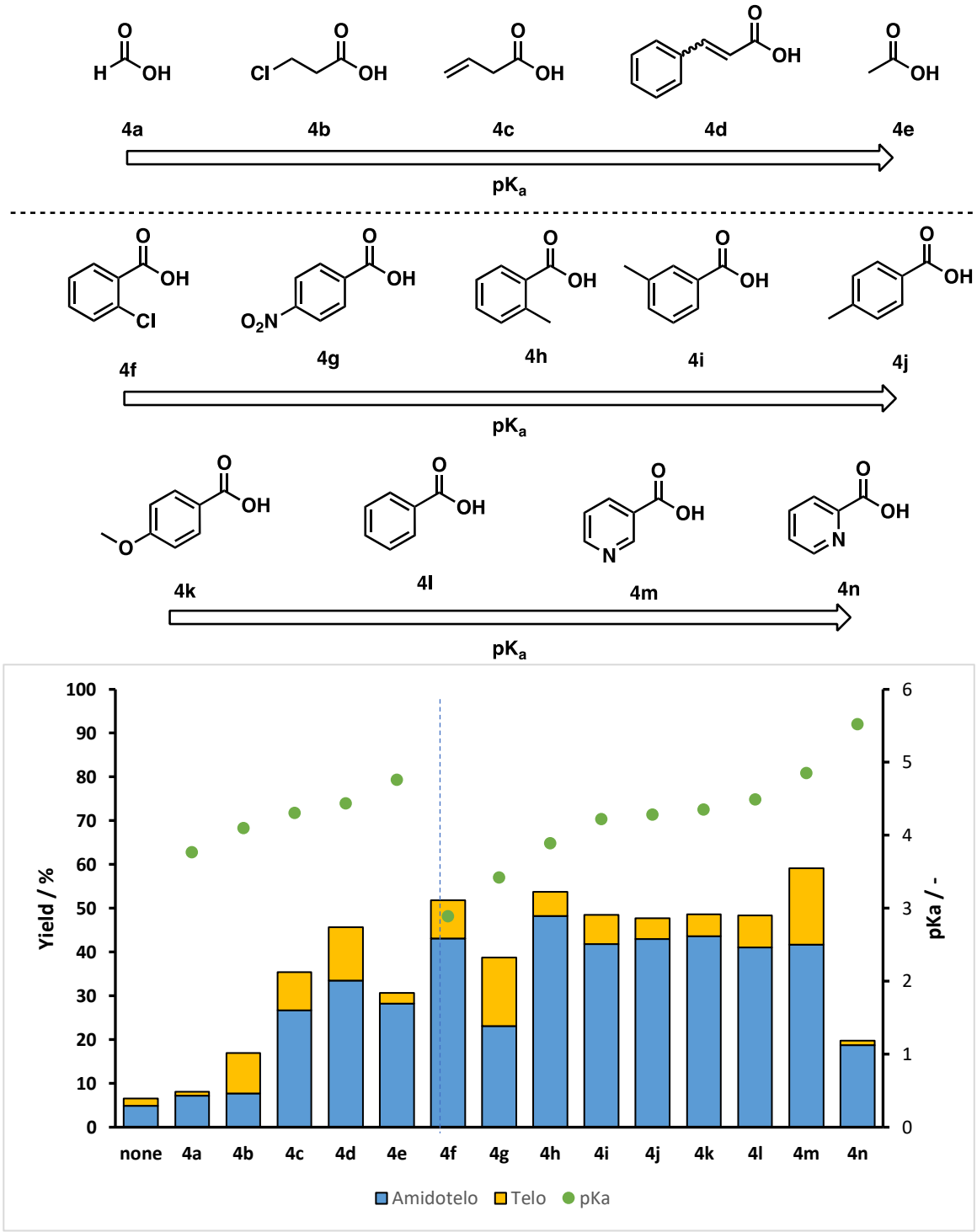

*Figure 33: Results of the acid screening. Conditions: 3 mmol piperidine **1**, 8 eq. butadiene **2**, 0.3 eq. carboxylic acid **4a-n**, 0.03 mmol $Pd(OAc)_2$, 0.09 mmol PCy_3 **21g**, 3 mL 1,4-dioxane, p_{CO} = 20 bar, t_R = 20 h, T_R = 93 °C and 600 rpm. Yield determined via GC-analysis with n-decane as internal standard (adapted from Milius 2020[76]).*

In the control experiment, conducted without the addition of an acid, a yield of only 5 % of the C9-amide was observed. Notably, alkyl carboxylic acids, in general, revealed a reduction in amide yield, with a plateau being observed within a pKa range of 4.31 to 4.76, resulting in an approximate 27 % yield. However, **4d** due to its conjugated acid nature, with a π-system attached to an

aromatic ring, resulted in the highest yield of 33% in the category. The influence of substituents on the aromatic acids, which possess a delocalized π-electron system, causing electron-poor systems to have a lower pK_a value. This reduction in pK_a correlates with reduced nucleophilicity, with some exceptions like chlorobenzoic acid showing relatively high yields despite having the lowest pK_a among the tested acids. Furthermore, the -M-effect of nitrobenzoic acid significantly affects nucleophilicity when compared to the -I-effect of 2-chlorobenzoic acid. Interestingly, a peak in yield is observed at a medium pK_a of 3.89 for 2-methylbenzoic acid, resulting in a 48 % yield. The plateau continues until **4m** with a pK_a of 4.85, yielding 42 % of the desired amide. A sharp decline in yield is observed with, the highest pK_a of 5.52, reducing it by half to 19 %. In summary, methylbenzoic acid and anisic acid outperform benzoic acid, unlike non-aromatic acids, which do not improve the amide yield.

4.6.3. Solvent screening

Dioxane has been identified as the solvent of choice for palladium catalyzed reactions in the past, due its ability to form coordination complexes with metals, particularly due to its Lewis-basic properties. This characteristic allows stabilizing metals in solution, a critical factor in the success of palladium catalyzed carbonylative telomerization. This is especially relevant because Pd(0), is inherently prone to forming agglomerates, which can compromise its activity and efficiency. Utilizing these coordinating abilities, agglomerates can be prevented, ensuring a higher number of active metal complexes in the reaction.

However, dioxane does not align with green chemistry principles. It has a relatively low acute toxicity, but concerns persist regarding its potential to cause cancer in humans. Therefore, the search for alternative solvents with similar coordinating properties becomes imperative.

A promising alternative is 2-methyltetrahydrofuran (2-MeTHF), a solvent derived from renewable resources. Due to its structure 2-methylTHF has similar coordination properties as 1,4-dioxane and could also stabilize the Pd(0) species in solution.

Table 10: Solvent Screening.

Entry	Solvent	$Y_{C9\text{-amides}}$ / [%]	$Y_{C8\text{-amines}}$ / [%]
1	1,4-dioxane[a]	42	7
2	2-MeTHF[a]	40	6
3	2-MeTHF[a,b]	40	9
4	1,4-dioxane[c]	48	6
5	2-MeTHF[c]	*49*	*7*

*Conditions: 3 mmol piperidine **1**, 8 eq. butadiene **2**, a: 0.3 eq. benzoic acid **4i**, c: 0.3 eq. o-toluic acid **4h**, 0.03 mmol $Pd(OAc)_2$, 0.09 mmol PCy_3 **21g**, 3 mL solvent, b: degassed via freeze-pump-thaw method, p_{CO} = 20 bar, t_R = 20 h, T_R = 93 °C and 600 rpm. Yield determined via GC-analysis with n-decane as internal standard (from Milius 2020[76]).*.

In a first comparison both solvents were tested using benzoic acid. 2-MeTHF yielded only 2 % less amides than dioxane. The solvents are dried *via* mole sieves prior to use and stored under argon. Since oxygen was a crucial factor in the amidotelomerization, freshly degassed solvent was also tested under otherwise identical conditions. Which increased only the telomerization yield by 3 %, but no significant impact on the carbonylative telomerization was observed.

With the use of *o*-toluic acid the result changed in favor of 2-MeTHF and the yield of the desired amide increased to 49 %. These findings suggest that substitution of the solvent by 2-MeTHF is even beneficial for the performance of the reaction. Therefore, 2-MeTHF is used in future experiments in combination with *o*- toluic acid.

The screening of ligands, acids and solvent already filtered the reaction conditions, reducing the parameters for a more detailed study *via* a design of experiments approach.

4.6.4. Optimization via DOE

The design of experiments approach can reduce the number of experiments necessary for an optimization drastically while taking cross effects between the parameters into account as described above. Since the additional amine changes the reaction system significantly, the optimization was repeated due to more acid-base reactions and a larger number of side reactions. The parameters butadiene amount, CO pressure and temperature were tested again. Additionally, the amount of o-toluic acid and the amount of ligand were investigated.

Table 11: Starting point for the optimization via DOE (adapted from Milius 2020[76]).

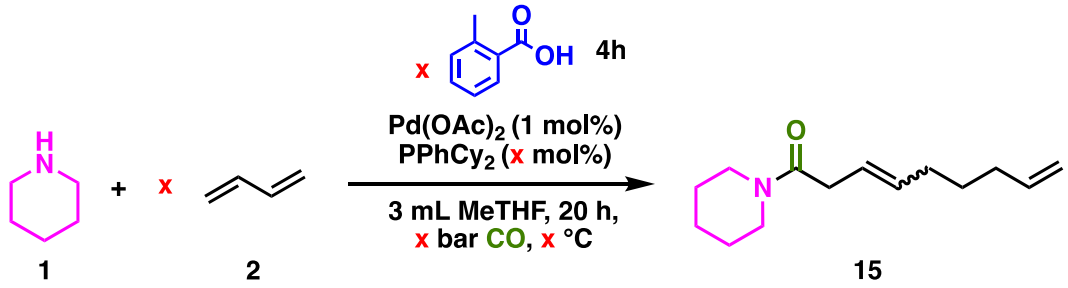

Factors	Abbreviation	Minimum Value	Maximum Value
Temperature [°C]	T	80	120
CO Pressure at RT [bar]	p	5	35
Butadiene eq. [-]	But	2	12
Ligand/Pd [-]	L/P	1	8
***o*-Toluic Acid eq. [-]**	Ac	0,1	1,5
Yield [%]	Yield MP	40	100
Selectivity [%]	Selectivity MP	70	100

The reaction parameters for the input of the DoE were chosen from previous research and for economic reasons. The temperature was varied between 80 and 120 °C to keep the required energy relatively low. Similar for the pressure which was tested between 5 and 35 bar. Another crucial parameter is the excess of butadiene for carbonylative telomerization, as it displayed a large influence on the yield of the reaction in all the previous studies (Chapter 4.5). Butadiene was used from 2 eq. up to 12 eq.. In theory the nonconverted butadiene can be recycled for the next reaction, however a lower excess is preferred, due to oligomerization of butadiene in the reaction mixture at elevated temperatures. The ligand amount was investigated from 1 up to 8 mol% which includes a P/Pd ratio of 1/1 up to 8/1. Toluic acid was used from sub stoichiometric 0.1 eq. up to an excess of 1.5 eq.. Ideally, the acid can be used in a sub-stoichiometric amount and function as a co-catalyst (Figure 30).

Using the MODDE software, as described above, the Design of Experiments (DoE) was conducted. A reaction plan was arranged by MODDE to minimize systemic errors. With this plan, the reactions were conducted, and the raw results were fed into the software. However, this data must be refined for an optimal fit of the model because outliers and insignificant parameters can lead to false calculations and low model quality. The summary of fit (Figure 34) contains the essential model conditions, which describe its reliability.

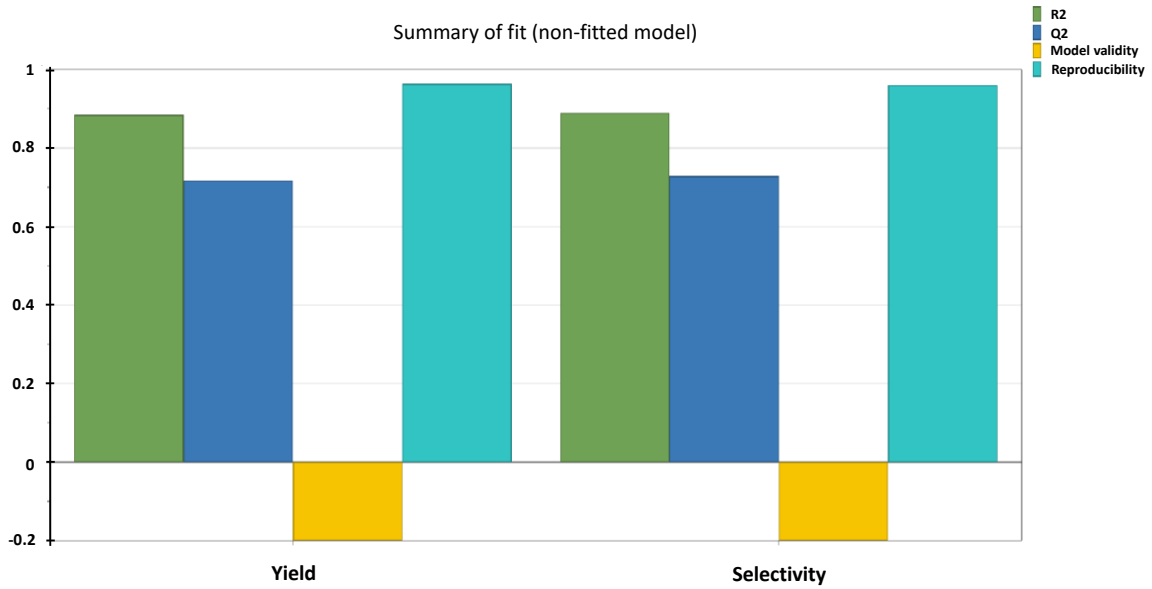

Figure 34: Summary of the model for the response yield and selectivity (from Milius 2020[76]).

A value for the model validity larger than 0.25 indicates no lack of fit, thus the model error is in the same range as the pure error. Reasons for an existing lack of fit in this case could be outliers, broad distribution and the non-correct model form. The probability of measuring errors is low, shown by the high reproducibility, however systemic errors not detected by this system.

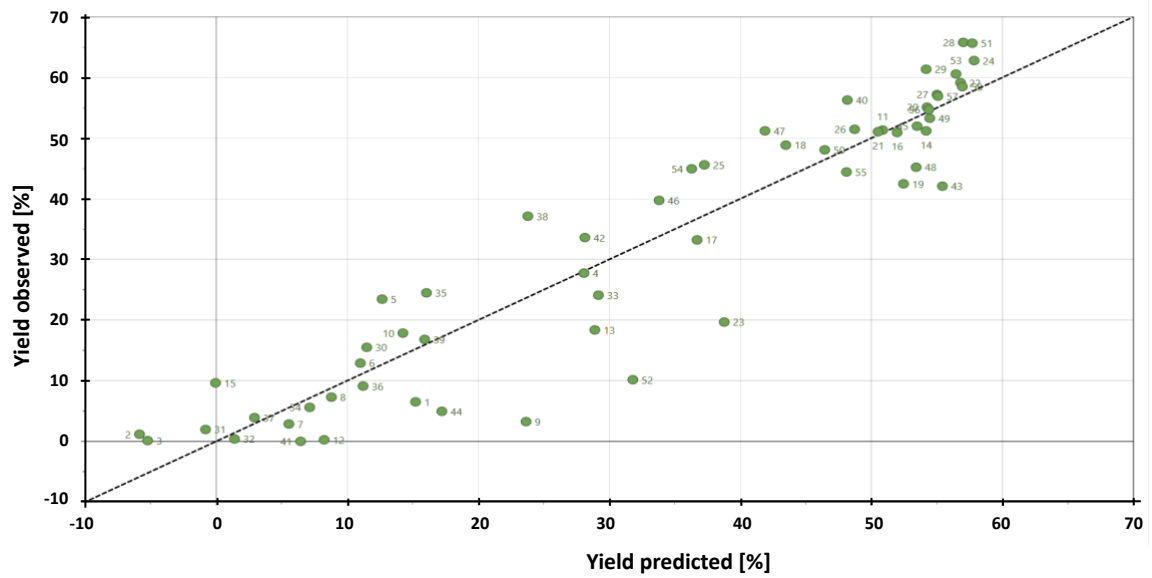

Figure 35: Plot of observed versus predicted values for the yield of C9-amides (adapted from Milius 2020[76]).

A perfect model would only have data points along the bisector. Due to experimental imperfections and a non-ideal model the actual results are scattered around the bisector. Some experiments (9, 23, 52) are relative far away from the bisector and are considered outliers. If this discrepancy is caused by an experimental error, the data point does not add value to the calculation. By removing the outliers from the model, the data can be refined and lead to a better fit of the model.

Another way of optimizing the model is to reduce the complexity by excluding insignificant parameters. From the start the model includes the main parameters, *i.e.*, T, p(CO), L/P, But, Ac, and a combination of each. This adds complexity to the system and could improve the model's accuracy. However, if some of the parameters are not significant the quality of the model

decreases, and all insignificant parameter combinations were removed. The result are the main parameters and the following combinations remain: T*T, But*But, Ac*Ac, T*L/P, p(CO)*L/P, p(CO)*Ac.

The removal of outliers and insignificant terms could drastically increase the model validity as displayed in Figure 36.

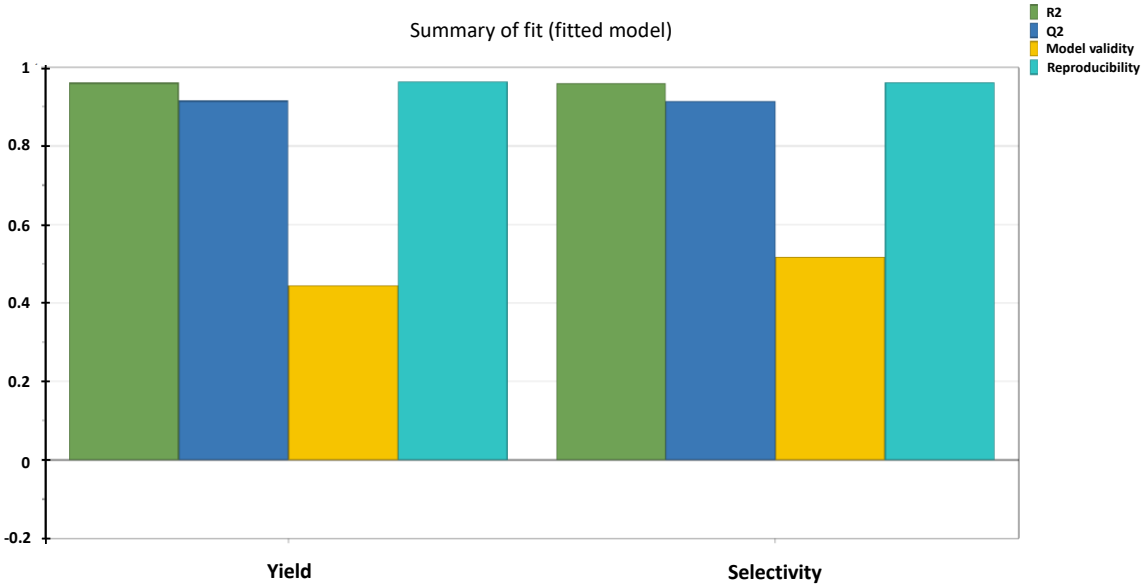

Figure 36: Summary of fit of the fitted model for responses yield and selectivity of C9-amides(from Milius 2020[76]).

The main improvement can be seen in the validity followed by Q^2 and R^2 for yield and selectivity respectively.

With the newly established model it is now possible to calculate the optimal reaction conditions concerning the maximum C9-amide yield and selectivity (Table 12).

Table 12: Optimal reaction parameters calculated by MODDE resulting from the fitted model (from Milius 2020[76]).

Yield 15 [%]	Selectivity 15 [%]	T_R [°C]	p_{CO} [bar]	Butadiene 2 [eq.]	L/P-ratio [-]	Acid [eq.]
68	68	106	18	11	8	0.86

Using MODDE the optimized yield and selectivity is predicted to be 68%, since full conversion is expected at the given reaction time. In comparison to the carbonylative telomerization directly with carboxylic acids the predicted yield is lower by 8%. To test the prediction the parameters were used for a control experiment (Table 13).

Table 13: Results of the optimized reaction conditions.

Y_{15} / [%][a]	$Y_{9/10}$ / [%][a]
63	8

*Conditions: 3 mmol piperidine **1**, 11 equiv. butadiene **2**, 0.03 mmol $Pd(OAc)_2$, 0.24mmol PCy_3 **21g**, 0.86 equiv. o-toluic acid **4h**, 3 mL 2-MeTHF, t_R = 20 h, p_{CO} = 20 bar, T_R = 105 °C and 600 rpm. a: duplicates. Yield determined via GC-analysis with n-decane as an internal standard (adapted from Milius 2020[76]).*

Under the optimized conditions described above, a yield of 63 % with full conversion was achieved. This result is 5 % lower than predicted, yet in the same range. Due to the limited data points and validation experiments the model is still prone to errors. For example, the experiments were conducted as duplicates, which gives a small possibility for eliminating outliers. However,

statistical more precise data could be obtained by triplicates, or duplicates of duplicates, *i.e.*, measuring each experiment twice or preparing two samples from the same batch. Performing the experiments as triplicates would increase the number of experiments by 50 % and therefore the required time and cost, in form of materials used. For this reason, duplicates were chosen as a compromise of some control mechanism and low time and material consumption.

Nevertheless, the initial performance of less than 10 % yield of the desired C9-amide **15** could be significantly increased to 63 %, by the predicted reaction parameters.

4.6.5. Critic remarks on the optimization

At the end of the optimization, an additional signal was identified as the telomerization product of the *o*-toluic acid **4h** with butadiene **2**.

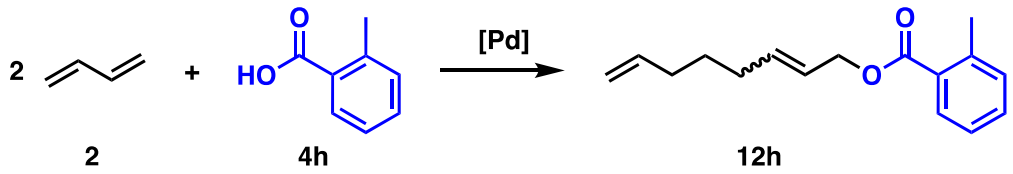

Figure 37: Telomerization of o-toluic acid.

At high concentrations of the acid in combination with high concentrations of butadiene, telomerization of the acid was observed. Unfortunately, the GC signal of the telomer is close to one of the desired amide isomers and with a large signal an overlapping occurred. Although, under optimized conditions the concentration is relatively low and no overlapping is observed some signal during the optimization had to be corrected due to overlapping which may lead to inaccurate results and therefore a decreased model quality.

4.6.6. Scale up and time resolved measurements

For a more detailed insight into the reaction, its kinetic, and possible side reactions, a time resolved analysis of the reaction is necessary. Therefore, the next step was the scale up to a reaction volume of 100 mL which is equal to a scale up factor of about 20. A pressure autoclave reactor manufactured by PARR INSTRUMENTS with additional sampling valves was used to perform the reactions.

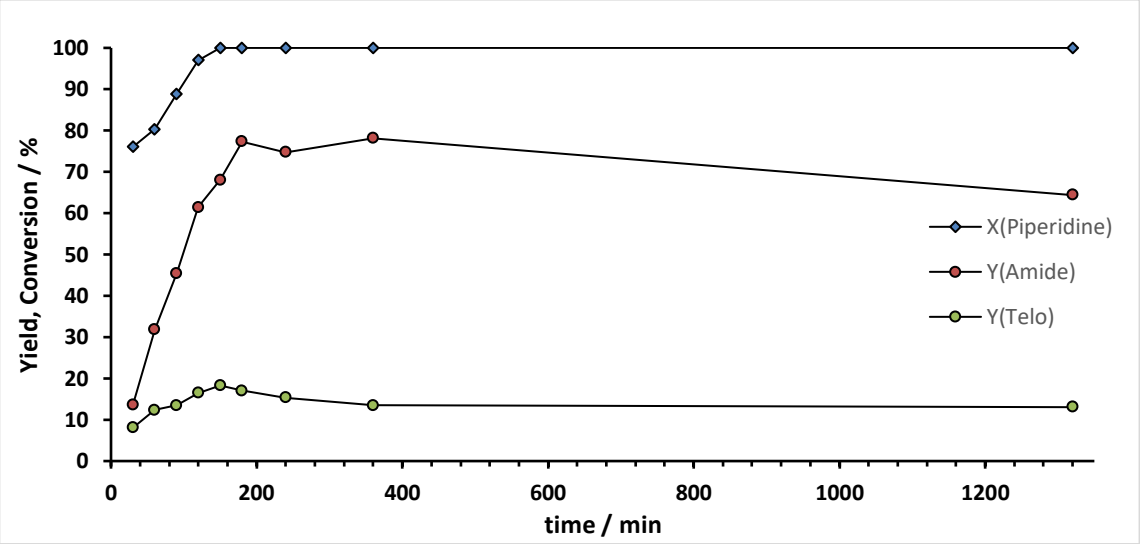

*Figure 38: Conversion time plot of the carbonylative telomerization of piperidine in the presence of acid. Conditions: 30 mmol piperidine **1**, 11 eq. butadiene **2**, 1 mol% $Pd(OAc)_2$, 2 mol% PCy_3 **21g**, 0.86 eq. o-toluic acid **4h**, 60 mL 2-MeTHF, t_R = 20 h, p_{CO} = 20 bar, T_R = 105 °C and 600 rpm. Yield determined via GC-analysis with n-decane as an internal standard (adapted from Milius 2020[76]).*.

Initially, the reaction occurs notably faster than anticipated. Previously published results on carbonylative telomerization suggest that at least 8-12 h of reaction time are necessary for high yields and conversion.[36–39,42] In comparison the presented acid assisted amide synthesis requires only 3 h for the reaction to complete and reaches a yield of 77 %. The acceleration is caused by the presence of the acid, which acts as a catalyst, expediting the reaction. Additionally, the acid engages with the amine to form an acid-base adduct, as expected. The formation of the adduct could also be beneficial for the reaction, since deprotonating the acid enhances its nucleophilic character, providing support for the intermediate anhydride theory. The anhydride formed subsequently recombines with an additional proton, thus facilitating the opening of the amine for further reaction.

During the reaction with the amine, the anhydride releases the initial acid, which can then reinitiate the cycle, demonstrating a self-sustaining reaction loop. However, some inefficiency is introduced as a portion of the anhydride reacts with its nonadienoic side, resulting in the production of nonadienoic acid and benzylic amides-products that are not the desired outcome (Figure 31, formation of 19).

Looking at the samples, a color difference is visible over the course of the reaction, form yellow to brown (Figure 39). Vials 5 and 6 have a grayish tan, which might be caused by Pd-black. Pd-black is a typical sign for catalyst degradation. Especially Pd(0) is prone to agglomeration, which leads to larger particles which are no longer solubilized. In vial 7 there is a visible black precipitate (Figure 39) indicating a progression of the degradation. These three vials resemble the top of the yield curve and indicate, that the catalyst was destroyed latest at vial 7 (Figure 39). Longer reaction times do not increase the yield for the desired amides, conversely the yield decreases due to additional side reactions. The darker brown color after that is caused by butadiene oligomerization, caused by prolonged exposure to elevated temperatures. The oligomerization has to be obviated to avoid a reduction of the overall resource efficiency of the reaction, due to not recyclable butadiene.

Figure 39: Samples of the reaction in the larger reactor directly after the reaction (top) and after 24h (bottom) (from Milius 2020[76]).

After 24 h of storage all samples turned brown similar to the end of the reaction. Therefore, butadiene is not stable in the reaction solution over a long time, which make the reaction speed even more relevant. The shorter the reaction time the less butadiene is lost to oligomerization. Since no reaction profile available for other reaction conditions the reaction was repeated with a lower acid content, to show the difference of the reaction profile (Figure 40).

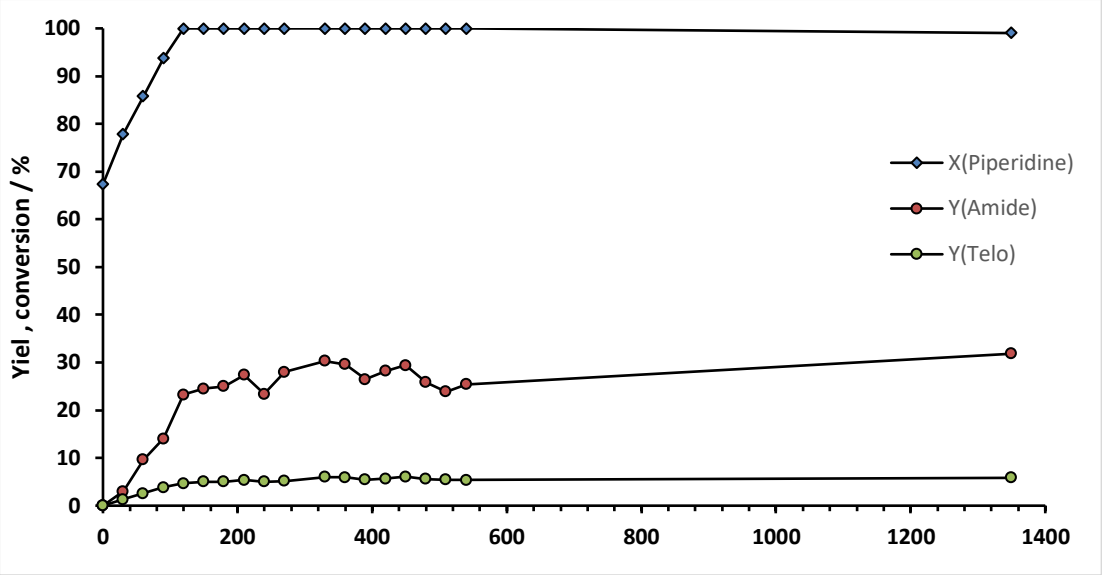

*Figure 40: Reaction profile of the carbonylative telomerization with toluic acids and piperidine. Conditions: 30 mmol piperidine **1**, 11 eq. butadiene **2**, 1 mol% $Pd(OAc)_2$, 2 mol% PCy_3 **21g**, 0.6 eq. o-toluic acid **4h**, 60 mL 2-MeTHF, t_R = 20 h, p_{CO} = 20 bar, T_R = 105 °C and 600 rpm (adapted from Milius 2020*[76]).

At a lower acid concentration of 0.6 eq., the reaction does not only proceed slower, but the maximum selectivity is also reduced to 32 %. Even after 23 h 32 % amide yield could not be exceeded. Again, the reaction stalled after Pd-black was observed in the reaction mixture, so not enough catalyst is left for the reaction to proceed. The acid concentration can influence the reaction outcome in many ways. First, the pH of the reaction mixture is influenced. Due to less acid in the mixture, a higher pH is expected; Second, the amount of acid base adducts changes and with less acid leaves more unreacted piperidine stays in solution, which can be seen by comparing the initial amount of piperidine. In the first experiment with 0.86 eq. acid the first sample was drawn after 30 min, so a direct comparison is not possible. However, the slope of the continuing data points suggests a lower starting amount of piperidiene; And third, the formation of possible intermediate anhydrides is also influenced.

In conclusion the scale up under optimized reaction conditions could increase the performance of the reaction in terms of reaction speed, yield, and selectivity. However, for further investigations the precipitation of palladium and therefore the catalyst deactivation should be studied in more depth, since catalyst recycling would be highly desirable for the homogeneously catalyzed reaction.

Additionally, a larger scale the reaction should tolerate different functional groups in the substrates for a more general reaction.

4.6.7. Direct Amide formation

In theory, a condensation of amine and carboxylic acid could take place under elevated temperatures. Although, usually good leaving groups such as halides or activated carboxylic acids are necessary for the formation of amides, a test reaction was carried out again under the adapted reaction conditions (Figure 41).

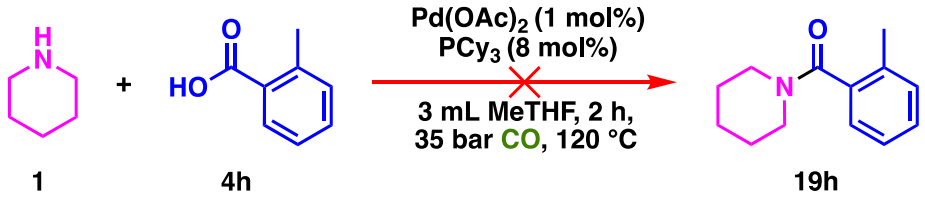

Figure 41: Combination of amine and amide under carbonylative telomerization conditions in the absence of butadiene (adapted from Milius 2020[76]).

Similar to the control reaction in chapter 1.1, no amide formation could be observed, and the only product was the expected ammonium salt of both reagents. These results may indicate the formation of an intermediate anhydride, since the resulting mixture has less active amine left for the direct carbonylative amidation and simultaneously increases the nucleophilicity of the carboxylic acid. In a future work the direct use of ammonium salts in the carbonylative telomerization should be investigated.

4.6.8. Investigation of the reaction scope

In general, there are two possibilities for the scope expansion for carbonylative telomerization as described above. Either the diene or the nucleophiles can be varied. First the reaction conditions were applied to different dienes (Figure 42). Isoprene leads to methyl branches at the main chain of the unsaturated amide. This would be the first example of isoprene as the substrate for carbonylative telomerization. Additionally, β-myrcene is used in the reaction, which was also used in the direct amidation reaction (chapter 0). However, the necessary catalyst amount was relatively high with 5 mol% Pd precursor and could be reduced significantly with this set up.

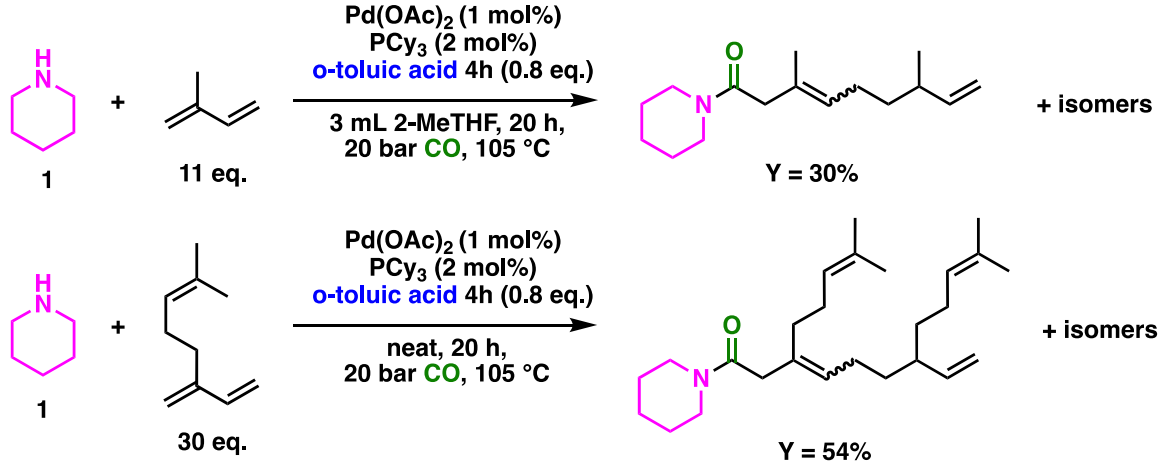

Figure 42: Diene scope in the carbonylative telomerization amidation one-pot reaction (adapted from Milius 2020[76]).

The successful utilization of both dienes, isoprene and β-myrcene was possible. Notably, isoprene, despite achieving only a 30% yield (Figure 42, top), reveals promising prospects. Until now isoprene was not published in the literature for carbonylative telomerization. The dimerization of the diene in the initial step introduces additional branches, resulting in an increased steric strain around the catalyst complex. This increased steric hindrance can potentially reduce the reaction rate emphasizing the need for optimization of the reaction conditions.

Conversely, in the second reaction, β-myrcene served as both the diene and solvent. Under otherwise identical conditions, 54% yield of the desired amide was observed despite the even higher steric demand of β-myrcene (Figure 42, bottom). Nevertheless, further optimization of the reaction conditions when using β-myrcene is required also. The reduction in the catalyst amount required, being only 1 mol% instead of 5 mol% in the direct reaction (chapter 0), is a remarkable improvement. Considering the current price for palladium a more cost-effective synthesis of

unsaturated amides is possible. This trade-off between yield and catalyst cost is a critical aspect in selecting the most suitable reaction pathway.

Furthermore, the amine was varied for a versatile product spectrum. A noncyclic amine, aromatic amines and morpholine were tested and compared (Table 14).

Table 14: Scope of the one pot amide synthesis via carbonylative telomerization and amidation.

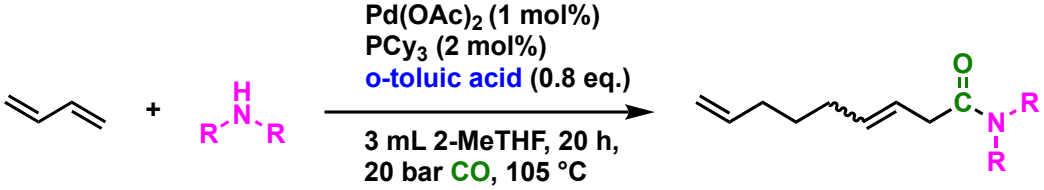

Entry	Substrate	Product	Y [%]
1	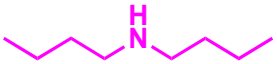 **30a**	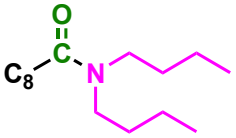 **31a**	74
2	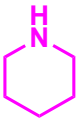 **1**	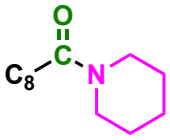 **15**	66
3	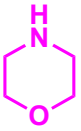 **30b**	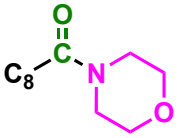 **31b**	19
4	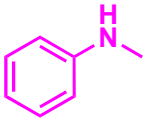 **30c**	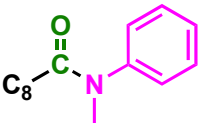 **31c**	51
5	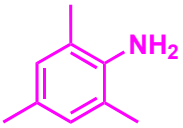 **30d**	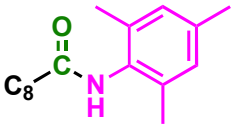 **31d**	26

*Conditions: 3 mmol amine **1** and **30a-30d**, 30 mmol butadiene **1**, 2.4 mmol o-toluic acid **4h**, 0.03 mmol $Pd(OAc)_2$, 0.06 mmol PCy_3, 3 mL 2-MeTHF, t_R = 20 h, p_{CO} = 20 bar, T_R = 105 °C and 600 rpm. Yield determined via GC-analysis with n-decane as internal standard (adapted from Milius 2020[76]).*

The highest yield of 74% was obtained with the noncyclic dibutylamine **30a** (Table 14, entry 1). Piperidine **1** has been favored in previous research due to its more readily available electron lone pair, which enhances its nucleophilicity and thus its reactivity in the direct carbonylative telomerization. The optimized conditions yielded 66% of the piperidinylamide **15** (Table 14, entry 2).

Morpholine **30b**, on the other hand, has a lower nucleophilicity due to the electronegative oxygen present in the ring, resulting in a poor amide **31b** yield of 19% (Table 14, entry 3).

Aromatic amines result in a moderate yield of 51% achieved for N-methylaniline **30c** (Table 14, entry 4), while a poor yield of 26% was obtained for 2,4,6-trimethylaniline **30d** (Table 14, entry 5). The diminished yield for 2,4,6-trimethylaniline **30d** can be explained with its high steric demand, which restricts the nucleophilic attack on the reactants, leading to decreased reactivity.

Additionally, 2,4,6-trimethylaniline **30d** is a primary amine which are typically less reactive than secondary amines.

4.6.9. Conclusions and Outlook

In conclusion, the carboxylic acid co-catalyzed carbonylative telomerization was presented. A variety of amides could be synthesized in a one-pot reaction based on the previous chapter. Combining the carbonylative telomerization of carboxylic acids with amines results in the synthesis of unsaturated amides with up to 74 % yield.

The scope of the reaction was investigated with different dienes and amines. Isoprene was used successfully for the first time in carbonylative telomerization, and β-myrcene could be converted with only one fifth of the catalyst amount compared to the conditions presented in chapter 0. However, the selectivity was lower, with only 54% of the highly branched amides. Notably, the reaction conditions were optimized for butadiene, and a new optimization for other dienes could improve the system's performance.

Different kinds of amines were implemented as well, which underline the dependency of the reaction on the nature of the nucleophile.

The sub-stoichiometric use of carboxylic acid could theoretically increase the atom economy (AE) of the reaction. If the acid is referred to as an additional catalyst for the reaction and excluded from the AE, since it is not consumed, the AE would be only limited by the selectivity of the reaction.

A scale-up and time-resolved measurements already indicated a possible boost in the performance of the reaction. Therefore, further research should focus on scaling up and fine-tuning the reaction time.

4.6.10. Experimental

General

Chemicals used in this chapter with respective purities are listed in the annex. The solvents were distilled and stored over 3 Å mole sieve. Piperidine **1** was also distilled and stored in a flask covered with aluminum foil to prevent light from entering. If not explicitly mentioned, all applied chemicals were used as obtained from the distributor.

All procedures involving oxygen- and moisture-sensitive chemicals, especially the transition metal catalyst precursor and the ligands, were carried out in a dry, inert argon atmosphere *via* standard Schlenk technique.

Procedure for autoclaves

First the carboxylic acid **4** and the internal standard (0.6 mmol, 85.4 mg, 0.2 eq.) were weighed into the reactor, and a magnetic stirring bar was added. Afterward the reactor was closed and purged with argon.

Next a catalyst stock solution was prepared with palladium acetate (0.03 mmol, 6.7 mg, 0.01 eq.) and PCy_3 (0.09 mmol, 26 mg, 0.03 eq.) in a 10 mL headspace vial. The vial was sealed with a crimp cap and purged with 3 argon/vacuum cycles. Then 3 mL of 2-MeTHF were added *via* syringe and the suspension was placed in an ultrasonic bath until it became homogeneous.

The catalyst solution and piperidine **1** (3 mmol, 258 mg, 1 eq.) were added *via* syringe under an argon counter flow. Next, 1,3-butadiene **2** (24 mmol, 1298 mg, 8 eq.) was filled into the reactor *via* differential weighing. Then the reactor was pressurized with 20 bar CO, before being placed in a heating block at 93 °C for 20 hours and 600 rpm. After completion of the reaction, the reactor was cooled with an ice/water bath and carefully depressurized. The reaction solution was analyzed *via* GC-FID.

For the larger 300 mL autoclave experiments the proportion were kept the same, but the catalyst solution was added at reaction temperature through a pressure dropping funnel. Samples were drawn during the reaction time *via* a sampling valve at the reactor and analyzed via GC-FID.

4.6.11. Analytics

NMR-Spectroscopy: ^{1}H- and ^{13}C-NMR-spectra were recorded using Bruker Avance III HD NanoBay - 400 MHz, Bruker Avance NEO – 500 MHz or Bruker Avance III HD – 600 MHz spectrometers at ambient temperature with the frequency and solvent noted. Chemical shifts δ are given in ppm relative to tetramethylsilane (0 ppm) and were referenced to residual solvent signals (^{1}H: $CDCl_3$ 7.26 ppm, ^{13}C: $CDCl_3$ 77.16 ppm).

Gas chromatography (GC): Conversion and yield of the reactions were determined *via* GC on an Agilent Technologies INC. chromatograph of the type 7890B with a flame ionization detector (FID). A HP-5 column was used (30 m long, 0.32 mm diameter, 0.25 µm thickness of the layer, 5 min at 50 °C, heating rate 15 °C/min to 290°C, heating rate 40 °C/min to 320 °C, holding for 10 min). The split was set to 1:75. *n*-Dodecane was chosen as internal standard and response factors of the substrates and products were obtained experimentally by analyzing known quantities of the substances (calibration) or were calculated form literature known methods.[60]

The response factor f_i for piperidine was determined to be 1.7778 *via* a multilevel calibration and equals the slope of the regression line (Figure 43).

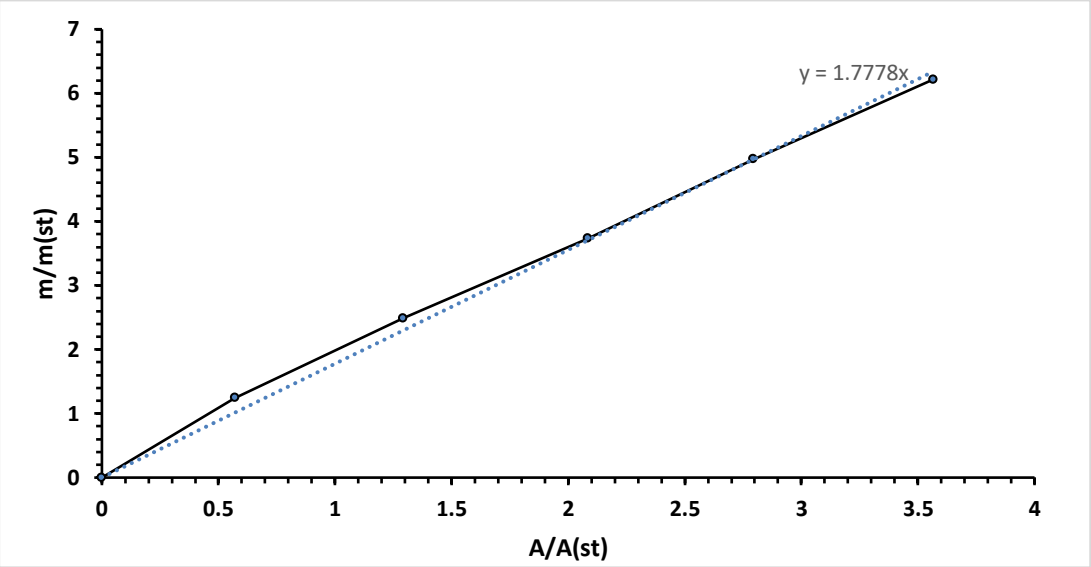

Figure 43: GC calibration of piperidine.

The specification of the response factors for the amide product was not accessible by the calibration method, due to insufficient product separation. Nevertheless, for those substances, the so-called STERNBERG factor was calculated after STERNBERG.[60]

Table 15: Sternberg factor of evaluated product substances.

Substance	Sternberg Factor
Piperidinyl nonadien-1-one **15/16**	1.2395
Octadienyl piperidine **9/10**	1.0826
Butenyl piperidine **8**	1.1315
Piperidinyl penten-1-one **11**	1.3589
Phenyl piperidinyl methanone	1.2159
N,N-dibutyl nonadien amide **31a**	1.1997
1-morpholinononadien-1-one **31b**	1.4877
N-methyl-N-phenyl-nonadienamide **31c**	1.1795
N-mesityl nonadienamide **31d**	1.2110
Dimethyl-1-piperidinyl nonadien-1-one **24/25**	1.2935
C21-amide **28/29**	1.1130

The STERNBERG factor approximates the response factor, and the calculated factors can be extracted from Table 15.

Mass Spectrometry (MS): Qualitative mass analysis was performed *via* GC. A HP-5MS UI (30 m long, 0.25 mm diameter, 0.25 µm thickness of the layer) column was used. The carrier gas was Helium, and the detector was of the Type 5977A MSD of Agilent Technologies INC.

Product Separation *via* Flash Chromatography - FC

Before the desired product was separated the reaction mixture was extracted with a 0.1 M sodium hydroxide solution, to remove the carboxylic acid. The aqueous phase was washed with ethyl acetate. Afterward the combined organic phases were dried over magnesium sulfate. Volatile compounds were removed in a rotary evaporator under reduced pressure. The residue was loaded to a silica oxide C18 packed cartridge (12g)

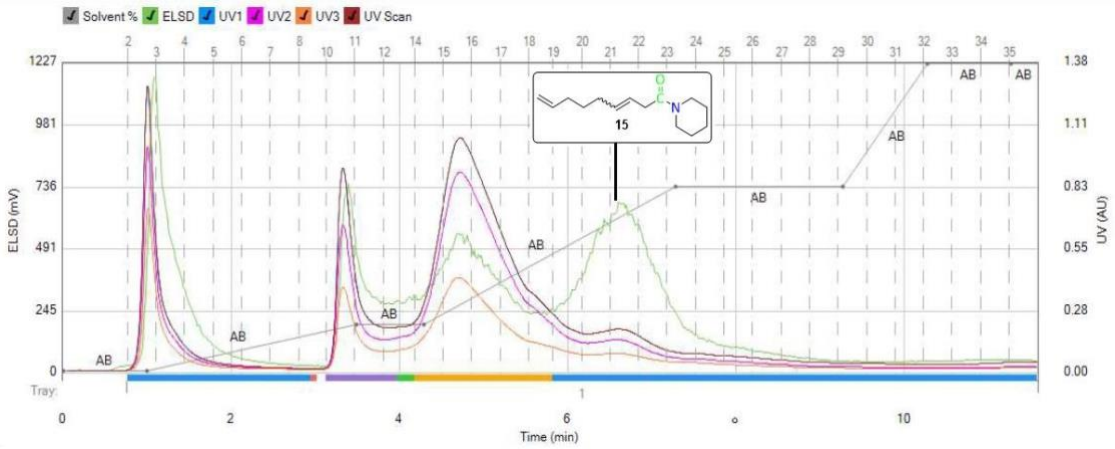

Figure 44:Product separation with the FC, first run.

The separation was carried out on a BÜCHI flash chromatograph, the Flash Pure. The solvent gradient was created using Rf-values determined earlier via thin layer chromatography (TLC). After completing the flash chromatography, the detected peaks (Figure 44) were characterized in the GC-MS and combined. The pure product was obtained by evaporating the solvent mixture.

1-(piperidin-1-yl) nona-3,8-dien-1-one (15)

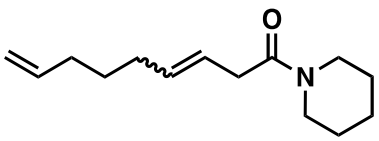

^{1}H NMR (400 MHz, $CDCl_3$): δ = 5.78 (m, 1H), 5.59 – 5.45 (m, 2H), 5.02 – 4.95 (m, 1H), 4.95-4.90 (m,1H), 3.57-3.48 (m, 2H), 3.43-3.32 (m,2H), 3.07(m, 2H),

2.04 (m, 4H), 1.66-1.57 (m, 2H), 1.57-1.49 (m, 4H), 1.45 (m, 2H) ppm
^{13}C {^{1}H} NMR (101 MHz, $CDCl_3$): δ = 169.90, 138.79, 133.47, 123.41, 114.63, 77.16, 47.01, 42.81, 38.03, 33.31, 32.07, 28.57, 26.59, 25.65, 24.62 ppm
LR-MS m/z (%): 221 (7), 178 (14), 166 (15), 152 (9), 138 (100), 137 (2), 127 (3), 112 (11), 84 (43)

1-(piperidin-1-yl)-2-vinylhept-6-en-1-one (16)

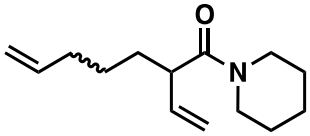

LR-MS m/z (%): 221 (8), 180 (8), 166 (8), 164 (16), 152 (6), 138 (10), 112 (100), 109 (1), 84 (21)

1-(octa-2,7-dien-1-yl) piperidine

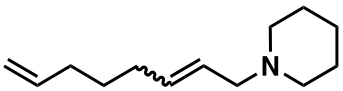

LR-MS m/z (%): 193 (7), 192 (20), 150 (22), 138 (12), 124 (27), 110 (19), 109 (1), 98 (50), 95 (3), 84 (100)

1-(but-2-en-1-yl) piperidine

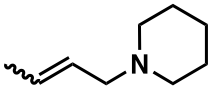

LR-MS m/z (%): 139(30), 124(37), 110(37), 98(95), 84(85), 68(20), 55(100)

1-(piperidin-1-yl) pent-3-en-1-one

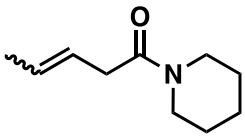

LR-MS m/z (%): 167(17), 152(4), 112(88), 84(18), 69(100), 55(42)

phenyl(piperidin-1-yl)methanone

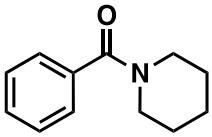

^{1}H NMR (400 MHz, $CDCl_3$): δ = 7.38 (1/2/3/4/6, s, 5H), 3.70 (8, br s, 2H), 3.33 (12, bs s, 2H), 1.67 (9/11, br s, 4H), 1.51 (10, br s, 3H)
^{13}C {^{1}H} NMR (101 MHz, $CDCl_3$): δ = 170.44 (7), 136.61 (5), 129.45 (2), 128.50 (4/6), 126.89 (1/3), 48.86 (8), 43.25 (12), 26.62 (9), 25.68 (11), 24.70 (10).
HR-MS (APCI): calcd. $[M+H]^+$ = 190.1226, found $[M+H]^+$ = 190.12279.
LR-MS m/z (%): 189 (27), 188 (82), 105 (100), 84 (8), 77 (70)

octa-2,7-dien-1-yl 2-methylbenzoate

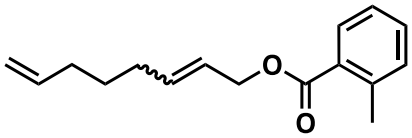

LR-MS m/z (%): 244 (0.1), 203 (0.1), 189 (0.2), 136 (5), 119 (100), 109 (3)

3,8-dimethyl-1-(piperidin-1-yl)nona-3,8-dien-1-one

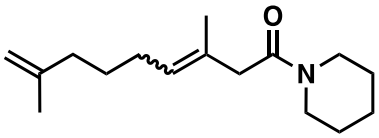

LR-MS m/z (%): 249(9), 234 (8), 194 (31), 180 (10), 166 (6), 152(5), 138 (3), 127 (21), 112 (100)

C21-amide

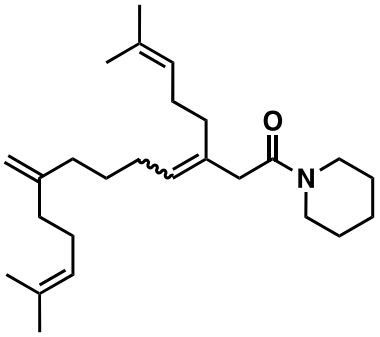

LR-MS m/z (%): 385 (8), 342 (4), 316 (78), 303 (7), 248 (15), 220 (6), 189 (12), 127 (86), 112 (100)

N,N-dibutylnona-3,8-dienamide

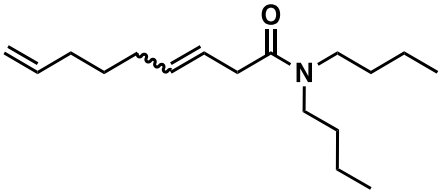

LR-MS m/z (%): 265 (35), 224 (22), 210 (15), 182 (23), 156 (95), 137 (2), 128 (30), 109 (7), 86 (100)

1-morpholinonona-3,8-dien-1-one

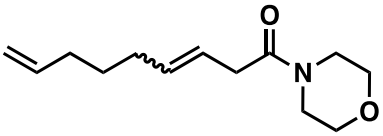

LR-MS m/z (%): 223 (25), 208 (16), 180 (84), 154 (18), 140 (98), 114 (27), 109 (67), 95 (57), 86 (100), 81 (96), 72 (7)-.

N-methyl-N-phenylnona-3,8-dienamide

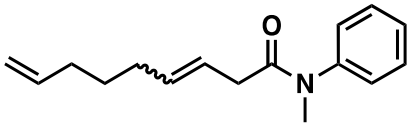

LR-MS m/z (%): 243 (6), 228 (1), 200 (2), 188 (3), 175 (16), 160 (5), 137 (3), 107 (100), 95 (6), 77 (25).

N-mesitylnona-3,8-dienamide

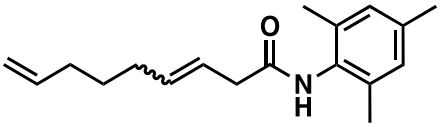

LR-MS m/z (%): 271 (12), 216 (1), 188 (2), 174 (2), 135 (100), 120 (11), 91 (14).

5. Amination of carboxylic esters

5.1. Abstract

This chapter investigates the direct conversion of esters into primary amines. Fatty esters are a readily available and renewable resource, making them a desirable starting material for the chemical industry. The presented approach aims to reduce the number of reaction steps, increasing overall efficiency and saving energy and resources. Several ruthenium catalysts were tested. Milstein's catalyst yielded 82 % in the amination of alcohols, but it was not effective in reducing esters. The Ru/triphos catalyst system was successful in both parts of the reaction, achieving the highest yield of 68 % in the ester hydrogenation. Additionally, the catalyst was capable of facilitating the combined ester amination, which was achieved as a one-pot reaction with a yield of up to 49 % for hexylamine. Ammonia had to be added to the reaction after the ester reduction step for successful conversion. To achieve auto-tandem catalysis, a modified triphos-xyl ligand was synthesized. However, we did not observe any improvement despite using the new ligand.

This chapter is in parts based on the following works which were adopted in parts, extended and modified:

Bachelotheses:

a) Niklas Kost (2019): Synthese des Milsteinliganden und seine Anwendung in der Esteraminierung, TU Dortmund
b) Annika Schmidt (2020): Ester amination and other homogeneous catalyzed applications of a xylene-modified triphos ligand, TU Dortmund
c) Bernd Rienhof (2020): Synthesis of xanthene-based pyrrole-functionalised ligands and investigation of their performance in hydroaminomethylation, TU Dortmund

Masterthesis:

d) Georg Beckmann (2021): Amination of esters - Investigation and optimization of ligands and reaction conditions, Master Thesis, TU Dortmund

5.2. Introduction

The demand for products from renewable resources are constantly rising, due to the increasing avoidance of fossil based raw materials. A common drawback for renewable feedstocks is their availability. Limited space for agriculture and the competition with food production must be considered.[77]

Fatty acids and esters are a readily available class of renewable compounds that can be sourced from vegetable fats and oils. They are produced on a very large scale, but when produced from plants, they compete with the food sector. Therefore, algae and yeast are gaining increasing attention in the research community for the purpose of producing bio-based oils.[78,79] Although mainly focused on the production of bio fuels, algae and yeast cells can be modified to produce fatty acids more effectively than growing crops and avoids the rivalry with food production.[80] Fatty acids and esters have the advantage that they already consist mainly of hydrocarbon chains, which makes them similar to petrol based feedstock and a good fuel source. The same is true for the chemical industry, as many processes relay on low functionalized carbon chains to start with. Also, the ester or acid group can be targeted selectively for chemical conversions.

Besides reduction to alcohols and aldehydes, amines can be synthesized consecutively. As described in the previous chapter amines are popular intermediates in the chemical industry. In the industry fatty amines are often used for the production of surfactants, which are typical

additives for dyes or detergents.[81,82] Due to their long carbon chain and the amine functionality, fatty amines can be readily converted into amphiphilic tensides.

There are three main synthesis routes (Figure 45) starting form carboxylic acids or esters:[83]

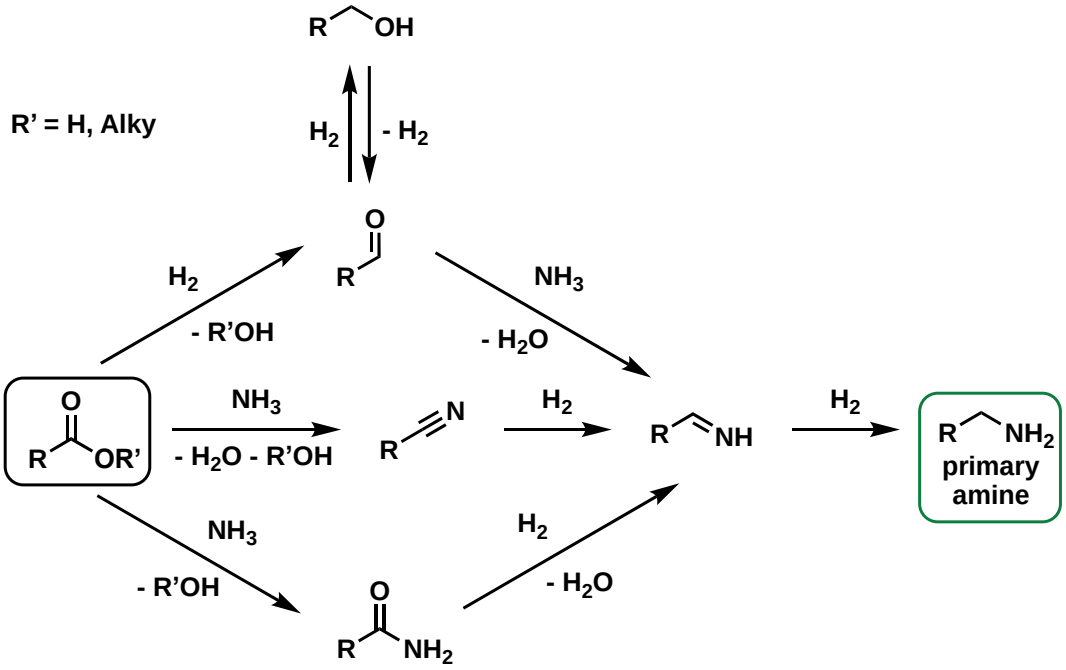

Figure 45: Amination of carboxylic acids and esters.

Starting from the acid or ester all three pathways proceed *via* different intermediates, *i.e.* aldehyde, nitrile, or amides. Notably, all pathways come together and continue *via* an imine and finally yield the desired primary amine in a final hydrogenation step.

In the amide route, the synthesis commences with the condensation of the carboxylic acid and ammonia (Figure 45, bottom), forming an amide. This is followed by a second step, which involves the hydrogenation of the carbonyl group within the amide, ultimately producing the imine intermediate (Figure 46).

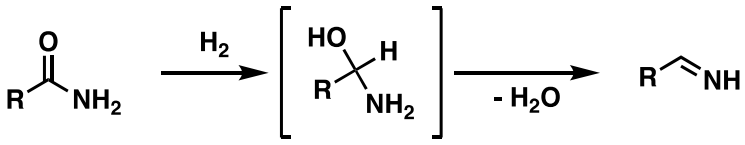

Figure 46: Hydrogenation of amides proceeding via C–O cleavage.[84]

The nitrile route begins with the conversion of the ester to a nitrile using ammonia (Figure 45, middle). Subsequently, the nitrile is hydrogenated to form an imine, which is further hydrogenated. This results in the coexistence of significant amounts of both imine and amine in the reaction vessel. The primary amine formed may react with the imine, leading to the formation of secondary amines. This undesired side-reaction can reduce the overall selectivity of the reaction.

For the alcohol route, the synthesis typically starts with the hydrogenation of the ester to form the corresponding alcohol (Figure 45, top). Notably, the conversion of carboxylic esters to the alcohol is favored over employing carboxylic acids as the stating material due to the milder reaction requirements. Afterward, alcohol is transformed through a hydrogen shuttle type reaction, wherein no additional hydrogen is introduced into the reaction; instead, the hydrogen originating from the oxidation of the alcohol remains bound at the catalyst center.[85] Following the formation of the imine through condensation of the aldehyde with ammonia, and a hydrogen transfer reaction, converting the imine into the desired amine. Consequently, only catalytic

amounts of the imine remain present within the reactor, with an excessive supply of ammonia serving to prevent undesired reactions with the product amine. This specific approach allows for high selectivity to be achieved while operating under mild reaction conditions. However, it is worth noting that the reaction tends to proceed at a relatively slow rate.

Although a tandem catalytic amination starting form a carboxylic acid or ester would save at least one reaction step. Only few studies on the subject were published (Figure 47).

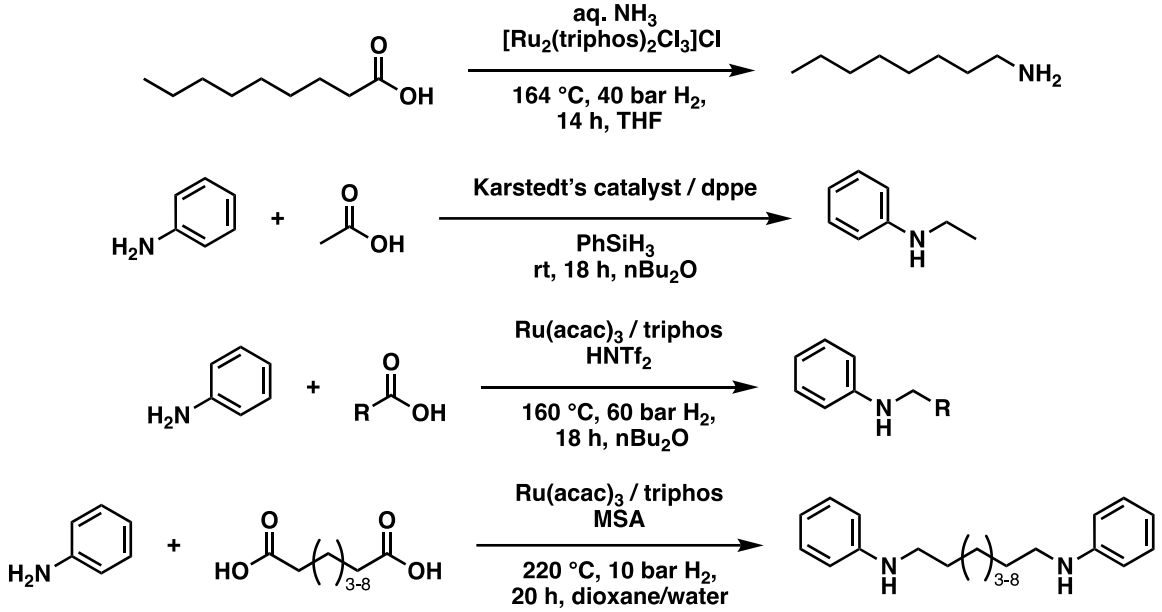

Figure 47: Amination of esters describes in the literature.[86–89]

The group of COLE-HAMILTON published an alkylation of ammonia with nonanoic acid in 2007.[87] Utilizing a $[Ru_2(triphos)_2Cl_3]Cl$ catalyst the group achieved 49 % of primary nonylamine. In the study aqueous ammonia was the key since liquid ammonia only reached 15 % yield.

This preference leans toward the reduction pathway involving aldehydes or alcohols. Given the utilization of reductive reaction conditions, the likelihood of hydrogen-shuttling mechanisms is low.

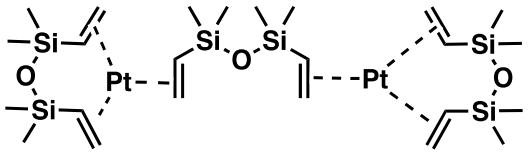

Figure : KARSTEDT's catalyst.

In 2014, BELLER and coworker published an article about the alkylation of amines using carboxylic acids using KARSTEDT'S catalyst. However, silanes were employed quantitatively as the reducing agent, which leads to the production of large amounts of waste.[88] One year later, the same group published the same reaction conducted with molecular hydrogen using a Ru/triphos catalyst system.[89] In 2017, the COLE-HAMILTON research group contributed two papers addressing the conversion of diacids through this amination route.[86,90] One of these papers focused on the synthesis of cyclic amines, while the other aimed at producing α-ω-diamines, a development of significant interest to the polymer industry. A one-pot reaction involving aniline as the amine source accomplished impressive results, with yields reaching up to 98 % form α-ω-diacids. In the case of phenyl esters, yields of 96 % were reached.[86]

However, ammonia-based reactions appear to be more challenging, since only sequential reactions proved successful. In this approach, the reduction occurs first without the presence of ammonia, followed by the amination step, resulting in yields of up to 83 % for the conversion of 1,12-dodecandiacid and 79 % for the dimethyl ester.[86]

In 2020, DE VOS proposed an amide pathway catalyzed by a heterogeneous $RuWO_x$-catalyst, demonstrating high selectivity within a one-pot reaction.[84] Branched acids could be efficiently converted into their corresponding amines, achieving yields of up to 96%. However, linear acids present a more formidable challenge, offering yields of only 81%. A drawback of their work is the high catalyst concentration of 5 mol% Ru and the large excess of ammonia. Since linear aliphatic amines are in high demand by the chemical industry, achieving improved performance in their synthesis remains an area of interest, despite the inherent challenges.

5.3.Goals

With the continuously rising demand for renewable and plant-based products the synthesis of primary amines form fatty acids, and their esters is a highly anticipated path since they can be sourced in relatively large quantities. The transformation has already been shown in the literature, however under not ideal conditions.

Currently the reaction sequence suffers from either poor selectivity or is carried out sequentially in more than one reaction step. To reduce the amount of waste produced during the process**, a one pot reaction and ideally tandem-catalyzed reaction profile** could eliminate workup procedures in between the reaction steps.

Another way to reduce the resource demand of the reaction is to optimize the efficiency of the reaction. Large excess of starting material might increase the selectivity of the reaction or lead to the complete conversion of the other reactants. However, this leads to high recycle streams or excessive waste production. Additionally, very expensive transition metals, such as ruthenium are used as the catalyst, which lead to high cost, if used in large amounts, especially on large scale processes.

Therefore, **optimized reaction conditions** and a **tailored catalyst system** are essential for an efficient transformation. Since at least two reaction steps are required both reactions are investigated separately at first to obtain a deeper understanding of each reaction. Following the work of COLE-HAMILTON and coworkers the ester reduction and alcohol amination are examined. For the alcohol amination the benchmark system is MILSTEIN'S catalyst and was tested for both partial reactions. The Ru/triphos catalyst system was chosen for ester reduction and investigated likewise for both partial reactions. First, the commercially available triphos is tested and used to find the optimal reaction condition in the present hardware. Afterwards, the ligand will be modified to improve the catalyst's performance. By adding more sterically demanding and electron rich ligands to the catalyst higher activities and yields should be possible.

However, these **ligands and catalyst have to be first synthesized**.

5.4. Alcohol amination

The commercial synthesis of primary amines is mostly done via the reaction of alcohols with ammonia (Figure 48). Even though the process requires harsh reaction conditions and results in a mixture of primary, secondary, and tertiary amines.[91]

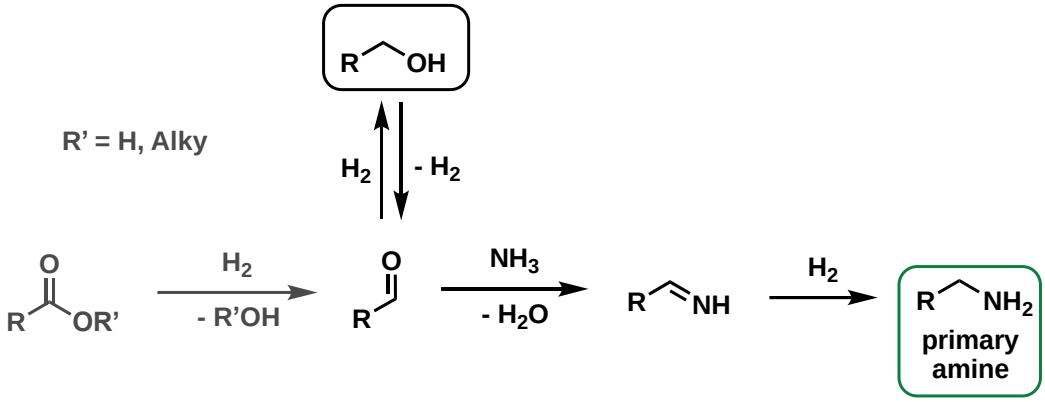

Figure 48: Reaction overview: alcohol amination for the synthesis of primary amines.

One reason for the mixture of products in the heterogeneous catalyzed process is the formation intermediate aldehydes and the fact that the primary amine is more nucleophilic than ammonia. Additionally, the first conversion into the primary amine is almost thermoneutral, while the second alkylation being exothermic and therefore favored. Hence, the desired primary amine undergoes consecutive reactions (Figure 49).[83]

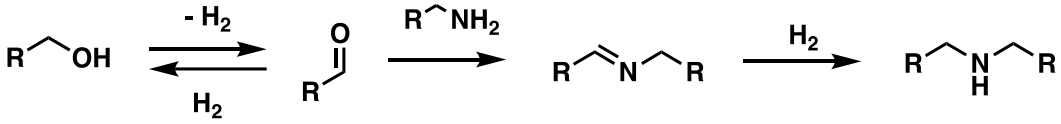

Figure 49: Amination of alcohols resulting in consecutive reactions.

Nevertheless, the process is used on large scale for the production of simple amines, *e.g.* ethylamine and butylamine. In this process the side products can also be sold as valuable intermediates or reactants.[83] Depending on the demand for each product the products can also be recycled into the process and therefore control the output. Especially for the selective synthesis of the primary amine large recycle streams are necessary, reducing the overall efficiency of the process. The primary benefit of using a heterogeneous catalyst is its recyclability, which justifies lower selectivities. In comparison homogeneous catalyst can achieve higher selectivities for the primary amine, but they are difficult to recycle.[83]

In 2008 MILSTEIN and coworkers discovered, that a variation of their PNP pincer ligands based on an acridine backbone can selectively form primary amines using alcohols and ammonia.[92] This new ligand lacks the typically pyridinylic group which promotes a hydrogen borrowing mechanism (Figure 50).[92–94]

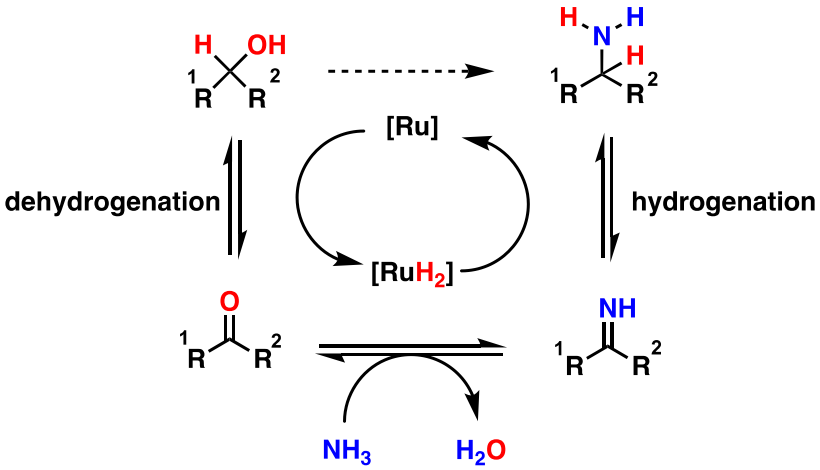

Figure 50: Hydrogen shuttle mechanism for the amination of alcohols.

The mechanism was described by MILSTEIN and BELLER for primary and tertiary amines respectively.[92,95] In 2014, the group of VOGT investigated the mechanism more in more detail using a Ru/Xantphos catalyst system.[94] A dihydrido Ru species was identified as the main catalytic intermediate. Additionally, the publication describes the low steady state concentration of the intermediate imine species as a crucial bottleneck in the reaction which leads to low reaction speeds and long reaction times. The solution of the group was to add a small amount of ketone to the reaction mixture, which sped up the reaction significantly. The model reaction used was the amination of cyclohexanol, hence leading to branched primary amines.[94]

In the same year HOFMANN and coworkers studied the mechanism for the acridine based catalyst system discovered by MILSTEIN with cyclohexanyl modifications.[96] Since then the catalyst has been used many different types of alcohol to amine conversion and led to more sustainable amine synthesis.[97] One explanation for the outstanding performance of the acridine base pincer ligands is the corporation of the ligand with the Ru metal center by reversible dearomatization (Figure 51).

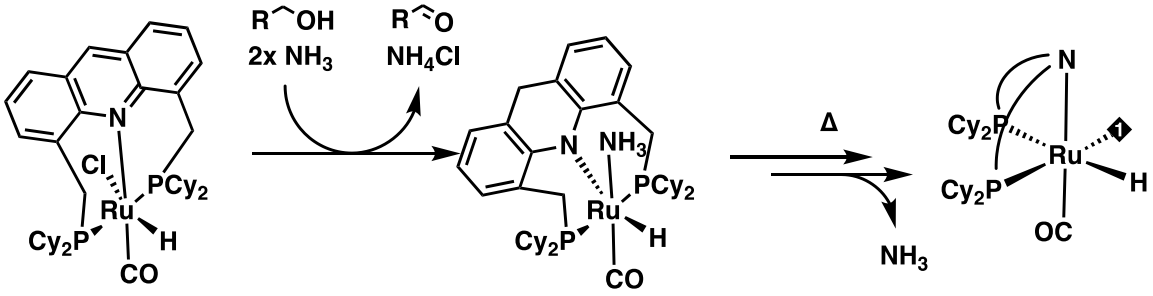

Figure 51: Dearomatization of the acridine based ligand.

This complex is readily formed by the oxidation of the alcohol and stores hydrogen. Subsequently, the ligand is reduced to a new species at elevated temperatures (Figure 51). The reduction of the imine, involving the formation of a penta coordinated Ru amide intermediate and subsequent protonation by an alcohol, was identified as the turnover- and selectivity-determining step (Figure 52).

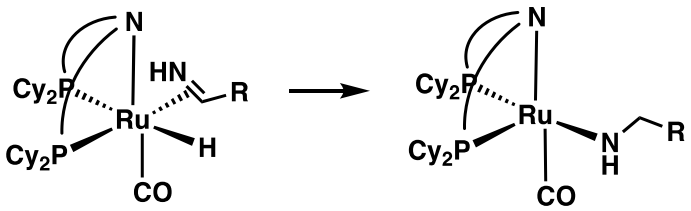

Figure 52: Rate-limiting step of the catalytic alcohol amination.[96]

Interestingly, the group of HOFMANN found with their DFT calculations that the catalytic cycle is completed assisted by an alcohol rather than the ligand. The ligand stays in his hydrogenated form and does not undergo re-aromatization for the course of the catalysis.[96] In 2015 the group of SCHAUB, who was also involved in the studies by HOFMANN, published cationic catalyst species for the amination with ammonia.[98] This, for the reaction new, type of catalyst undergoes a different catalytic mechanism and requires a minimal amount of aldehyde which is formed in a catalytic cycle involving ammonium chloride ions. When compared to MILSTEIN'S catalyst the new triphos based catalyst cannot achieve such high yields and reaches up to 52 % without additives (Table 16, entry 3).[98] However, the triphos system performs better than the xantphos based system which reaches only 11 % primary amine yield with the lowest selectivity of 69 % under the tested conditions (Table 16, entry 6).[98] In a different set up with p-xylene as the solvent instead of toluene, the performance could be more than doubled (Table 16, entry 7).

One year later, the same group was able to increase the selectivity of the triphos system and could achieve similar yields and selectivities compared with Milstein's catalyst (Table 16, entry 4, 5). The challenge is the selectivity towards the linear primary amines since they are more prone to consecutive reaction due to lack of sterically hindrance.

Table 16: Comparison of literature reaction systems for primary aliphatic amines.

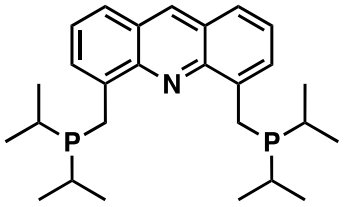

L1

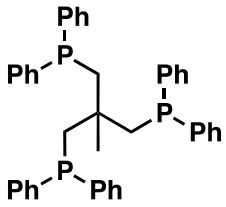

L2

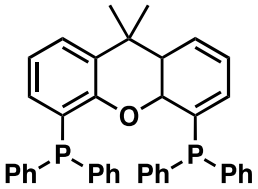

L3

Entry	Ligand	t [h]	T [°C]	NH_3	Ru [mmol]	X [%]	S [%]
1[92]	L1[a]	12	155	7.5 bar	0.1	99	79
2[98]	L1[a]	12	155	35-40 bar	0.1	99	95
3[98]	L2	15	165	6 bar	0.2	63	83
4[99]	L2[a]	15	165	7-8 bar	0.2	99	97
5[99]	L2	15	165	7-8 bar	0.2	98	95
6[98]	L3	12	155	35-40 bar	0.1	16	69
7[100]	L3	12	155	6 eq.	0.1	30	77
8[101]	L3	20	140	60 eq.	3	99	79

a: Catalyst used as an ex situ formed complex.

A big advantage of the triphos reaction system, compared with the acridine-based system, is the commercial availability. The acridine-based ligands are not available on the market, whereas triphos and xantphos are readily available. Nonetheless, MILSTEIN'S catalyst is an interesting starting point since similar catalyst are also known for ester hydrogenation capabilities.

5.4.1. Starting with the benchmark

Due to the ligand being not commercially available the first step was to synthesize the 4,5-bis((diisopropylphosphinyl)methyl)acridine ligand from acridine (Figure 53).

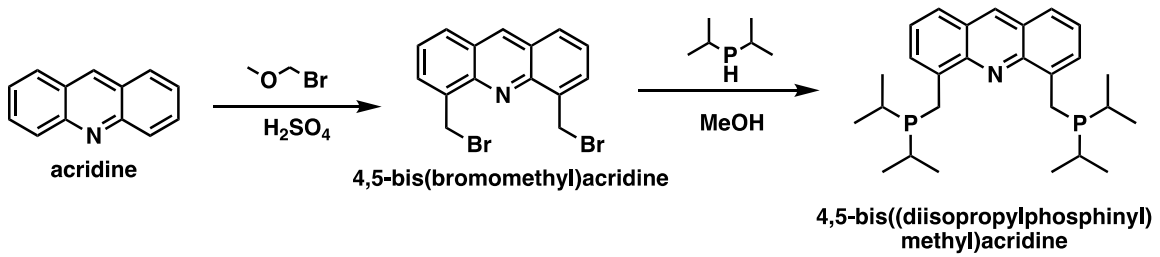

Figure 53: Reaction scheme for the synthesis of 5-bis((diisopropylphosphinyl)methyl)acridine.

The ligand is synthesized starting from the acridine which is bromomethylated in sulfuric acid with bromomethyl methyl ether (BMME) in the first step to give 4,5-bis(bromomethyl)acridine.[102] Phosphorous is added by nucleophilic substitution of the bromide with diisopropylphosphine in methanol. To form the active catalyst an *ex situ* preformation is necessary. For the complex formation $HRu(PPh_3)_3Cl(CO)$ is combined with the acridine based ligand in toluene (Figure 54).

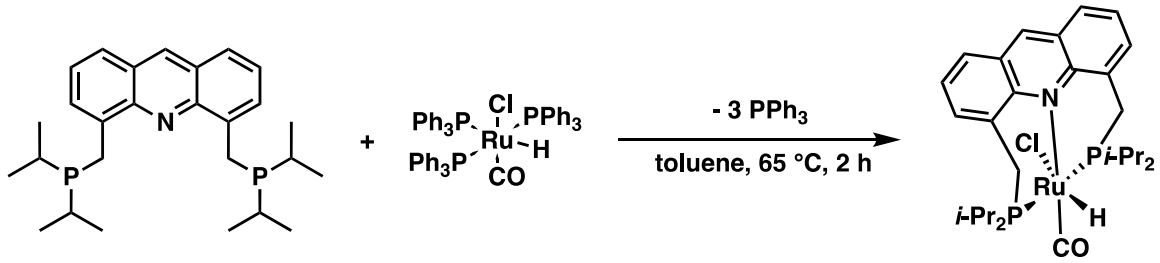

Figure 54: Formation of the Ru catalyst complex with the acridine based ligand.

This step yields the desired complex as solid, describes as stable in air for several month, in contrast to oxidation prone free ligand.[92]

5.4.1.1. Synthesis of 4,5-bis(bromomethyl)acridine – BMME route

The synthesis was carried out after Galy[102] with BMME (Figure 55).

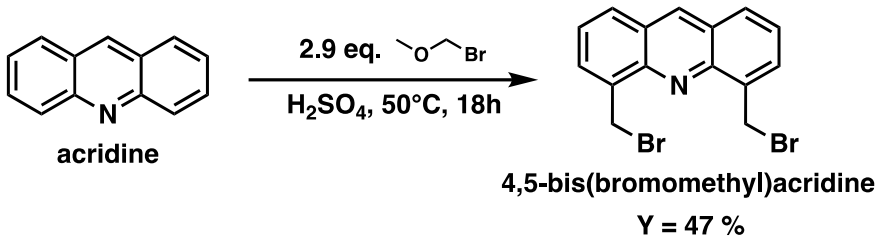

Figure 55: Synthesis of 4,5-bis(bromomethyl)acridine.

In the initial experiment, conducted on a 5 mmol scale, the reaction mixture was quenched by pouring it onto ice after 34 h reaction time. A bright orange solid precipitated, necessitating filtration. However, the obtained solid was sticky and remained at the flask's wall, despite using 170 mL of chloroform to wash out the product. The residue was filtrated off and discarded, which could still contain a small portion of the desired product. A subsequent crystallization from chloroform and diethyl ether yielded a pure product with a poor yield of 24 %. This low yield could be attributed to losses in the remaining solid and during the recrystallization process. Additionally, the dissolution of the product under reflux chloroform required a larger quantity than anticipated, reducing the effectiveness of the recrystallization.

A second attempt at recrystallization resulted in co-crystallization and a product of low purity. The recrystallization procedure was then modified, with the crude product being dissolved in dichloromethane and cyclohexane was used to decrease solubility. This adjustment increased the yield to 47 % of the desired product.

To scale up production to 33.8 mmol, dichloromethane (DCM) was employed for product extraction, dissolving more of the side product. Consequently, the crude product was dissolved in chloroform, and the side products were filtered off. The recrystallization, following the modified procedure from the second synthesis, yielded 41 % of the product. The lower yield can be explained with the second filtration step, which sacrificed some of the product to achieve higher purity.

For future syntheses BMME should be replaced since it is carcinogenic, toxic, and volatile. Alternatives are longer chain bromomethyl ether such as bromomethyl octyl ether, which is also suspected to cause cancer, but has a high boiling point rendering it less volatile and easier to handle.[103,104] Another alternative is a different synthesis route.

5.4.1.2. Synthesis of 4,5-bis(bromomethyl)acridine – zinc bromide route

An alternative is a reaction analogous to the BLANC reaction, which is a chloromethylatation[105–107]

Figure 56: BLANC reaction with benzene.

In this process paraformaldehyde, HCl and zinc chloride are used to chloromethylated aromatics. A combination of HBr and zinc bromide leads to the bromine analog.[108] For the desired ligand the first step is the electrophile addition of a protonated formaldehyde to the acridine backbone, promoted by the zinc bromide. Then a nucleophilic substitution of the protonated hydroxyl group by bromine.

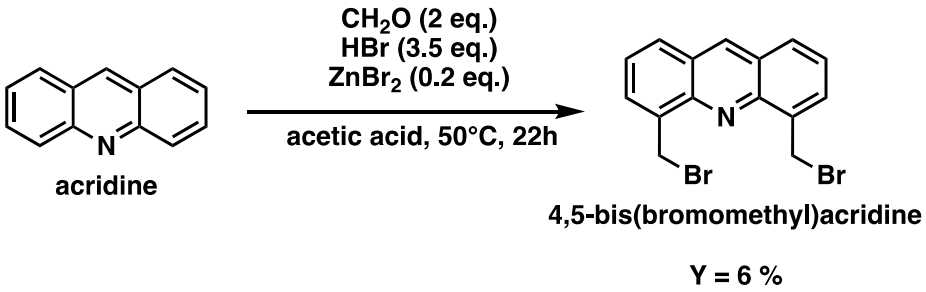

Figure 57: Bromomethylation of acridine with paraformaldehyde and HBr.

The reaction was carried out after VAN DER MADE.[108] Only 6 % yield could be achieved and a low purity of the desired product. This could be explained by low activity of acridine, as also observed above. VAN DER MADE used activated xylene derivatives which resulted in excellent yields.[108] The nitrogen is a most likely protonated under the given conditions, hence is loses its π-electron donating effect and does not contribute with a +M-effect to the reactivity of the acridine system. In addition, nitrogen has a low -M-effect, resulting in a deactivation of the system. Even with the extended reaction time no sufficient yield could be achieved, also leading to a poor selectivity. The side products have an almost equal polarity resulting in a difficult separation and poor purity. Other activation mechanism should be considered in follow up research on synthesis of acridine-based ligands.

5.4.1.3. Synthesis of 4,5-bis((diisopropylphosphinyl)methyl)acridine

The next step in the synthesis sequence is the introduction of diisopropyl phosphine. According to MILSTEIN a 2.55 fold excess of the phosphine was used (Figure 58).[92]

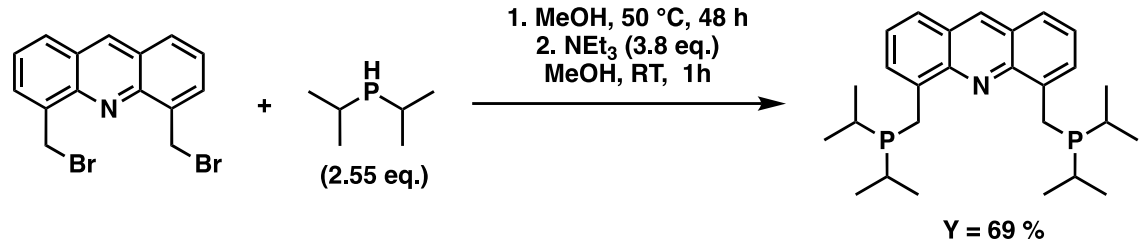

Figure 58: Synthesis of 4,5-bis((diisopropylphosphinyl)methyl)acridine.

After completion of the reaction time, triethylamine was added. The amine deprotonates the intermediate phosphonium ion to the desired phosphine and a color change from orange to yellow could be observed, confirming the progress of the reaction. The crude product was separated from the solid triethylammonium bromide and the remaining yellow oil was crystallized from a mixture of acetone and pentane. At first minimal amount of hot acetone was used to dissolve the solid and then pentane was used to lower the solubility. Afterward, the mixture was cooled down slowly. For the formation of crystals, the mixture was stored at 4 °C for several days. Crystals have formed, however they immediately melted during the filtration process at room temperature.

Finally, the crystallization was carried out over night at -20 °C, followed by cold bath at -50 °C. This procedure led to a larger quantity of crystals, which were washed with cold acetone seven times at -50 °C. The desired ligand could be isolated as a bright yellow solid with a yield of 54 %. In a final batch directly applying the improved purification procedure a yield of 69 % could be achieved. The yield could potentially be improved by a longer period at lower temperatures, e.g. in a -40 °C freezer.

5.4.1.4. Synthesis of Milstein's catalyst

Since the ligand is rarely used as an *in situ* catalyst and higher stability of the Ru complex the ligand was converted completely. The synthesis of the catalyst complex was carried out after MILSTEIN (Figure 59).[92]

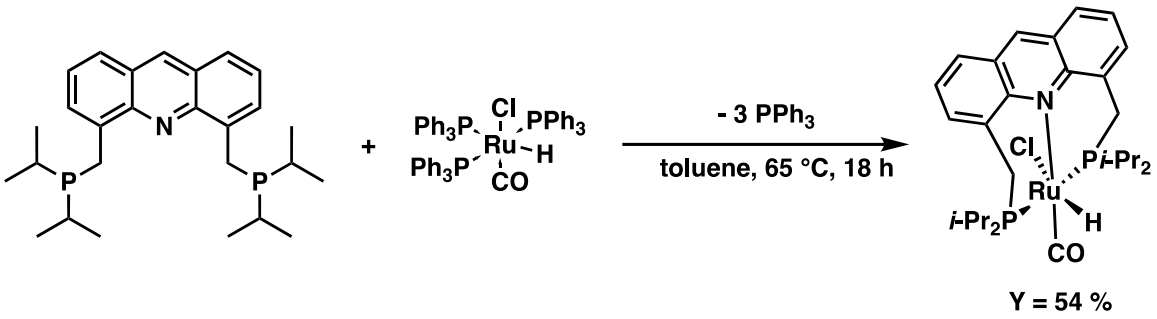

Figure 59: Synthesis of Milstein's catalyst. [92]

Freshly washed ligand and the Ru precursor were combined and stirred for 2 h, but the ligand was still not converted fully so the reaction was prolonged until the next day. After the reaction there was a black precipitate at the bottom of the flask, which points to elemental ruthenium. The elemental ruthenium could be caused by impurities in the Ru precursor, or some of the catalyst was already destroyed during the synthesis. Therefore, a more precise control of the reaction time should be implemented in further synthesis.

Nevertheless, the crude yield of the catalyst could be increased to 80 % from prior failed attempts. The key was a precipitation from tetrahydrofuran (THF) at room temperature with pentane. In prior attempts a hot crystallization was carried out at 60 °C and lead to insufficient purification.

High purity could be achieved by washing the complex several times with small amounts of cold (0 °C) toluene and pentane subsequently. Afterwards the catalyst was dried under vacuum. Due to the many NRM samples during the purification the overall yield was only 54 %.

For future syntheses the use of freshly washed ligand is important, or ligand that was stored in a glove box which was not available at the time of the synthesis. This prevents oxidized or partial oxidized ligand which is difficult to remove from the catalyst in the purification step at the end. As mentioned, a shorter reaction time would also be helpful to prevent unnecessary side product. Additionally, less pentane and colder temperatures should be used for recrystallization for a longer time to obtain a more complete crystallization. finally soring the ligand and the catalyst in a glove box under inert conditions would help to prevent oxidation, since the alkyl phosphine ligand is relative labile.

In the next step the complete catalyst is used for alcohol amination as the first part of the

5.4.1.5. Note on the literature

Especially for the synthesis of the acridine based Milstein ligand the existing literature lacks detail. Therefore, trial and error procedure was necessary, which resulted in several unsuccessful experiment that could have been prevented. Some mistakes seem obvious retrospectively, however a more detailed and clear description of the procedure could have prevented this. The use of the correct terminology is of high importance when describing chemical experiments *e.g.* “wash” *vs*. “extract”. To wash a compound implies washing out impurities which have a higher solubility in the washing medium than the desired product. In contrast to extract a compound is the opposite i.e., the desired product has a higher solubility in the extraction medium than the impurities leading to a product enriched extract.

Furthermore, exact condition for purification steps such as pressure, temperature or ratio of solvents used in a mixture are rarely provided. This was especially problematic during the synthesis of the ligand. A normal -23 °C freezer was not sufficient for the crystallization and since no temperature was provided, we looked for the problem elsewhere, hence wasting time and recourses. At the time no -40 °C freezer was available so, reducing the temperature to this level was not possible for an extended time. Finally, a discussion with DENNIS PINGEN lead us to the conclusion that lower temperatures are necessary and paved the way for the successful synthesis.

5.4.1.6. Alcohol amination with the acridine based Milstein ligand

The MILSTEIN ligand is very promising for the overall reaction due to its high performance in alcohol amination. The first step is to reproduce these results and the second to align the reaction conditions with the reaction conditions of the ester hydrogenation to prepare the overall reaction for ester amination. Hexanol was chosen as the model substrate since it is readily available and easy to quantify *via* GC (Figure 60).

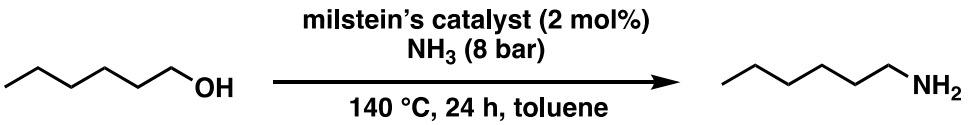

Figure 60: Initial reaction conditions.

At first the ligand was tested, as other systems such as Ru/Xantphos can be carried out without degassed substrates (Figure 61).

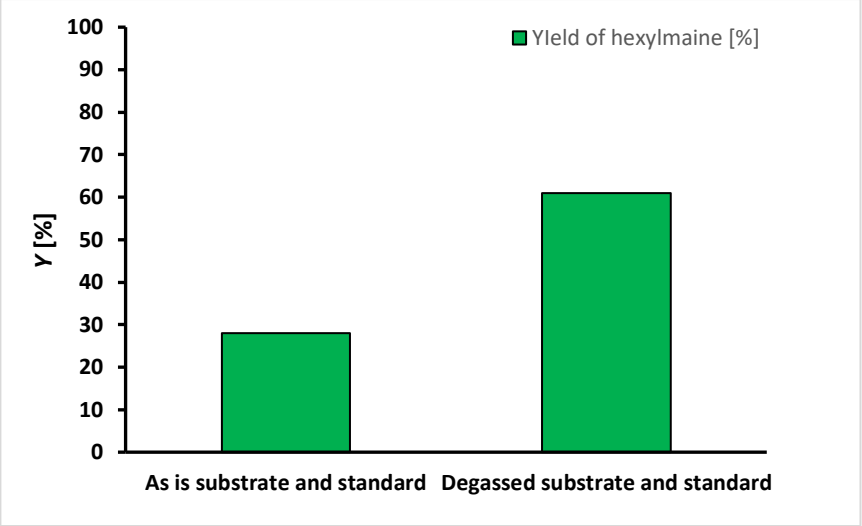

Figure 61: Comparison of as is and degassed standard and substrate in the amination of hexanol. Conditions: 9.5 mmol hexanol, 10 mg catalyst, 200 mg NH_3, 3 mL toluene 24 h, 140 °C, 700 rpm. Quantification via GC with decane as internal standard.

The results show, a high dependency on the oxygen content in the reactor. In contrast to the highly stable Ru/Xantphos catalyst system, which was investigated by other members of our group, MILSTEIN'S catalyst requires the complete absence of oxygen in the reactor for high yields.

Next, the dilution of the alcohol was investigated, which can influence the reaction performance in two ways. First, the reaction solution is more diluted which can reduce the formation of secondary amines, due to fewer collisions. Second, the amount of ammonia is kept the same, so the ratio of ammonia:alcohol also increases with a higher dilution.

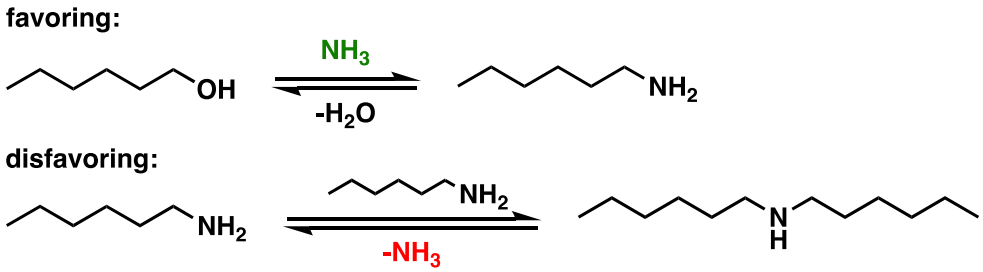

Figure 62: Influence of an excess of ammonia in the amination of alcohols.

After LECHATELIER the equilibrium of a reaction will oppose the excess of reactants or products, hence an ammonia excess would favor the formation of hexylamine with ammonia and disfavor the formation of dihexylamine from two hexylamines which releases ammonia (Figure 62). The alcohol content in the reaction mixture was reduced from 9.5 mmol to 1.5 mmol (Figure 63).

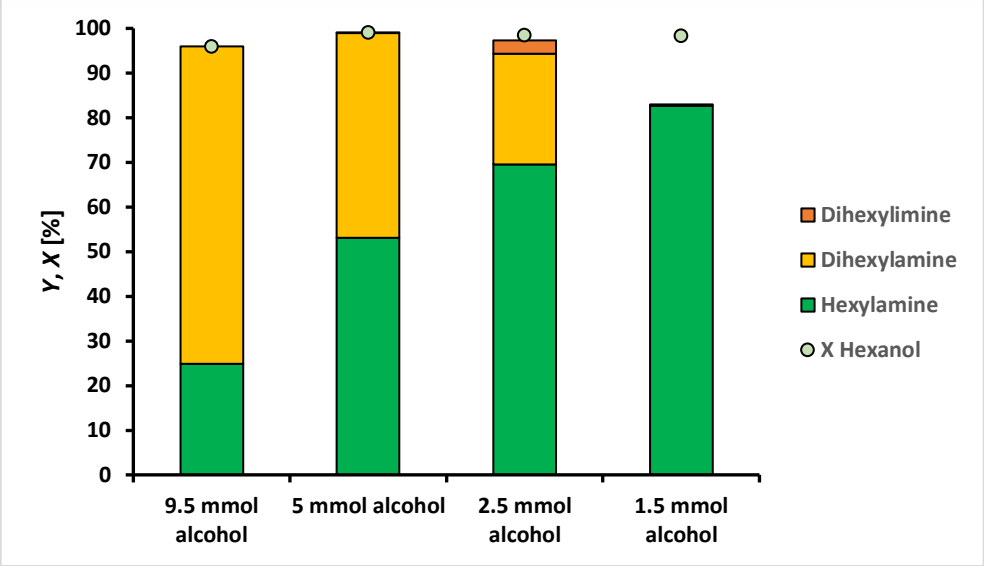

Figure 63: Reduction of the alcohol amount in the amination reaction with MILSTEIN's ligand. Conditions: Conditions: hexanol, 1.7 µmol MILSTEIN's catalyst, 200 mg NH_3, 3 mL toluene 24 h, 140 °C, 700 rpm. Quantification via GC with decane as internal standard.

The alcohol was almost fully converted in each case. Since the reaction time was relatively long even 9.5 mmol alcohol, which correspond to a small excess of 1.2 NH_3, could be converted completely. However, the main product in this reaction is dihexylamine. As explained above, hexylamine is more reactive than ammonia in the amination reaction of alcohols and results in an exothermic reaction, while the formation of hexylamine with ammonia is thermo-neutral. By diluting the alcohol amount in the reaction mixture, in this case using less alcohol, increases the amount of the desired primary amine as expected. At 1.5 mmol hexanol 83 % hexylamine are achieved (Figure 63). Surprisingly, only traces of dihexylamine were detected and some alcohol reacted to unknown side products.

During the dilution series the ammonia excess increases from 1.2 to 7.8 eq. since the amount of ammonia is kept constant. However, this method reduces the scale of the time-space-yield of the reaction with decreasing reference amount for higher excess of ammonia and dilution. Additionally, the catalyst loading is decreased by the dilution. In terms of mol% the relative amount changed from 0.18 mol% to 1.1 mol% catalyst. Another method is adding more ammonia to the reaction to increase the excess of the reagent without diluting the alcohol significantly (Figure 64).

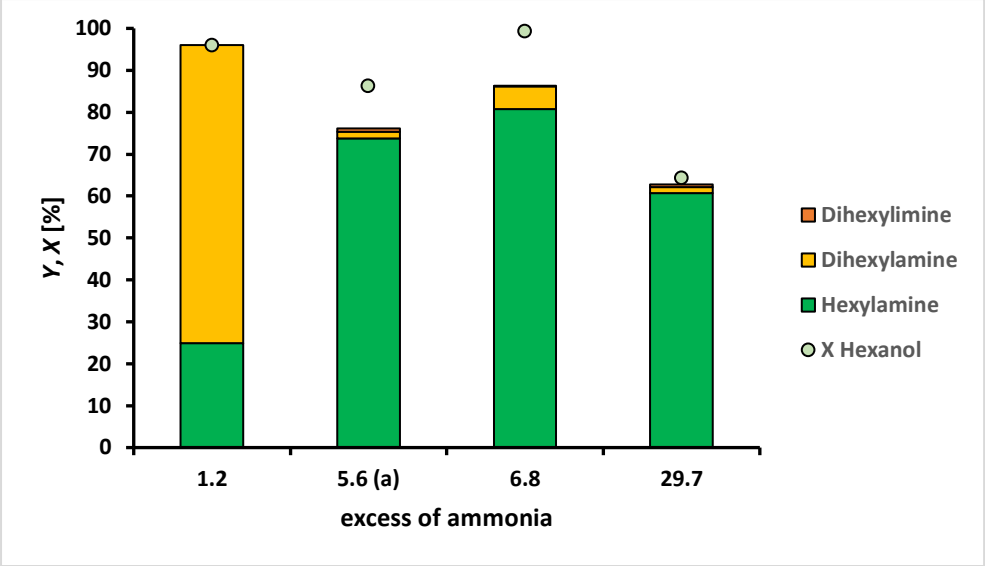

Figure 64: Influence of elevated ammonia content in the amination of hexanol with Milstein's catalyst. Conditions: hexanol 9 mmol, 0.18 mol% Milstein's catalyst, NH_3, 3 mL toluene 24 h, 140 °C, 700 rpm. Quantification via GC with decane as internal standard.

Rising the ammonia content in the reaction mixture results in a better performance of the reaction until 6.8 eq. of ammonia with a yield of 81 %. Under these reaction conditions the relative catalyst amount is 0.18 mol% and reaches a similar yield compared to the experiment with less alcohol and a relative catalyst amount of 1.1 mol%. The ammonia excess is with 6.8 and 7.8 in a similar range.

Increasing the ammonia content further to an excess of 29.7 leads to a drop in conversion and yield which can be caused by too much ammonia in the coordination sphere of the catalyst. In this case the ammonia inhibits the access of hexanol to the active catalyst center and slowing down the reaction significantly.

Another catalyst system well known for the amination of alcohols and for the desired consecutive reaction is the Ru/triphos catalyst.

5.4.2. Triphos as a commercially available alternative

In 2016 SCHAUB and colleagues, have demonstrated that triphos can be a viable alternative to MILSTEIN'S catalyst. Triphos, like MILSTEIN'S catalyst, maintains a stable coordination sphere around the central ruthenium atom, resulting in high selectivity for primary amines.[99]

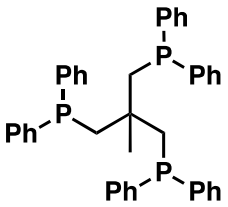

Figure 65: Triphos ligand.

Additionally, the triphos system has already been utilized by COLE-HAMILTON'S group for ester amination reactions which is the main goal for this chapter. Therefore, the focus was on the Ru/triphos catalyst system for this part dissertation. Another advantage of triphos is that it is commercially available, especially with larger scale reactions. For a direct comparison, hexanol was chosen as the model substrate (Figure 66).

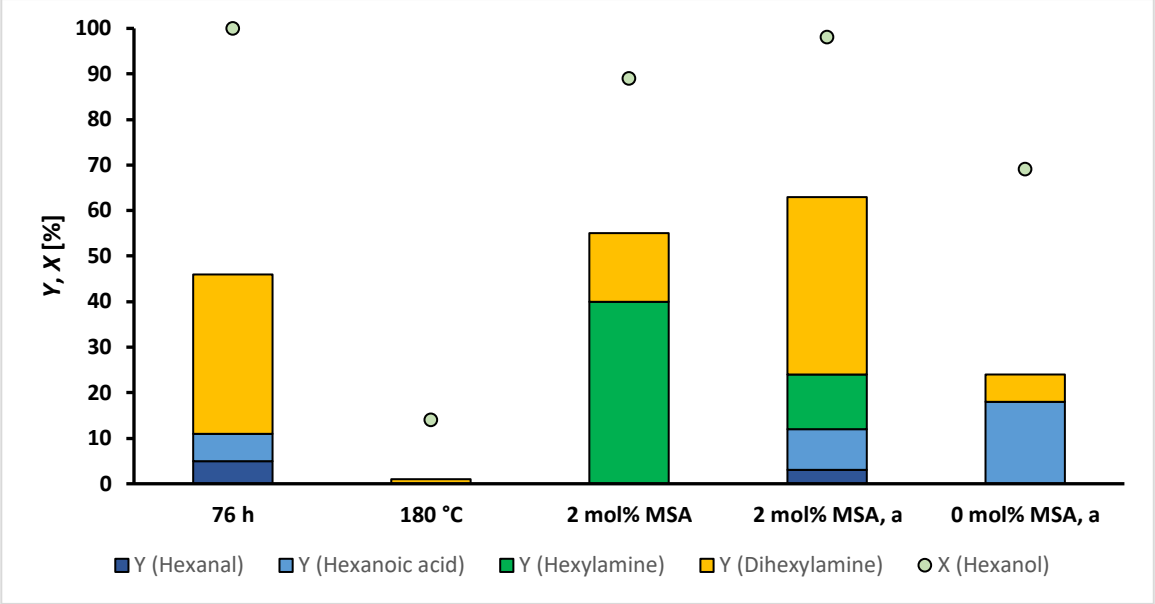

Figure 66: Optimization of alcohol amination of hexanol. Conditions: $Ru(acac)_3$ 2 mol%, triphos 4 mol%, 0.38 mmol hexanol, MSA 4 mol%, dioxane (3.5 mL), water (1 mL), di-n-butyl ether (100 mg), 10 bar H_2, NH_3 10 eq., 220 °C, 20 h. a = $HRuCl(CO)(PPh_3)_3$ (adapted from SCHMIDT 2020[109]).

Different reaction times, temperatures and methanesulfonic acid (MSA) content was screened at first (Figure 66). Long reaction times of 76 h lead mainly to a formation of dihexylamine and high amounts of products that are not detectable by GC since the difference between the combined yield and conversion is large. As most of the other amination reactions in literature[101,110,111] are carried out at lower temperatures, next, the reaction temperature was decreased to 180°C. However, almost no conversion of hexanol was observed with only modest amounts of the secondary amine being formed. With the system proposed by COLE-HAMILTON using MSA (Figure 66, 2 % MSA) hexylamine was formed with 40 % yield and dihexylamine with 15 % as a side product. Higher catalyst activity could be achieved by the use of $[HRuCl(CO)(PPh_3)_3]$ as precursor because it is closer to the active catalyst species and only the triphenyl phosphine ligands must be changed by the triphos ligand. However, this system (Figure 66, 2 mol% MSA, a) showed reversed selectivity between the primary and secondary amine with a higher conversion of hexanol but more side products like hexanoic acid and hexanal. It is assumed that the task of the methane sulfonic acid is the formation of the active catalyst species. As the $[HRuCl(CO)(PPh_3)_3]$ precursor already provides an active catalyst species a reaction without methane sulfonic acid was carried out (Figure 66, 0 mol% MSA, a). No hexylamine was being formed and only small amounts of dihexylamine were detected, also resulting in a reduced conversion. Notably, both too high and too low amounts of MSA influence the performance negatively. This shows the importance of MSA in the reaction medium.

The results of COLE-HAMILTON[86] with conversions of 100 % and yields of the primary amine up to 98 % could not be achieved. In further investigations, the use of aqueous ammonia should be studied in more depth.

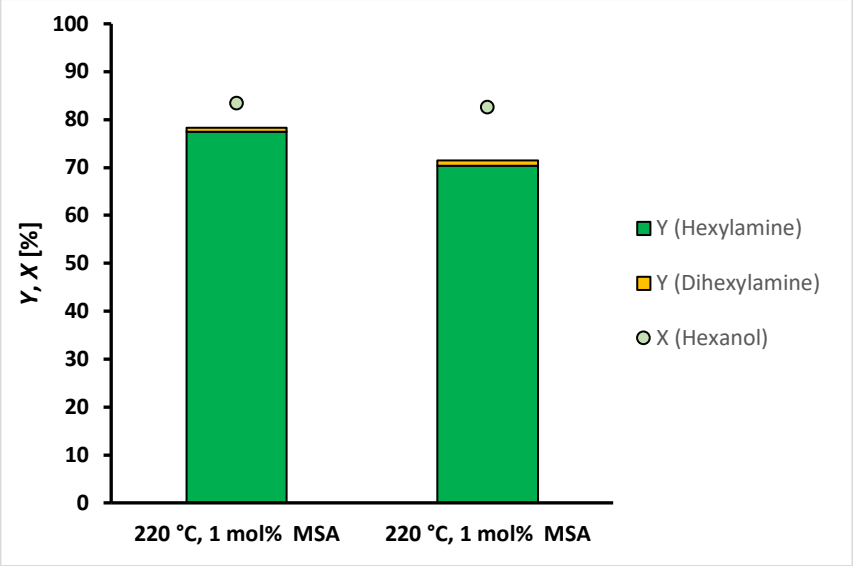

Figure 67: Alcohol amination of hexanol at 220 °C. Conditions: hexanol (0.5 mmol), $Ru(acac)_3$ (1 mol%), triphos (2 mol%), MSA (1 mol%) in dioxane (2.4 mL), water (1.6 mL), aq. NH_3 (26 %, 5 mL), H_2 (10 bar), 20 h, 220 °C (adapted from Reichert 2022[112]).

The conversions of the reaction are 83 % and 82 % with a selectivity of 93 % and 85 % to the desired product hexylamine. In addition, dihexylamine is formed in small amounts, each with a selectivity of about 1 %. The formation of unknown side products was also reduced. Using aqueous ammonia as the amine source seems to be beneficial for the alcohol amination with the Ru/triphos system.

5.4.3. Experimental

General

Solvents and Chemicals: All solvents and chemicals were purchased from ABCR, Acros Organics, TCI, Sigma Aldrich, VWR or UMICORE. Solvents was dried over 3 Å molecular sieve for at least 24 h and distilled before use under argon. All precursors and ligands were stored in Schlenk flasks under an argon atmosphere.

Synthesis of 4,5-bis-(bromomethyl)-acridine (I)

Acridine (926 mg, 5.01 mmol) was heated to 50 °C in H_2SO_4 (10 mL) under an argon atmosphere, producing a yellow suspension. After addition of the BMME at 50 °C (1.2 mL, 44.64 mmol, 8.9 eq.) in one portion, the mixture turned red. The reaction mixture was then stirred at 50 °C for 18 h. A slight formation of Br_2 could be observed (brown gas). The suspension was then added to 70 mL of ice and stirred for an additional 2 h. A yellow precipitate could be observed which was filtered off and washed with 50 mL distilled water. To the solid 170 mL chloroform were added, leaving some of the solid undissolved on the surface of the liquid. The undissolved solid was filtered off and the liquid organic phase was dried with $MgSO_4$. The solvent was then removed using a rotary evaporator, yielding a yellow powder. This yellow powder was then dissolved in 12 mL chloroform in reflux and recrystallized with 5 mL diethyl ether and then dried under reduced pressure to give 4,5-bis-(bromomethyl)-acridine (442 mg, 1.21 mmol, 24 %) as a yellow solid.

Synthesis of 4,5-bis-(bromomethyl)-acridine (II)

The second attempt was scaled up to 33.8 mmol acridine (6245 mg) and carried out as described in (I), except for the purification. To obtain a better yield form the crystallization dichloromethane was used for the process instead of chloroform and a minimal amount of cyclohexane was added to reduce the solubility of the product until the mixture became cloudy. Then the product was

filtered off and dried under reduced pressure. The desired product was obtained as a bright yellow solid (5039 mg, 13.8 mmol, 41 %).

Synthesis of 4,5-bis-(bromomethyl)-acridine (III)

The third attempt was carried out on an 8.3 mmol scale (acridine 1530 mg) as described in (I) with the modifications of (II). To further increase the yield from the crystallization the mixture was stored over night at -18 °C, before the product was filtered off and dried under reduced pressure. The desired product was obtained as a bright yellow solid (1423 mg, 3.9 mmol, 47 %).

Alternative synthesis of 4,5-bis-(bromomethyl)-acridine (zink bromide route)

Acridine (902 mg, 5.0 mmol, 1 eq.), zinc bromide (228 mg, 1.0 mmol, 0.2 eq) and paraformaldehyde (938 mg, 10.0 mmol, 2 eq) were successively suspended in dry acetic acid (3 mL). A 31 w% hydrogen bromide solution in acetic acid (2.9 mL, 17.6 mmol, 3.5 eq) was then added and stirred at 50 °C for 22 h. The reaction mixture was then added to approx. 30 mL of water. Afterward, 70 mL of chloroform were added to the reaction mixture and the organic phase was separated. The aqueous phase was extracted four times with 70 mL chloroform four times. The combined organic phases were then dried with $MgSO_4$. The solvent was then removed using a rotary evaporator and an NMR sample was prepared. As this showed little product signal (6 % yield), this method of purifying the product was discarded.

Synthesis of 4,5-bis((diisopropylphosphinyl)methyl)acridine (I)

The 4,5-bis-(bromomethyl)-acridine (302 mg, 0.8 mmol, 1 eq.) was suspended in dry and degassed methanol (4 mL) under argon atmosphere resulting in a yellow suspension. Diisopropylphosphine (250 mg, 2.1 mmol, dissolved in 2.25 g cyclohexane, 2.56 eq.) was added dropwise *via* syringe, during the addition the suspension changed to an orange color. The flask was then sealed, stirred at 50 °C for 45 h and then cooled for 1 h. Freshly distilled triethylamine (0.45 mL, 3.2 mmol, 3.8 eq) was then slowly added and stirred at room temperature for 1 h 50 min. The solvent was carefully distilled under reduced pressure at RT into a cold trap and the yellow residue was washed with 3 mL of dry diethyl ether four times, leaving the triethylammonium bromide as a white residue in the flask. The organic phases were combined, and diethyl ether was removed by distillation into a cold trap. A yellow-orange oil, which contained the product was obtained, but the isolation of the product was not successful.

Synthesis of 4,5-bis((diisopropylphosphinyl)methyl)acridine (II)

The reaction was repeated with the following changes: The reaction was carried out in a 4.1 mmol scale; the reaction time was increased to 68 h; the extraction of the desired product from the solid residue was conducted with two times 12 mL, two times 10 mL und once with 5 mL dry diethyl ether. After the solvent was removed the raw product was dried under reduced pressure (3 mbar, 30 min). The solid was dissolved in 1.7 mL acetone and stored at -22 °C over night. The next day the formed crystals were washed with 2 mL (-50 °C) cold acetone seven times. 4,5-Bis- (diisopropylphosphinyl)methyl)-acridin was obtained as a yellow solid (1246 mg, 2.8 mmol, 69 %).

Synthesis of (4,5-Bis-(Diisopropylphosphinyl)methyl)-acridin)-hydridochlorido-carbonylruthenium(II)

Freshly washed 4,5-bis(diisopropylphosphinyl)methyl)acridine (167 mg, 0.4 mmol, 1.1 eq) was dissolved in 22 mL of dry and degassed toluene in a Schlenk flask. $HRuCl(CO)(PPh_3)_3$ (329.1 mg, 0.346 mmol, 1 eq) is added to this mixture and stirred at 65 °C for 18 h. After cooling down, the solvent is slowly removed and the remaining solid is taken up in 2.5 mL THF at room temperature. Subsequently, 23.5 mL of pentane is slowly added to precipitate the desired complex. The solvent is then decanted off and the remaining solid is washed with 5 mL pentane and dried under educed

pressure at 1 mbar for 5 h to obtain a brown-orange powder. Washing with 2 mL toluene at 0 °C, washing with 4 mL pentane and subsequent drying gives the final milestone catalyst (113.2 mg, 0.2 mmol, 54 % yield).

5.5. Hydrogenation of carboxylic acid esters – Generation of the intermediate

For the desired ester to amine transformation in cascade reaction, a conversion of the ester into an intermediate is the first step. Based on the work of COLE-HAMILTON the hydrogenation to obtain primary, aliphatic alcohols was chosen, which can be aligned with the above describes amination of alcohols (Figure 50). Fatty acids usually occur in the form of triglycerides in nature and are processed into methyl esters for further use in the chemical industry. Therefore, methyl hexanoate was chosen as the model reaction in this work, which can be converted into hexanol *via* hydrogenation (Figure 68, when R = n-pentyl).

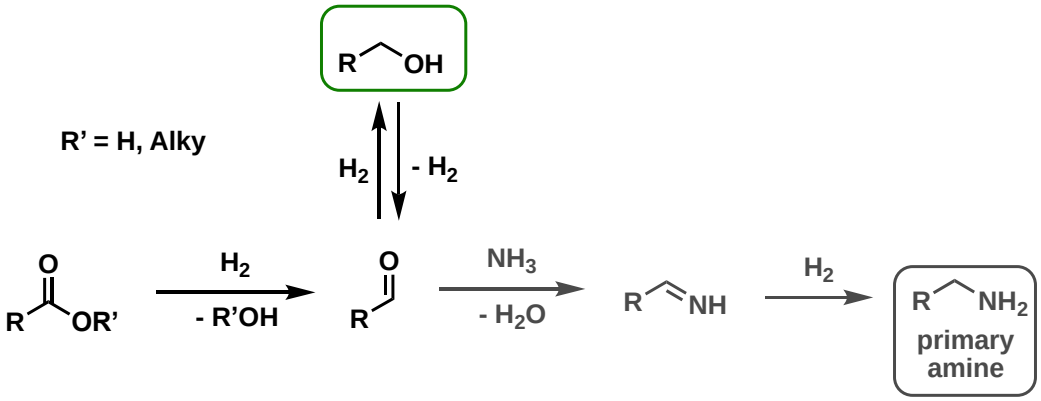

Figure 68: Schematic hydrogenation of carboxylic acid esters in the context of ester amination.

In theory, a reduction of the ester into an aldehyde would be enough for the total conversion from ester to amine. However, under reductive conditions, *i.e.,* in the presence of hydrogen and a catalyst, aldehydes are readily hydrogenated to form a more stable alcohol.

MILSTEIN'S catalyst shows remarkable performance in the amination of alcohols, which makes this catalyst a promising candidate for the total reaction. Additionally, the Ru/triphos catalyst system is investigated, since it is capable of a similar reaction with aniline instead of ammonia.

5.5.1. Hydrogenation of hexanoic acid with Milstein's catalyst

At first MILSTEIN'S catalyst was tested in the hydrogenation of methyl hexanoate. The acridine based ligand is like the pyridine base catalyst complexes, also developed by the same group, are well suited for the hydrogenation of esters.[113–119]

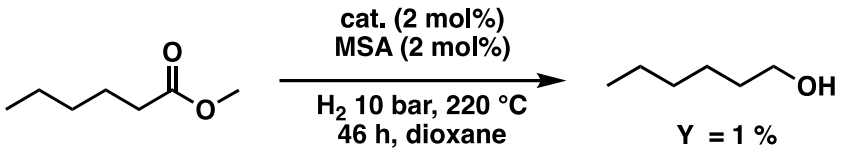

Figure 69: Hydrogenation of methyl hexanoate with MILSTEIN'S catalyst.

The ester could not be converted into the alcohol successfully, as only traces of the desired alcohol could be detected. Due to lack of catalyst a wider range of reaction conditions could not be tested, which underlines the convenience of a commercially available catalyst for the optimization of a catalytic reaction.

5.5.2. Hydrogenation of hexanoic acid with a triphos based system

Hydrogenation with a homogeneous ruthenium catalyst is well known, but the Ru/triphos system which is the focus of this work because it can also alkylate ammonia with alcohols. Already in 1997,

TEUNISSEN et al. discovered that $Ru(acac)_3$ in combination with the triphos ligand can convert dimethyloxalate to ethylengycol.[120] Since then the catalyst system was established and used in similar compositions for the reduction of different kinds of carboxylic acids and esters.[110,120–125]

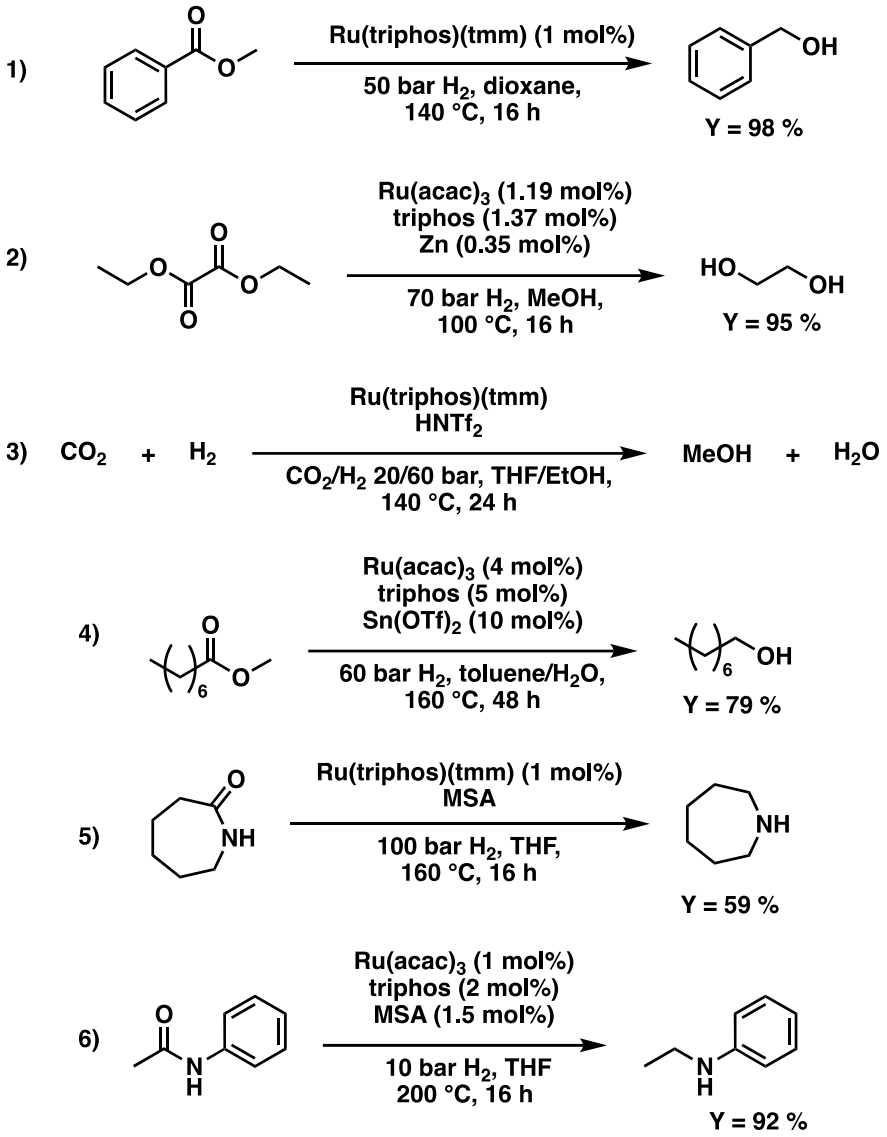

Figure 70: Examples of hydrogenations of carboxylic acid derivatives.

In general, high yields can be achieved using a Ru-based catalyst with the triphos ligand. However, the reaction speed is relatively low and harsh conditions are required. For the hydrogenation of aliphatic carboxylic acids for example requires 60 bar of hydrogen and 4 mol% ruthenium catalyst, resulting in overall high costs. Most catalyst systems depend on an additional activation co-catalyst, which can be either a strong base or a strong acid. These activation agents promote different ionic catalyst complexes.

Similar to entry 6 in Figure 70 which is capable of the hydrogenation of amides, the ester amination procedure of Cole-Hamilton used an Ru/triphos catalyst system with MSA for activation under a comparable mild pressure of 10 bar. Therefore, these conditions were used as the starting conditions and tested with different solvents and concentrations of the acid.

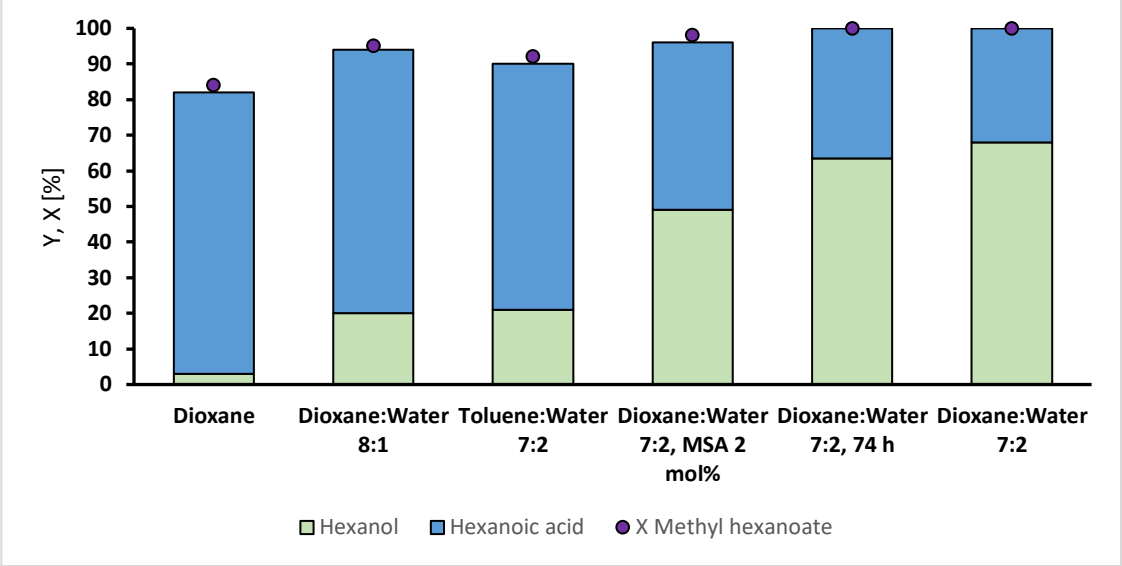

Figure 71: Optimization of reduction of methyl hexanoate. Conditions: methyl hexanoate 0.38 mmol, $Ru(acac)_3$ 2 mol%, triphos 4 mol%, MSA 4 mol%, dioxane 3.5 mL, water 1 mL, H_2 10 bar, 220 °C, 20 h. Yields determined via GC and dibutyl ether as an internal standard(adapted from SCHMIDT 2020[109]).

Starting with only dioxane as the solvent a poor yield of hexanol was achieved. The main product was the free acid, which results form probably hydrolysis of the ester and might also indicate water residue in the solvent. When water is added to the mixture the yield increases to 20 % with an ration of dioxane:water 8:1 and increases even to 68 % when a ratio of 7:2 was used. Replacing dioxane by toluene in this set up results in a drop of the yield to 21 %. Also, using only 2 mol% of MSA could not increase the yield of the alcohol.

Afterward the same conditions were applied to methyl undecanoate and both carboxylic acids respectively (Figure 72).

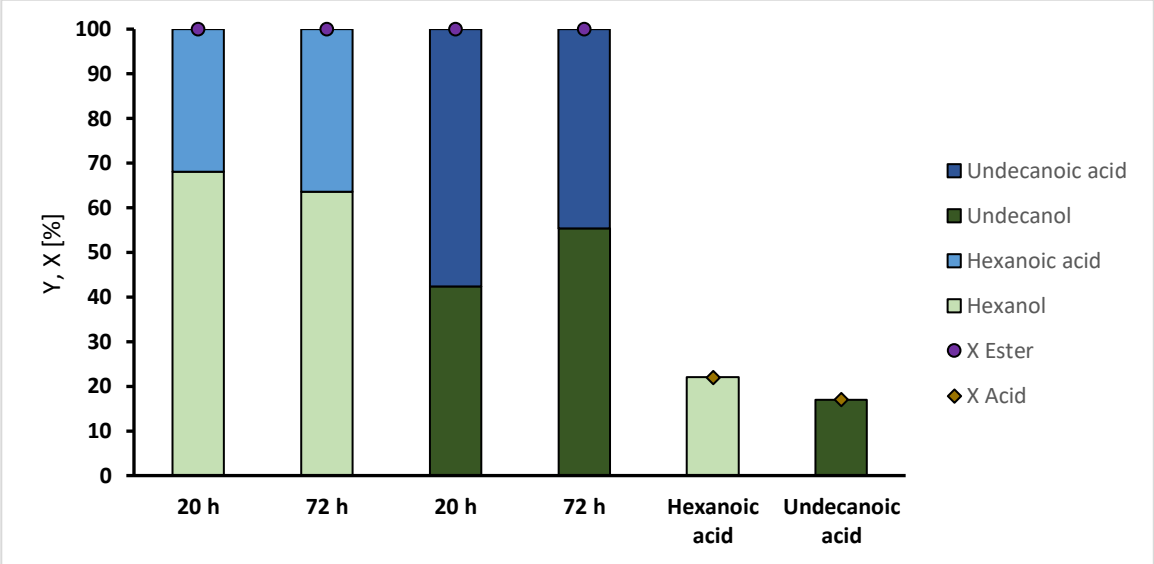

Figure 72: Comparison of reducing activity of the catalyst system for methyl hexanoate and methyl undecanoate. Conditions: ester 0.38 mmol, $Ru(acac)_3$ 2 mol%, triphos 4 mol%, MSA 4 mol%, dioxane 3.5 mL, water 1 mL, 10 bar H_2, 220 °C, 20 h. Yields determined via GC and dibutyl ether as an internal standard (adapted from SCHMIDT 2020[109]).

Compared with hexanol (Figure 72), the yield of undecanol was lower, but the conversion was also completed. Notable, the yield increased from 42 % to 55 % when the reaction time was increased form 20 h to 72 h. A longer chain length of the ester could lead to higher sterically

demand and a slower exchange of the substrate at the active catalyst complex When the respective acids are used the conversion drops below 22 %, indicating a slower conversion of the acid compared to the ester.

Next, the reaction was investigated in a larger reactor with 100 mL volume and 30 mL solvent.

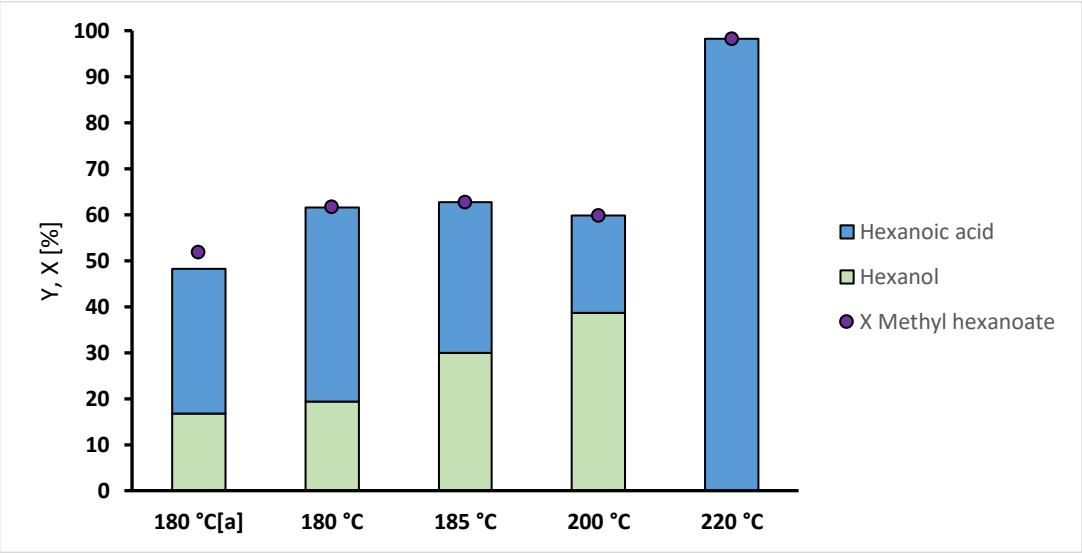

Figure 73: Scale-up and temperature dependency of the hydrogenation of methyl hexanoate. Conditions: ester 3.75 mmol, $Ru(acac)_3$ 1 mol%, triphos 2 mol%, MSA 1 mol%, dioxane 18 mL, water 12 mL, 10 bar H_2, 2 h preforming of the catalyst, 20 h reaction time. Yields determined via GC and decane as an internal standard. [a] = no preforming (adapted from Reichert 2022[112]).

The overall yields and conversion were lower than expected. These lower results can be attributed to the larger reactor and the new procedure for charging it. The smaller 25 mL autoclaves only have two valves on the top, leaving fewer possibilities for trace oxygen left behind in the reactor. In comparison, the 100 mL autoclaves have a more complex set up and are equipped with a pressure dropping funnel, an addition valve, a gas inlet, a temperature, and pressure sensor. Although the reactor was flushed with argon 5 times, trace oxygen could have been trapped in the apparatus. Additionally, the catalyst solution was transferred into the reactor *via* reduced pressure in the reactor through a cannula. The procedure was optimized later but could have caused oxygen contamination at this stage.

Nevertheless, a temperature trend can be observed and the hexanol yield increases from 19 % to 39 % from 180 °C to 200 °C. At 220 °C the temperature of the reaction mixture reached 235 °C, before settling at 220 °C. The higher than planned temperature caused a deactivation of the catalyst as no formation of hexanol could be observed. Instead, only hydrolysis took place. At 180 °C and 185 °C, hydrolysis was the main reaction probably caused by the lower activity of the hydrogenation. Only at 200 °C the catalyst system was active enough to promote the desired hydrogenation resulting in the alcohol being the main product.

The lowest conversion was observed without preformation which indicates that the active catalyst is better formed in the absence of substrate and need some time to form. Due to the mentioned possibility of oxygen contamination the difference is not drastic.

Combining the ester hydrogenation with the alcohol amination results in the desired ester to amine conversion.

5.5.3. Experimental

General hydrogenation of esters in a 25 mL autoclave

$Ru(acac)_3$ (1.6 mg, 0.005 mmol, 0.01 eq.) and triphos (5.2 mg, 0.01 mmol, 0.02 eq.) were weighed into the reactor in air. The reactor is sealed and then inertized with argon. A stock

solution of 10 mL dioxane/water (3:2), methane sulfonic acid (0.78 µL, 0.013 mmol, 0.025 eq.) and hexanoic acid methyl ester (157.3 mg, 1.25 mmol, 2.5 eq.) was prepared, 4 mL of the solution were filled into the reactor under argon countercurrent. The reactor was flushed 6 times with H_2, pressurized with H_2 (10 bar) and then stirred in a preheated heating block at 220 °C for 20 h. At the end of the reaction time, the reaction was stopped by cooling the reactor in an ice bath and the reactor was depressurized. The reaction solution was then analyzed by GC-FID.

General hydrogenation of esters in a 100 mL autoclave

$Ru(acac)_3$ (12 mg, 0.038 mmol, 0.01 eq.) and triphos (38.6 mg, 0.075 mmol, 0.02 eq.) were weighed into the reactor in air. The reactor was sealed and inertized with argon. A solution of 20 mL dioxane/water (3:2) and methane sulfonic acid (2.34 µL, 0.038 mmol, 0.025 eq.) was prepared and completely transferred to the reactor via a cannula under reduced pressure in the reactor and the transfer flask under argon. A second solution of 10 mL dioxane/water (3:2) and hexanoic acid methyl ester (472.8 mg, 3.5 mmol, 1 eq.) was prepared, which was filled into the closed pressure dropping funnel of the reactor under argon counter flow. The reactor was flushed 6 times with H_2, pressurized with H_2 (10 bar) and then stirred for 2 h at the given reaction temperature.

After 2 h, the solution was released from the dropping funnel into the reactor and the reactor was stirred for 20 h at reaction temperature. At the end of the reaction time, the reaction mixture was cooled down with an water/ice bath. The reactor was depressurized and the reaction solution was then analyzed by GC-FID.

5.6. Ester amination – the tandem catalysis

The next step was to combine both reactions and add ammonia or another amine source directly to the reaction system. Both reactions precede *via* an intermediate aldehyde and especially since hydrogen is present in the reaction mixture, the whole reaction also proceeds *via* the aldehyde (Figure 74).

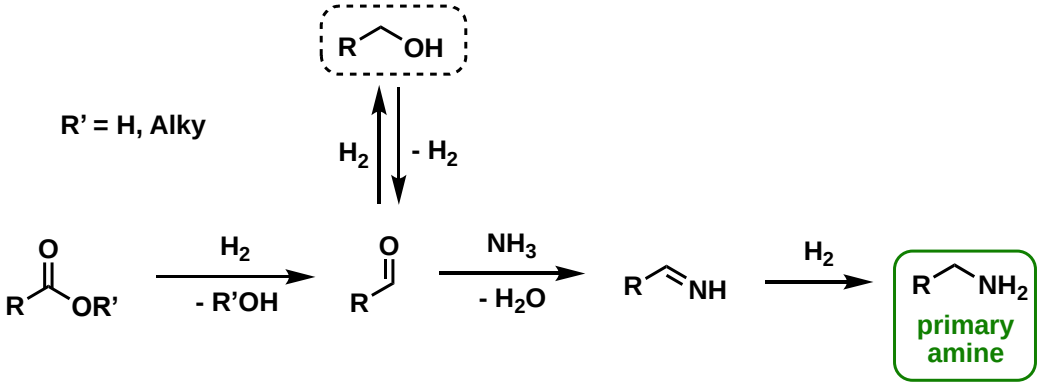

Figure 74: Ester amination with possible pathways.

COLE-HAMILTON and coworkers have described the amination of bifunctional acid and esters with aniline.[86] They proposed a sequential amination *via* an aldehyde, while the second amination could proceed with a diversion over an amide. However, the reaction speed was substantially faster when the reaction was carried out sequentially *via* the alcohol.

5.6.1. Amination of methyl hexanoate with MILSTEIN's catalyst

First, MILSTEIN'S catalyst was tested in the ester amination reaction under condition reported by COLE-HAMILTON[8486]. At the time ammonia was unavailable, so aniline was used as well.

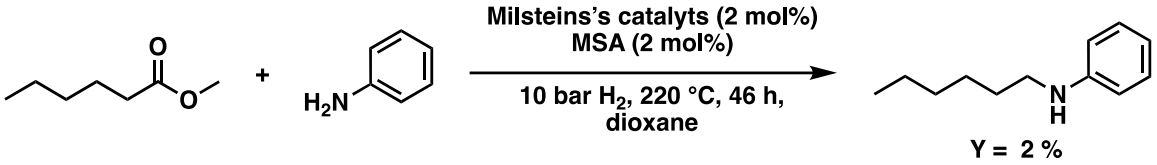

Figure 75: amination of methyl hexanoate with MILSTEIN'S catalyst.

Similar to the hydrogenation (chapter 5.5), the yield was poor, and the desired amine could be obtained with a yield of 2 %. Considering the better performance on the catalyst system for primary amines the reaction time could have been still too short. Especially the first hydrogenation step has been proven to be extremely oxygen sensitive, more freeze-pump-thaw cycles for each component of the reaction could be beneficial, as well as handling the catalyst in a glovebox which was not available at the time of the reaction. Additionally, the temperature could have been too high for this type of catalyst.

It could be insightful to repeat the experiment with ammonia in a larger reactor under strictly oxygen free conditions. Additionally, a better compromise of the reaction conditions of the amination and the hydrogenation could be found, e.g. no MSA and lower temperatures.

5.6.2. Amination of esters with the Ru/triphos catalyst

Next the combined reaction was carried out with the Ru/triphos system. Two catalyst precursors were investigated, and a small screening of the reaction conditions was carried out to combine both, hydrogenation, and amination reaction, in a single synthesis step.

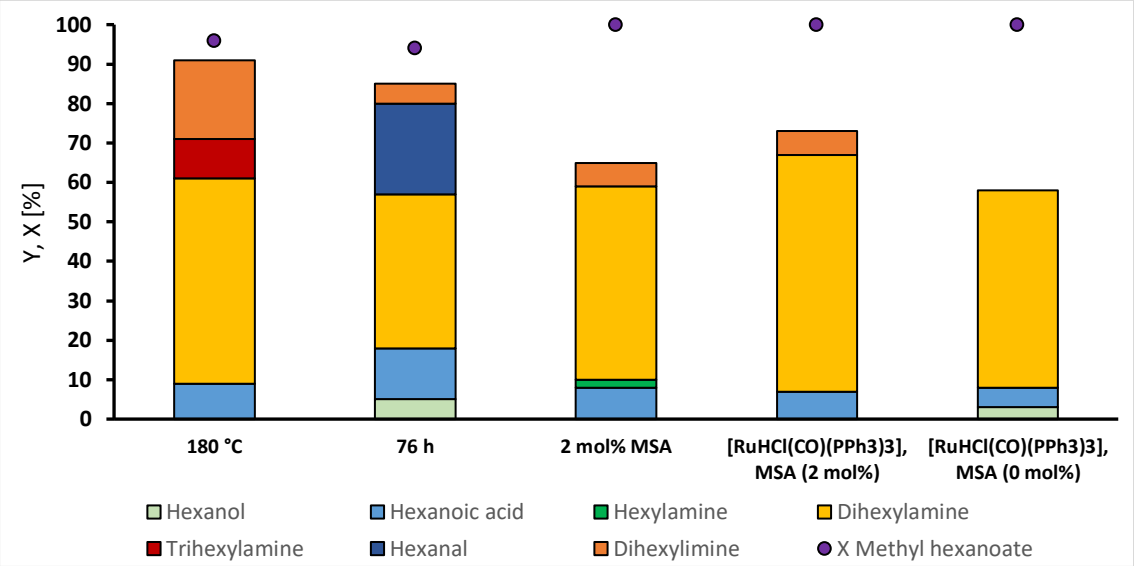

Figure 76: *Screening of ester amination of methyl hexanoate. Conditions: Methyl hexanoate 0.38 mmol [Ru(acac)$_3$] 2 mol%, triphos 4 mol%, MSA 4 mol%, dioxane 3.5 mL, water 1 mL, di-n-butyl ether 100 mg, H_2 10 bar, NH_3 10 eq., 220 °C, 20 h. Yields and conversion determined with GC-FID and di-n-butyl ether as the internal standard (adapted from SCHMIDT 2020*[109]*).*

The amination of methyl hexanoate yielded dihexylamine as the main product under all tested reaction conditions. Only by reducing the MSA amount to 2 mol% traces of the desired hexylamine could be detected. A reduction of the temperature to 180 °C even led to formation of trihexylamine and significant amounts of dihexylimine, which showcases a lower hydrogenation activity. Despite waste being a significant portion of the solvent hydrolysis was only observed in small amount.

Changing the catalyst precursor to alternative closer to the active catalyst. *i.e.*, $[HRuCl(CO)(PPh_3)_3]$, did not lead to an improvement of the results.

COLE-HAMILTON and coworkers reported only the direct amination of ester with amines thus the production of secondary amines. However, the group was able to obtain primary amine with ammonia through a two-step reaction set up. First, the hydrogenation of the ester and in the second step the addition of ammonia for the amination reaction. This way, the catalyst can successfully conduct both reactions consecutively.

In the next screening experiments both set ups were compared under similar condition (Figure 77).

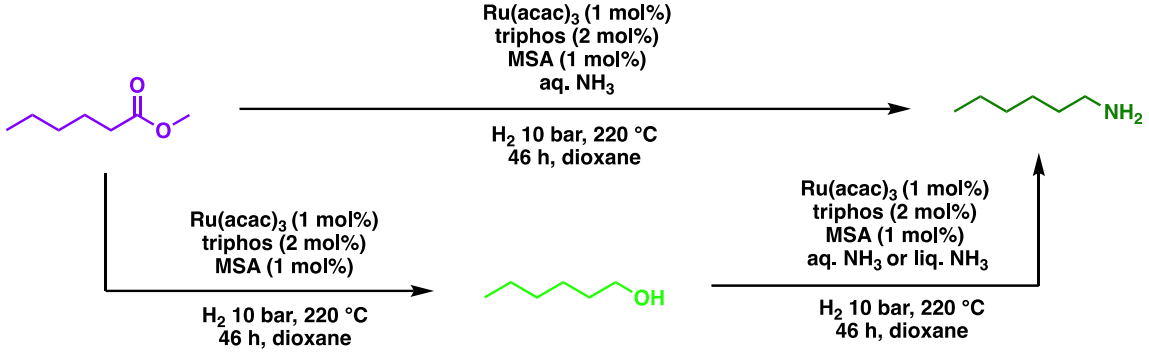

Figure 77: Single step reaction and two-step process for the amination of methyl hexanoate.

Additionally, ammonia can be added pure in its liquid, condensed form or as an aqueous solution. The latter is much easier to handle but could take up oxygen over time.

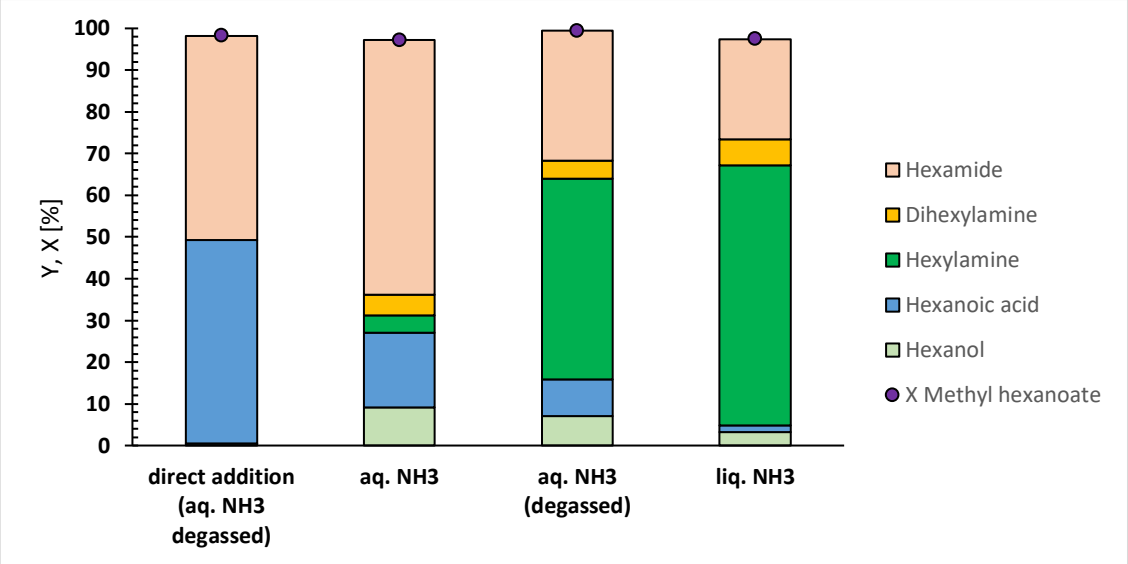

Figure 78: Comparison of the one-step reaction with the consecutive synthesis of primary amines form esters. Conditions: 0.5 mmol methyl hexanoate, $Ru(acac)_3$ 1 mol%, triphos 2 mol%, MSA 1 mol%, dioxane 2.4 mL, water 1.6 mL, 10 bar H_2, 20 h, 220 °C; then addition of NH_3 (26%, 5 mL), 10 bar H_2, 20 h, 220 °C (adapted from REICHERT 2022[112]).

Again, the direct addition does not result in significant amounts of amine. Only unwanted reaction paths can be observed, namely amidation and hydrolysis of the ester. With the sequential addition of aqueous ammonia, a small amount of hexylamine is detected in the reaction solution. However, the amount of amide increased, and hydrolysis was still the second largest reaction by yield. These results point to a low overall ester reduction activity which is heavily depended on the oxygen content in the reaction solution. Since ammonia was stored as an aqueous solution over a longer period, oxygen could be dissolved into the solution form the atmosphere. Therefore, the ammonia solution was degassed by three freeze-pump-thaw cycles. Although ammonia is also

a gas, oxygen can be removed selectively form the solution. A small part of ammonia is bound as ammonium hydroxide in solution (Figure 79) and ammonia has a relatively to oxygen high melting point of -77.73 °C so it can be frozen at liquid nitrogen temperatures.

Figure 79: Hydrolysis of ammonia.

With the degassed aqueous ammonia solution, the amination became the main reaction and resulted in 48 % yield. The main side reaction again was amidation with 31 %. Without oxygen the catalyst activity did increase, so the addition of liquid ammonia seems a suitable alternative. With liquid ammonia the yield could be increased to 62 %.

5.6.3. Experimental

Ester amination with MILSTEIN'S catalyst

First, the MILSTEIN'S catalyst (10.2 mg, 0.02 mmol, 2 mol%) was weighed into the steel reactor, then a stirring bar was added, and the reactor was closed. The reactor was then evacuated and flooded with argon three times. A 20 mL crimp cap vial was closed for each of the stock solutions. These were then inertized with argon. Then freshly distilled aniline (118 mg, 1.27 mmol, 1.5 eq), methyl sulfonic acid (1.64 mg, 0.02 mmol, 2 mol%) and methyl hexanoate (111 mg, 0.84 mmol, 1 eq.) were each added to a prepared vial *via* syringe. 2 mL dioxane was added to the aniline and methyl hexanoate stock solutions and 1 mL to the MSA stock solution. The prepared stock solutions were then added to the reactor in the argon counter flow. The reactor was flushed 6 times with H_2, was pressurized with 10 bar H_2, and then stirred at 700 rpm at a temperature of 220 °C for 67 h. Afterward, the reactor was cooled with ice/water bath. The reaction solution was analyzed *via* GC with decane as an internal standard.

Ester amination with Ru/triphos

$Ru(acac)_3$ (1.6 mg, 0.005 mmol, 1 mol%) and triphos (5.2 mg, 0.01 mmol, 2 mol%) were weighed into the reactor in air. The reactor is sealed and then inertized with argon. A stock solution with 10 mL dioxane/water (3 : 2), methanesulfonic acid (0.78 µL, 0.013 mmol, 2.5 mol%) and hexanoic acid methyl ester (157.3 mg, 1.25 mmol, 2.5 eq.) was prepared, 4 mL of which were filled into a 25 mL reactor under argon countercurrent. The reactor was flushed 6 times with H_2, pressurized with H_2 (10 bar) and then stirred in a preheated heating block at 220 °C for 20 h. Afterward, the reactor was cooled down depressurized and then charged with 5 mL aqueous ammonia solution in an argon counter flow. Alternatively the reactor was attached to a syringe pump after the first reaction step an 2 mL liquid ammonia was added. The reactor was then pressurized with H_2 (10 bar) and then stirred in a preheated heating block at 220 °C for 20 h. At the end of the reaction time, the reaction was stopped by cooling the reactor in an ice bath and the reactor was depressurized. The reaction solution was analyzed via GC-FID with dodecane as an internal standard.

5.7. Substituted-Triphos – The better alternative?

The optimization of the reaction conditions of a reaction can improve the reaction outcome significantly. However, the nature of the catalyst can also have a significant influence on the reaction and even overcome limitations by changing the catalytic mechanism of the reaction. Another way of improving the reaction outcome is eliminating the deactivation pathways of the catalyst to maintain highest activity for an extended period, ideally for the entire reaction time a longer in case of catalyst recycling. Above the deactivation by oxygen was already mentioned, which can affect the ligand by oxidation or the catalyst metal. Additionally, the catalyst can form stable complexes which are no longer available for catalytic reactions.

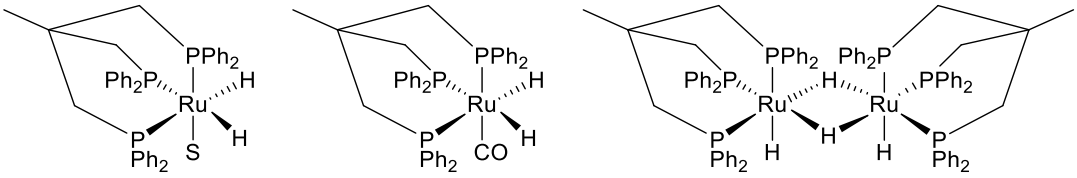

Figure 80: The proposed active catalyst complex and deactivated forms.

The group of KLANKERMAYER described the dimerization of the active Ru/triphos yielding stable dimers (Figure 80, deactivated complex II) a major influence on the reactivity.[125] The hydride bridges can be inhibited by adding larger substituents at the phosphorus atoms of the ligand. In their work tolyl and xylyl derivatives of triphos were tested.

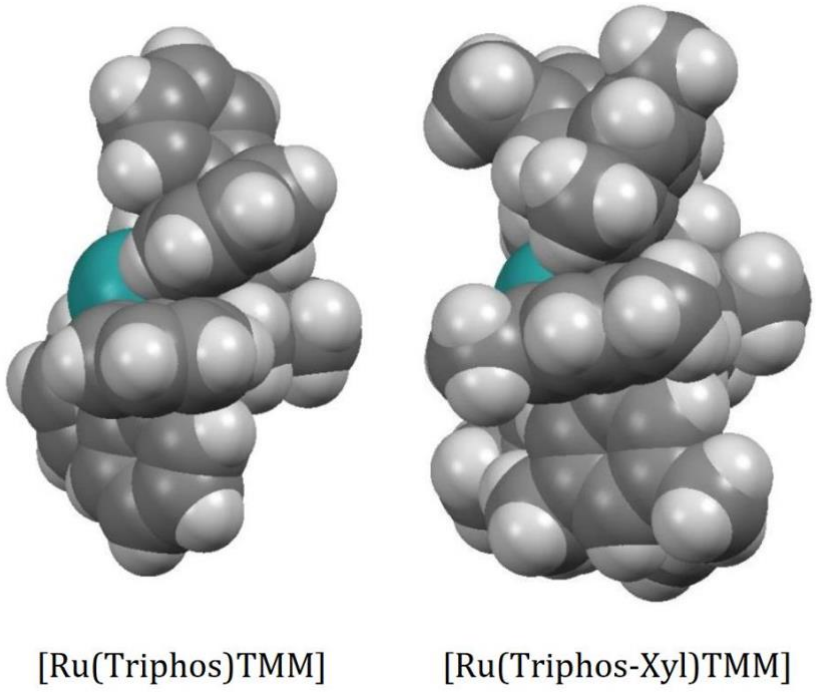

Figure 81: Comparison of the spatial orientation of [Ru(triphos)TMM] complex with [Ru(triphos-Xyl)TMM] complex.

As Figure 81 depicts, the triphos-xyl can shield the Ru center better than the normal phenyl triphos ligand due to the extra methyl groups occupying more space. Therefore, less dimers are formed and the activity of the catalyst in the hydrogenation of esters increased significantly. The yield could be increased form 25 % with triphos to a remarkable yield of 98 % with triphos-xyl. Also, the hydrogenation of lactams to form cyclic amines could be improved significantly. Triphos reached a yield of 13 % with a TON of 25 while triphos-xyl reaches 95 % with a TON of 200.[125]

There are two mechanism which improve the performance of the triphos-xyl ligand. First, the additional methyl groups add electron density to the aromatic system and through this they add electron density to the phosphorous. Usually, electron rich catalysts have an increased hydrogen activation capability. Second, the 3,5-positioning of the rests improve the sterical demand and thus improve the shielding of the metal center, avoiding dimerization.

Similar improvements could be possible with ester amination since the hydrogenation activity is crucial for the transformation. A drawback is, that the ligand is not commercially available and hast to be synthesized.

5.7.1. Synthesis of Substituted-triphos

The synthesis is carried after previous work of our group and Klankermayer[121].[125] First, dixyly (xyl) phosphine **4a** and 3,5-dimethoxyphenyl (DMOP) phosphine **4b** are synthesized *via* a GRIGNARD reaction followed by a reduction of the phosphine oxide and in the second step the phosphine is combined with the ligand backbone **5** to form the final triphos-xyl **6a** or triphos-DMOP **6b** ligand.

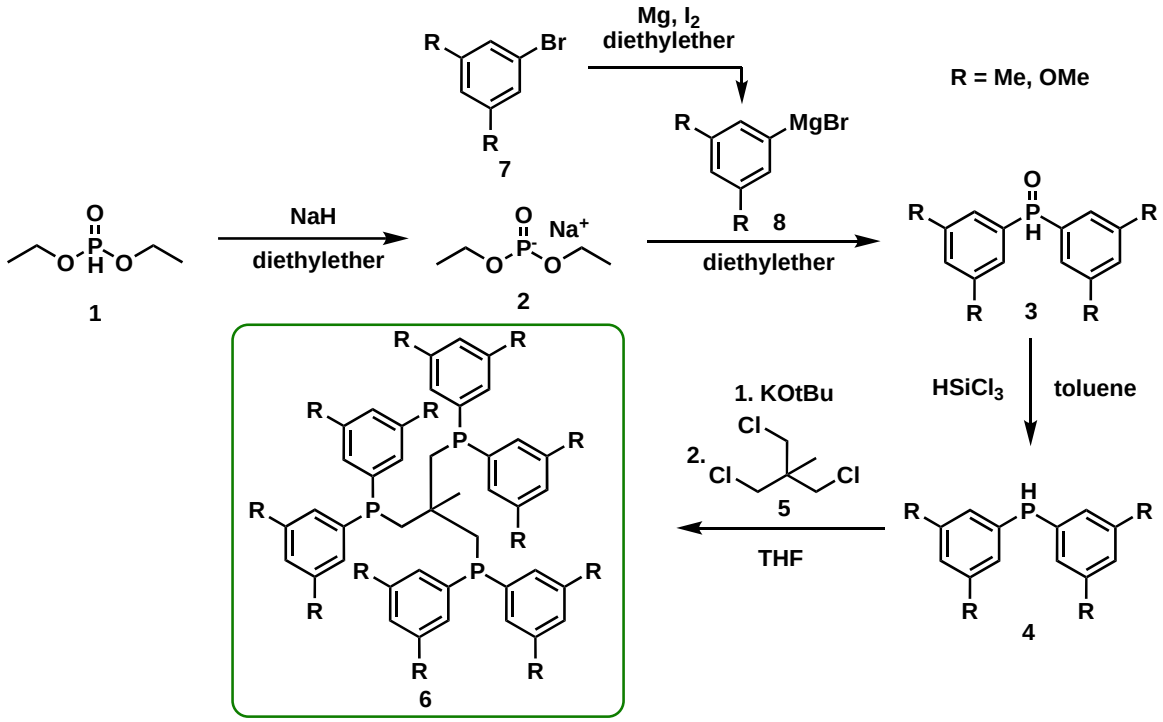

Figure 82: Synthesis plan of the triphos ligand substituted with 3,5-xylyl and 3,5-dimethoxyphenyl groups.

To avoid an overreaction at the phosphorus atom, diethyl phosphite is protected as a sodium salt. The GRIGNARD reagent was produced freshly prior to use from the bromine substituted aryls.

Additionally, the synthesis of a 2,8-dimethyl-10*H*-phenoxaphosphine (POP) **4c** substituted triphos ligand was attempted, which still consist of the synthesis of the phosphine and the attachment to the backbone. In this case the synthesis of the phosphine starts form ditolylether **9** and phosphorous tri chloride (Figure 83).

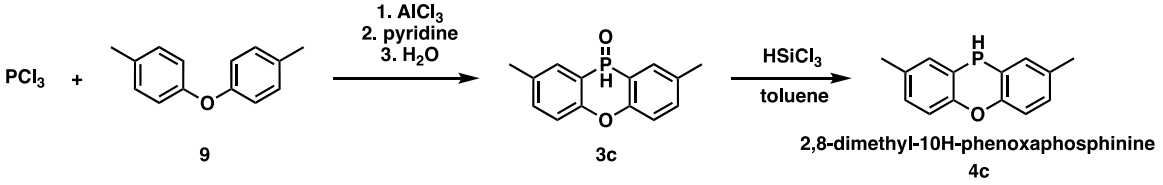

Figure 83: Synthesis plan for 2,8-dimethyl-10H-phenoxaphosphine.

By pouring the intermediate phosphine chloride on ice, it gets oxidized quickly and can then be reduced to form the desired phosphine.

This phosphine is an interesting structural motive for the triphos type ligand, because it also has additional methyl groups comparable to the triphos-xyl **6a**, but is less free in movement due to the oxygen bridge between the two benzyl rings. In the past POP-Xantphos was already used for hydroaminomethylation, which also requires the selective hydrogenation of an imine.[126]

5.7.2. Synthesis of phosphine oxides

Deprotonation of diethyl phosphonate

The aim of the first reaction is to deprotonate the diethyl phosphonate **1** for the following GRIGNARD reaction, so that less side-products are formed. Inspired by a method from CASALNUOVO[123127], modified with NaH instead of KH.

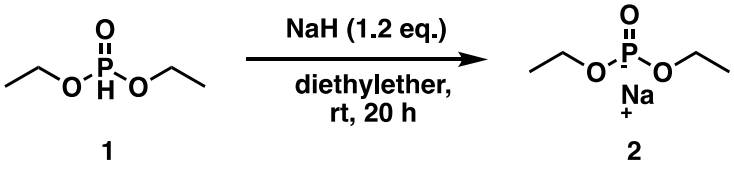

Figure 84: Deprotonation of diethyl phosphonate.

Firstly, a grey suspension of sodium hydride in diethyl ether was formed. Slowly, diethyl phosphonate was added by syringe when the formation of gas and the change in color to a lighter suspension was observed. Because of high room temperatures or leaking lids, additional adding of diethyl ether was necessary. After stirring for 20 h a yellow solution could be observed and was analyzed by ^{31}P-NMR spectroscopy.

Figure 85: Sodium hydride suspension (left), addition of diethyl phosphonate (middle), after reaction (right) (from SCHMIDT 2020[109]).

During the reaction the consumption of the solid NaH could be observed as the reaction solution turned from turbid to clear. Drying of diethyl phosphonate **1** was necessary, as the consumption of NaH was higher than expected in the first run. Therefore, the phosphite was distilled and stored over 3 Å mole sieve. With dried substrate the analytical yields achieved in the ^{31}P-NMR spectra reached up to 93 % and the reaction solution was filtered before use to remove excess NaH.

Synthesis of bis(3,5-dimethylphenyl)phosphine oxide

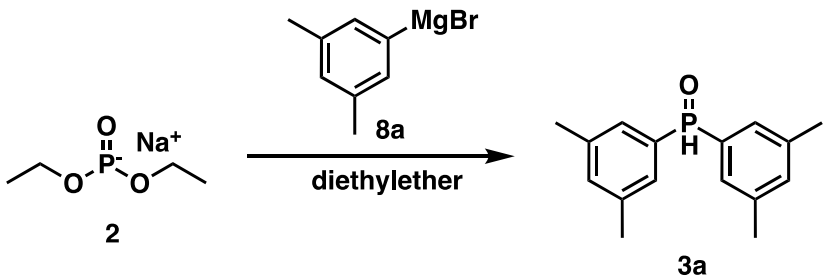

*Scheme 1: GRIGNARD reaction towards bis(3,5-dimethylphenyl)phosphine oxide **3a**.*

Different parameters were tested to optimize the GRIGNARD reaction. Initially a synthesis of the GRIGNARD-magnesium bromide was carried out with magnesium powder, but the reaction did not start on its own. Magnesium easily passivates on the outer surface of the powder. Therefore, diluted hydrochloric acid was used to activate the magnesium. Additionally, iodine crystals were mixed with the magnesium for further activation. The GRIGNARD reaction was started by alternating addition of diethyl ether and 5-bromo-*m*-xylene **7a** at 35 °C. An ultrasonic bath could also help to start the reaction at times. The start of the reaction was accompanied by heat and vapor development and a change in color to dark brown/black.

After the reaction different purification methods were tested. Column chromatography led to a loss in purity of 3 %. Potentially, the loss in purity is due to differences in the concentration of the NMR samples and not that a contamination was caused by column chromatography. This method did not lead to a purification and a substantial part of the product was lost in the process. Due to strong interactions the product could be absorbed into the silica gel column.

With crystallization in ethanol the purity could be improved by 2 % according to ^{31}P-NMR.

Next, filtration from toluene and a following extraction was tested. When similar reactions were carried out, a phosphorous species believed to be the phosphorous oxide (δ = 19.32) was purely extracted from other oxides with a mixture of water and dioxane in toluene. However, after extraction the organic phase still contained the desired oxide according to ^{31}P-NMR. Extraction led to an improvement of purity of 5 %.

As none of the purification methods led to particularly good results, finally the cured product was used as is.

In general, low yields were achieved as the following table (Table 17) shows.

As different purification methods were used, a comparison can only be made qualitatively. Stirring the GRIGNARD reaction for a shorter time leads to higher conversions of the phosphine oxide **3a** whereas a longer reaction time after addition of the phosphonate leads to higher yields of **3a**. It can be assumed that reaction 3 shows a higher conversion as actually noted because a violent reaction with foaming after quenching the reaction solution led to a loss of product. Another important influence factor that explains the different results may be the dryness of the used substrates and solvents.

Table 17: Overview of the synthesis of xyl-phosphine oxide.

Entry	Activation of magnesium	Addition of Iodine	Mg [eq.]	Addition of Bromoxylene 7a	GRIGNARD reaction	Crude purity	Purification	Yield/Purity 3a
1	0.01 M HCl	Dry, stirred for 19 h	1.1	37 °C, 9 h, diethyl ether	rt, 66 h, diethyl ether	90 %	Column chromatography / Crystallization	44 % /92 %
2	0.05 M HCl	Dry, stirred 2 h	1.1	40 °C, 71 h, diethyl ether	rt, 21 h, diethyl ether	65 %	Extraction	31 % / 70 %
3	0.05 M HCl	Dry, stirred 4 h	1.1	20 °C, 71 h, diethyl ether	rt, 80 h, diethyl ether	80 %	None	35 % / 80 %
4	None	Dry stirred over night	1.1	50 °C, 14 h, THF	rt, 22 h, THF, phosphite in GRIGNARD	20 %	discarded	-
5	0.01 M HCl	Dry, stirred for 20 h	1.1	50 °C, 16 h, THF	rt °C, 11 h, THF	66 %	None	65 % / 66 %
6	0.01 M HCl	Dry, stirred for 16 h	1.5	50 °C, 16 h, THF	rt °C, 20 h, THF	96 %	None	91 % / 96 %

With the addition of 1.5 eq. magnesium the highest yield could be achieved. Although the magnesium oxide layer should have been removed by the diluted hydrochloric acid, some of the magnesium still was not available for the reaction. Therefore, increasing the amount led to almost full conversion of the xylyl bromide **7a**. In general, the purification process was not trivial and best result were achieved with a high yield to avoid purification.

Synthesis of bis(3,5-dimethoxyphenyl)phosphine oxide

Analogously, bis(3,5-dimethoxyphenyl)phosphine oxide **3b** was synthesized form sodium dieethylphosphonate **2**. However, the experiment was carried out before the amount of magnesium was identified as the limiting component and thus carried out with only 1.1 eq. of magnesium.

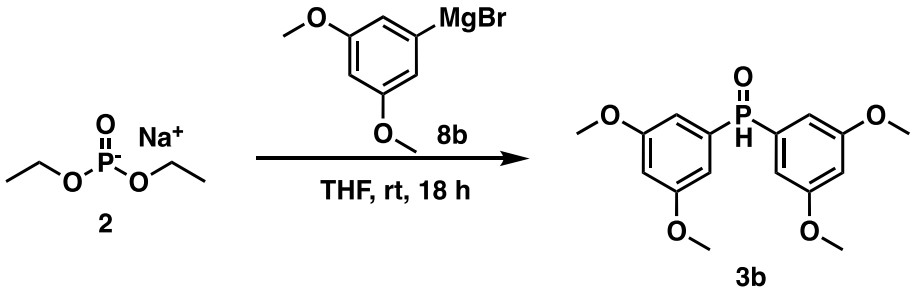

Figure 86: Synthesis of

After the workup, the desired product bis-(3,5-dimethoxyphenyl)-phosphine oxide **3b** was obtained with yield of 83 % and a purity of 87 %. The low yield is a result of not enough active magnesium available for the reaction and should be adapted in the future.

Synthesis of *10*-phenoxyzinphosphine oxide

The synthesis of *10*-phenoxyzinphosphine oxide **3c** (POP oxide) was carried out after PONOMAREV who published the synthesis in 2004 and is the only literature available (Figure 87).[128] For other ligands containing POP, the phosphine chloride route is preferred and more commonly used.

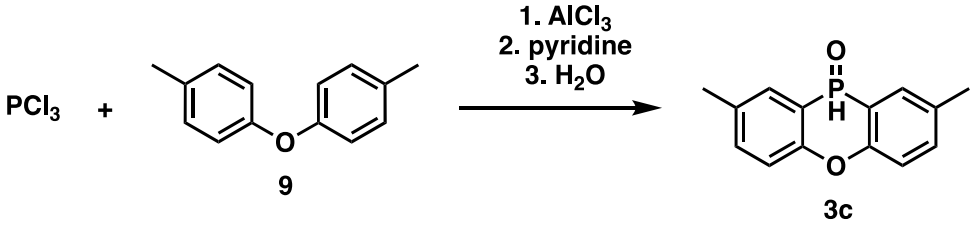

Figure 87: Synthesis of POP oxide.

The initial two reaction steps lead to the creation of POP chloride, which reacts easily with water to produce the desired phosphine oxide and HCl. The reaction is highly exothermic, so the reaction mixture was poured onto ice to cool it simultaneously. The crude product was purified *via* column chromatography, which did not lead to such a high loss of product compared to dixylylphosphine **4a**. Instead, the pure POP oxide **3c** was obtained as bight white solid which showed the characteristic P–H coupling of over 500 Hz in the ^{1}H NMR spectrum. A yield of 82 %could be achieved. Next, the phosphine oxides were reduced to produce the phosphine intermediates.

5.7.3. Reduction to bis(3,5-dimethylphenyl)phosphine

Using Trichlorosilane

In the context of secondary phosphine oxide reduction, a substantial body of research has been dedicated to reactive silanes as reducing agents.[129] Trichlorosilane stands out as the most widely employed reducing agent in this context.[130]

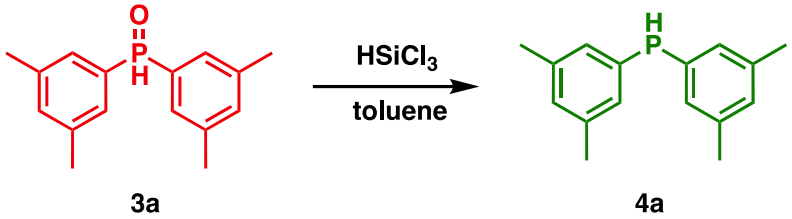

*Figure 88: Reduction towards bis(3,5-dimethylphenyl)phosphine **4a**.*

A suggested mechanistic pathway is depicted in Figure 89. Initially, a four-step transition-state is established, wherein the oxygen is abstracted by the silane. Simultaneously, a concerted hydrogen transfer occurs to the phosphine. Subsequently, the resultant acidic siloxane anion facilitates the return of the hydrogen, leading to the regeneration of the phosphine, while generating trichlorosilanol as a by-product.[129]

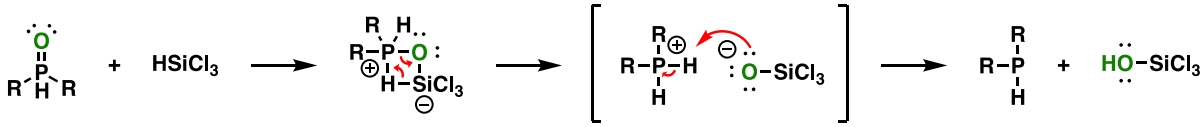

Figure 89: Proposed mechanism for reduction of secondary phosphine oxides with trichlorosilane.[41]

The silanol as the only by-product is an advantage of this reaction in comparison to other reducing agents like DIBAL-H. Due to its low boiling point, it can be vaporized under reduced pressure alongside excess trichlorosilane without laborious work-up processes.

Other phosphine species undesirably formed during the reaction sequences were also able to be reduced using trichlorosilane, so that starting from different phosphine species this method led

to comparable good results. Different ratios of toluene and trichlorosilane, different reaction times and work-up procedures were tested.

Because of the air sensitivity of the phosphine and the reducing agent trichlorosilane all reactions were carried out in degassed, dry toluene. When trichlorosilane was added in argon countercurrent, the formation of gas and vapor was observable. The reaction mixture and the products after work up were analyzed *via* ^{31}P-NMR spectroscopy to differentiate the formed phosphorous species.

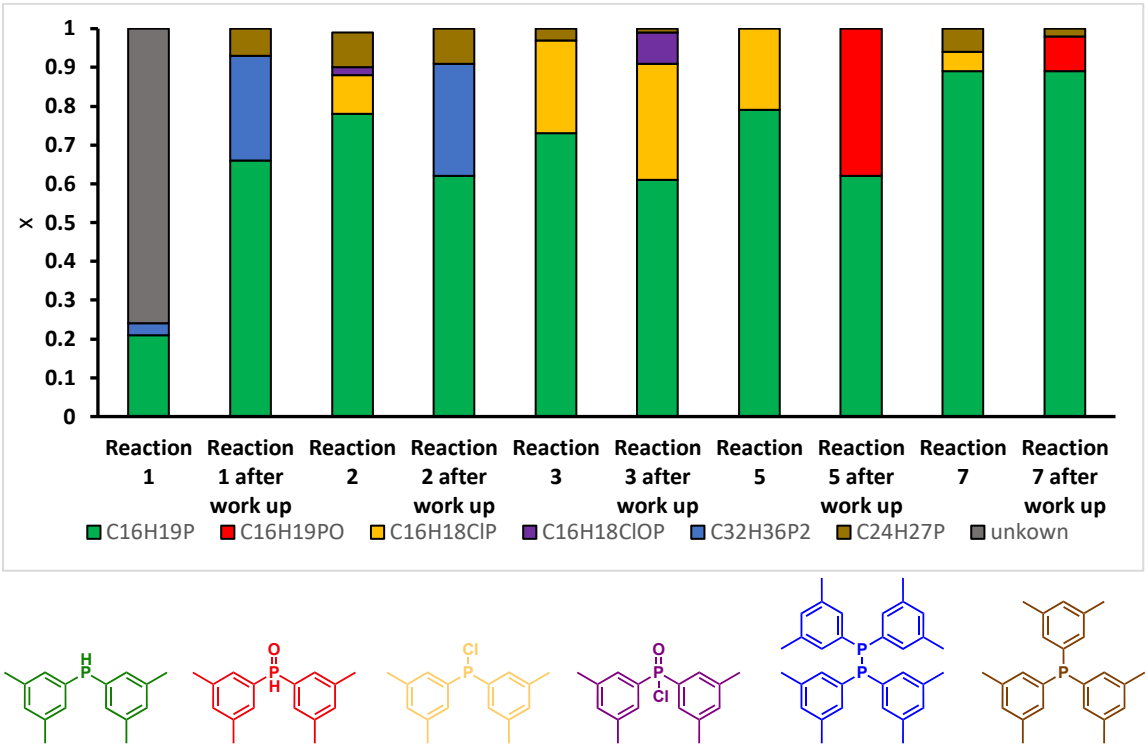

Figure 90: Overview of obtained phosphorus species during and after reaction (Proposed structure based on ^{31}P-NMR chemical shift) (adapted from SCHMIDT 2020[109]).

In reaction 1, a full conversion was achieved within 2.5 h, so less reduction agent was used for the next reaction. A predominant side-product, i.e., 1,1,2,2-tetrakis(3,5-dimethylphenyl)-diphosphine, was observed. By increasing the solvent content in reaction 2, dilution of the reaction mixture could prevent the undesired dimer formation. However, the formation of the dimer persisted, which could be attributed to the removal of trichlorosilane at 50 °C during the workup procedure and the presence of chloro bis(3,5-dimethylphenyl)phosphine. The phosphine chloride can react with the desired phosphine, leading to the formation of a dimer (Figure 91).

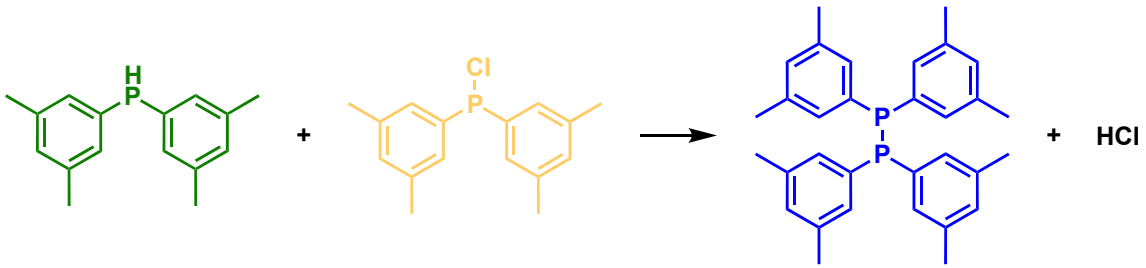

Figure 91: Side-reaction: formation of the phosphine dimer.

As this reaction points out the most prominent side-reaction, it was tried to suppress the formation of the phosphine chloride as well as the coupling with the phosphine. In reaction three, the removal of solvent was carried out at room temperature which proved that a lower

temperature did not lead to the coupling towards the dimer ($C_{32}H_{36}P_2$) but instead to the preservation of the phosphine chloride.

In reaction 4 the dependence of the formation of the phosphine chloride from trichlorosilane was investigated. 3.6 eq., 5 eq. and 6.4 eq. of trichlorosilane were added and each heated to reflux for an hour. As visible in Figure 92 with little amount of trichlorosilane a lot of phosphine chloride was formed, with addition of more trichlorosilane the amount auf the phosphine chloride is reduced to the phosphine **4a** and the dimer while the amount of the triphenylphosphine remains constant.

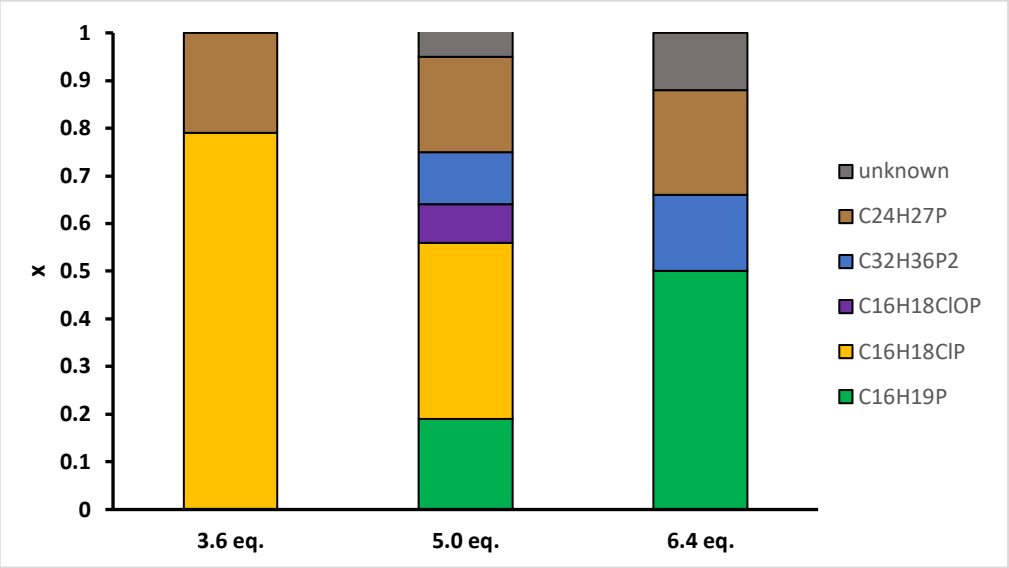

Figure 92: Dependence of formation of phosphine chloride from amount of trichlorosilane(adapted from SCHMIDT 2020[109]).

As an amount of 6.4 eq. trichlorosilane did not form any phosphine chloride, in reaction 5 the same amount was used. However, the phosphine chloride was formed, so that different workup procedures were tried in the next three reactions to avoid the formation of the dimer. In reaction 5, quenching with a degassed aqueous NaOH-solution (20 %) was tested. No dimer was formed but apparently the phosphine chloride and parts of the phosphine were oxidized.

As reaction 6 showed, a large excess of trichlorosilane of 11 eq. did not result in a more selective formation of the phosphine but to a species not detectable by our ^{31}P-NMR investigations, possibly the deprotonated phosphine. Quenching with isopropanol as well was assumably unsuccessful because no quenching characteristics like gas formation or color change were observable. The ^{31}P-NMR confirmed these observations as still no phosphorus species except for a small amount of oxide (maybe due to leaks during the preparation of the NMR sample) were found. The phosphorus species was still undetectable.

In reaction 7, 5 eq. of trichlorosilane were enough to obtain the desired phosphine **4a** in good analytical yields. The dropwise addition of a small amount of degassed aqueous NaOH-solution (20 %) led to precipitation of the excess silane as white solid and after filtration and removing of toluene under reduced pressure, the phosphine **4a** was obtained as a yellow liquid with high purity of 89 %. After the successful formation of in high purity, a successful sequential reaction towards the ligand is promising.

Temperature Dependency

A significant gas development was observed during the addition of trichlorosilane, even before the completion of the addition or heating of the reaction. This suggests that the reaction occurs at room temperature and may require less trichlorosilane. To simplify the overall reaction

procedure, it is advisable to avoid heating and perform the reactions at room temperature. This would also enable the use of a solvent with a lower boiling point than toluene for the reaction.

The solvent was replaced with THF, and the reaction was carried out at 22 °C (Figure 93). The amount of trichlorosilane added was reduced to 2.5 equivalents. The reaction was not quenched, but instead, the volatile trichlorosilane, the siloxanes received as coupling products, and the THF were removed under vacuo. The reaction progress and product were investigated via NMR-spectroscopy.

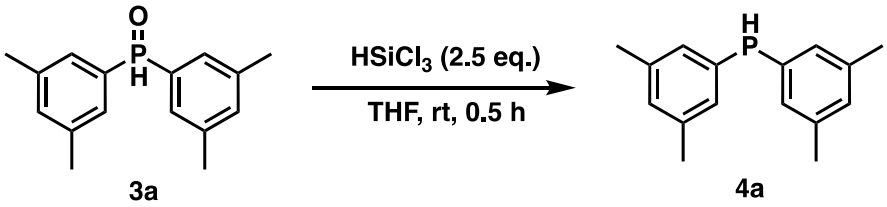

Figure 93: Reduction of the dixylene-phosphine-oxide using trichlorosilane.

The NMR-spectroscopy investigation revealed that full conversion of the phosphine oxide **3a** could be achieved within 30 min even at room temperature, as determined by the product signal at around -39.6 ppm. The product mixture analysis showed a second signal at a chemical shift of 84.0 ppm, accounting for 16% of the phosphorus. This signal indicates that the dixylene-phosphine-chloride was produced as a by-product during the reaction. A third signal was detected at -14.8 ppm, but its intensity was very low. This signal may have been caused by a reaction between dixylene-phosphine-chloride and moisture in the NMR sample. The reaction between water and phosphine-chloride may have formed dixylene-phosphine-hydroxide. Dixylene-phosphine **4a** was received as an off white solid in a good yield of 80 % and a purity of 84 %.

The reaction can be carried out at much lower temperatures, resulting in two phosphorus species. With the lower temperatures, no phosphorus dimers were observed, and the main product is the desired phosphine **4a** with only 2.5 eq. of silane. However, the presence of 16 % phosphine chloride is still high and could be reduced by using a chloride-free reduction agent.

Reduction of POP oxide

Next POP oxide **3c** was reduced with the same procedure.

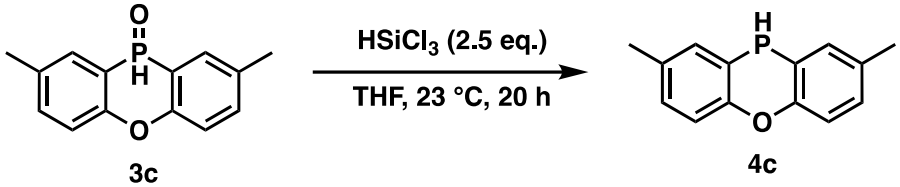

Figure 94: Reduction of POP oxide with trichlorosilane.

The product mixture obtained consisted mainly of POP chloride (62 %), with only 29 % representing the intended phosphine **4c** product. The remaining 9 % was attributed to POP hydroxide. To improve the POP synthesis, the reaction conditions were adjusted by lowering the reaction temperature to 0°C and limiting the reaction duration to one hour. Subsequent analysis using NMR spectroscopy revealed a modified product mixture.

Under the revised conditions, the ^{31}P-NMR spectrum displayed two distinct signals: one at 37.2 ppm corresponding to POP chloride and another at 15.1 ppm indicative of POP hydroxide. It is noteworthy that the desired POP could not be detected. Instead, POP chloride was received as an off-white solid, with a high yield of 90 % and a purity of 93 %. Under the given reaction condition the different nature of the phosphine oxide **3c** leads to its chlorination instead of the reduction to the desired phosphine **4c**.

A different reduction agent without chlorides could prevent the chlorination, hence DiBAl-H was tested as an alternative.

Using DiBAl-H

In 2005 BUSACCA and coworkers at BÖHRINGER-INGELHEIM published a new method using diisobutylaluminium hydride (DiBAl-H).[131] With the goal of finding a safe and effective reduction method even on larger scale. The group claimed DiBAl-H to be superior to previously described reduction routes. The reduction was also possible at room temperature in only 10 min with their procedure.

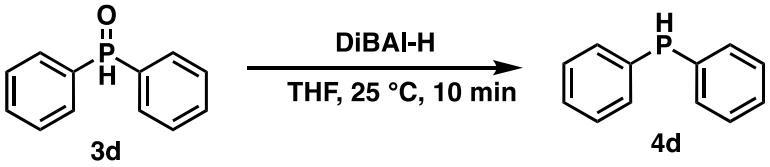

Figure 95: Reduction of dixylylphosphineoxide with DiBAl-H.[131]

In contrast to neutral diphenylsilane which is often used but requires 200 °C in many cases or the electron deficient trichlorosilane which is described with elevated temperatures and was also used in this work.[132,133] As presented above trichlorosilane requires refluxing in toluene to avoid chlorinated side product or a precise control of the reaction time. Regarding larger scale synthesis trichlorosilane also holds additional risks such as a low flash and boiling point at -13 °C and 31 °C respectively.[134,135] Under reaction conditions the temperature is higher than both resulting in high-risk due to possible oxygen contamination during malfunction.

The group of BUSACCA reached yield of up to 92 % with their reduction protocol for a variety of phosphine oxides **3**. Notably, the reaction was carried out under very mild conditions. A drawback of the presented methodology is the requirement of special glass ware for best results. The work up of the crude product consists of several extraction and washing steps with aqueous NaOH solution and brine. Nevertheless, the more complex workup promises a higher purity of the final product.

At first, the procedure was tested on phosphine oxide **3a**, that was recovered from a previous reduction experiment that showed splitting of the secondary phosphine resulting in primary phosphine.

Since the exact apparatus described in the publication was not available a three-neck Schlenk flask was used with Teflon tubes as a sparge line and for the removal of the aqueous phase. The phosphine oxide was successfully converted into the desired phosphine, while the primary phosphine did not increase (Figure 96).

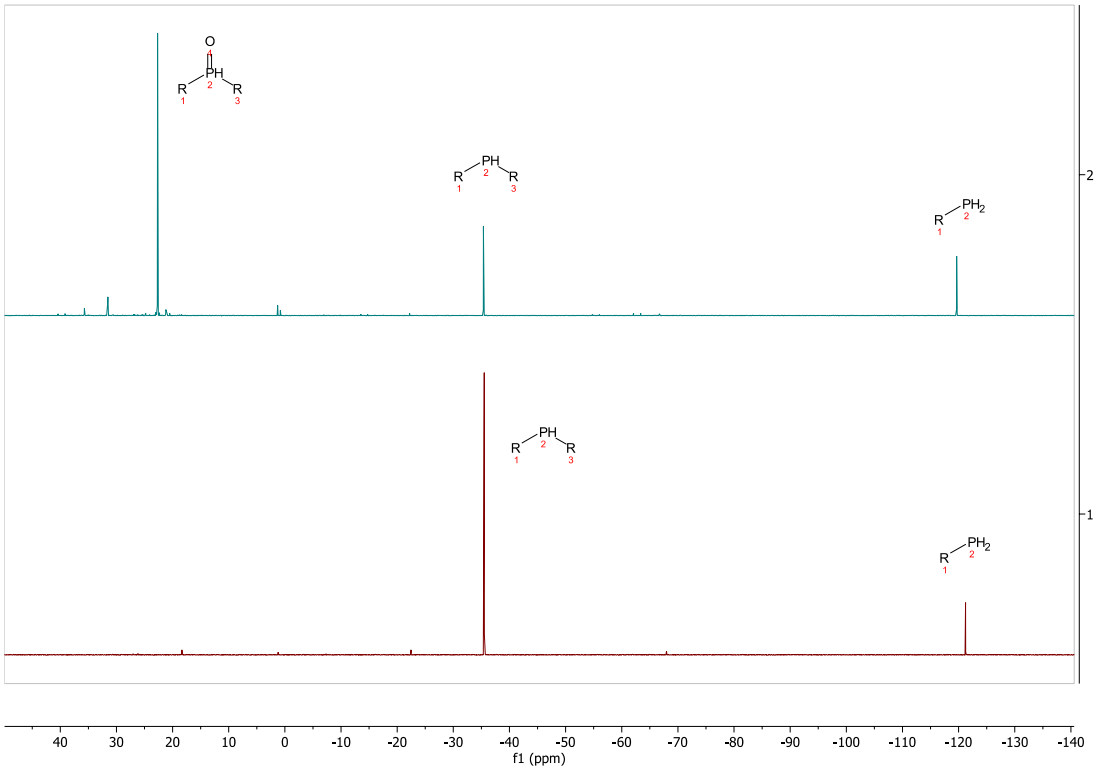

Figure 96: Comparison of the ^{31}P-NMR before and after the reduction with DiBAl-H including work up (R = Xylyl).

After this promising result the same reaction conditions were applied to POP-oxide **3c**. Instead of the desired POP-H phosphine **4c**, a primary phosphine was detected as the only product.

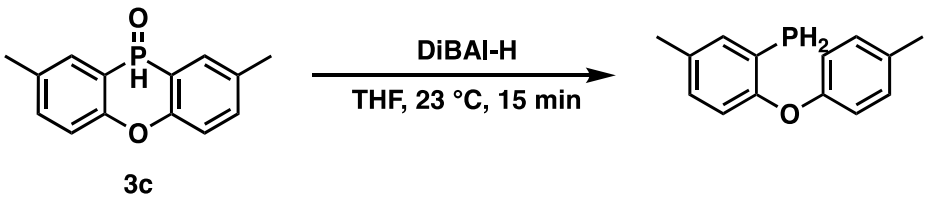

3c

*Figure 97: Reduction of POP-oxide **3c** with DiBAl-H resulting in a primary phosphine.*

The cyclic structure of POP-H **4c** seems to be not sufficiently stable and promotes the ring opening under reductive conditions. This could explain that POP-H was reported in the literature only once in 1965.[136] FRITZSCHE and coworkers investigated the reduction of secondary and primary phosphine oxides with silanes.

5.7.4. Synthesis of xyl-triphos

In general, the synthesis of the final ligand is carried out by deprotonation the phosphine **4a**, which can then react with the tripodal backbone **5**. In a nucleophilic substitution the desired ligand is formed with a chloride salt formation as the driving force.

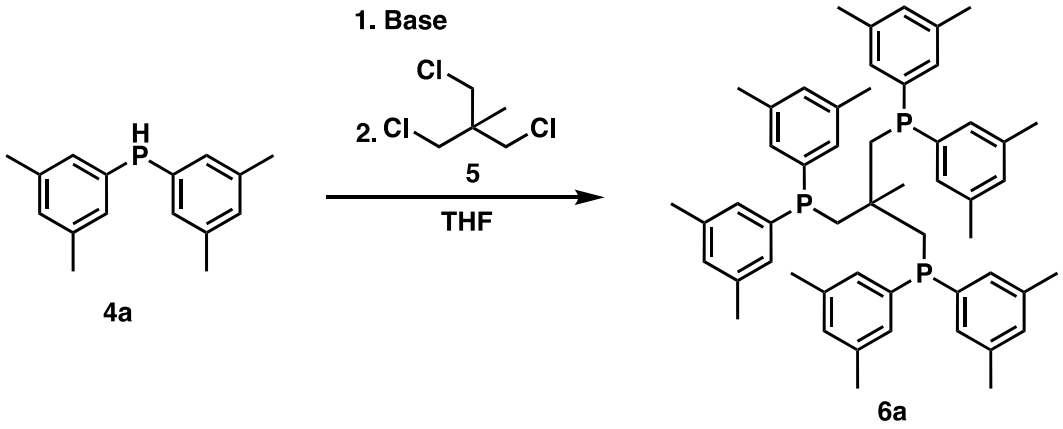

*Figure 98: Synthesis of triphos-xly **6a**.*

In a first test reaction the deprotonation of dixylylphosphine **4a** was not successful, hence LDA was tested which is also a strong base and simultaneously a weak nucleophile due to steric hindrance. A successful deprotonation is indicated by the formation of a dark red solution upon addition of LDA. The yellow color of the phosphine shifts to red due to the delocalized π-electron system of the aromatic rings, which is now expanded beyond the phosphorus atom (bathochromic shift). Therefore, the color of the solution is a first sign for a successful deprotonation. Moreover, the solution was analyzed by ^{31}P-NMR and the absence of a phosphine peak at 40 ppm confirmed full conversion. Although the deprotonation was successful, no ligand **6a** was obtained from the reaction with the backbone **5**. Also, heating to reflux for two days only lead to 14% analytical yield in the reaction mixture. Due to the poor yield no separation of the ligand **6a** was possible.

Sodium hydride was not able to deprotonate the phosphine as no red color was observable and phosphine was still present in the ^{31}P-NMR spectrum.

KLANKERMAYER[43] proposed using potassium *tert*-butoxide and DMSO. The order of addition (first phosphine **4a**, then KO*t*Bu, then solvent) seems not to be recommendable, as the solid KO*t*Bu reacts heavily with the oily **4a** under coloration towards red and formation of heat and bubbles. Although the reaction time and temperature were increased step by step, no triphos-xyl **6a** ligand was observable.

Since the results obtained in THF were more favorable than those in DMSO, THF was used with KOtBu as the deprotonating agent. However, the deprotonation using KOtBu was not successful probably due to still present water in the substrate, despite long drying times under reduced pressure. After adding more KOtBu until no more bubbling occurred and complete deprotonation was achieved, the ^{31}P-NMR spectrum showed no remaining phosphine. After stirring for 19 h at 60 °C and quenching with saturated ammonia chloride solution, no ligand but only phosphorus oxides were obtained.

The phosphine **4a** was thoroughly dried using toluene-water azeotropic distillation. It was then added dropwise to a colorless solution of KOtBu in THF, resulting in a color change from yellow to deep red (Figure 99).

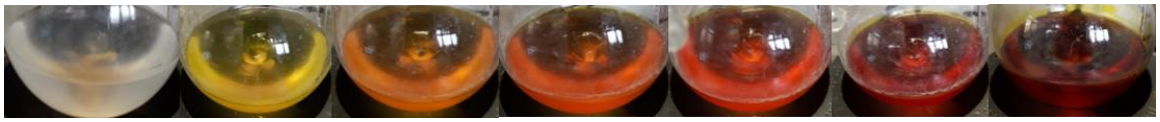

Figure 99: Color gradient during the addition of KOtBu (from SCHMIDT 2020[109]).

The transparent red solution indicates successful deprotonation and the ^{31}P-NMR spectrum shows the presence of ligand in the cloudy red solution (Y_{ana} = 67 %). After quenching with degassed saturated ammonia chloride solution and concentrating under reduced pressure, the ligand was isolated via crystallization. The resulting yellow oil was dissolved in degassed isopropanol and water was added until a 1:1 ratio was achieved, causing a fine white solid to

precipitate. After several washing cold washing steps with 2-propanol and methanol the triphos-xyl **6a** ligand was obtained as a white solid in a poor yield of Y_{iso} = 5.

The procedure was repeated with an improved isolation step. The desired ligand was recrystallized from iso-propanol (40 mL, 95 % 2-propanol, 5 % water, mixing 70 °C, crystallization -20 °C). With this crystallization the isolated yield could be improved to 38 %.

5.7.5. Ester amination with triphos-xyl

The newly synthesized triphos-xyl **6a** ligand was then tested in ester amination (Figure 102) and first in the separate reactions (Figure 100, Figure 101).

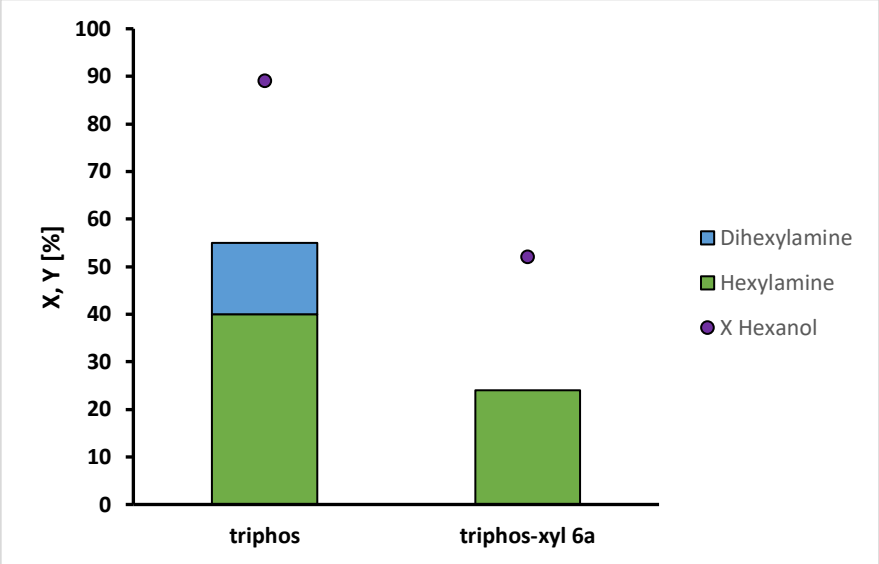

*Figure 100: Comparison of triphos and triphos-xyl **6a** ligand in amination of hexanol. Conditions: $Ru(acac)_3$ 2 mol%, triphos 4 mol%, hexanol 0.38 mmol, MSA 2 mol%, dioxane 3.5 mL, water 1 mL, di-n-butyl ether 100 mg, H_2 10 bar, NH_3 10 eq., 220 °C, 20 h (adapted from SCHMIDT 2020[109]).*

Compared to triphos under the same conditions, triphos-xyl shows a lower conversion, but achieves a higher amine selectivity. No dihexylamine was detected in the reaction with triphos-xyl **6a**. However, both reactions showed a discrepancy between conversion and yield, which cannot be explained by the gas chromatogram.

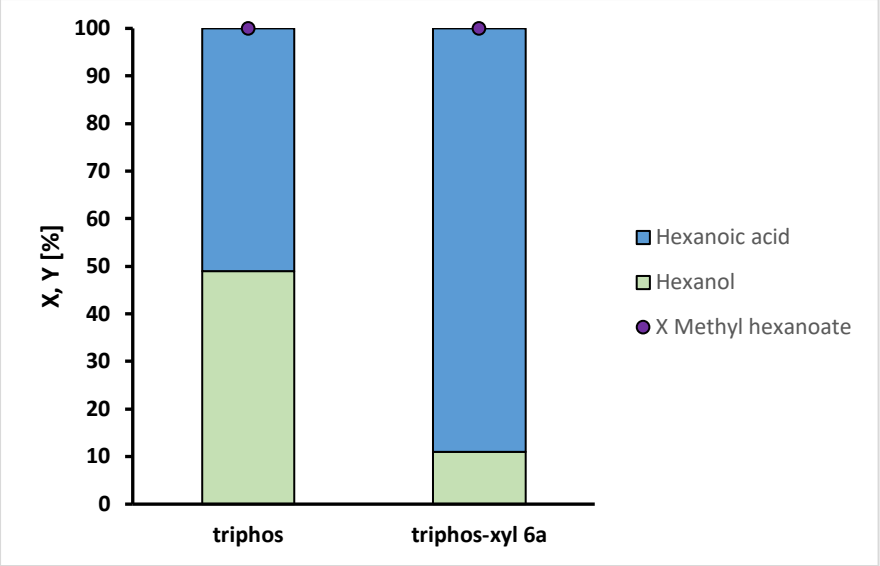

*Figure 101: Comparison of triphos and triphos-xyl **6a** ligand in reduction of methyl hexanoate. Conditions: $Ru(acac)_3$ 2 mol%, triphos 4 mol%, methyl hexanoate 0.38 mmol, MSA 2 mol%, dioxane 3.5 mL, water 1 mL, di-n-butyl ether 100 mg, H_2 10 bar, 220 °C, 20 h (adapted from SCHMIDT 2020[109]).*

The ester hydrogenation was less successful and resulted mainly in the hydrolysis of the ester. Chronologically, this experiment was conducted before the successful hydrogenation with Ru/triphos was achieved. Therefore, trace oxygen could have been affecting the reaction, as described in chapter 5.5.2. Nevertheless, the same conditions were applied to both ligands and in comparison, triphos-xyl could not obtain better results in the hydrogenation reaction, which contradicts the finding in from the literature.[125] This could result from not ideal reaction conditions for triphos-xyl, e.g. the literature used only 160 °C and 100 bar H_2.

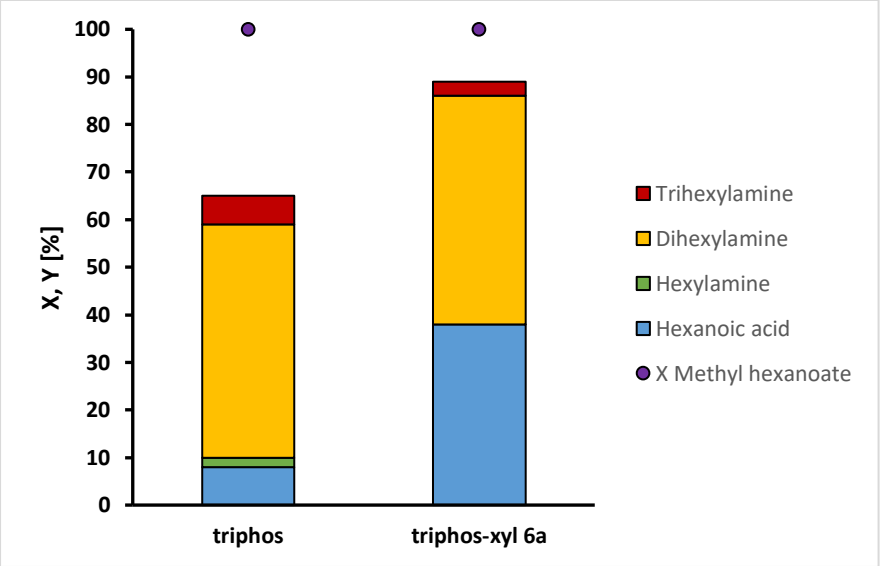

*Figure 102: Comparison of triphos and triphos-xyl **6a** ligand in amination of methyl hexanoate. Conditions: $Ru(acac)_3$ 2 mol%, triphos 4 mol%, methyl hexanoate 0.38 mmol, MSA 2 mol%, dioxane 3.5 mL, water 1 mL, di-n-butyl ether 100 mg, H_2 10 bar, NH_3 1000 mol%, 220 °C, 20 h (adapted from SCHMIDT 2020[109]).*

In the combined ester amination, hexylamine was only detected when the triphos ligand was used. Both ligands showed significant formation of dihexylamine, showing the potential ability for amination, but not the desired primary amine formation. In the case of triphos-xyl **6a**, more hydrolysis was observed, but the secondary and tertiary amine yields were comparable.

For future studies on the ligand, an optimization of the reaction conditions is recommended, which was not possible in this study due to the low amounts obtained in the synthesis. It was assumed that the reaction parameters of Ru/triphos could be applied to Ru/triphos-xyl due to their similarity. However, the results indicate otherwise.

5.7.6. Experimental

Ester amination with triphos-xyl

The ligand and catalyst precursor were placed in a reactor and closed. The reactor was purged with 3 argon/vacuum cycles. A stock solution, along with the solvents di-n-butyl ether and substrate, were added in an argon countercurrent. The reactor was then pressurized with 10 bar of hydrogen, and if applicable, ammonia was pumped into the reactor at 10 bar with the *via* a syringe pump. The reactor was stirred at 220°C for 20 h. After cooling down, the reactor was opened, and the reaction solution was analyzed using GC/MS.

Synthesis of sodium diethyl phosphonate

Sodium hydride (1457 mg, 57.7 mmol, 1.16 eq.) was placed in a heated out Schlenk flask under argon and diethyl ether (100 mL) was added and a gray suspension formed. Afterward diethyl phosphonate **1** (6.5 mL, 49.8 mmol, 1 eq.) was added under an argon countercurrent. The suspension was stirred for 20 h at room temperature. After completion of the reaction time excess sodium hydride filtered off and the solution transferred to a heated out Schlenk flask. The residue was rinsed with diethyl ether. The resulting solution was used directly in the next reaction.

Synthesis of bis(3,5-dimethylphenyl)phosphine oxide (I)

Magnesium activated with 0.05 M hydrochloric acid (3002 mg, 122 mmol, 2.45 eq.) was stirred in a heated Schlenk tube with 3 iodine beads for 4 h, a brown coloration of the magnesium being observable. 5 mL diethyl ether were added at 40 °C as well as 5-bromo-*m*-xylene **7a** (9.5 mL) in portions of 1 mL and in between two 1 mL portions of ether. The solution was kept in an ultrasonic bath. 1 mL 5-bromo-*m*-xylene **7a** and 10 mL ether were alternately added until all 5-bromo-*m*-xylene **7a** (15 mL, 108 mmol, 2.17 eq.) and ether (60 mL) had been added. The reaction solution was stirred at 40 °C. for 20 h. The resulting greenish-brown solution was added to a heated flask with the reaction solution of the synthesis of sodium diethyl phosphonate **2**; reaction 3 using a syringe and excess magnesium was rinsed with 15 mL ether. Another 70 mL ether was added due to a violent reaction. The reaction solution was stirred at room temperature for 80 h. The red solution with a gray sticky solid was quenched with saturated aqueous ammonium chloride solution (70 mL). The yellow solution was extracted with 3 × 50 mL diethyl ether, dried with magnesium sulfate, filtered off and concentrated on a rotary evaporator. The bis(3,5-dimethylphenyl)phosphine oxide **3a** was obtained as a yellow oil (4.438 g, 17.18 mmol, 0.35 eq.).

Synthesis of bis(3,5-dimethylphenyl)phosphine oxide (II)

Magnesium (120 mmol, 2946 mg, 3 eq) was prepared under an argon atmosphere and stirred with an iodine crystal over 16 h. Distilled THF (5mL) was added and 5-bromo-xylene **7a** (22 mmol, 3 mL, 0.54 eq) was added. the mixture was heated to 50 °C and stirred for 15 min. An iodine crystal was added leading an exothermic reaction and boiling of the solution. Additional THF (10 mL) and 5-bromo-m-xylene **7a** (29 mmol, 4 mL, 0.72 eq) were added leading to more boiling. The solution was stirred at 50 °C 5 min. THF (10 mL) and 5-bromo-m-xylene **7a** (29 mmol, 4.1 mL, 0.74 eq) were added. The reaction was stirred about 15 min before more distilled THF (15 mL) was added. The reaction was stirred at 50 °C 16 h.

The sodium diethyl phosphonate **2** was filtered into a heated out flask and the GRIGNARD was slowly filtered into it. The reaction was stirred at 24 °C about 20 h.

The reaction was quenched with a concentrated aqueous ammonium chloride solution (50 mL) leading to a gas development. Additional water (50 mL) and diethyl ether (40 mL) were added, the phases were separated, and the aqueous phase was extracted with diethyl ether (2x 50 mL). The organic phases were combined dried over magnesium sulphate and the solvent was removed under reduced pressure yielding a yellow liquid. The liquid was investigated via NMR-spectroscopy. Dixylenephosphineoxide **3a** (36.2mmol, 9360mg, Y=91%, 96%) was received as a yellow viscous liquid.

Synthesis of bis(3,5-dimethoxyphenyl)phosphine with $HSiCl_3$

Bis-(3,5-dimethoxyphenyl)-phosphine oxide **3b** (5.600 g, 17.4 mmol) was dissolved in a small amount of dry toluene and transferred into a Schlenk flask. The amount of solvent was increased to 180 mL toluene and this solution was degassed using an ultrasonic bath under argon atmosphere for one hour. After that, trichlorosilane (8.9 mL, 87 mmol, 5 eq.) was added dropwise over 15 min. After the first drops some white precipitate was formed and the reaction mixture was heated to 110 °C for 2.5 h. After this aqueous NaOH-Solution (20 %) was added dropwise until no solid was formed any more (30 mL). The phases were separated, and the organic solvent was removed under reduced pressure, resulting in a brown oily residue. (3.965 g, 74 % (70% phosphine **4b**, 30 % phosphine oxide **3b**)).

The phosphine / phosphine oxide mixture from the first reduction (1.815 g, 5.63 mmol, 1 eq.) was dissolved in dry toluene (50 mL) and degassed using an ultrasonic bath under argon atmosphere for an hour. After that, trichlorosilane (2.27 mL, 22.3 mmol, 4 eq.) was added dropwise. The reaction mixture was heated to 110 °C and after an hour, it was cooled down to rt and NaOH Solution (20 %, 17 mL) was added, the phases were separated and the organic solvent was removed under reduced pressure, resulting in a brown oil (1.935 g, (86 % phosphine **4b**, 14 % phosphine oxide **3b**).

Synthesis of bis(3,5-dimethoxyphenyl)phosphine with DiBAl-H

The reaction was carried out after BUSACCA *et al.*[131] A 3-neck Schlenk flask equipped with a magnetic stirrer, addition funnel, and an argon sparge line was evacuated/Ar filled (3X), then charged with 48 mL 1M DIBAL-H/THF (48.0 mmol, 7 eq.) through the addition funnel (Figure 103). 10 mL THF were used to rinse the walls of the addition funnel into the flask. The addition funnel was then charged with a solution of 2.2 g phosphine oxide **3b** (6.8 mmol, 1 eq.) in 20 mL THF. This solution was then added dropwise over 10 min (CAUTION: gas evolution). 10 mL THF were used to rinse the walls of the addition funnel into the flask. The resulting mixture was then stirred at room temperature for 20 min, after which 80 mL of MTBE was added dropwise over 10 min via an addition funnel. After 10 min, the sparge line was inserted below the surface of the solution and a slow flow of argon was initiated and maintained throughout all subsequent operations. After sparging for 10 min, the mixture was cooled with a water/ice bath. The addition funnel was then charged with 50 mL 2 N NaOH. This solution was then added dropwise via addition funnel over 20 min. 15 mL saturated aq. NaCl was then added via an addition funnel over 10 min. After 5 min, stirring was stopped and the lower aqueous phase was removed *via* a Teflon tube and argon pressure. 50 mL 5 % (w/v) NaCl in H_2O was then added dropwise through a funnel for 10 min, and the lower aqueous phase was again removed as before. Then in a second Schlenk flask 10 g $MgSO_4$ was inertized with argon and the organic phase was transferred into the flask *via* a Teflon tube. After e few minutes of shaking the dried organic phase was filtered off. 25 mL MTBE were used to extract the remaining $MgSO_4$ and the solvent of combined organic phase war removed under

reduced pressure. The product was received as colorless oil (2.8 g, Containing the secondary and primary phosphine 4:1).

Figure 103: Apparatus for the reduction with DiBAl-H.

Synthesis of 1,1,1-tris(bis(3,5-dimethylphenyl)phosphinyl)methyl)ethane (triphos-xyl)

Potassium *tert*-butoxide (1405 mg, 12.1 mmol, 3.67 eq.) was placed in a heated Schlenk flask and dissolved in 100 mL THF. Bis(3,5-dimethylphenyl)phosphine **4a** (2802 mg, 11.6 mmol, 3.5 eq.) was added dropwise. The solution was stirred for 30 min and 1,3-dichloro-2-chloromethyl-2-methylpropane **5** (0.51 mL, 3.31 mmol, 1 eq.) was added. The mixture was stirred for 20 h at 60 °C. The reaction solution was quenched with 30 mL of saturated ammonium chloride solution. The resulting yellow aqueous phase was extracted once with 30 mL of diethyl ether. The solvents of the combined organic phases were removed under vacuum, resulting in a white solid precipitate that disappeared upon further concentration. The remaining yellow oil was dissolved in 10 mL of isopropanol. Water was gradually added to the solution until a 1:1 mixture of water and isopropanol was formed, and the solution was then centrifuged. A brown oil was separated from a white, milky solution. The milky solution was concentrated and a white solid was crushed out. The oil was taken up in isopropanol and recrystallized -23 ° C. A yellow solution was separated from solid oil. Fresh isopropanol was added in the cold and white, fine-grained solid was slowly washed out of the oil. This solid was separated and allowed to sink so that an orange solution could be separated. The white solid was washed with isopropanol. The washing solution was stored at -23 ° C for 30 min, during which time again a lot of white solid precipitated. The white solid was washed again with methanol in the cold, dried in a high vacuum and the ligand **6a** was obtained as a white solid (145 mg, 0.183 mmol, 0.05 eq.).

5.7.7. Analytics

Sodium diethyl phosphonate

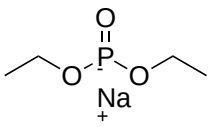

^{31}P NMR (25 MHz, diethyl ether) δ =154.43 - 155.75 (s, 1 P; O=PNa(OR)$_2$) ppm.).

Synthesis of bis(3,5-dimethylphenyl)phosphine oxide

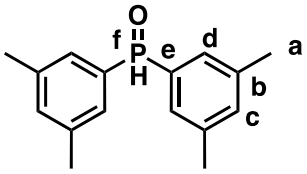

^{1}H NMR (500 MHz, $CDCl_3$) δ = 8.52 (s, 2H, f), 7.33 – 7.26 (m, 4H, d), 7.17 (s, 2H, c), 2.33 (s, 12H,a)
^{13}C NMR (126 MHz, $CDCl_3$) δ = 138.84, 138.71, 134.37, 134.34, 131.88, 130.87, 128.32, 128.21, 68.05, 25.70, 21.33.
^{31}P NMR (202 MHz, $CDCl_3$) δ = 22.93.

1,1,1-tris(bis(3,5-dimethylphenyl)phosphinyl)methyl)ethane (triphos-xyl)

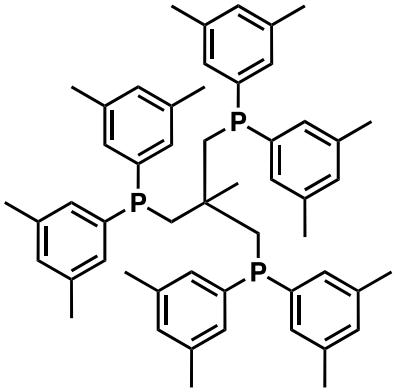

^{1}H NMR (400 MHz, $CDCl_3$): δ = 1.07 (s, 9 H; $C\underline{H}_3(CH_2)_3$), 2.17 (s, 6 H; $C\underline{H}_2$), 2.29 (s, 36 H; $C\underline{H}_3$-C_6H_3), 6.95 (s, 6 H; para-$C_6\underline{H}_3$), 7.07 (d, $J_{H,H}$ =8.3 Hz, 12 H; ortho-$C_6\underline{H}_3$) ppm.
^{13}C NMR (101 MHz, $CDCl_3$): δ = 21.32 (s, 12 C; $\underline{C}H_3$-C_6H_3), 130.46 (s, 7 C; para-$\underline{C}_6H_3$), 130.58 - 130.67 (m, 16 C; ortho-$\underline{C}_6H_3$), 137.89 (s, 4 C; meta-$\underline{C}_6H_3$), 138.24 (s, 1 C; ipso-$\underline{C}_6H_3$) ppm.
^{31}P NMR (162 MHz, $CDCl_3$): δ = -27.07 (s, 3P) ppm.

Synthesis of bis(3,5-dimethoxyphenyl)phosphine

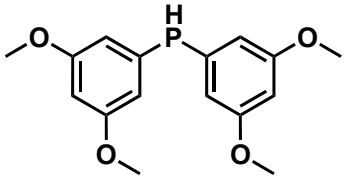

^{31}P-NMR (202 MHz, $CDCl_3$): *δ* = -35.37 ppm.

5.8.N-triphos – A preparative advantage?

Deprotonation of the phosphine presented a significant challenge in synthesizing triphos derivatives. Another class of tripodal ligands is the N-centered N-triphos, which the MILLER group extensively studied. They described two synthetic routes for synthesizing N-centered triphos ligands. (Figure 104).[137,138] Routes **A** and **B** are both phosphorus based MANNICH reactions. In route **A**, the secondary phosphine is converted with formaldehyde under acidic conditions in methanol into a stable phosphonium salt. This salt is then isolated and further transformed with ammonia under basic conditions into the desired N-triphos ligand. An advantage of this procedure is the stability of the phosphonium salt, which is air stable.[137] In route **B**, the secondary phosphine is similarly converted with formaldehyde, but under neutral conditions. This process results in the

formation of a hydroxymethyl phosphine intermediate, which is then directly converted into the desired N-triphos ligand through a one-pot reaction with ammonia under basic conditions.

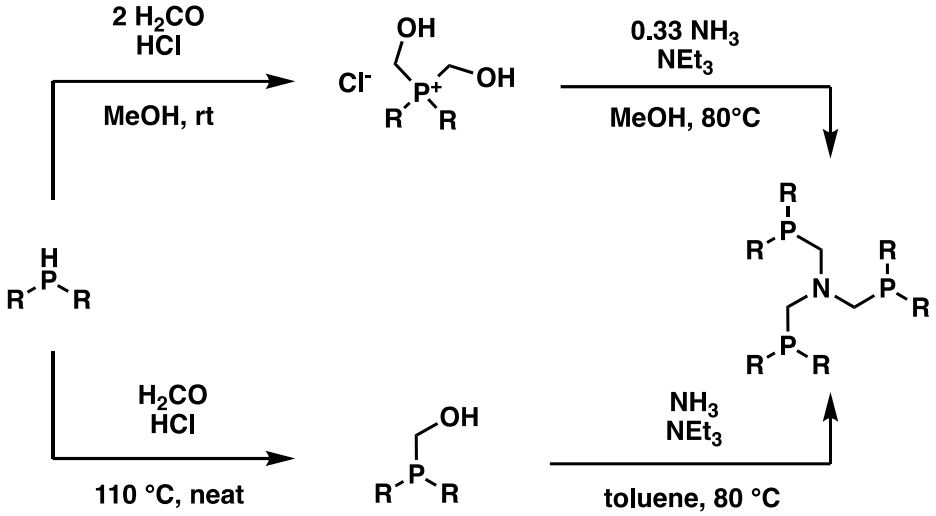

Figure 104: Two literature described routes towards N-triphos and derivates.[138]

5.8.1. Synthesis of N-triphos

Since the intermediate is directly converted into the next step the one pot synthesis seemed favorable. Furthermore, there are reports in the literature, that route **A** showed a decreased yield for some derivatives, because of a decreased reactivity of the phosphonium salt.[138,139] Therefore, a modified synthesis based on route **B** was performed (Figure 105).

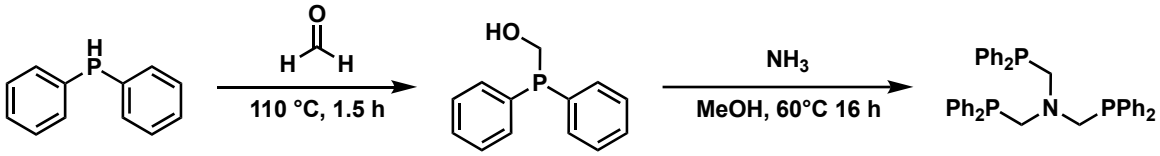

Figure 105: Modified synthesis route towards N-triphos.

Diphenyl phosphine as a commercially available secondary phosphine was taken as the starting point of the synthesis. A weakness in the synthesis of route **B** is the instability of the formed hydroxymethyl phosphine intermediate in organic solvents, especially methanol, causing the reverse reaction (Figure 106), which resulted in an equilibrium distribution and therefore reduces the yield.[140]

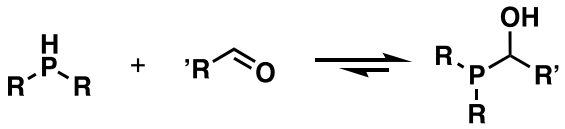

Figure 106: Synthesis and reversible decomposition of α-hydroxyphosphines.[140]

Since the diphenyl phosphine a liquid, the reverse reaction was prevented by performing the reaction without solvent. This had the additional advantage, that the reaction temperature could be increased to 110 °C, which should increase the reaction speed next to the higher concentrations of substrates.

Paraformaldehyde is insoluble in the secondary phosphine, resulting in a suspension when mixed. After 1.5 hours, the suspension cleared, indicating the end of the reaction. Methanol was added to the solution and to prevent the reverse reaction from occurring ammonia was passed through the reaction solution immediately. Instead of using an aqueous ammonia solution as reported for this synthesis, liquid ammonia was evaporated in an autoclave and passed through the reaction mixture. Adding a higher amount of ammonia increases the solubilized amount and

should lead to a higher product yield. It is important to note that the thermodynamically favored product is the trisubstituted one, compared to the mono- and disubstituted ligand. To complete the reaction, heat the reaction mixture with a slow argon current to remove the resulting ammonia. This will drive the reaction to completion.

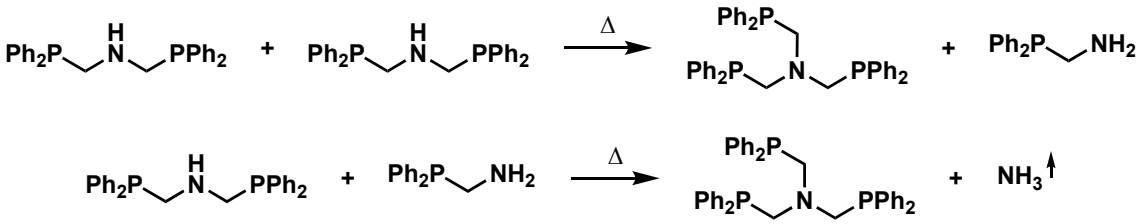

Figure 107: Recombination of secondary amines to form N-triphos.

The reaction mixture was stirred overnight at 50 °C to enhance the yield. The following day, a white suspension formed, which was an advantage of using MeOH as a solvent. The product was easily separated from the solution by filtration and purified by washing with additional MeOH. N-triphos was obtained with high purity and a yield of 65 %, consistent with reported yields in literature.[137,139]

5.8.2. Synthesis of N-triphos^{Xyl}

The synthesis of the third ligand N-triphos-xyl was performed like the synthesis of N-triphos (Figure 108)**.**

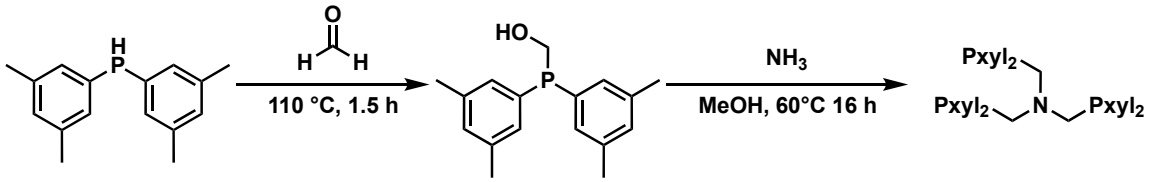

Figure 108: Synthesis of N-triphos-xyl starting from bis-(3,5-dimethylphenyl)-phosphine.

The bis-(3,5-dimethylphenyl)-phosphine was a yellow oil, therefore no solvents were needed and the N-triphos-xyl ligand was obtained in the same manner as N-triphos. First, the purity of N-triphos-xyl was only about 91%, therefore the solid was again stirred in boiling MeOH and hot filtered. After that the product showed a purity of 97 %, but the yield was only about 22 %. This was probably caused by the hot filtration to ensure to obtain a pure product but lead to losses because of the enhanced solubility of the product. Therefore, the parent solution was stored at -30 °C, no more precipitate had formed.

5.8.3. Experimental

Synthesis of N-triphos

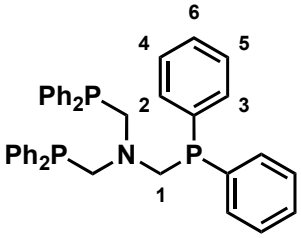

Paraformaldehyde (3 g, 31.7 mmol, 1 eq) was given into a Schlenk flask equipped with a Teflon coated stirring bar and dried under reduced pressure for 10 min. Diphenylphosphine (5.5 mL, 31.7 mmol, 1 eq.) was added via syringe in an argon counter current. The suspension was heated to 110 °C and stirred for two h. A clear solution was formed, which was filtered into a Schlenk finger. MeOH (15 mL) was added, and the mixture was heated to 55 °C. Ammonia (5 mL) was

passed through the reaction mixture during 15 min, resulting in a white suspension. The mixture was stirred overnight and the next day a yellow solution had formed. It was filtered and MeOH (15 mL) was added to the white solid again and heated to 65 °C for an additional hour. The solution turned yellow and was separated from the solid, which was washed with MeOH (2 x 5 mL) and dried under reduced pressure resulting in N-Triphos (4.2 g, 6.9 mmol, 65 %).

^{31}P-NMR (202 MHz, C_6D_6): δ = -28.77 ppm.

^{1}H-NMR (500 MHz, C_6D_6): δ = 7.53 – 7.46 (m, H2, H3, total: 12H), 7.05 – 7.01 (m, H4, H5, H6, total: 18H), 3.91 (d, J = 3.8 Hz, H1, total: 6H) ppm.

Synthesis of N-tiphos-xyl

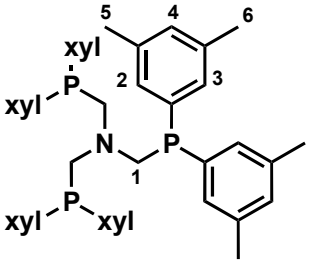

Paraformaldehyde (193 mg, 2.05 mmol, 1.1 eq) was placed in a Schlenk flask and dried under reduced pressure for 10 min. Afterwards it was added to bis-(3,5-dimethylphenyl)-phosphine (450 mg, 1.86 mmol, 1 eq) resulting in a white suspension and heated to 110 °C for 2 h until a clear, yellow solution was obtained. This was transferred into another Schlenk flask via a cannula, dissolved in MeOH (7 mL) and heated to reflux. Ammonia (2.5 mL, liquid) was evaporated and passed through the reaction mixture slowly in bubbles for 2 h. After the first bubbles, a white precipitate was formed but disappeared after 10 min stirring again. The heat was decreased to 50 °C and the reaction mixture was stirred overnight. The next day a white precipitate has formed, which blocked the stirring bar at the bottom of the flask. Additional 4 mL of methanol was added, and the mixture was heated to reflux again for 2 h. Afterwards the solution was filtered, using a filter cannula and the white solid was washed with MeOH (2 x 3 mL) and dried under reduced pressure. The NMR analysis showed 91 % purity, with many signals around -28 ppm (the desired product peak). The solid was refluxed in MeOH (8 mL) for 4 h again, the solution was hot filtered, and the white solid showed 97 % product purity (111 mg, 0.14 mmol, 22%).

^{31}P-NMR (202 MHz, $CDCl_3$): δ = 28.53 (s, 1P) ppm

^{1}H-NMR (400 MHz, $CDCl_3$): δ = 7.03 (m, H2, H3, 12H), 6.86 (s, H4, total: 6H), 3.70 (s, H1, total: 6H), 2.15 (s, H5, H6, total: 36H).

5.9. Conclusions and outlook

First, the two parts of the ester amination were studied separately. The best results in alcohol amination were obtained with MILSTEIN'S catalyst, which is not commercially available and had to be synthesized. With the same catalyst, no successful conversions were observed in the ester hydrogenation and ester amination. However, the parameters tested were limited and could be extended in future optimization experiments.

The Ru/triphos system was able to perform both reaction steps separately and the combined ester amination. The results reported in the literature could be reproduced with lower yields and were not matched even after screening experiments.

Esters were converted to primary amines with a yield of up to 49 % hexylamine. The successful reaction was attributed to the use of liquid ammonia and the addition of ammonia after the reduction of the ester. As a result, an alternative triphos-xyl was synthesized, demonstrating exceptional performance in hydrogenation reactions in previous studies.

The synthesis of triphos-xyl encountered initial struggles, as the initial plan did not yield the expected results. However, through optimization and adaption to the present equipment, successful synthesis of triphos-xyl was achieved. However, the ligand did not outperform the present triphos system. In alcohol amination, triphos-xyl showed better results compared to the performance of triphos, but not to the extent expected. The poor performance in ester hydrogenation was especially disappointing. Looking ahead, further optimization of reaction conditions for triphos-xyl could lead to an improvement in the results. Additionally, ex-situ formed catalyst complex might be beneficial for the catalysis.

The preparative procedure of N-triphos involves more steps than the triphos synthesis. However, the purification of the final product is more straightforward and does not rely on the quality of the deprotonating agent. Heating is used to control the mono-, di-, and tri-substituted ligands, which enables the easier use of excess gaseous ammonia that can be bubbled through the solution instead of aqueous NH_3. A simple precipitation of the pure ligand at the end of the reaction can avoid the more difficult crystallization and reduce the points of entry for oxygen.

The reaction can also be carried out on a larger scale by directly using gaseous ammonia, which may be future syntheses. The N-triphos ligands show promise as an alternative for hydrogenation and amination reactions. However, it is important to test the stability of the ligand under a NH_3 atmosphere. Next to the catalyst system the reaction could be improved by more advanced reaction engineering. For example, the ester hydrogenation could be carried out in a batch reactor and the following alcohol amination could be carried out in a plug-flow reactor, which allows a better control of the reaction temperature and reaction time.

6. Hydrogenation of oximes

6.1. Abstract

The efficient production of aliphatic primary amines is still a major challenge despite their production on large scale. Particularly when considering the overall production route starting from alkenes, current strategies suffer in at least one reaction step from poor regio- or chemoselectivity. This work presents an efficient and selective synthesis protocol for primary aliphatic amines *via* their corresponding aldoximes. These are readily produced from the condensation of hydroxylamine and the respective aldehydes. This straightforward condensation can be carried out either with isolated aldehydes or with crude reaction solutions from the hydroformylation of alkenes. It allows a straightforward separation of the aldoximes via their precipitation, which then serve as intermediates for the final reduction. In a newly developed protocol for aldoxime reduction, yields of up to 90 % of the desired primary amines from several different aldoximes are achieved. The ruthenium/triphos catalyst system showed activities (TOF) exceeding 7500 h^{-1}, which is significantly faster than other amination protocols, and complete conversion is achieved within minutes. Our new approach allowed the synthesis of the precursor for polyamide-12 (methyl 12-aminododecanoate) from the unsaturated, renewable oleochemical methyl 10-undecenoate *via* the hydroformylation, condensation, reduction sequence on a 6 g scale with 77 % overall yield.

This chapter is in parts contain the results of the following works which were adopted in parts, extended and modified:

Bachelorthesis:

Rene Reichert (2022): Untersuchung der Ruthenium-katalysierten Esteraminierung sowie Synthese alternativer tridentater Phosphorliganden, TU Dortmund

Masterthesis:

Hannes Wegener (2022): Optimization of a homogeneous, ruthenium-based catalyst system for the selective hydrogenation of aldoximes, Master Thesis, TU Dortmund

Publication:

Hares, K.; Wegener, H.W.; Roth, T.F.H.; Reichert, R.; Vogt, D.; Seidensticker, T. Primary amines from alkenes and carbonyl compounds: highly selective hydrogenation of oximes using a homogeneous Ru-catalyst. *Catal. Sci. Technol*. **2024**; DOI: 10.1039/D4CY00368C

Adapted in parts, extended and modified.

6.2. Introduction

Today, primary amines play a vital role in producing pharmaceuticals, agrochemicals, polymers and other chemical intermediates, which contribute to many everyday products.[93,141–143] Especially the synthesis of primary aliphatic amines remains challenging, as most routes suffer from low selectivities or poor atom economy.[27] This is a significant drawback for industrial-scale production due to the immense waste and byproducts generated. Hence, there is a large environmental and economic interest in new, more efficient synthesis protocols to produce primary amines. The most industrially abundant chemicals are alkenes, which render them desirable starting materials. However, the direct transformation into amines is complex and remains one of the critical challenges in catalysis (Figure 109).[27]

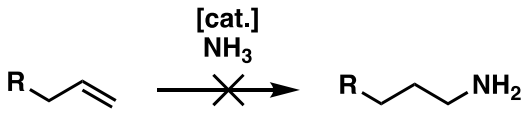

Figure 109: Catalytic, regioselective hydroamination of non-activated alkenes with ammonia towards primary amines remains a dream reaction.

The direct hydroamination of non-activated alkenes with ammonia would yield amines in a 100 % atom economic reaction and was titled the "holy grail of catalysis".[27] The main challenges are the high dissociation energy required for activating the N–H bond in ammonia,[144] the fact that the reaction is thermoneutral, and the controlled transformation into the *anti*-Markovnikov product.[27] Therefore, a wide variety of synthesis routes have been explored to address these problems (Figure 110).

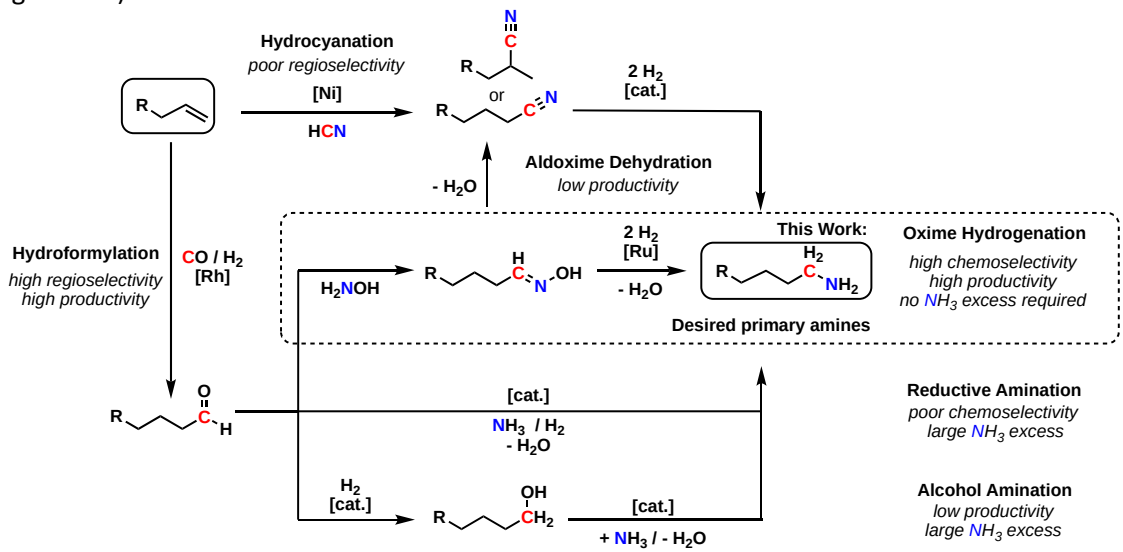

Figure 110: Reaction pathways toward primary amines starting from alkenes.

Since the direct hydroamination of non-activated aliphatic 1-alkenes with ammonia to produce primary amines is still one of the major challenges in organic chemistry,[27] the chemical industry commonly uses related hydrofunctionalizations. For instance, Ni-catalyzed **hydrocyanation** transforms alkenes into nitriles, a highly atom-economic process using hydrogen cyanide.[145–147] However, the control of regioselectivity is challenging since the desired linear amine resembles the *anti*-Markovnikov product and is, therefore, not the thermodynamically favored product.[146] Thus, hydrocyanation is only established for the synthesis of adiponitrile from 1,3-butadiene.[148] For linear, aliphatic 1-alkenes, *poor regioselectivity* is obtained. In a consecutive hydrogenation, the corresponding nitriles are transformed into the desired aliphatic primary amines with high yields and selectivities, a process that is well understood and already highly optimized.[149,150]

Alternatively, the Rh-catalyzed hydroformylation of aliphatic 1-alkenes affords aldehydes with the *highest regioselectivity* at *high productivity*.[151] These aldehydes are valuable platform intermediates for a range of different products, among them aliphatic primary amines. Three different routes generally exist: The **reductive amination** of aliphatic aldehydes directly with ammonia is still suffering from *poor chemoselectivity*.[152,153] Secondary and tertiary amines are formed by consecutive reactions of the primary amines since the produced amines are more reactive than ammonia.[28,153–155] Typically, a *large excess of ammonia* is thus used to shift the product distribution toward the primary amine, hampering productivity.

Secondly, aldehydes can be reduced to the corresponding alcohols, which can be transformed into amines by **alcohol amination**.[92,96,98,101,111,156] Excellent chemoselectivities towards primary amines, even with linear aliphatic alcohols, can be achieved using ammonia.[98] However, the high

chemoselectivity comes with the price of *high ammonia excess* and long reaction times. The reaction time often exceeds 12 h, resulting in *low productivity*.

A third but underrepresented way of synthesizing primary amines is *via* oximes as intermediates. Aldehydes stoichiometrically and highly selectively react with hydroxylamine to form aldoximes, which is why this reaction is used to identify aldehydes in complex mixtures.[157] In this way, nitrogen is introduced into molecules without risking consecutive reactions to secondary or tertiary amines, thus *avoiding a high excess of the nitrogen source.* Recently, the potential of combining Rh-catalyzed hydroformylation with aldoxime formation has been demonstrated in the context of nitrile formation *via* biocatalytic aldoxime dehydration.[158–161] We recently showed that an aqueous hydroxylamine solution does not inhibit biphasic Rh-catalyzed hydroformylation, so aldoximes can be obtained in a one-pot reaction starting from alkenes.[162] This offers an elegant way to produce aldoximes since the isolation of the reactive aldehydes is circumvented. Interestingly, it is possible to increase the already *high regioselectivity* from the hydroformylation step by aldoxime formation: In some cases, the linear oximes selectively crystallize from the reaction mixture.[161] Therefore, rendering the otherwise difficult separation of linear and branched products very efficient, making aldoximes very interesting intermediates on the way to primary amines.

As interesting as the biocatalytic transformation of aldoximes into nitriles for circumventing the use of hydrogen cyanide is, this reaction sequence has two major drawbacks for the synthesis of primary aliphatic amines: Firstly, **aldoxime dehydration** has a relatively *low productivity*, and secondly, starting from aliphatic 1-alkenes, four reaction steps are required in total.

Therefore, that direct **aldoxime hydrogenation** is more straightforward and could thus be an essential step for the highly desired primary aliphatic amines. It perfectly complements the established reaction sequence of Rh-catalyzed hydroformylation and aldoxime formation. In contrast to hydrocyanation, *high regioselectivity* and *high productivity* from the initial hydroformylation can be at least preserved. In contrast to reductive amination and alcohol amination, minimal to *no excess of the N-source* hydroxylamine is required, and consecutive reactions may be efficiently suppressed, resulting in *high chemoselectivity*.

Aldoximes are common intermediates in organic synthesis on a laboratory scale. Usually, activated hydride species are utilized for their reduction, as these reactants are easy to handle in a conventional synthesis laboratory. Boron-based reduction agents can achieve a high primary amine selectivity of over 90 %. Another recent example is the synthesis of a new *anti*-ulcer agent by IVANKIN, which relies on lithium aluminum hydride to produce the intermediate primary amine.[163] However, this reaction produces inorganic salts as byproducts, and the reagents are challenging to handle on a larger scale as they are pyrophoric and toxic. High selectivity towards the primary amine is often achieved only under harsh conditions or elongated reaction times.[164–167]

The cleanest reducing agent is molecular hydrogen in combination with a catalyst and dates to 1956; REEVE and CHRISTIAN showed excellent activity for Raney Cobalt.[168] The challenge here is to selectively stop the reaction at the primary amine and avoid consecutive reactions. The reaction mechanism for the heterogeneously catalyzed reaction was investigated by MÜLLER *et al.*[169] Who used oxide-supported Ni and Co catalysts, which are less active but show higher selectivity for primary amines, as well as Pd and Rh on activated carbon, which are more active but yield the secondary amine as the main product. This study revealed that the selectivity of the oxime reduction is highly dependent on the nature of the substrate.[169] More branched, thus, more sterically demanding substrates yield higher selectivities than entirely linear oximes, and ketoximes produce the highest primary amines selectivity.[169]

Very recently, the reduction of aldoximes was used to synthesize heterocyclic primary amines, which can be used to produce polymers and liquid crystal coordinating agents. With a heterogeneous Ni-Mo/ZrO_2 catalyst, BAI-CHENG *et al.* achieved yields above 90 % after two to four

hours of reaction time on a 60 g scale. However, excess ammonia was necessary for high yields, and the products were *beta*-cyclic compounds.[170]

In 2019, the group of WANG reported excellent hydrogenation results using a palladium-based catalyst consisting of nanoparticles with nitrogen-containing ligands.[171] They obtained a 99 % yield of benzylamine and its derivatives. The yield of aliphatic amines was reduced to 83 % in the case of octylamine and 71 % in the case of butylamine. Remarkably, the conversion takes place at an atmospheric pressure of H_2 and room temperature, and even after 10 recycling runs, the performance did not decrease significantly. However, the reaction is limited to a highly diluted substrate on an extremely small scale, namely 0.05 mmol in 10 mL H_2O.[171]

In the reviewed literature, there is no example of the homogeneously catalyzed reduction of aldoximes with molecular hydrogen as the reductant, especially for aliphatic linear oximes. This is a reaction with high potential for the chemical industry and the synthesis of intermediates and pharmaceuticals since it makes a wide variety of primary amines accessible selectively. Additionally, combined with previous work from our group, this reaction offers an efficient synthesis of primary aliphatic amines starting from alkenes, which remains a significant challenge. A highly relevant example would be the synthesis of green PA 12 starting from the renewable methyl 10-undecenoate, which can be sourced from the oil of the Ricinus plant.[172,173]

6.3. Results and Discussion

The introduction of nitrogen into a molecule *via* hydroxylamine at a carbonyl group is a well-known and straightforward reaction, as they usually readily react and form the desired oxime intermediate. This reaction is highly selective to carbonyls and can target them directly from a mixture of compounds. However, the subsequent hydrogenation requires a well-optimized catalyst for selective conversion.

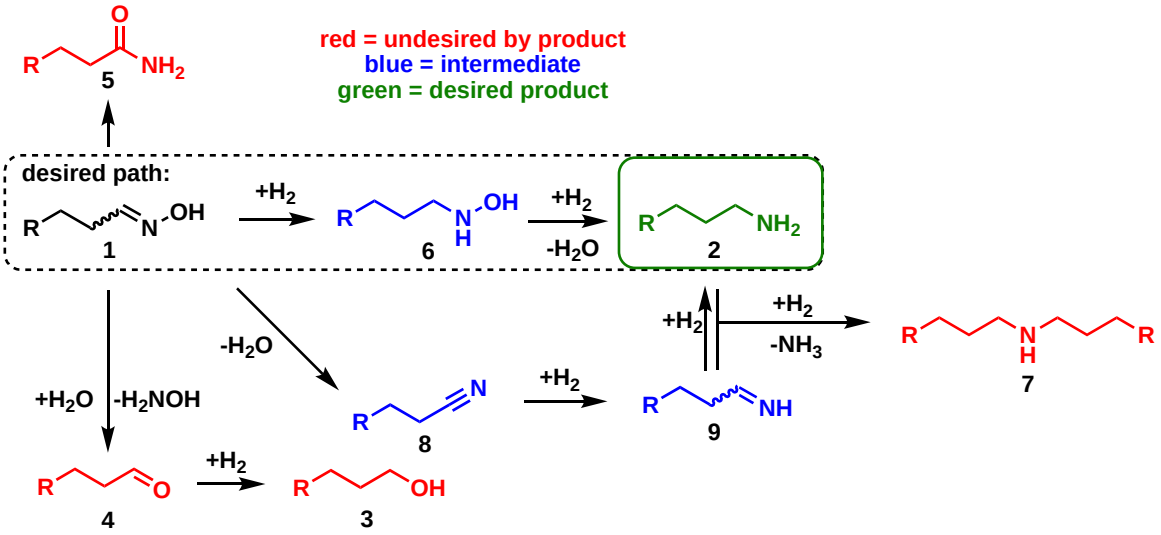

Figure 111: Possible side reactions in the hydrogenation of aldoximes.

In their pure form, aldoximes (**1**) are usually more stable compared to the corresponding aldehydes (**4**). However, several side reactions may occur in the reaction solution and in contact with the catalyst (Figure 111): Acidic conditions result in a Beckmann rearrangement forming amides (**5**), which are relatively stable and not readily hydrogenated.

The oxime (**1**) can also be hydrolyzed at elevated temperatures to the aldehyde (**4**) and hydroxylamine, which are rapidly converted into the corresponding alcohol (**3**) and ammonia under reducing conditions. Theoretically, the alcohol (**3**) can react with ammonia to form the desired primary amines (**2**) *via* alcohol amination. However, secondary amine formation is more likely, since the more reactive primary amine (**2**) is already present in the reaction mixture and will preferably react with the alcohol (**3**).

Additionally, there are two main pathways to form the desired primary amine (**2**). On the one hand, the aldoxime (**1**) can be dehydrated to form a nitrile (**8**), which in turn is hydrogenated into the corresponding imine (**9**). Subsequent hydrogenation yields the desired primary amine (**2**). The imine (**9**) must be hydrogenated rapidly to obtain high selectivities since it is prone to react with the primary amine to form secondary amines.

On the other hand, the pathway promising the highest selectivities is *via* the direct oxime hydrogenation to the organic hydroxylamine intermediate (**6**), which is subsequently hydrogenated to the desired primary amine (**2**), liberating water.

Due to all these side reactions, the reaction system must be finely tuned, ideally favoring the organic hydroxylamine path (Figure 111, dashed box), as it has a lower potential for side reactions.

Therefore, the reaction conditions were optimized in a single-point optimization manner.

The precursor, ligand, catalyst amount, solvent, temperature, and pressure were chosen as the optimization parameters, with a starting point selected from common hydrogenation conditions. The model reaction was the reduction of hexanal oxime (**1a**) to hexylamine (**2a**) (Figure 112).

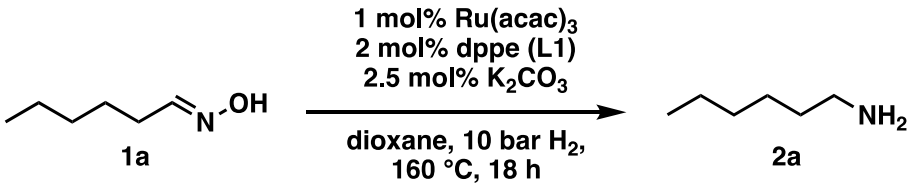

*Figure 112: Starting conditions for optimizing the reaction conditions in the hydrogenation of hexanal oxime (**1a**).*

At first, the reaction was carried out on a 1 mmol scale in a 20 mL autoclave with the above-stated reaction conditions (Figure 112). However, this setup was not ideal for this reaction since the selectivity was low, and reaction monitoring was impossible due to the small reaction volume the lack of suitable periphery. The main side product was hexanol (**3a**), indicating a reverse reaction of the oxime **1a** with water yielding hexanal (**4a**), which is readily reduced under the present conditions. Additionally, a 12 % yield of hexanamide (**5a**) was observed, resulting from a Beckmann rearrangement.

6.3.1. Preliminary Experiments

Before parameter optimization, experiments were performed to set the limits for optimization. Screening experiments were performed in 20 mL autoclaves equipped with a magnetic stirring bar to get a first impression of the reactions. A ruthenium $Ru(acac)_3$ / dppe system was chosen as a benchmark, and different solvents were tested.

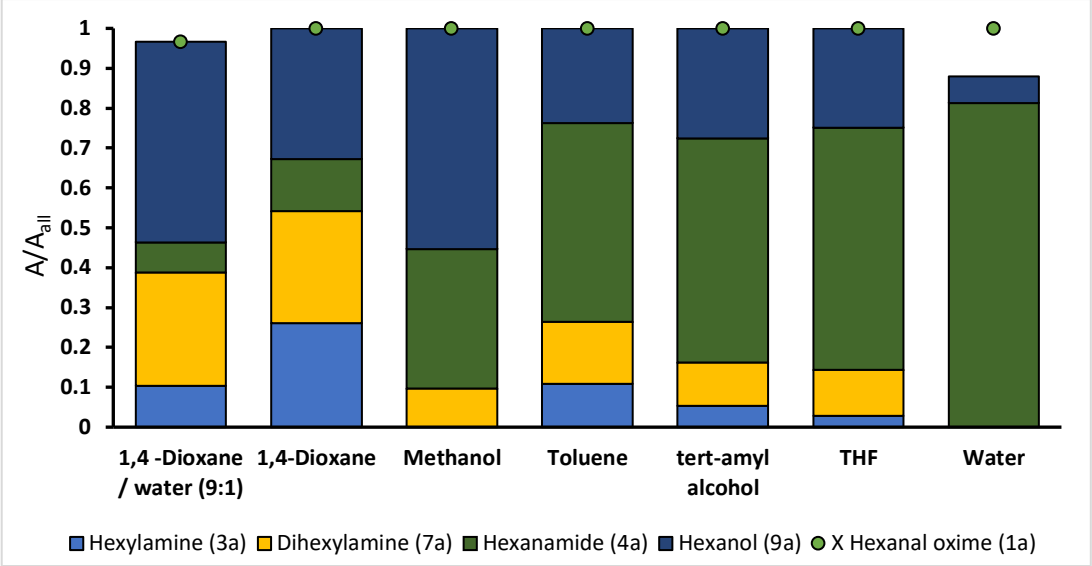

Figure 113: First solvent screening in 20 mL autoclaves. The ratio of substance area to overall area in GC/FID chromatogram for different solvents (Reaction conditions: Hexanal oxime (1a) (1 mmol), $Ru(acac)_3$ (0.01 eq.), dppe L1 (0.02 eq.), K_2CO_3 (0.025 eq.), solvent (2 mL; $p(H_2)$ = 10 bar, 160 °C, 18 h).

The desired amine was detected with all the solvents investigated except for water. The highest amount of hexylamine (**3a**) was found with 1,4-dioxane as solvent. An interesting observation is that the amount of hexanamide (**4a**) seems to increase with the idle time of the prepared reactor. All the reactions presented were carried out in parallel in separate 20 mL autoclaves and charged in the reverse order shown in the graph. The longest time after the preparation of the reactor seems to have the highest amount of amide, i.e., water. A possible explanation is that the active catalyst only forms under reaction conditions and performs the Beckmann rearrangement first. Since dioxane had the best selectivity for the desired primary amine, it was the solvent of choice. To observe the formation of different compounds during the reaction a larger 100 mL reactor was chosen, and samples were taken approximately every hour.

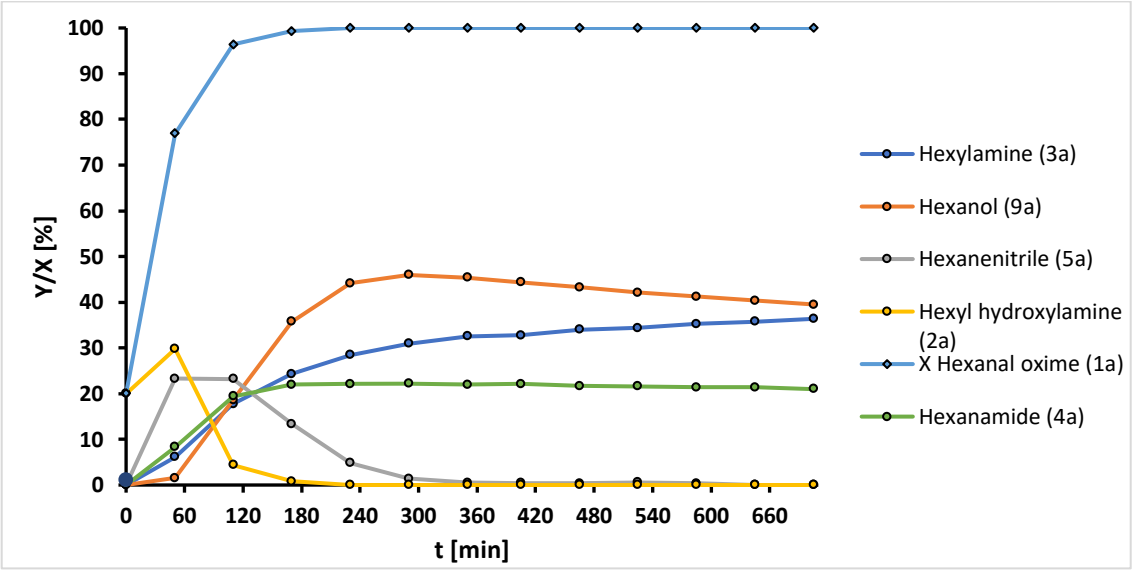

*Figure 114: Reaction profile for ruthenium catalyzed hydrogenation of hexanal oxime (**1a**) with KOH as basic additive and triphos as ligand. Conditions: Hexanal oxime (**1a**) (25 mmol), $Ru(acac)_3$ (0.005 eq.), triphos (0.01 eq.), KOH (0.025 eq.), 1,4-dioxane (50 mL), $p(H_2)$ = 10 bar, 160 °C, 12 h.*

Amide formation stops after complete conversion of the hexanal oxime (**1a**) and is not consumed afterward. Relatively large amounts of alcohol and nitrile formation were also observed.

While drawing samples, it became visible that the reaction system seems to undergo a relatively slow catalyst-forming process. The reaction mixture's color changed over 2 h from red, the color of the dissolved $Ru(acac)_3$, to yellow, which is typically the color of Ru-phosphine complexes in solution (Figure 115).

Figure 115: Sample color gradient over the reaction time (5, 10, 15, 20, 25, 30, 60, 90, 120, 150 min).

After opening the reactor upon completion of the reaction under the non-optimized conditions, the typical odor of ammonia was present. A handheld ammonia detector could confirm relatively large amounts of ammonia in the reactor, indicating the reverse reaction of the oxime (**1a**), resulting in hydroxylamine, which is readily reduced to ammonia under the present conditions. This might be caused by a slow hydrogenation of the hexanal oxime (**1a**) due to the not yet formed active catalyst, allowing the backreaction to hexanal (**4a**) and hydroxylamine. Interestingly, the alcohol is converted under the present reaction conditions, which the presence of ammonia can explain.

To avoid the reverse reaction and Beckmann rearrangement in subsequent experiments, the catalyst is run for 2 h. This was the time when the sample turned yellow and the red color of the precursor disappeared. In addition to preformation, another ligand can enhance the formation of an active catalyst complex suitable for oxime hydrogenation.

6.3.2. Ligand Screening

In previous works of alcohol amination and the amination of esters, ruthenium reached high primary amine selectivity. Therefore, we did focus on ruthenium. For hydrogenation reactions, there is a wide variety of ligands available, which were screened first.

The conversion of the oxime was complete in all cases, but the distribution of the products varied. The results suggest that tridentate ligands favor the hydrogenation into the primary amine (

Table 18), which is, in all cases, the main product. However, **L2** and **L7** stand out with more than 65 % selectivity towards the primary amine. With the mono and bidentate ligands, the nitrile was the main product. This suggests that the tridentate ligands have higher activity in the hydrogenation of oximes and nitrile since less nitrile remains in the product mixture. Alternatively, the reaction route *via* the hexyl hydroxylamine (**2a**) is the preferred route, resulting in less nitrile formation in the first place.

Table 18: Ligand screening in the hydrogenation of hexanal oxime.

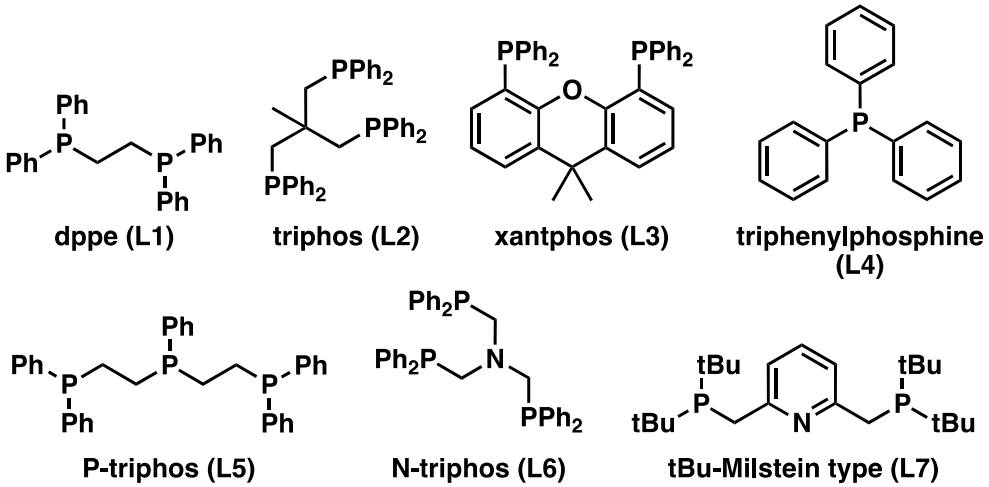

Ligand	X [%]	$S_{(hexylamine\ 3a)}$ [%]	$S_{(dihexylamine\ 7a)}$ [%]	$S_{(hexanitrile\ 5a)}$ [%]	$S_{(hexanamide\ 4a)}$ [%]	$S_{(hexanol\ 9a)}$ [%]
L1	98	6	36	42	4	7
L2	>99	69	8	2	2	3
L3	>99	12	23	45	5	5
L4	98	1	26	57	9	7
L5	>99	30	26	11	6	16
L6	>99	34	15	22	4	10
L7	>99	68	7	2	9	1

*Conditions: 8.33 mmol hexanal oxime (**1a**), 0.5 mol% $Ru(acac)_3$, 2.5 mol% KOH, 160 °C, 5 h, 700 rpm, 1,4-dioxane (30 mL), 10 bar H_2, Monodentate: 1.65 mol%, Bidentate: 0.825 mol%, Tridentate: 0.55 mol%. Determined via GC with dodecane as an internal standard.*

For subsequent work, **L2** was chosen because it has the highest selectivity and is known to be stable at elevated temperatures. Additionally, the so-called triphos ligand (**L2**) is about 1/5 the price of **L7** while achieving similar results.[174,175]

After the ligand was selected, the pressure of the reaction was investigated. Typically, hydrogen pressure is one of the most critical parameters for the hydrogenation reaction because it directly affects the amount of hydrogen in solution.

6.3.3. Pressure Screening

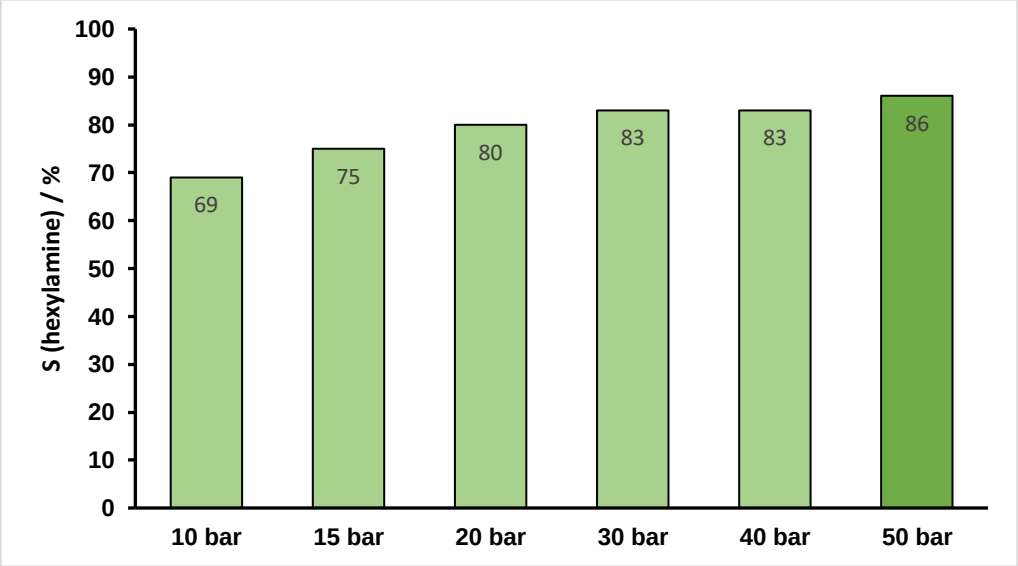

*Figure 116: Screening of the hydrogen pressure. Conditions: 8.33 mmol hexanal oxime (**1a**), 0.5 mol% $Ru(acac)_3$, 0.55 mol% triphos (**L2**), 2.5 mol% KOH, 160 °C, 5 h, 700 rpm, 1,4-dioxane (30 mL). Determined via GC with dodecane as an internal standard.*

As expected, higher hydrogen pressure correlates with a higher selectivity of the reaction. Besides the amount of hydrogen, its activation is also crucial for the outcome of the reaction since this is often the rate-limiting step.

A common way to increase the activation of hydrogen is the use of additives. For the selected Ru-triphos system, base or acid additives are usually used. However, under acidic conditions, the oximes tend to undergo a rapid Beckmann rearrangement. Therefore, different bases were investigated for the hydrogenation of aldoximes (Figure 117).

6.3.4. Base Screening

In the base screening, several oxygen and nitrogen bases were investigated.

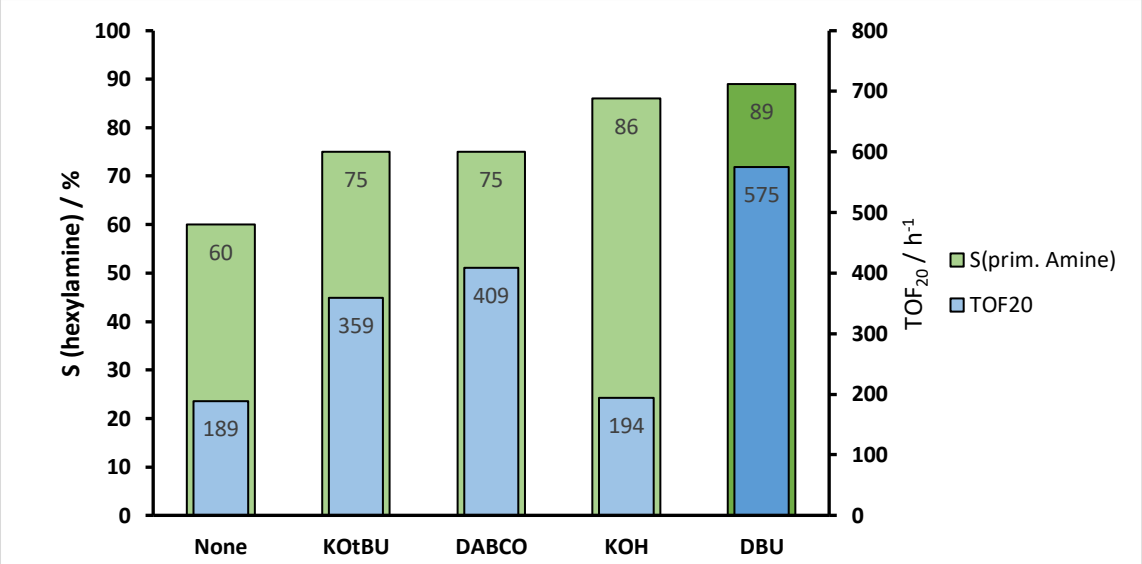

*Figure 117: Variation of the base additives. Conditions: 8.33 mmol hexanal oxime (**1a**), 0.5 mol% $Ru(acac)_3$, 0.55 mol% triphos (**L2**), 2.5 mol% base, 160 °C, 50 bar H_2, t = 5 h, 700 rpm, 1,4-dioxane (30 mL). Determined via GC with dodecane as an internal standard.*

The Ru-triphos system is often used in combination with KO*t*Bu as a basic activation agent. In the reduction of aldoximes, it reached a selectivity of 75 % and a TOF_{20} of 359 h^{-1}. KOH scored higher in selectivity with the price of a slower reaction. This could be caused by the low solubility of KOH in dioxane. A few drops of water were necessary to dissolve the required amount of base, which could interfere with the catalyst or trigger the backward reaction of hexanal oxime (**1a**) into hexanal (**8a**). Additionally, the amine bases 1,4-diazabicyclo[2.2.2]octane (DABCO) and 1,8-diazabicyclo[5.4.0]undec-7-ene (DBU) were tested. Both have shown a higher reaction rate, but the best results were achieved with DBU, *i.e.,* a selectivity of 89 % and a TOF_{20} of 575 h^{-1}. The higher selectivity is caused by less nitrile (Figure 118) formed during the reaction, thus probably favoring the hydroxylamine path and the lack of water in the system inhibits the backward reaction of hexanal oxime (**1a**).

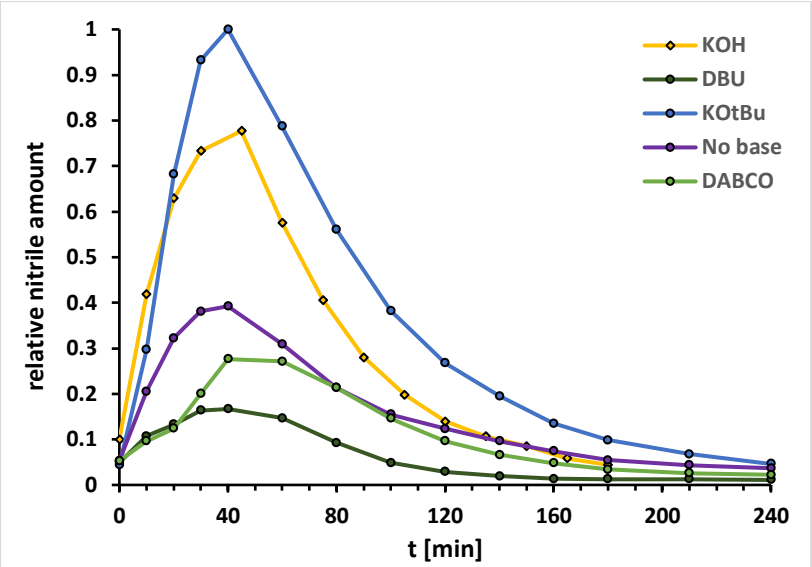

*Figure 118: Relative hexanenitrile (**5a**) amount formed during the hydrogenation with different bases. The highest amount detected with KOH as the reference. Conditions: 8.33 mmol hexanal oxime (**1a**), 0.5 mol% $Ru(acac)_3$, 0.55 mol% triphos (**L2**), 2.5 mol% base, 160 °C, 50 bar H_2, t = 5 h, 700 rpm, 1,4-dioxane (30 mL). Determined via GC with dodecane as an internal standard.*

Looking closely at the GC chromatograms, additional signals could be observed when amine bases such as DABCO and DBU were used. To clarify which side products belong to those signals, HPLC-HRMS experiments were carried out. These experiments revealed the formation of two new condensates (Figure 119) that were not observed using KO*t*Bu (**B3**) and KOH (**B4**). This could hint at a nitrogen-based catalytic step or acid-base reaction taking place at different pH.

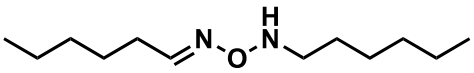

11
Chemical Formula: $C_{12}H_{26}N_2O$
Exact Mass: 214.20
Molecular Weight: 214.35

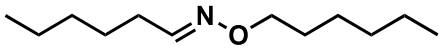

12
Chemical Formula: $C_{12}H_{25}NO$
Exact Mass: 199.19
Molecular Weight: 199.34

*Figure 119: New condensates observed in the hydrogenation of hexanal oxime (**1a**) in the presence of amine bases.*

The masses shown above (Figure 119) were found in the measurement for the sample after 5 min, corresponding to the time when there were high intensities of the former unknown signal. The left compound (**11**) can result from the condensation of a hexanal oxime (**1a**) with a hexyl hydroxylamine (**2a**). In contrast, the right compound (**12**) can be built by condensing hexanal oxime (**1a**) with hexanol (**9a**). Both condensate molecules are intermediates in the reaction system since both can be reduced to the desired primary amine (**3a**). However, the oxime ether (**12**)

releases an additional hexanol (**9a**) in the process and explains the formation of hexanol (**9a**) when the oxime is already completely converted.

6.3.5. Precursor screening

Several different precursors were tested in the hydrogenation of hexanal oxime under the above established conditions.

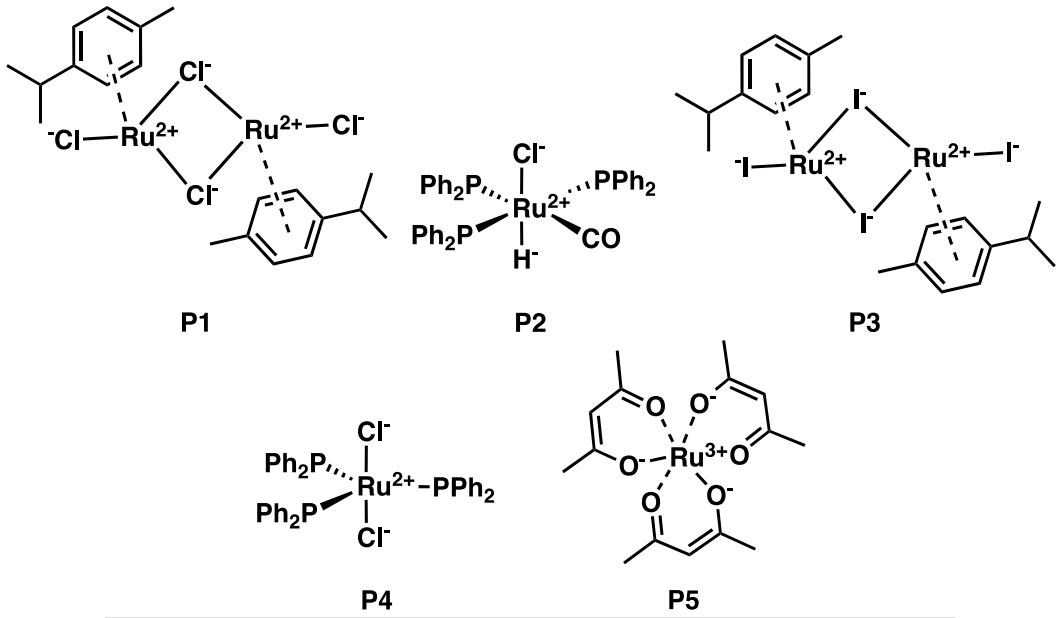

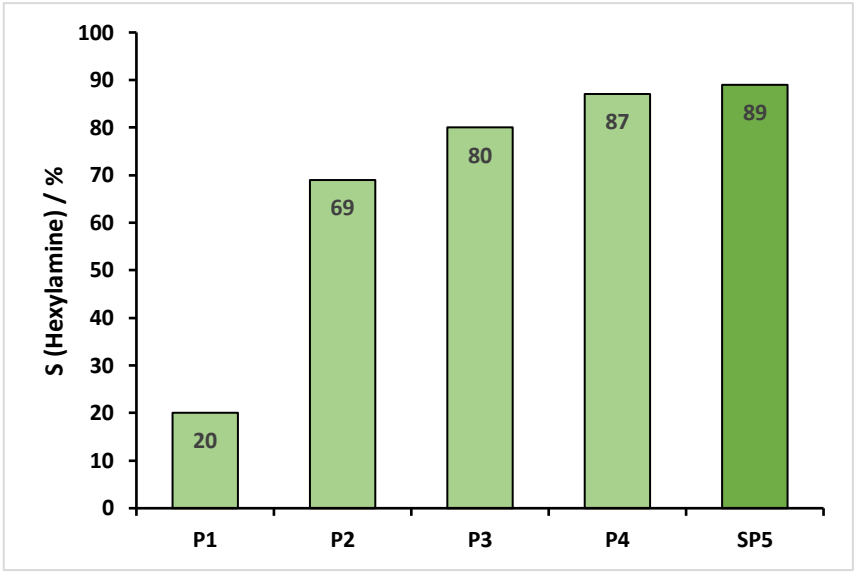

*Figure 120: Precursor screening. Conditions: 8.33 mmol hexanal oxime (**1a**), 0.5 mol% (Ru), 0.55 mol% triphos (**L2**), 2.5 mol% DBU, dioxane (30 mL), p(H_2) = 50 bar, 160 °C, 5 h, rpm = 700. Selectivity of hexylamine (**3a**) was calculated by GC by using dodecane as an internal standard.*

The optimization was started with $Ru(acac)_3$ (**P5**) since this system is also often used in the literature.[86,90,121] Additionally, Ru^{II} precursors were tested, which are commonly used for other ruthenium catalyzed amination reactions.

Surprisingly, **P2** exhibited a selectivity of only 69 % despite being the preferred precursor for numerous analogous catalyst systems. **P4** demonstrated a comparable selectivity; however, it led to the accumulation of hexyl hydroxylamine (**2a**) during the reaction, potentially resulting in additional side reactions. The best results were achieved with **P5,** and the reaction system was not altered after the precursor screening.

6.3.6. Solvent screening

Another essential factor for the homogeneous catalyst system is the solvent since it influences the solubility of the catalyst and the substrates. 1,4-Dioxane is an excellent solvent for Ru catalyzed hydrogenation reactions, but it is suspected to cause cancer, making it desirable to find an alternative. Referring to the principles of green chemistry, harmful solvents should be replaced with less dangerous substitutes.

Toluene is also an established solvent that has a stabilizing effect on the catalyst, so it was tested along with anisole. Anisole contains an aromatic ring with a methyl ether, thus combining the structural properties of dioxane and toluene. They were compared in the hydrogenation of hexanal oxime (**1a**) (Figure 121).

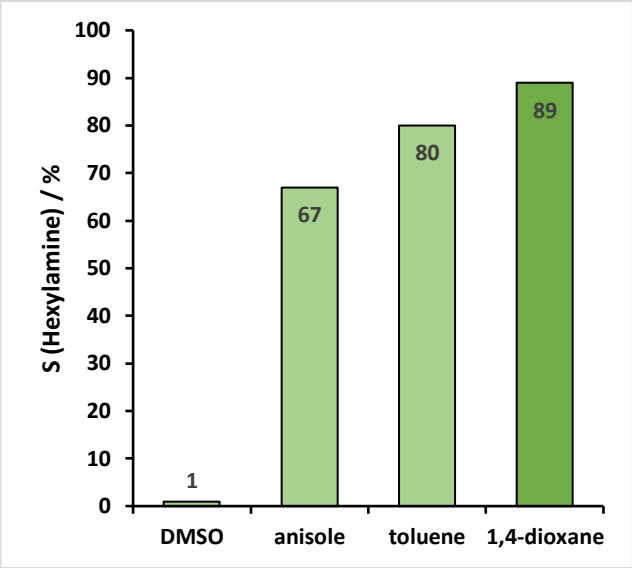

*Figure 121: Solvent screening for the hydrogenation of hexanal oxime (**1a**). Conditions: hexanal oxime (**1a**) (8.33 mmol), $Ru(acac)_3$ (0.5 mol%), triphos (**L2**))(0.55 mol%), DBU (2.5 mol%), solvent (30 mL), t = 5 h, rpm = 700 T = 160 °C, $p(H_2)$ = 50 bar. Selectivity of hexylamine (**3a**) was calculated by GC by using dodecane as an internal standard.*

Despite the additional ether functionality, anisole performed the worst with only 67 % selectivity, and toluene also underperformed dioxane. The structural difference could explain the difference. Both toluene and anisole are aromatic and can coordinate mainly through π-π-interactions, which seems less effective than the coordinating oxygen atoms in dioxane. Moreover, dioxane can act as a bidentate ligand, increasing its stabilizing effect on the catalyst. Hence, the performance of dioxane with 89 % selectivity remains the best.

DMSO was tested because of the inadequate solubility of long-chain oximes and dioximes. It is capable of dissolving these specific oximes, which cannot be dissolved in small enough amounts of solvents for the reaction to be carried out in the current reactor system. However, the hydrogenation was not successful, since only traces of the amine could be observed. Additionally, the distinct odor of cabbage indicates the hydrogenation of DMSO to dimethyl sulfide.

Therefore, dioxane was the solvent of choice.

6.3.7. 1Temperature – A key factor

Generally, the reaction rate is highly dependent on the reaction temperature. Preferably, the desired reaction path is favored at elevated temperatures, further increasing the selectivity. The results of the temperature screening are presented in Figure 122.

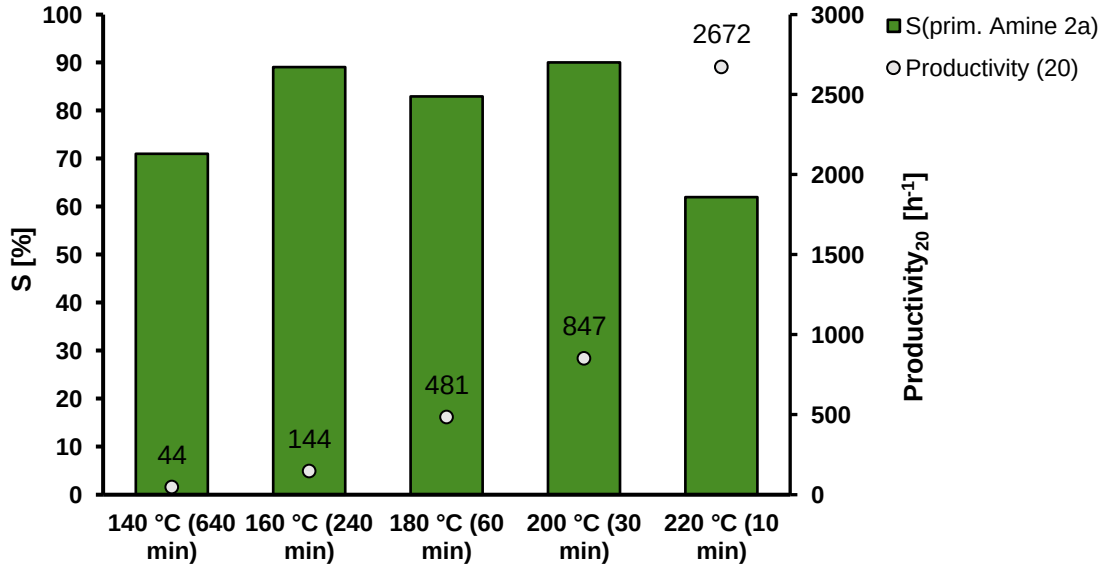

*Figure 122: Temperature dependency of the hydrogenation of hexanal oxime (**1a**). Conditions: Hexanal oxime (**1a**, 8.33 mmol), Ru(acac)$_3$ (0.5 mol%), triphos (**L2**) (0.55 mol%), DBU (2.5 mol%), dioxane (30 mL), H_2 (50 bar at rt), 700 rpm, preforming 2 h under reaction conditions without substrate. The selectivity (S) of hexylamine (**2a**) was calculated by GC-FID using n-dodecane as an external standard. All data points for the selectivity arise from time-dependent measurements and were chosen for the highest selectivity (compare in SI). Productivity calculated at 20 % yield of hexylamine (**2a**).*

As expected, the reaction speed increases with increasing temperatures. The selectivity also increases with the temperature reaching a maximum of 90 % at 200 °C. At 220 °C, the consecutive reaction takes over and reduces the selectivity towards the primary amine. The formation of **7a** (Scheme 3) after complete conversion of 1a can occur either via dimerization of the primary amine (**3a**) or in a reaction of the imine (**6**) and (**3**), both liberating ammonia At this temperature, the highest selectivity of 62 % was reached after 10 min, and the secondary amine formation (**7a**) occurred faster (compared with the X/t-plot in the SI). At 200 °C the highest selectivity was accomplished after 30 min. At 160 °C, a similar selectivity was reached, but it took significantly longer, as the maximum was reached after only 240 min. The maximum selectivity at 200 °C is probably the result of two factors. First, a higher reaction rate reduces the time of intermediates being present in the reaction mixture, thus suppressing side reactions and increasing selectivity. Second, at higher temperatures than 200 °C, the activation energy of the dehydrogenation of primary amine (**2b**) to the corresponding imine **9a** is overcome. Hence, so-called deaminative coupling proceeds, in which two primary amines react to form the corresponding secondary amine (**7a**) under the liberation of ammonia, thus decreasing the selectivity at higher temperatures.

Comparing the productivity at 20 % yield (equation 3) at the presented temperatures reveals an almost exponential relation: From 44 h^{-1} at 140 °C to an increased productivity of 2672 h^{-1} at 220 °C. The productivity was chosen for comparison of the different reaction parameters, because the hexanal oxime is converted extremely fast.

$$\text{productivity}(20) = \frac{\text{n(product at 20 \% yield)}}{n(catalyst) \times t(for\ 20\ \%\ yield)} \qquad (3)$$

Due to the different possible reaction paths (Figure 111) it does not indicate a better performance of the reaction, so comparing the TOF_{20} could be misleading, e.g. a high TOF_{20} could be reached *via* the nitrile path but the overall reaction would be slower. In contrast, the productivity is calculated *via* the yield and therefore, includes the selectivity of the conversion.

6.3.8. Scale up of the reaction

Next, we performed the reaction in a 300 mL autoclave with 25 mmol hexanal oxime (**1a**), representing a scale-up factor of 3 (Figure 124, graph B). Additionally, the reactor was equipped with a gas inlet stirrer to improve the hydrogen availability for the reaction. In this setup, the productivity could be increased to 1074 h^{-1} at 200 °C (from 847 h^{-1}). The selectivity, however, was a bit lower at 83 %. Longer preparation time with the larger reactor could have led to more side products. Noteworthy is the decay of the amine (**3a**) yield after it reached a maximum at 40 min of reaction time. Simultaneously, an increase in the dihexylamine (**7a**) yield can be observed, which suggests a deaminative coupling occurs, despite the pressurized hydrogen atmosphere. Interestingly, more nitrile (**8a**) was observed with this reaction setup. Therefore, the secondary amine (**7a**) could result from the imine (**9a**) intermediate.

In contrast, the alcohol (**3a**) and amide (**5a**) could only be detected in trace or not at all, respectively. Theoretically, the amide could also be converted under the present conditions.

6.3.9. Enlightening the reaction path

For a better understanding of the results, the path of the reaction can reveal more details. First, we investigated whether the formation of the primary amine is possible *via* the reduction of the corresponding amide. As described above, the amide can be built from a Beckmann rearrangement of the oxime, typically under acidic conditions (Figure 111, reaction **1** to **5**). Although basic conditions were present, the amide was a significant side product at the start of our investigations. Under optimized conditions, no amide was observed. To exclude the reaction path *via* an amide, we tested the hydrogenation of the hexanamide **5a** under optimized conditions.

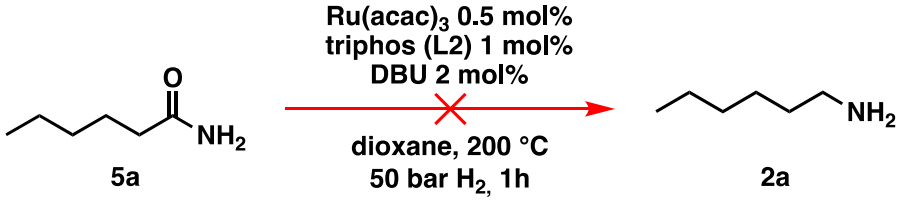

Figure 123: Hydrogenation of hexanamide under oxime hydrogenation conditions.

No conversion was observed after 1 h of reaction time, confirming no amide reduction under the given reaction conditions. Therefore, the amide indeed represents a dead end in this reaction setup.

The other two possible reaction paths can proceed either *via* the dehydration of the aldoxime forming the nitrile (**8**), which is subsequently hydrogenated to the imine (**9**), or *via* a direct hydrogenation resulting in hydroxyl hexylamine (**6**). Both intermediates are then hydrogenated to the desired primary amine. Due to the lack of an imine species (**9**), the direct hydrogenation path should be more selective.

To obtain more details, we compared the hydrogenation of hexanenitrile (**8a**) with the hydrogenation of the hexanal oxime (**1a**). Both reactions are displayed in Figure 124.

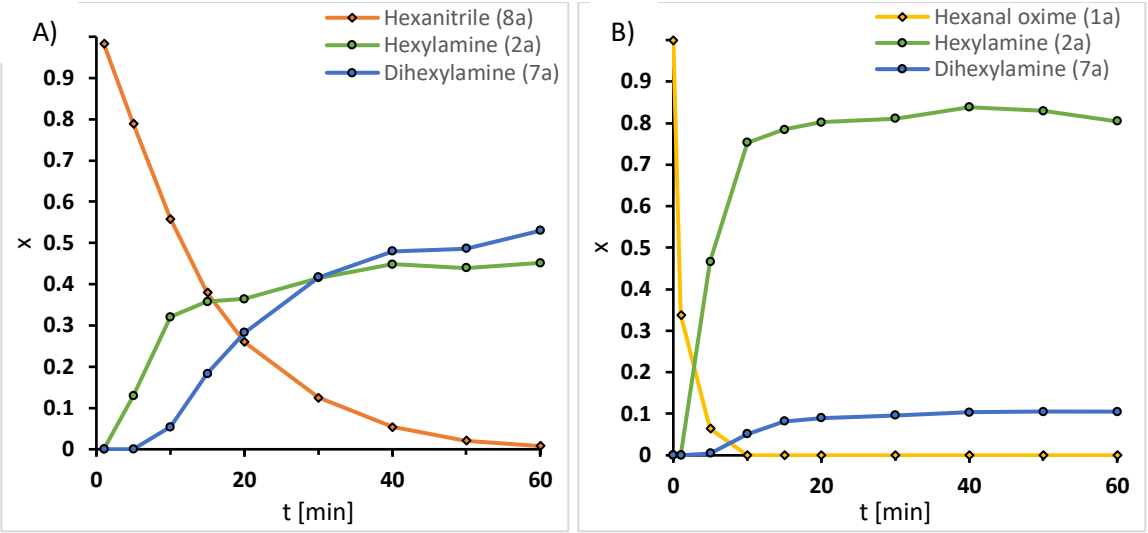

Figure 124: Comparison of the hydrogenation of hexanenitrile A) hexanal oxime B) under optimized conditions. Conditions: Substrate (25 mmol), $Ru(acac)_3$ (0.5 mol%), triphos (0.55 mol%), DBU (2.5 mol%), dioxane (100 mL), H_2 (50 bar at RT), 750 rpm at 200 °C. Amounts as a fraction of the substrate at the reaction start were calculated by GC using dodecane as an external standard.

In comparison, the nitrile reduction (Figure 124, A) is slower than the oxime hydrogenation (Figure 124, B). While the nitrile reaches full conversion only after 60 min, the oxime (**1a**) is already converted after 10 min under the same conditions. This trend is also reflected by the productivities (at 20 % yield) of the reactions, which are 1074 h^{-1} for the oxime hydrogenation and 350 h^{-1} for the nitrile reduction. Therefore, the main reaction path is likely through the hexyl hydroxylamine (**6a**). Another hint is the selectivity of the reaction. As mentioned before, the imine intermediate **9** is prone to side reactions, leading to an increased dihexylamine (**7a**) formation. The test reaction confirms this hypothesis since the selectivity of the nitrile reduction after full conversion of 45 % is significantly lower than the 83 % of the oxime hydrogenation.

These findings underline the importance of a fast hydrogenation reaction for the selectivity toward the desired primary amine.

6.3.10. Scope of the reaction

Next, we have investigated the scope of the reaction (Table 19).

Table 19: Conversion of different oximes under optimized conditions.

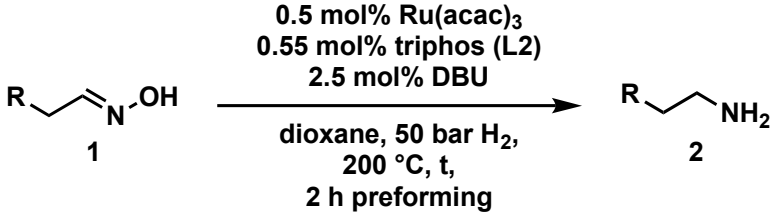

Entry	Substrate	t [min]	Product	Yield [%]
1[a]	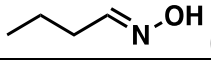 (1h)	5	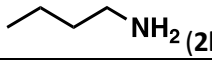 (2h)	51
2	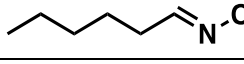 (1a)	30	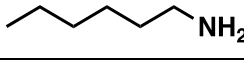 (2a)	90
3[a]	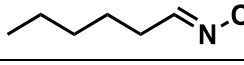 (1a)	40	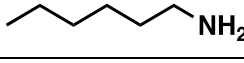 (2a)	83
4	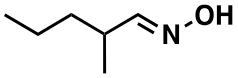 (1c)	120	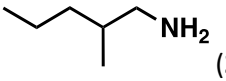 (2c)	80
5	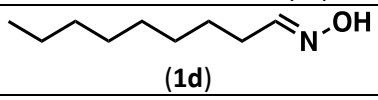 (1d)	120	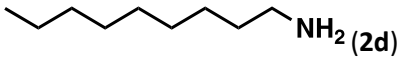 (2d)	77
6	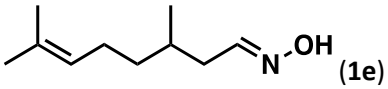 (1e)	120	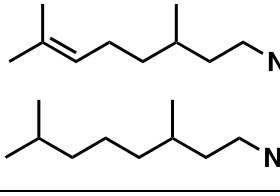 (2e) (2e')	47 (9:1)[b]
7[a]	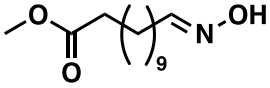 (1g)	15	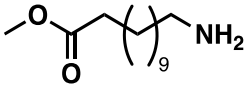 (2g)	80
8	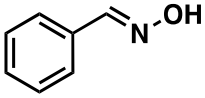 (1b)	120	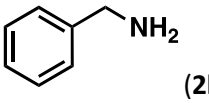 (2b)	67
9	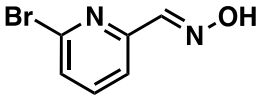 (1f)	120	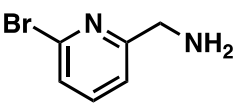 (2f)	68
10[a]	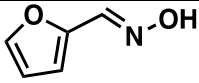 (1i)	15	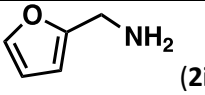 (2i)	53

*Conditions: oximes (8.33 mmol), $Ru(acac)_3$ (0.5 mol%), triphos (**L2**) (0.55 mol%), DBU (2.5 mol%), dioxane 30 mL, H_2 (50 bar at RT), 700 rpm at 200 °C. The yields of the amines were calculated by GC-FID by using dodecane as an internal standard. a: 25 mmol scale in 100 mL dioxane. b: determined via ^{1}H-NMR.*

All tested oximes could be fully converted with up to 90 % selectivity. Since hexylamine (**3a**) was used for optimization, it reached the highest yield of 90 %, with the secondary amine (**7a**) being the main side-product. The branched (**1c**) and other chain length oximes (**1b**, **1d**) could be converted successfully with slightly less yield (Table 19, entry 1-5). The main side products were the secondary amine and the alcohol, indicating a lower selectivity toward the organic hydroxylamine (**2**) path.

Surprisingly, the NMR spectrum revealed that the double bond in citronellal oxime (**1e**) stayed 90 % intact (Table 19, entry 6). Other functional groups are also tolerated, such as bromide, benzyl and furfuryl moieties (Table 19, entry 8-10), showcasing the high chemoselectivity of the Ru/triphos system towards carbonyl compounds. Again, the secondary amine is the main side product.

Compared to other amination reactions, our newly developed protocol combines great chemoselectivity with high reaction speed. Therefore, adding a valuable tool for the synthesis of primary amines. Noteworthy, the best results were achieved for aliphatic aldoximes, which are synthesized from aldehydes usually produced *via* hydroformylation.

In order to demonstrate the feasibility and direct applicability of the catalyst system for industrial processes, further investigations were carried out with readily available bulk chemicals.

6.3.11. Combination with Hydroformylation

To realize the desired alkene to primary amine conversion path, a hydroformylation was added to the reaction procedure, now consisting of three reaction steps. At first, we chose a cyclodextrin assisted biphasic hydroformylation with a Rh/Sulfoxantphos catalyst system, which yields a relatively pure product phase (Table 20, entry 1-3).[176,177] This product phase was then combined with an aqueous hydroxylamine solution to form the oximes. In the last step the oximes were hydrogenated with our newly developed protocol.

Table 20: Synthesis of primary amines from alkenes.

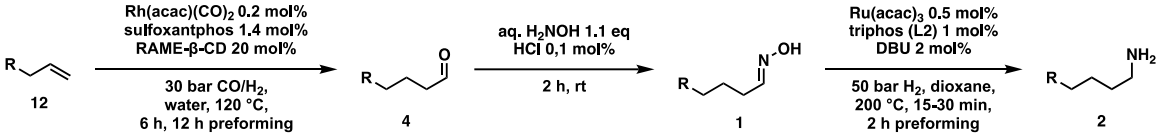

Entry	R =	Yield 4 [%]	Yield 1 [%][b]	Yield 2 [%][b]
1	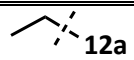 **12a**	76	71	60
2	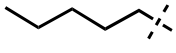 **12d**	80	76	57
3	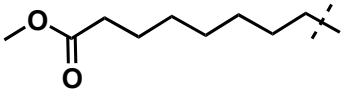 **12g**	83	79	63
4	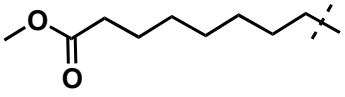 **12g**	91[a]	85	68

Conditions: Hydroformylation: preforming: CO/H_2 (30 bar), $n(CO)/n(H_2)$ = 1, 12 h, at 120 °C; reaction: 32 mmol, 10 CO/H_2 (30 bar), $n(CO)/n(H_2)$ = 1, 6 h, at 120 °C $m(H_2O)/m$(substrate) = 0.2, n(substrate)/n(Rh) = 500, nCD/nRh = 100, n(P)/n(Rh) = 7. Oximation: product phase of hydroformylation, aq. H_2NOH (1.1 eq.), HCl (0.1 mol%) 2 h at 30 °C. Hydrogenation: 8.33 mmol 1, $Ru(acac)_3$ (0.5 mol%), triphos (L2) (0.55 mol%), DBU (2.5 mol%), 1,4-dioxane 30 mL, H_2 (50 bar at RT), 700 rpm at 200 °C. The yields were calculated by GC-FID by using dodecane as an internal standard. b: cumulated yield with previous reactions.

The hydroformylation is already established and the combined oximation reaction was carried out with excellent yields in all cases (Table 20, yields **1**). With regard to the alkene the yields were between 71 % and 79 %.

The oximation yields crystalline products, which were filtrated off readily. With hexanal oxime (**1a**) as an exception, which had to be crystallized from diethyl ether.

All side products and remaining substrate from the hydroformylation step were separated by washing the oxime crystals. Only for hexanal oxime (**1a**) a small portion of the branched oxime would co-crystallize. Afterwards, the oximes were investigated in the hydrogenation reaction under optimized conditions, which results in good to very good yields of the primary amine and moderate overall yields (Table 20, yields **2**).

The yield obtained from the hydrogenation of hexanal oxime (**1a**) after the full reaction set-up starting from the alkene were slightly lower than those synthesized from the purchased aldehyde (Table 20, entry 1, yield **2**). This could be caused by the presence of branched oxime or other small impurities resulting from the hydroformylation. In terms of l/b-ratio, the performance was increased by two points to 29.2. For nonylamine (**2d**) and methyl 12-aminododecanoate (**2g**), the linearity improves significantly due to an easier separation, as the crystals of the linear product already form during the oximation reaction, and the branched products remain liquid.[161] Therefore, the intermediate oximation reaction also allows an easy separation of linear and branched products which otherwise requires costly separation methods for the aldehyde or amine products.

To improve the overall yield of the amine we carried out the same reaction sequence with a monophasic hydroformylation reaction. The upside is its better performance, and the usual downside is the more difficult separation of the products, since it's a monophasic mixture. With our reaction sequence, the separation of the oxime intermediate remains easy. With the monophasic hydroformylation an increase of the total amine yield to 68% could be achieved (Table 20, entry 4).

As a proof of concept, a sample of a hydroformylation reaction solution of a continuously operated mini plant was used as the substrate.[178] The result is a diluted aldehyde **4g** solution, which was then converted into the amine **2g** *via* its oxime **1g** (Figure 125).

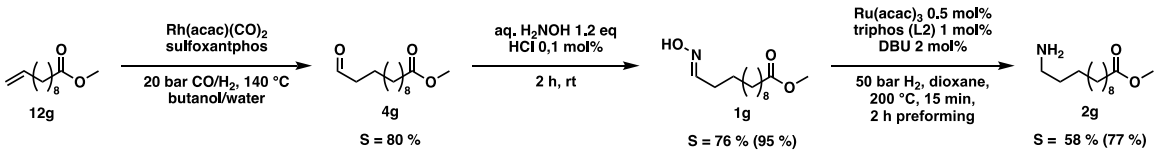

Figure 125: Reaction sequence starting with a reaction solution sample of a continuous operated miniplant. Selectivity combined for the alkene and each reaction in parentheses.

The oximation was carried out with 145 g of the product phase, which contained 58 wt% aldehydes. Hydroxylamine was directly added to this mixture and in a two-step crystallization the oxime **1g** was obtained in 95 % yield. Noteworthy, only 1.2 eq. of the amines source were necessary for the conversion which is significantly lower compared to the large ammonia excess in reductive amination and alcohol amination. This reaction step allows a decoupling of both reactions and can convert even diluted aldehyde solutions. The hydrogenation of the oxime can then be carried out independently.

In the final hydrogenation was carried out in a 300 mL autoclave with 25 mmol oxime **1g**. Full conversion was achieved after only 5 min, resulting in a high TOF_{20} of 8934 h^{-1}. After 15 min of reaction time, the highest selectivity of 77 % was reached. Continuing the reaction after that point favors the deaminative coupling, reducing the amount of primary amine while the secondary amine is built up. The productivity (at 20 % yield) was high with 1004 h^{-1}. With the new protocol a fast and selective conversion of methyl 11-undecanoate **12** into 12-aminododecanoate **2g** *via* the oxime **1g** in a multigram scale was achieved, thus offering a new and efficient alternative to the desired but not feasible hydroamination reaction of aliphatic alkenes.

6.4.Conclusions and outlook

The first homogeneously catalyzed hydrogenation of aldoximes into primary aliphatic amines with high selectivity of up to 90 % and a productivity(20) of up to 2897 h^{-1} was presented. The reaction is significantly faster than existing protocols and does not require a significant excess of the amine source. In addition, the hydrogenation procedure is selective for the conversion of oximes and tolerates reduceable moieties such as double bonds aromatic rings and esters. Especially the latter provides an appealing route for the preparation of bifunctional polymer precursors.

Using this protocol, a new reaction sequence that starts from common alkenes *via* hydroformylation, utilizes the resulting aldehydes for oxime synthesis and ultimately yields aliphatic primary amines was developed. The reaction sequence offers a viable alternative to the highly desired but not feasible hydroamination of standard alkenes and is a new approach for synthesizing primary aliphatic amines.

The overall yield from alkene to the primary amine in the three-step reaction setup reaches up to 68 %, with water being the only byproduct. The reaction sequence can be directly applied to current hydroformylation processes, whether mono or biphasic. Since the oxime intermediate can be easily separated, even a purification of linear and branched oxime intermediates is readily possible due to their crystallization behavior, allowing greatly improved l/b ratios of the final products. Methyl 10-undecenoate was converted into the PA-12 precursor methyl 12-aminododecanoate, allowing the production of bio-based PA-12 with water as the only byproduct. Especially the high l/b-ratio of the product is remarkable. Up to 77 % yield of pure linear ω-amino ester was achieved on a 25 mmol scale with a productivity of 1004 h^{-1} in the hydrogenation step starting from the aldoxime.

Our next goal is the conversion of dioximes to obtain diamines such as hexamethylene diamine. Due to the poor solubility in dioxane further reaction engineering and change of the reactor set up is required. Additionally, further improvements in the reaction's selectivity *via* a flow-reactor, separating the product from the substrate on the reactor length, would be attractive for future studies.

6.5. Experimental

6.5.1. Used Chemicals and Materials

All chemicals used within this work are given in

Table 25.

Oxime hydrogenation in 20 mL autoclave

Hexanal oxime (**1a**) (1 mmol, 1 eq.), metal precursor (0.01 mmol, 0.01 eq.), ligand (0.02 mmol, 0.02 eq.) and the base (Na_2CO_3, K_2CO_3 as solid; NaOH, KOH, KO*t*Bu as solution in water/dioxane) were weighed into multiplex reactors. The reactors were closed, flushed with argon, and degassed solvent (2 mL) was added. The reactors were gassed with hydrogen at 10 bar and stirred at 160 °C for 18 h. The reactors were opened, and 1 mL of the solution was analyzed by GC/FID or GC/MS.

The internal standard was added either after solvent addition before the reaction or after the reaction in the same GC vial.

Oxime hydrogenation in 100 mL autoclave

First, the reactor was equipped with a stirring bar and then tightly closed. Then, KO*t*Bu **B3** / 1,4-dioxane stock solution was prepared (0.00832 mmol/mL), and this was degassed under argon atmosphere in an ultrasonic bath. $Ru(acac)_3$ (16.6 mg, 0.0417 mmol, 0.005 eq.) and the ligand **L1**-**L7** were placed in another Schlenk flask and then dissolved in 25 mL of the degassed base/solvent solution. The reactor was evacuated and purged with argon and vacuum was used to pull the catalyst and ligand solution into the reactor *via* the sampling valve. During this, the hexanal oxime (**1a**) (8.33 mmol, 959 mg, 1 eq.) was dissolved in 5 mL of solvent and degassed for 1 h. Then, the oxime solution was filled into the dropping funnel with a syringe under argon counter flow. Then, the reactor was gassed with 30 bar of hydrogen and heated to 160 °C internal temperature, and the catalyst was allowed to preform for 2 h while stirring. At the end of the 2 h, the oxime was added *via* the dropping funnel, and the first sample was taken.

Samples were prepared *via* the sampling valve into GC vials, which were frozen in liquid nitrogen. The collected sample volume was then weighed and prepared for GC measurements using dodecane as an external standard and 2-propanol as solvent.

Oxime hydrogenation in 300 mL autoclave

In a Schlenk flask under argon atmosphere, $Ru(acac)_3$ **P5** (49.8 mg, 0.125 mmol, 0.005 eq.) and triphos **L2** (88.6 mg, 0.138 mmol, 0.0055 eq.) were weight in. The flask was flushed with argon before dioxane (65 mL) was added. Then DBU (97 mg, 0.625 mmol, 0.025 eq.) was added through a septum and the mixture was mixed.

A 300 mL overhead stirred pressure autoclave was purged with argon. Vacuum was pulled on the reactor, and the catalyst mixture was transferred in the reactor through a Teflon tube attached to the sampling valve utilizing the low pressure inside. The oxime (25 mmol, 1 eq.) was weighed in a separate Schlenk flask under argon atmosphere and dissolved in 35 mL dioxane. The substrate mixture was transferred into a pressure-dropping funnel mounted to the reactor *via* a syringe under an argon flow. The reactor was charged with 50 bar H_2 and heated to 200 °C (80 bar pressure at reaction temp.). The catalyst was preformed for 2 h, stirring at 750 rpm with a gas-inlet stirrer. After the preforming period, the dropping funnel was opened, and the reaction started. Samples were drawn after 1, 5.30, 10.30, 15, 20, 30, 40, and 60 min and analyzed *via* GC using dodecane as the internal standard.

Oximation of aldehydes

Hydroxylamine solution (50 % aq., 144 mmol, 1.44 eq.) was placed in a 3-neck flask equipped with a dropping funnel. The dropping funnel was charged with the corresponding aldehyde (100 mmol, 1 eq.).

The flask was cooled to 0 °C in an ice bath, and the solution was stirred with 600 rpm. The aldehyde was added dropwise to the solution. 5 mL of water were used to rinse the addition funnel. After the addition was completed, HCl (conc., 0.01 eq.) was added, the reaction mixture was allowed to warm up to rt, and the stirring speed was increased to 900 rpm.

The mixture was extracted with diethyl ether 3 times. The organic phases were combined, and the solvent was removed under reduced pressure.

Oximation of hydroformylation reaction solution

Starting with a hydroformylation reaction solution (145 g) in butanol with a 60.4 wt% aldehyde 1.1 eq. Hydroxylamine as a 50 wt% aqueous solution was added slowly at 0 °C before adding conc. HCl (0.1 mol%) *via* a 1 mL syringe. Following the addition of the acid, the reaction was allowed to warm to rt and was stirred overnight to ensure reaction completion. Subsequently, the solids that had formed were filtered off, washed with water, and then rinsed with pentane. After the washes, the solid precipitate was dried under reduced pressure to remove any residual solvents or impurities.

Another filtration step was conducted to improve the yield. Additional product was further precipitated by adding water to the filtrate.

Synthesis of hexanamide (4a)

Hexanal oxime (**1a**) (1 mmol, 1 eq.), $Ru(acac)_3$ **P5** (0.01 mmol, 0.01 eq.), triphos **L2** (0.02 mmol, 0.02 eq.) and KOH (0.025 mmol, 0.02 mmol) were weighed into a 20 mL reactor. The reactor was closed, flushed with argon, and degassed 1,4-dioxane (2 mL) was added. The reactor stirred at 160 °C for 18 h. The reactor was opened, and 1 mL of the solution was analyzed by GC/FID and GC/MS. The remaining solution was united with the sample solution, and the solvent was evaporated by a rotary evaporator, yielding a brown oil. The oil was worked up by column chromatography with pure ethyl acetate, yielding the hexanamide as an off-white solid (44 mg, 0.38 mmol, 38 %).

6.5.2. Analytics

GC Analysis: All chromatograms were recorded by an AGILENT 7890A gas chromatograph with an HP-5-column (length = 30 m, diameter = 0.25 mm, film thickness = 25 µm). Each sample was measured with a split ratio of 75:1 and a sample volume of 1 µL. The species were determined by previous calibrations (Figure 126). The corresponding heating profile for the hydrogenation of hexanal oxime (**1a**) is shown in Figure 127. The heating profiles for the substrate screening are shown subsequently).

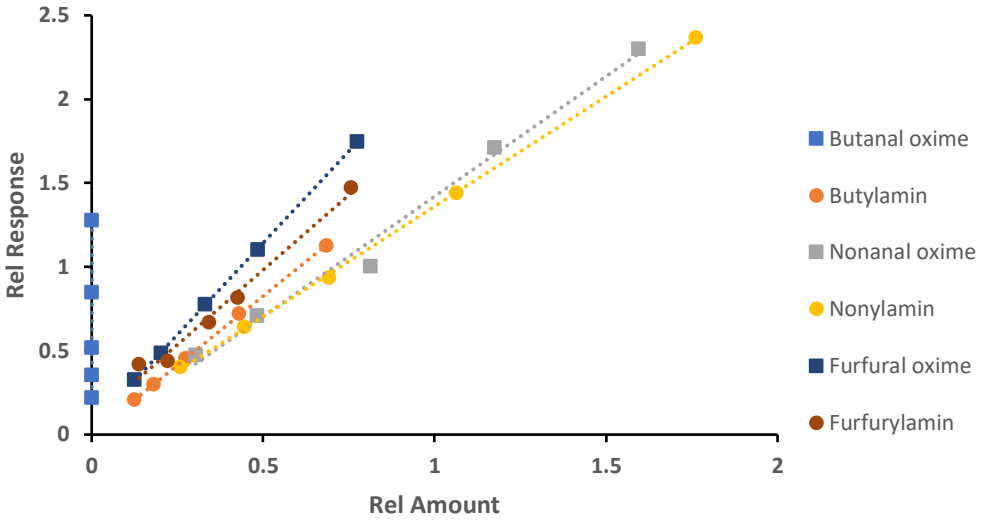

Figure 126: Calibration curve for GC Analysis.

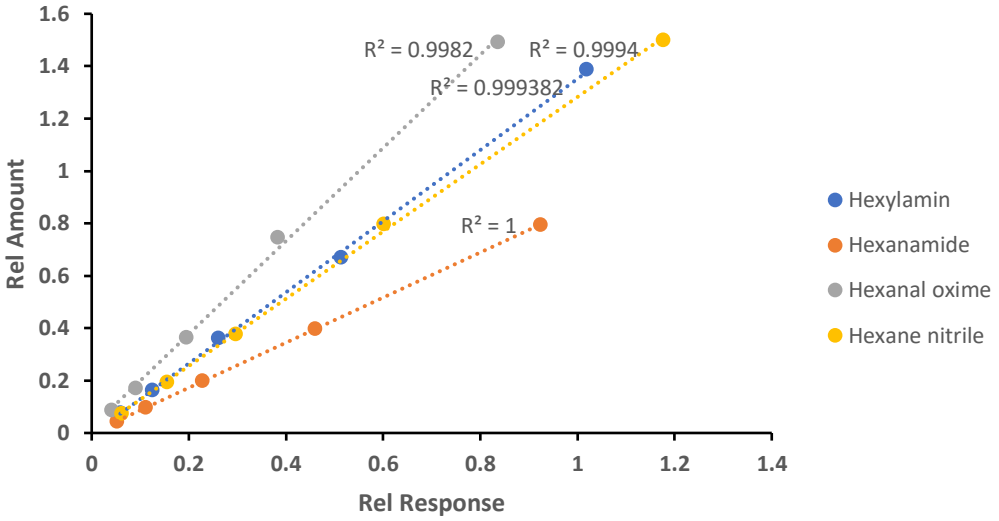

Figure 127: Calibration curve for C_6 substrates and intermediates.

Table 21: Temperature profile of GC measurements with the method.

	Rate / °C min-1	Value / °C	Hold Time / min	Run Time / min
Initial	0	60	0.5	0.5
Ramp 1	10	100	0	4.5
Ramp 2	15	110	0	5.17
Ramp 3	50	120	0	5.37
Ramp 4	15	130	0	6.0
Ramp 5	50	165	0	6.7
Ramp 6	18	275	0	12.8

Table 22: Temperature profile for longer chained aliphatic oximes (C_9)

	Rate / °C min^{-1}	Value / °C	Hold Time / min	Run Time / min
Initial	0	60	0.5	0.5
Ramp 1	50	120	0	1.7
Ramp 2	10	140	0	3.7
Ramp 3	5	150	1	6.7
Ramp 4	5	160	0	8.7
Ramp 5	15	200	0	11.37
Ramp 6	18	275	0	15.5

Table 23: Temperature profile for long chains aliphatic oximes (C_{12}).

	Rate / °C min^{-1}	Value / °C	Hold Time / min	Run Time / min
Initial	0	60	0.5	0.5
Ramp 1	50	165	0	2.6
Ramp 2	20	275	3	11.1

Hexanal oxime (1a)

^{1}H NMR (600 MHz, $CDCl_3$) δ = 9.35 (s, 1H), 7.40 (t, *J* = 6.2 Hz, 1H), 6.70 (t, *J* = 5.5 Hz, 1H), 2.36 (td, *J* = 7.6, 5.4 Hz, 1H), 2.17 (td, *J* = 7.6, 6.2 Hz, 1H), 1.52 – 1.42 (m, 2H), 1.35 – 1.25 (m, 4H), 0.92 – 0.83 (m, 3H).

E/Z: 1:1.08

^{13}C NMR (151 MHz, $CDCl_3$) δ = 153.00, 152.45, 31.63, 31.32, 29.52, 26.36, 25.80, 25.07, 22.44, 14.01, 14.00.

LC-HRMS ($C_6H_{13}NO$) $[M+H]^+$: calculated: 116.1070; detected: 116.1071 (-1.3 ppm deviation).

Hexanamide (4a):

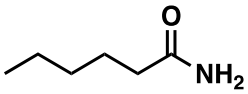

^{1}H NMR (400 MHz, $CDCl_3$) δ = 0.87 - 0.94 (m, 3 H), 1.28 - 1.38 (m, 4 H), 1.64 (q, 2 H), 2.22 (t, 2 H), 5.62 (d, 2 H) ppm.

^{13}C NMR (101 MHz, $CDCl_3$) δ = 13.92, 22.39, 25.23, 31.40, 35.94, 175.81 ppm.

Butanal oxime (1b)

^{1}H NMR (400 MHz, $CDCl_3$) δ = 8.88 (s, 1H), 8.48 (s, 1H), 7.42 (t, *J* = 6.1 Hz, 1H), 6.72 (t, *J* = 5.4 Hz, 1H), 2.36 (td, *J* = 7.5, 5.5 Hz, 1H), 2.18 (td, *J* = 7.4, 6.1 Hz, 1H), 1.53 (q, *J* = 7.4 Hz, 2H), 0.96 (q, *J* = 7.3 Hz, 3H).

E/Z = 1:1.06

^{13}C NMR (101 MHz, $CDCl_3$) δ = 152.95, 152.30, 31.55, 27.01, 20.04, 19.57, 14.01, 13.73.

2-Methylpentanal oxime (1c)

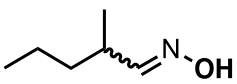

^{1}H NMR (400 MHz, $CDCl_3$) δ = 8.24 (s, 1H), 7.29 (d, *J* = 7.0 Hz, 1H), 6.50 (d, *J* = 7.8 Hz, 0H), 3.15 (p, *J* = 7.1 Hz, 0H), 2.38 (qd, *J* = 7.0, 5.6 Hz, 1H), 1.48 – 1.26 (m, 4H), 1.05 (dd, *J* = 13.3, 6.8 Hz, 3H), 0.96 – 0.85 (m, 3H).

^{13}C NMR (101 MHz, $CDCl_3$) δ = 157.66, 156.73, 36.97, 36.92, 34.27, 29.38, 20.54, 20.27, 18.06, 17.58, 14.17, 14.12.

2-Methylpentylamin (3c)

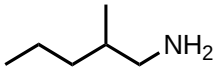

^{1}H NMR (600 MHz, $CDCl_3$) δ = 8.35 (s, 4H), 2.99 – 2.91 (m, 1H), 2.81 – 2.71 (m, 1H), 1.99 – 1.88 (m, 1H), 1.71 (s, 2H), 1.45 – 1.34 (m, 2H), 1.34 – 1.26 (m, 1H), 1.26 – 1.19 (m, 1H), 1.07 (d, *J* = 6.7 Hz, 3H), 0.91 (t, *J* = 7.0 Hz, 3H).

^{13}C NMR (151 MHz, $CDCl_3$) δ = 45.68, 36.26, 31.60, 19.74, 17.53, 14.18

Nonanal oxime (1d)

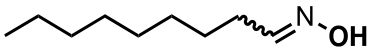

^{1}H NMR (500 MHz, $CDCl_3$) δ = 7.42 (t, *J* = 6.1 Hz, 1H), 6.72 (t, *J* = 5.4 Hz, 0H), 2.37 (td, *J* = 7.6, 5.4 Hz, 1H), 2.19 (td, *J* = 7.6, 6.2 Hz, 1H), 1.52 – 1.44 (m, 2H), 1.38 – 1.19 (m, 10H), 0.88 (td, *J* = 7.0, 1.5 Hz, 3H).

E/Z = 1:1.31

^{13}C NMR (126 MHz, $CDCl_3$) δ = 153.26, 152.58, 77.41, 77.16, 76.91, 31.96, 29.63, 29.52, 29.42, 29.32, 29.30, 29.24, 26.66, 26.19, 25.08, 22.79, 14.24.

Nonylamine (3d)

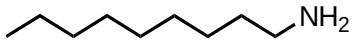

LC-HRMS of nonylamine (**3d**) ($C_9H_{21}N$) $[M+H]^+$: calculated 144.1747; detected: 144.1751 (-3.2 ppm deviation).

Citronellal oxime (1e)

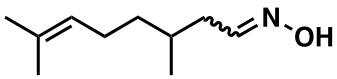

^{1}H NMR (400 MHz, $CDCl_3$) δ = 8.74 (s, 1H), 8.36 (s, 1H), 7.42 (t, *J* = 6.5 Hz, 1H), 6.74 (t, *J* = 5.5 Hz, 1H), 5.08 (dddq, *J* = 7.2, 5.8, 2.9, 1.5 Hz, 2H), 2.43 – 2.16 (m, 3H), 2.10 – 1.89 (m, 5H), 1.68 (t, *J* =1.3 Hz, 7H), 1.60 (t, *J* =1.2 Hz, 7H), 1.36 (dd, *J* = 6.7, 5.7 Hz, 1H), 1.30 – 1.16 (m, 2H), 0.94 (dd, *J* = 7.7, 6.7 Hz, 7H).

^{13}C NMR (101 MHz, $CDCl_3$) δ = 152.15, 151.69, 131.68, 124.49, 124.44, 36.98, 36.78, 36.56, 32.07, 31.06, 30.65, 25.85, 25.61, 25.55, 19.87, 19.58, 17.79.

3,7-dimethyloct-6-en-1-amine (3e)

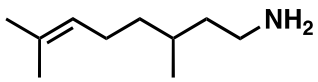

^{1}H NMR (600 MHz, $CDCl_3$) δ = 5.09 (ddp, *J* = 8.4, 5.8, 1.4 Hz, 1H), 3.47 (qd, *J* = 7.0, 0.9 Hz, 2H), 2.77 – 2.62 (m, 2H), 2.04 – 1.89 (m, 2H), 1.67 (s, 2H), 1.60 (s, 2H), 1.54 – 1.41 (m, 2H), 1.36 – 1.22 (m, 2H), 1.22 – 1.18 (m, 3H), 0.92 – 0.84 (m, 3H).

^{13}C NMR (151 MHz, $CDCl_3$) δ = 131.31, 124.96, 65.99, 41.36, 40.25, 37.36, 30.28, 25.85, 25.63, 19.69, 17.78, 15.41.

LC-HRMS of 3,7-dimethyloct-6-en-1-amine ($C_{10}H_{22}N$) $[M+H]^+$: calculated 156.17075; detected: 156.1745 (-1.32 ppm deviation).

3,7-dimethyloctan-1-amine (3e')

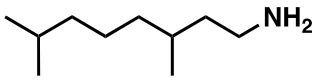

LC-HRMS ($C_{10}H_{24}N$) $[M+H]^+$: calculated 158.18640; detected: 158.1900 (-1.8847 ppm deviation)

Methyl-12-oxododecanoate oxime (1f)

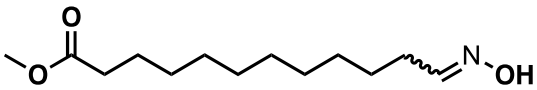

^{1}H NMR (600 MHz, $CDCl_3$) δ = 7.56 (s, 1H), 7.42 (t, *J* = 6.1 Hz, 0H), 7.25 (s, 0H), 6.71 (t, *J* = 5.5 Hz, 1H), 3.67 (s, 3H), 2.37 (td, *J* = 7.6, 5.5 Hz, 1H), 2.30 (t, *J* = 7.6 Hz, 2H), 2.19 (td, *J* = 7.5, 6.1 Hz, 1H), 1.65 – 1.57 (m, 5H), 1.36 – 1.25 (m, 12H).

E/Z: 3.19:1

^{13}C NMR (151 MHz, $CDCl_3$) δ = 174.55, 153.42, 152.68, 51.61, 34.26, 29.54, 29.52, 29.50, 29.47, 29.45, 29.35, 29.33, 29.25, 29.15, 26.63, 26.20, 25.08, 24.96.

Methyl 12-oxododecanoate (8f)

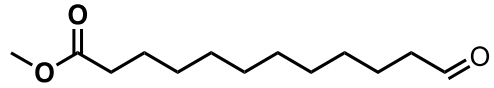

^{1}H NMR (400 MHz, C_6D_6) δ = 9.34 (t, *J* = 1.7 Hz, 1H), 3.37 (s, 3H), 2.13 (t, *J* = 7.4 Hz, 2H), 1.83 (td, *J* = 7.3, 1.7 Hz, 2H), 1.57 (t, *J* = 7.3 Hz, 2H), 1.31 (p, *J* = 7.3 Hz, 2H), 1.24 – 1.00 (m, 12H).

Methyl 12-aminododecanoate (3f)

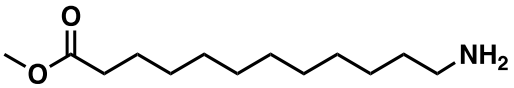

^{1}H NMR (500 MHz, $CDCl_3$) δ = 3.65 (s, 3H), 2.68 – 2.62 (m, 2H), 2.28 (t, *J* = 7.6 Hz, 2H), 1.58 (dt, *J* = 15.1, 7.4 Hz, 2H), 1.44 – 1.38 (m, 2H), 1.29 – 1.23 (m, 14H).

^{13}C NMR (151 MHz, $CDCl_3$) δ = 174.49, 51.58, 42.43, 34.26, 34.06, 29.73, 29.66, 29.63, 29.56, 29.38, 29.28, 27.04, 25.10.

Benzaldehyde oxime (1g)

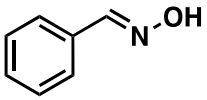

^{1}H NMR (600 MHz, $CDCl_3$) δ = 8.18 (t, *J* = 1.5 Hz, 1H), 7.59 (dd, *J* = 6.7, 3.0 Hz, 2H), 7.42 – 7.37 (m, 3H).

^{13}C NMR (151 MHz, $CDCl_3$) δ = 150.47, 132.02, 131.11, 130.37, 130.24, 128.94, 128.65, 128.59, 127.19.

(6-bromopyridin-2-yl)methanamine (3h)

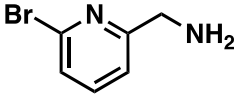

^{1}H NMR (600 MHz, CDCl3) δ = 7.50 (t, *J* = 7.7 Hz, 1H), 7.34 (dd, *J* = 7.8, 0.9 Hz, 1H), 7.27 – 7.24 (m, 1H), 3.94 (s, 2H), 1.72 (s, 2H).

^{13}C NMR (151 MHz, CDCl3) δ = 163.99, 141.95, 139.07, 126.28, 120.08, 47.54.

Furfuryl oxime (1i):

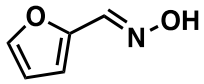

^{1}H NMR (400 MHz, $CDCl_3$) δ = 10.01 (s, 5H), 8.03 (s, 1H), 7.54 (s, 4H), 7.50 (dd, *J* = 1.7, 0.7 Hz, 2H), 7.48 (dd, *J* =1.7, 0.7 Hz, 5H), 7.35 (dd, *J* =3.4, 1.0 Hz, 5H), 6.65 (d, *J* = 3.4 Hz, 2H), 6.54 (ddd, *J* = 3.5, 1.8, 0.7 Hz, 6H), 6.46 (dd, *J* = 3.5, 1.8 Hz, 2H).

^{13}C NMR (101 MHz, $CDCl_3$) δ = 147.22, 145.23, 144.45, 143.59, 140.32, 137.21, 118.38, 112.87, 112.44, 111.72.

Additional HRMS data:

LC-HRMS of hexyl hydroxylamine (**2a**) ($C_6H_{15}NO$) $[M+H]^+$: calculated 118.1226; detected: 118.1228 (-1.3 ppm deviation).

LC-HRMS of hexylamine (**3a**) ($C_6H_{15}N$) $[M+H]^+$: calculated 102.1277; detected: 102.1280 (-2.9 ppm deviation).

LC-HRMS of hexanenitrile (**5a**) ($C_6H_{11}N$) $[M+H]^+$: calculated 98.0964; detected: 98.0961 (2.8 ppm deviation).

LC-HRMS of hexylimine (**6a**) ($C_6H_{13}N$) $[M+H]^+$: calculated 100.1121; detected: 100.1118 (-2.5 ppm deviation).

LC-HRMS of dihexylamine (**7a**) ($C_{12}H_{27}N$) $[M+H]^+$: calculated 186.2216; detected: 186.2222 (-2.9 ppm deviation).

LC-HRMS of dihexylimine ($C_{12}H_{25}N$) $[M+H]^+$: calculated 184.2060; detected: 184.2065 (-2.7 ppm deviation).

7. Conclusions and outlook

The research presented in this work has advanced the field of catalytic synthesis through the development and optimization of innovative methodologies for amide and amine production. These new methods help to reduce waste and the impact on the environment.

1. This work marks a significant advancement by incorporating highly branched amides into the toolbox of carbonylative telomerization. β-Myrcene and amines were combined for the first time in this reaction. By optimizing the reaction parameters, the desired branched amide was obtained with up to 97% yield. Using the monodentate PCy_2Ph proved crucial for enhancing the selectivity and overall efficiency of the reaction. A drawback is the high amount of Pd-catalyst necessary to facilitate the reaction.
   To overcome this challenge, a new approach was successfully implemented. Again, carbonylative telomerization was used and combined with carboxylic acids. In a novel palladium-catalyzed reaction, the synthesis of mixed carboxylic anhydrides from bulk chemicals was achieved for the first time, with yields up to 82%. The investigation of various benzoic acid derivatives revealed the influence of electronic properties on the yields. Their quantitative analysis was complicated since the resulting mixed carboxylic anhydrides are highly reactive. Therefore, a new protocol was developed, which derivatized the anhydrides into stable amides for precise quantification.
   Afterward, this concept was used to establish a carboxylic acid co-catalyzed carbonylative telomerization to synthesize unsaturated amides. 74% yield were achieved with several dienes and amines. Moreover, the sub-stoichiometric use of carboxylic acid presents a strategy for enhancing reaction efficiency, with scaling-up efforts showing increased performance and an 80 % reduction in catalyst quantity.
2. The desired conversion of amines into esters was achieved, although a two-step process was necessary. The reproduction of the literature results was partially difficult, as the obtained yields were up to 62 % lower. After investigating each part reaction separately, the ester reduction was identified as the limiting step.
   To improve the reaction, triphos-xyl was successfully synthesized. However, the desired higher yields in ester amination were obtained.
   As an alternative, the study focused on the synthesis of N-triphos ligands and their potential application in alcohol amination reactions. Compared to triphos, the work-up of the N-centered ligand is straightforward and leads to higher yields of 65%. N-triphos-xyl was also successfully obtained, but the yield was lower at 22%.
3. Finally, the hydrogenation of aldoximes into primary aliphatic amines was carried out with a homogeneous ruthenium catalyst for the first time. The reaction showcased remarkable selectivity of up to 90 % and productivity of up to 2900 h^{-1}. A new route for synthesizing primary aliphatic amines from common alkenes was developed by combining hydrogenation with previous hydroformylation. This new reaction sequence resembles a viable alternative to the highly anticipated hydroamination of alkenes with ammonia. The demonstrated three-step reaction sequence presents an attractive combination with straightforward purification steps, thus resulting in an efficient overall process. Using this process, the conversion of the renewable methyl 10-undecenoate into the polyamide precursor methyl 12-amminoundecanoate could be realized with high yields of up to 77 %.

In conclusion, the comprehensive research presented in this study underscores the importance of catalyst design, reaction optimization, and mechanistic understanding in advancing catalytic synthesis methodologies. This study contributes valuable insights and sets the stage for further catalysis and chemical synthesis advancements by addressing key challenges and exploring new reaction pathways.

While the methods introduced in this work already offer more sustainable synthesis methods for amides and amines, further enhancements are necessary for an industrial application.

Carbonylative telomerization uses a palladium-based catalyst, which is responsible for a significant portion of the cost of the reaction. A recycling strategy must be implemented for a sustainable and profitable scale-up. Ideally, the product can be separated from the catalyst while keeping the latter in its active form. A challenge here is the use of the solvent 1,4-dioxane, which is miscible with water and many organic solvents, making liquid-liquid phase separation difficult.

In terms of the amination of esters, the one-pot reaction is theoretically possible but requires more optimization. The one-pot, two-step reaction setup could also be further improved by higher reaction speed and yield. Modified triphos ligands have shown promising results in the literature; however, their synthesis, especially the work-up, requires fine tuning to be applied on larger scales.

Finally, the amination of alkenes with oxime intermediates should be transferred to a continuous reaction setup. Crystallizing the oxime intermediates from the hydroformylation reaction solution while maintaining the catalyst's activity seems promising. The catalyst recycling seems more challenging for the hydrogenation step due to the dioxane solvent. A separation using CO_2 to form carbamates, which are separable from a non-polar reaction solution, could be a viable option.

8. References

(1) Drauz, K.; Grayson, I.; Kleemann, A.; Krimmer, H.; Leuchtenberger, W.; Weckbecker, C. Amino Acids. *Ullmann's Encyclopedia of Industrial Chemistry*; Wiley, **2007**. https://doi.org/10.1002/14356007.a02_057.pub2.

(2) Electrochemically-produced ammonia could revolutionize food production. https://phys.org/news/2018-07-electrochemically-produced-ammonia-revolutionize-food-production.html (accessed 2023-11-09).

(3) World Population Clock: 8.1 Billion People (LIVE, 2023) - Worldometer. https://www.worldometers.info/world-population/# (accessed 2023-11-09).

(4) Smil, V. Detonator of the Population Explosion. *Nature* **1999** 400:6743 1999, 400 (6743), 415–415. https://doi.org/10.1038/22672.

(5) The Nobel Prize in Chemistry 1918. https://www.nobelprize.org/prizes/chemistry/1918/summary/ (accessed 2023-11-11).

(6) The Nobel Prize in Chemistry 1931. https://www.nobelprize.org/prizes/chemistry/1931/summary/ (accessed 2023-11-11).

(7) Williams, R. E.; Marshall, C. M. Top 200 Brand Name Drugs by Retail Sales in 2022. Arizona **2022**.

(8) Pattabiraman, V. R.; Bode, J. W. Rethinking Amide Bond Synthesis. *Nature* **2011** 480:7378 2011, 480 (7378), 471–479. https://doi.org/10.1038/nature10702.

(9) Roughley, S. D.; Jordan, A. M. The Medicinal Chemist's Toolbox: An Analysis of Reactions Used in the Pursuit of Drug Candidates. *J Med Chem* **2011**, 54 (10), 3451–3479. https://doi.org/10.1021/JM200187Y/SUPPL_FILE/JM200187Y_SI_001.PDF.

(10) Brown, D. G.; Boström, J. Analysis of Past and Present Synthetic Methodologies on Medicinal Chemistry: Where Have All the New Reactions Gone? *J Med Chem* **2016**, 59 (10), 4443–4458. https://doi.org/10.1021/ACS.JMEDCHEM.5B01409/ASSET/IMAGES/LARGE/JM-2015-01409Z_0006.JPEG.

(11) Gaspa, S.; Raposo, I.; Pereira, L.; Mulas, G.; Ricci, P. C.; Porcheddu, A.; De Luca, L. Visible Light-Induced Transformation of Aldehydes to Esters, Carboxylic Anhydrides and Amides. *New J Chem* **2019**, 43 (27), 10711–10715. https://doi.org/10.1039/C9NJ01984G.

(12) Mevan Dissanayake, D. M. M.; Melville, A. D.; Vannucci, A. K. Electrochemical Anion Pool Synthesis of Amides with Concurrent Benzyl Ester Synthesis †. *Green Chem* **2019**, 21. https://doi.org/10.1039/c9gc00707e.

(13) Liu, Y.; Shi, S.; Achtenhagen, M.; Liu, R.; Szostak, M. Metal-Free Transamidation of Secondary Amides via Selective N-C Cleavage under Mild Conditions. *Org Lett* **2017**, 19 (7), 1614–1617. https://doi.org/10.1021/ACS.ORGLETT.7B00429/SUPPL_FILE/OL7B00429_SI_001.PDF.

(14) De Souza, G. F. P.; Von Zuben, T. W.; Salles, A. G. On Water Metal-Catalyst-Free Oxidative Coupling-Amidation of Amines to Access Imines and Amides. *ACS Sustain Chem Eng* **2017**, 5 (9), 8439–8446. https://doi.org/10.1021/ACSSUSCHEMENG.7B02353/ASSET/IMAGES/LARGE/SC-2017-02353P_0007.JPEG.

(15) Zhan, W.; Ji, L.; Ge, Z. mei; Wang, X.; Li, R. tao. A Continuous-Flow Synthesis of Primary Amides from Hydrolysis of Nitriles Using Hydrogen Peroxide as Oxidant. *Tetrahedron* **2018**, 74 (13), 1527–1532. https://doi.org/10.1016/J.TET.2018.02.017.

(16) Loukrakpam, D. C.; Phukan, P. Metal-Free One-Pot Conversion of Olefins and Alkynes to Amides Using TsNBr2, I2 and Aqueous NH3 at Room Temperature. *ChemistrySelect* **2019**, 4 (31), 8978–8982. https://doi.org/10.1002/SLCT.201901530.

(17) Massolo, E.; Pirola, M.; Benaglia, M. Amide Bond Formation Strategies: Latest Advances on a Dateless Transformation. *Eur J Org Chem* **2020**, 2020 (30), 4641–4651. https://doi.org/10.1002/EJOC.202000080.

(18) Sabatini, M. T.; Boulton, L. T.; Sneddon, H. F.; Sheppard, T. D. A Green Chemistry Perspective on Catalytic Amide Bond Formation. *Nat Catal* **2019**, 2 (1), 10–17. https://doi.org/10.1038/s41929-018-0211-5.

(19) Ishihara, K.; Ohara, S.; Yamamoto, H. 3,4,5-Trifluorobenzeneboronic Acid as an Extremely Active Amidation Catalyst. *J Org Chem* **1996**, 61 (13), 4196–4197. https://doi.org/10.1021/JO9606564/SUPPL_FILE/JO4196.PDF.

(20) Gernigon, N.; Al-Zoubi, R. M.; Hall, D. G. Direct Amidation of Carboxylic Acids Catalyzed by Ortho-Iodo Arylboronic Acids: Catalyst Optimization, Scope, and Preliminary Mechanistic Study Supporting a Peculiar Halogen Acceleration Effect. *J Org Chem* **2012**, 77 (19), 8386–8400. https://doi.org/10.1021/JO3013258/SUPPL_FILE/JO3013258_SI_002.CIF.

(21) Lundberg, H.; Adolfsson, H. Hafnium-Catalyzed Direct Amide Formation at Room Temperature. *ACS Catal* **2015**, 5 (6), 3271–3277. https://doi.org/10.1021/ACSCATAL.5B00385

(22) Gunanathan, C.; Ben-David, Y.; Milstein, D. Direct Synthesis of Amides from Alcohols and Amines with Liberation of H2. *Science* **2007**, 317 (5839), 790–792. https://doi.org/10.1126/SCIENCE.1145295

(23) Fang, X.; Jackstell, R.; Beller, M. Selective Palladium-Catalyzed Aminocarbonylation of Olefins with Aromatic Amines and Nitroarenes. *Angew Chem* **2013**, 125 (52), 14339–14343. https://doi.org/10.1002/ANGE.201308455.

(24) Nageswara Rao, S.; Reddy, N. N. K.; Samanta, S.; Adimurthy, S. I2-Catalyzed Oxidative Amidation of Benzylamines and Benzyl Cyanides under Mild Conditions. *J Org Chem* **2017**, 82 (24), 13632–13642. https://doi.org/10.1021/ACS.JOC.7B02211

(25) Popov, K. K.; Campbell, J. L. P.; Kysilka, O.; Hošek, J.; Davies, C. D.; Pour, M.; Kočovský, P. Reductive Amination Revisited: Reduction of Aldimines with Trichlorosilane Catalyzed by Dimethylformamide–Functional Group Tolerance, Scope, and Limitations. *J Org Chem* **2022**, 87 (2), 920–943. https://doi.org/10.1021/acs.joc.1c01561.

(26) Afagh, N. A.; Yudin, A. K. Chemoselectivity and the Curious Reactivity Preferences of Functional Groups. *Angew Chem Int Ed* **2010**, 49 (2), 262–310. https://doi.org/10.1002/ANIE.200901317.

(27) Streiff, S.; Jérôme, F. Hydroamination of Non-Activated Alkenes with Ammonia: A Holy Grail in Catalysis. *Chem Soc Rev* **2021**, 50 (3), 1512–1521. https://doi.org/10.1039/C9CS00873J.

(28) Murugesan, K.; Wei, Z.; Chandrashekhar, V. G.; Neumann, H.; Spannenberg, A.; Jiao, H.; Beller, M.; Jagadeesh, R. V. Homogeneous Cobalt-Catalyzed Reductive Amination for Synthesis of Functionalized Primary Amines. *Nat Commun* **2019**, 10 (1), 5443. https://doi.org/10.1038/s41467-019-13351-7.

(29) Senthamarai, T.; Murugesan, K.; Schneidewind, J.; Kalevaru, N. V.; Baumann, W.; Neumann, H.; Kamer, P. C. J.; Beller, M.; Jagadeesh, R. V. Simple Ruthenium-Catalyzed Reductive Amination Enables the Synthesis of a Broad Range of Primary Amines. *Nat Commun* **2018**, 9 (1), 4123. https://doi.org/10.1038/s41467-018-06416-6.

(30) Maji, M.; Chakrabarti, K.; Panja, D.; Kundu, S. Sustainable Synthesis of N-Heterocycles in Water Using Alcohols Following the Double Dehydrogenation Strategy. *J Catal* **2019**, 373, 93–102. https://doi.org/10.1016/J.JCAT.2019.03.028.

(31) García-Ortiz, A.; Vidal, J. D.; Climent, M. J.; Concepción, P.; Corma, A.; Iborra, S. Chemicals from Biomass: Selective Synthesis of N-Substituted Furfuryl Amines by the One-Pot Direct Reductive Amination of Furanic Aldehydes. *ACS Sustain Chem Eng* **2019**, 7 (6), 6243–6250. https://doi.org/10.1021/ACSSUSCHEMENG.8B06631/ASSET/IMAGES/LARGE/SC-2018-066314_0001.JPEG.

(32) Billups, W. E.; Walker, W. E.; Shields, T. C. The Palladium-Catalysed Carbonylation–Dimerization of Butadiene. *J Chem Soc D* **1971**, 0 (18), 1067–1068. https://doi.org/10.1039/C29710001067.

(33) Tsuji, J.; Mori, Y.; Hara, M. Organic Syntheses by Means of Noble Metal Compounds-XLVIII. Carbonylation of Butadiene Catalyzed by Palladium-Phosphine Complexes. Tetrahedron **1972**, 28 (14), 3721–3725. https://doi.org/10.1016/S0040-4020(01)93818-9.

(34) Romanelli, M.; Romanelli, G. Preparation of Alkadienoic Acid Esters. US 3 780 074, **1973**. https://www.google.com/patents/US3780074.

(35) Knifton, J. F. Syngas Reactions. I. The Catalytic Carbonylation of Conjugated Dienes. *J Catal* **1979**, 60 (1), 27–40. https://doi.org/10.1016/0021-9517(79)90065-4.

(36) Dumont, C.; Belva, F.; Gauvin, R. M.; Sauthier, M. The Palladium-Catalyzed Carbonylative Telomerization Reaction with Phenols, Polyphenols and Kraft Lignin. *ChemSusChem* **2018**, 11 (22), 3917–3922. https://doi.org/10.1002/cssc.201802017.

(37) Wilson, E.; Dumont, C.; Drelon, M.; Suisse, I.; Penverne, C.; Sauthier, M. The Palladium-Catalyzed Carboxytelomerization of Butadiene with Agrobased Alcohols and Polyols. *ChemSusChem* **2019**, 12 (11), 2457–2461. https://doi.org/10.1002/cssc.201900381.

(38) Vogelsang, D.; Vondran, J.; Vorholt, A. J. One-Step Palladium Catalysed Synthetic Route to Unsaturated Pelargonic C9-Amides Directly from 1,3-Butadiene. *J Catal* **2018**, 365, 24–28. https://doi.org/10.1016/j.jcat.2018.06.004.

(39) Vogelsang, D.; Dittmar, M.; Seidensticker, T.; Vorholt, A. J. Palladium-Catalysed Carboxytelomerisation of β-Myrcene to Highly Branched C21-Esters. *Catal Sci Technol* **2018**, 8 (17), 4332–4337. https://doi.org/10.1039/c8cy00769a.

(40) Vogelsang, D.; Raumann, B. A.; Hares, K.; Vorholt, A. J. From Carboxytelomerization of 1,3-Butadiene to Linear α,ω-C 10 -Diester Combinatoric Approaches for an Efficient Synthetic Route. *Chem Eur J* **2018**, 24 (9), 2264–2269. https://doi.org/10.1002/chem.201705381.

(41) Hares, K.; Vogelsang, D.; Wernsdörfer, C. S.; Panke, D.; Vogt, D.; Seidensticker, T. Palladium-Catalyzed Synthesis of Mixed Anhydrides via Carbonylative Telomerization. *Catal Sci Technol* **2022**. https://doi.org/10.1039/D2CY00486K.

(42) Vogelsang, D.; Vondran, J.; Hares, K.; Schäfer, K.; Seidensticker, T.; Vorholt, A. J. Palladium Catalysed Acid-Free Carboxytelomerisation of 1,3-Butadiene with Alcohols Accessing Pelargonic Acid Derivatives Including Triglycerides under Selectivity Control. *Adv Synth Catal* **2020**, 362 (3), 679–687. https://doi.org/10.1002/adsc.201901383.

(43) Smutny, E. J. Oligomerization and Dimerization of Butadiene under Homogeneous Catalysis. Reaction with Nucleophiles and the Synthesis of 1,3,7-Octatriene. *J Am Chem Soc* **1967**, 89 (25), 6793–6794. https://doi.org/10.1021/ja01001a089.

(44) Walker, W. E.; Manyik, R. M.; Atkins, K. E.; Farmer, M. L. Palladium Complex Catalyzed Reactions of Conjugated Dienes. II Solvent and Ligand Effects on the Reaction of Butadiene with Acetic Acid. *Tetrahedron Lett* **1970**, 11 (43), 3817–3820. https://doi.org/10.1016/S0040-4039(01)98598-3.

(45) Takahashi, S.; Shibano, T.; Hagihara, N. The Dimerization of Butadiene by Palladium Complex Catalysts. *Tetrahedron Lett* **1967**, 8 (26), 2451–2453. https://doi.org/10.1016/S0040-4039(00)90830-X.

(46) Lopes, J. M.; Petrovski, Z.; Bogel-Łukasik, R.; Bogel-Łukasik, E. Heterogeneous Palladium -Catalyzed Telomerization of Myrcene with Glycerol Derivatives in Supercritical Carbon Dioxide: A Facile Route to New Building Blocks. *Green Chem* **2011**, 13 (8), 2013–2016. https://doi.org/10.1039/C1GC15313G.

(47) Behr, A.; Johnen, L.; Vorholt, A. J. Telomerization of Myrcene and Catalyst Separation by Thermomorphic Solvent Systems. *ChemCatChem* **2010**, 2 (10), 1271–1277. https://doi.org/10.1002/CCTC.201000116.

(48) Behr, A.; Becker, M.; Beckmann, T.; Johnen, L.; Leschinski, J.; Reyer, S.; Behr, A. Telomerisation – Fortschritte Und Anwendungen Einer Vielseitigen Reaktion. *Angew Chem* **2009**, 121 (20), 3652–3669. https://doi.org/10.1002/ANGE.200804599.

(49) Behr, A.; Becker, M.; Beckmann, T.; Johnen, L.; Leschinski, J.; Reyer, S. Telomerization: Advances and Applications of a Versatile Reaction. *Angew Chem Int Ed* **2009**, 48 (20), 3598–3614. https://doi.org/10.1002/anie.200804599.

(50) Brotzel, F.; Ying, C. C.; Mayr, H. Nucleophilicities of Primary and Secondary Amines in Water. *J Org Chem* **2007**, 72 (10), 3679–3688. https://doi.org/10.1021/JO062586Z/

(51) Rose, D.; Lepper, H. The Palladium-Catalysed Reaction of Butadiene with Acetic Acid in the Presence of Phosphites. *J Organomet Chem* **1973**, 49 (2), 473–476. https://doi.org/10.1016/S0022-328X(00)84238-2.

(52) Inanaga, J.; Hirata, K.; Saeki, H.; Katsuki, T.; Yamaguchi, M. A Rapid Esterification by Means of Mixed Anhydride and Its Application to Large-Ring Lactonization. *Bull Chem Soc Jpn* **1979**, 52 (7), 1989–1993. https://doi.org/10.1246/bcsj.52.1989.

(53) Wang, X.; Woo, L. K. Isomerization of Olefin Carboxylic Esters Catalyzed by Nickel and Palladium Compounds. *J Mol Catal A Chem* **1998**, 130 (1–2), 171–176. https://doi.org/10.1016/S1381-1169(97)00213-6.

(54) Kocen, A. L.; Brookhart, M.; Daugulis, O. Palladium-Catalysed Alkene Chain-Running Isomerization. *Chem Commn* **2017**, 53 (72), 10010–10013. https://doi.org/10.1039/c7cc04953f.

(55) Mamone, P.; Grünberg, M. F.; Fromm, A.; Khan, B. A.; Gooßen, L. J. [Pd(μ-Br)(PtBu3)]2 as a Highly Active Isomerization Catalyst: Synthesis of Enol Esters from Allylic Esters. *Org Lett* **2012**, 14 (14), 3716–3719. https://doi.org/10.1021/OL301563G.

(56) Peydecastaing, J.; Vaca-Garcia, C.; Borredon, E. Quantitative Analysis of Mixtures of Various Linear Anhydrides and Carboxylic Acids. *Chromatographia* **2008**, 68 (9–10), 685–688. https://doi.org/10.1365/s10337-008-0765-5.

(57) Peydecastaing, J.; Vaca-Garcia, C.; Borredon, E. Consecutive Reactions in an Oleic Acid and Acetic Anhydride Reaction Medium. *Eur J Lip Sci Technol* **2009**, 111 (7), 723–729. https://doi.org/10.1002/ejlt.200800189.

(58) Kikukawa, K.; Kono, K.; Nagira, K.; Wada, F.; Matsuda, T. Reaction of Diazonium Salts with Transition Metals. 6. Preparation of Mixed Acid Anhydrides from Arenediazonium Salts and Sodium Carboxylates under Palladium(O) Catalysis. *J Org Chem* **1981**, 46 (22), 4413–4416. https://doi.org/10.1021/jo00335a018.

(59) Wernsdörfer, C. S. Expansion of the Synthesis-Tool of Carboxytelomerization for the Two-Step Synthesis of Amides via Anhydrides. Bachelor Thesis, TU Dortmund, Dortmund, 2019.

(60) Jorgensen, A. D.; Picel, K. C.; Stamoudis, V. C. Prediction of Gas Chromatography Flame Ionization Detector Response Factors from Molecular Structures. *Anal Chem* **1990**, 62 (7), 683–689. https://doi.org/10.1021/ac00206a007.

(61) Lide, D. R.; Haynes, W. M. CRC Handbook of Chemistry and Physics, 90th ed.; *CRC Press*, **2010**.

(62) Schaller, H. F.; Tishkov, A. A.; Feng, X.; Mayr, H. Direct Observation of the Ionization Step in Solvolysis Reactions: Electrophilicity versus Electrofugality of Carbocations. *J Am Chem Soc* **2008**, 130 (10), 3012–3022. https://doi.org/10.1021/ja0765464.

(63) Jolly, P. W. η 3-Allylpalladium Compounds. *Angew Chem Int Ed* **1985**, 24 (4), 283–295. https://doi.org/10.1002/ANIE.198502831.

(64) Pedersen, D.; Rosenbohm, C. Dry Column Vacuum Chromatography. *Synthesis* **2004**, 2001 (16), 2431–2434. https://doi.org/10.1055/s-2001-18722.

(65) Vogelsang, D.; Vondran, J.; Hares, K.; Schäfer, K.; Seidensticker, T.; Vorholt, A. J. Palladium Catalysed Acid-Free Carboxytelomerisation of 1,3-Butadiene with Alcohols Accessing Pelargonic Acid Derivatives Including Triglycerides under Selectivity Control. *Adv Synth Catal* **2020**, 362 (3), 679–687. https://doi.org/10.1002/adsc.201901383.

(66) Neumann, H.; Brennführer, A.; Groß, P.; Riermeier, T.; Almena, J.; Beller, M. Efficient Carbonylation of Aryl and Heteroaryl Bromides Using a Palladium/Diadamantylbutylphosphine Catalyst. *Adv Synth Catal* **2006**, 348 (10–11), 1255–1261. https://doi.org/10.1002/ADSC.200606044/

(67) Trost, B. The Atom Economy—A Search for Synthetic Efficiency. *Science* **1991**, 254 (5037), 1471–1477. https://doi.org/10.1126/science.1962206.

(68) Behr, *A. Angewandte homogene Katalyse*; Wiley-VCH: Weinheim, **2008**.

(69) Bunten, K. A.; Moreno, C.; Poë, A. J. Electronic and Steric Effects in Fragmentation Reactions of Os3(CO)9(μ-C4Ph4). *Dalton Trans* **2005**, No. 8, 1416–1421. https://doi.org/10.1039/B418940J.

(70) Carrow, B. P.; Chen, L. Tri(1-Adamantyl)Phosphine: Exceptional Catalytic Effects Enabled by the Synergy of Chemical Stability, Donicity, and Polarizability. *Synlett* **2017**, 28 (3), 280–288. https://doi.org/10.1055/S-0036-1588128/ID/JR000-2001/BIB.

(71) Henderson, W. A.; Streuli, C. A. The Basicity of Phosphines. *J Am Chem Soc* **1960**, 82 (22), 5791–5794. https://doi.org/10.1021/JA01507A008/

(72) Schöbel, R. *Beiträge Zur Optimierung Und Katalysatorrückführung Der Carboxytelomerisation*, Technische Universität Dortmund, Dortmund, **2009**.

(73) Kégl, T. R.; Pálinkás, N.; Kollár, L.; Kégl, T. Computational Characterization of Bidentate P-Donor Ligands: Direct Comparison to Tolman's Electronic Parameters. *Molecules* **2018**, Vol. 23, Page 3176 2018, 23 (12), 3176. https://doi.org/10.3390/MOLECULES23123176.

(74) Kamer, P. C. J.; Van Leeuwen, P. W. N. M.; Reek, J. N. H. Wide Bite Angle Diphosphines: Xantphos Ligands in Transition Metal Complexes and Catalysis. 2001. https://doi.org/10.1021/ar000060.

(75) Glorius, F. N-Heterocyclic Carbenes in Transition Metal Catalysis; *Topics in Organometallic Chemistry*; Springer Berlin Heidelberg: Berlin, Heidelberg, **2007**; Vol. 21. https://doi.org/10.1007/978-3-540-36930-1.

(76) Milius, L. Tandem-Catalysed Conversion of 1,3-Dienes with Amine Nucleo- Philes via Carboxylic Acid-Assisted Carboxytelomerisation in a One-Step Reaction System. Master Thesis, TU Dortmund, Dortmund, **2020**.

(77) Muscat, A.; de Olde, E. M.; de Boer, I. J. M.; Ripoll-Bosch, R. The Battle for Biomass: A Systematic Review of Food-Feed-Fuel Competition. *Glob Food Sec* **2020**, 25, 100330. https://doi.org/10.1016/J.GFS.2019.100330.

(78) Karamerou, E. E.; Webb, C. Cultivation Modes for Microbial Oil Production Using Oleaginous Yeasts – A Review. *Biochem Eng J* **2019**, 151, 107322. https://doi.org/10.1016/J.BEJ.2019.107322.

(79) Bao, W.; Li, Z.; Wang, X.; Gao, R.; Zhou, X.; Cheng, S.; Men, Y.; Zheng, L. Approaches to Improve the Lipid Synthesis of Oleaginous Yeast Yarrowia Lipolytica: A Review. *Renewable and Sustainable Energy Rev* **2021**, 149, 111386. https://doi.org/10.1016/J.RSER.2021.111386.

(80) Zhou, Y.; Hu, C. Catalytic Thermochemical Conversion of Algae and Upgrading of Algal Oil for the Production of High-Grade Liquid Fuel: A Review. *Catalysts* **2020**, Vol. 10, Page 145 2020, 10 (2), 145. https://doi.org/10.3390/CATAL10020145.

(81) Borschel, E.-M.; Heimann, S.; Kromm, E. Textile Auxiliaries, 5. Deying Auxiliaries. *Ullmann's Encyclopedia of Industrial Chemistry* **2011**. https://doi.org/10.1002/14356007.O26_O09.

(82) Holmberg, K. Surfactants. *Ullmann's Encyclopedia of Industrial Chemistry* **2019**, 1–56. https://doi.org/10.1002/14356007.A25_747.PUB2.

(83) Roose, P.; Eller, K.; Henkes, E.; Rossbacher, R.; Höke, H. Amines, Aliphatic. *Ullmann's Encyclopedia of Industrial Chemistry* **2015**, 1–55. https://doi.org/10.1002/14356007.A02_001.PUB2.

(84) Coeck, R.; De Vos, D. E. One-Pot Reductive Amination of Carboxylic Acids: A Sustainable Method for Primary Amine Synthesis. *Green Chem* **2020**, 22 (15), 5105–5114. https://doi.org/10.1039/d0gc01441a.

(85) Pingen, D.; Diebolt, O.; Vogt, D. Direct Amination of Bio-Alcohols Using Ammonia. *ChemCatChem* **2013**, 5 (10), 2905–2912. https://doi.org/10.1002/cctc.201300407.

(86) Shi, Y.; Kamer, P. C. J.; Cole-Hamilton, D. J. A New Route to α,ω-Diamines from Hydrogenation of Dicarboxylic Acids and Their Derivatives in the Presence of Amines. *Green Chem* **2017**, 19 (22), 5460–5466. https://doi.org/10.1039/C7GC02838E.

(87) Núñez Magro, A. A.; Eastham, G. R.; Cole-Hamilton, D. J. The Synthesis of Amines by the Homogeneous Hydrogenation of Secondary and Primary Amides. *Chem Commun* **2007**, No. 30, 3154–3156. https://doi.org/10.1039/b706635j.

(88) Sorribes, I.; Junge, K.; Beller, M. Direct Catalytic N-Alkylation of Amines with Carboxylic Acids. *J Am Chem Soc* **2014**, 136 (40), 14314–14319. https://doi.org/10.1021/ja5093612.

(89) Sorribes, I.; Cabrero-Antonino, J. R.; Vicent, C.; Junge, K.; Beller, M. Catalytic N-Alkylation of Amines Using Carboxylic Acids and Molecular Hydrogen. *J Am Chem Soc* **2015**, 137 (42), 13580–13587. https://doi.org/10.1021/jacs.5b07994.

(90) Shi, Y.; Kamer, P. C. J.; Cole-Hamilton, D. J.; Harvie, M.; Baxter, E. F.; Lim, K. J. C.; Pogorzelec, P. A New Route to N-Aromatic Heterocycles from the Hydrogenation of Diesters in the Presence of Anilines. *Chem Sci* **2017**, 8 (10), 6911–6917. https://doi.org/10.1039/c7sc01718a.

(91) Hayes, K. S. Industrial Processes for Manufacturing Amines. *Appl Catal A Gen* **2001**, 221 (1–2), 187–195. https://doi.org/10.1016/S0926-860X(01)00813-4.

(92) Gunanathan, C.; Milstein, D. Selective Synthesis of Primary Amines Directly from Alcohols and Ammonia. *Angew Chem Int Ed* **2008**, 47 (45), 8661–8664. https://doi.org/10.1002/anie.200803229.

(93) Imm, S.; Bähn, S.; Neubert, L.; Neumann, H.; Beller, M. An Efficient and General Synthesis of Primary Amines by Ruthenium-Catalyzed Amination of Secondary Alcohols with Ammonia. *Angew Chem Int Ed* **2010**, 49 (44), 8126–8129. https://doi.org/10.1002/anie.201002576.

(94) Pingen, D.; Lutz, M.; Vogt, D. Mechanistic Study on the Ruthenium-Catalyzed Direct Amination of Alcohols. *Organometallics* **2014**, 33 (7), 1623–1629. https://doi.org/10.1021/om4011998.

(95) Tillack, A.; Hollmann, D.; Mevius, K.; Michalik, D.; Bähn, S.; Beller, M. Salt-Free Synthesis of Tertiary Amines by Ruthenium-Catalyzed Amination of Alcohols. *Eur J Org Chem* **2008**, No. 28, 4745–4750. https://doi.org/10.1002/ejoc.200800671.

(96) Ye, X.; Plessow, P. N.; Brinks, M. K.; Schelwies, M.; Schaub, T.; Rominger, F.; Paciello, R.; Limbach, M.; Hofmann, P. Alcohol Amination with Ammonia Catalyzed by an Acridine-Based Ruthenium Pincer Complex: A Mechanistic Study. *J Am Chem Soc* **2014**, 136 (16), 5923–5929. https://doi.org/10.1021/ja409368a.

(97) Kar, S.; Milstein, D. Sustainable Catalysis with Fluxional Acridine-Based PNP Pincer Complexes. *Chem Commun* 2022, 58 (23), 3731–3746. https://doi.org/10.1039/D2CC00247G.

(98) Derrah, E. J.; Hanauer, M.; Plessow, P. N.; Schelwies, M.; da Silva, M. K.; Schaub, T. Ru(II)-Triphos Catalyzed Amination of Alcohols with Ammonia via Ionic Species. *Organometallics* **2015**, 34 (10), 1872–1881. https://doi.org/10.1021/acs.organomet.5b00003.

(99) Nakagawa, N.; Derrah, E. J.; Schelwies, M.; Rominger, F.; Trapp, O.; Schaub, T. Triphos Derivatives and Diphosphines as Ligands in the Ruthenium-Catalysed Alcohol Amination with NH 3. *Dalton Trans* **2016**, 45 (16), 6856–6865. https://doi.org/10.1039/C5DT04870B.

(100) Schaub, T.; Buschhaus, B.; Brinks, M. K.; Schelwies, M.; Paciello, R.; Melder, J.-P.; Merger, M. Process for the Preparation of Primary Amines by Homogeneously Catalyzed Alcohol Amination. *US20120232292A1*, **2012**. https://patents.google.com/patent/US20120232292A1/en?oq=US+2012%2f0232292+A1%2c+2012. (accessed 2023-11-19).

(101) Imm, S.; Bähn, S.; Zhang, M.; Neubert, L.; Neumann, H.; Klasovsky, F.; Pfeffer, J.; Haas, T.; Beller, M. Improved Ruthenium-Catalyzed Amination of Alcohols with Ammonia: Synthesis of Diamines and Amino Esters. *Angew Chem Int Ed* **2011**, 50 (33), 7599–7603. https://doi.org/10.1002/anie.201103199.

(102) Chiron, J.; Galy, J.-P. Reactivity of the Acridine Ring: One-Pot Regioselective Single and Double Bromomethylation of Acridine and Some Derivatives. *Synlett* **2003**, No. 15, 2349–2350. https://doi.org/10.1055/s-2003-42104.

(103) Lu, W.; Shao, Z. G.; Zhang, G.; Li, J.; Zhao, Y.; Yi, B. Preparation of Anion Exchange Membranes by an Efficient Chloromethylation Method and Homogeneous Quaternization/Crosslinking Strategy. *Solid State Ion* **2013**, 245–246, 8–18. https://doi.org/10.1016/J.SSI.2013.05.005.

(104) Warshawsky, A.; Deshe, A.; Gutman, R. Safe Halomethylation of Aromatic Polymers via BCME-Free Long Chain Haloalkylethers. *Br Poly J* **1984**, 16 (4), 234–238. https://doi.org/10.1002/PI.4980160415.

(105) Li, J. J. Blanc Chloromethylation. *Name Reactions*; Springer Berlin Heidelberg: Berlin, Heidelberg, **2006**; pp 61–62. https://doi.org/10.1007/3-540-30031-7_30.

(106) Ivanov, V. S. International and Russian Methods of Synthesis and Use of Pyromelliticacid Dianhydrideand Tendencies of Their Development (Review). *Biosci Biotechnol Res Asia* **2014**. https://doi.org/10.13005/bbra/1583.

(107) Whitmore, F. C.; Ginsburg, A.; Rueggeberg, W.; Tharp, I.; Nottorf, H.; Cannon, M.; Carnahan, F.; Cryder, D.; FLeming, G.; Goldberg, G.; Haggard, H.; Herr, C.; Hoover, T.; Lovell, H.; Mraz, R.; Noll, C.; Oakwood, T.; Patterson, H.; Van Strien, R.; Walter, R.; Zook, H.; Wagner, R.; Weisgerber, C.; Wilkins, J. Production of Benzyl Chloride by Chloromethylation of Benzene. Laboratory and Pilot Plant Studies. *Ind Eng Chem* **1946**, *38* (5), 478–485. https://doi.org/10.1021/ie50437a013.Weisgerber, C. A.; Wilkins, J. P.; Whitmore, F. C. Production of Benzyl Chloride LABORATORY AND.

(108) van der Made, a. W.; van der Made, R. H. A Convenient Procedure for Bromomethylation of Aromatic Compounds. Selective Mono-,Bis-, or Trisbromomethylation. *J Org Chem* **1993**, 58 (5), 1262–1263. https://doi.org/10.1021/jo00057a046.

(109) Schmidt, A. Ester Amination and Other Homogeneous Catalyzed Applications of a Xylene-Modified Triphos Ligand. Bachelor Thesis, TU Dortmund, Dortmund, **2020**.

(110) Beydoun, K.; Thenert, K.; Streng, E. S.; Brosinski, S.; Leitner, W.; Klankermayer, J. Selective Synthesis of Trimethylamine by Catalytic N-Methylation of Ammonia and Ammonium Chloride by Utilizing Carbon Dioxide and Molecular Hydrogen. *ChemCatChem* **2016**, 8 (1), 135–138. https://doi.org/10.1002/CCTC.201501116.

(111) Pingen, D.; Müller, C.; Vogt, D. Direct Amination of Secondary Alcohols Using Ammonia. *Angew Chem Int Ed* **2010**, 49 (44), 8130–8133. https://doi.org/10.1002/anie.201002583.

(112) Reichert, R. Untersuchung Der Ruthenium-Katalysierten Esteraminierung Sowie Synthese Alternativer Tridentater Phosphorliganden. Bachelor Thesis, TU Dortmund , Dortmund, **2022**.

(113) Werkmeister, S.; Neumann, J.; Junge, K.; Beller, M. Pincer-Type Complexes for Catalytic (De)Hydrogenation and Transfer (De)Hydrogenation Reactions: Recent Progress. *Chem Eur J* **2015**, 21 (35), 12226–12250. https://doi.org/10.1002/CHEM.201500937.

(114) Zhang, J.; Balaraman, E.; Leitus, G.; Milstein, D. Electron-Rich PNP-and PNN-Type Ruthenium(Ii) Hydrido Borohydride Pincer Complexes. Synthesis, Structure, and Catalytic Dehydrogenation of Alcohols and Hydrogenation of Esters. *Organometallics* **2011**, 30 (21), 5716–5724. https://doi.org/10.1021/OM200595M/SUPPL_FILE/OM200595M_SI_001.CIF.

(115) Schwartsburd, L.; Iron, M. A.; Konstantinovski, L.; Diskin-Posner, Y.; Leitus, G.; Shimon, L. J. W.; Milstein, D. Synthesis and Reactivity of an Iridium(I) Acetonyl PNP Complex. Experimental and Computational Study of Metal-Ligand Cooperation in H-H and C-H Bond Activation via Reversible Ligand Dearomatization. *Organometallics* **2010**, 29 (17), 3817–3827. https://doi.org/10.1021/OM1004435/

(116) Feller, M.; Karton, A.; Leitus, G.; Martin, J. M. L.; Milstein, D. Selective Sp3 C-H Activation of Ketones at the β Position by Ir(I). Origin of Regioselectivity and Water Effect. *J Am Chem Soc* **2006**, 128 (38), 12400–12401. https://doi.org/10.1021/JA0641352/

(117) Ben-Ari, E.; Leitus, G.; Shimon, L. J. W.; Milstein, D. Metal-Ligand Cooperation in C-H and H2 Activation by an Electron-Rich PNP Ir(I) System: Facile Ligand Dearomatization-Aromatization as Key Steps. *J Am Chem Soc* **2006**, 128 (48), 15390–15391. https://doi.org/10.1021/JA066411I/SUPPL_FILE/JA066411ISI20060905_044738.CIF.

(118) Gunanathan, C.; Milstein, D. Metal-Ligand Cooperation by Aromatization-Dearomatization: A New Paradigm in Bond Activation and “Green” Catalysis. *Acc Chem Res* **2011**, 44 (8), 588–602. https://doi.org/10.1021/AR2000265/

(119) Khusnutdinova, J. R.; Milstein, D. Metall-Ligand-Kooperation. *Angew Chem* **2015**, 127 (42), 12406–12445. https://doi.org/10.1002/ange.201503873.

(120) Teunissen, H. T.; Elsevier, C. J. Ruthenium Catalysed Hydrogenation of Dimethyl Oxalate to Ethylene Glycol. *Chem Commun* **1997**, No. 7, 667–668. https://doi.org/10.1039/a700862g.

(121) Coetzee, J.; Dodds, D. L.; Klankermayer, J.; Brosinski, S.; Leitner, W.; Slawin, A. M. Z.; Cole-Hamilton, D. J. Homogeneous Catalytic Hydrogenation of Amides to Amines. *Chem Eur J* **2013**, 19 (33), 11039–11050. https://doi.org/10.1002/chem.201204270.

(122) Thenert, K.; Beydoun, K.; Wiesenthal, J.; Leitner, W.; Klankermayer, J. Ruthenium-Catalyzed Synthesis of Dialkoxymethane Ethers Utilizing Carbon Dioxide and Molecular Hydrogen. *Angew Chem* **2016**, 128 (40), 12454–12457. https://doi.org/10.1002/ange.201606427.

(123) Cui, X.; Li, Y.; Topf, C.; Junge, K.; Beller, M. Direct Ruthenium-Catalyzed Hydrogenation of Carboxylic Acids to Alcohols. *Angew Chem* **2015**, 127 (36), 10742–10745. https://doi.org/10.1002/ANGE.201503562.

(124) vom Stein, T.; Meuresch, M.; Limper, D.; Schmitz, M.; Hölscher, M.; Coetzee, J.; Cole-Hamilton, D. J.; Klankermayer, J.; Leitner, W. Highly Versatile Catalytic Hydrogenation of Carboxylic and Carbonic Acid Derivatives Using a Ru-Triphos Complex: Molecular Control over Selectivity and Substrate Scope. *J Am Chem Soc* **2014**, 136 (38), 13217–13225. https://doi.org/10.1021/ja506023f.

(125) Meuresch, M.; Westhues, S.; Leitner, W.; Klankermayer, J. Tailor-Made Ruthenium-Triphos Catalysts for the Selective Homogeneous Hydrogenation of Lactams. *Angew Chem Int Ed* **2016**, 55 (4), 1392–1395. https://doi.org/10.1002/anie.201509650.

(126) Ahmed, M.; Bronger, R. P. J.; Jackstell, R.; Kamer, P. C. J.; Van Leeuwen, P. W. N. M.; Beller, M. Highly Selective Hydroaminomethylation of Internal Alkenes To Give Linear Amines. *Chem Eur J* **2006**, 12 (35), 8979–8988. https://doi.org/10.1002/CHEM.200600702.

(127) Casalnuovo, A. L.; RajanBabu, T. V.; Ayers, T. A.; Warren, T. H. Ligand Electronic Effects in Asymmetric Catalysis: Enhanced Enantioselectivity in the Asymmetric Hydrocyanation of Vinylarenes. *J Am Chem Soc* **1994**, 116 (22), 9869–9882. https://doi.org/10.1021/ja00101a007.

(128) Ponomarev, I. I.; Rybkin, Y. Y.; Goryunov, E. I.; Petrovskii, P. V; Lyssenko, K. A. Reaction of 4,4´dimethyldiphenyl Ether with Phosphorus Trichloride in the Presence of Anhydrous Aluminum Chloride. *Russ.Chem.Bull., Int.Ed* **2004**, 53 (12), 2762–2765.

(129) Hérault, D.; Nguyen, D. H.; Nuel, D.; Buono, G. Reduction of Secondary and Tertiary Phosphine Oxides to Phosphines. *Chem Soc Rev* **2015**, 44 (8), 2508–2528. https://doi.org/10.1039/C4CS00311J.

(130) Podyacheva, E.; Kuchuk, E.; Chusov, D. Reduction of Phosphine Oxides to Phosphines. *Tetrahedron Lett* **2019**, 60 (8), 575–582. https://doi.org/10.1016/J.TETLET.2018.12.070.

(131) Busacca, C. A.; Lorenz, J. C.; Grinberg, N.; Haddad, N.; Hrapchak, M.; Latli, B.; Lee, H.; Sabila, P.; Saha, A.; Sarvestani, M.; Shen, S.; Varsolona, R.; Wei, X.; Senanayake, C. H. A Superior Method for the Reduction of Secondary Phosphine Oxides. *Org Lett* **2005**, 7 (19), 4277–4280. https://doi.org/10.1021/ol0517832.

(132) Hobbs, C. F.; Knowles, W. S. Asymmetric Hydroformylation of Vinyl Acetate with DIOP-Type Ligands. *J Org Chem* **1981**, *46* (22), 4422–4427. https://doi.org/10.1021/jo00335a020.

(133) Fritzsche, H.; Hasserodt, U.; Korte, F. Reduktion Organischer Verbindungen Des Fünfwertigen Phosphors Zu Phosphinen, II. Reduktion Tertiärer Phosphinoxyde Zu Tertiären Phosphinen Mit Trichlorsilan. *Chem Ber* **1965**, 98 (1), 171–174. https://doi.org/10.1002/CBER.19650980122.

(134) Wu, H. C.; Yu, J. Q.; Spencer, J. B. Stereospecific Deoxygenation of Phosphine Oxides with Retention of Configuration Using Triphenylphosphine or Triethyl Phosphite as an Oxygen Acceptor. *Org Lett* 2004, 6 (25), 4675–4678. https://doi.org/10.1021/OL048227C/

(135) Hayashi, T.; Hirate, S.; Kitayama, K.; Tsuji, H.; Torii, A.; Uozumi, Y. Asymmetric Hydrosilylation of Styrenes Catalyzed by Palladium-MOP Complexes: Ligand Modification and Mechanistic Studies. *J Org Chem* **2001**, 66 (4), 1441–1449. https://doi.org/10.1021/JO001614P/

(136) Fritzsche, H.; Hasserodt, U.; Korte, F. Reduktion Organischer Verbindungen Des Fünfwertigen Phosphors Zu Phosphinen, III: Darstellung Primärer Und Sekundärer Phosphine Mit Silanen. *Chem Ber* **1965**, 98 (5), 1681–1687. https://doi.org/10.1002/CBER.19650980547.

(137) Phanopoulos, A.; Long, N.; Miller, P. The Synthesis, Characterization and Reactivity of a Series of Ruthenium N-Triphosph Complexes. *J Vis Exp* **2015**, 2015 (98), 1–7. https://doi.org/10.3791/52689.

(138) Phanopoulos, A.; White, A. J. P.; Long, N. J.; Miller, P. W. Insight into the Stereoelectronic Parameters of N-Triphos Ligands via Coordination to Tungsten(0). *Dalton Trans* **2016**, 45 (13), 5536–5548. https://doi.org/10.1039/c6dt00170j.

(139) Phanopoulos, A.; Brown, N. J.; White, A. J. P.; Long, N. J.; Miller, P. W. Synthesis, Characterization, and Reactivity of Ruthenium Hydride Complexes of N-Centered Triphosphine Ligands. *Inorg Chem* **2014**, 53 (7), 3742–3752. https://doi.org/10.1021/ic500030k.

(140) Moiseev, D. V.; Marcazzan, P.; James, B. R. Reversible Decomposition of Mono(α-Hydroxy)-Phosphines and Their Reaction with α,β-Unsaturated Aldehydes. *Can J Chem* **2009**, 87 (4), 582–590. https://doi.org/10.1139/V09-021.

(141) Alex Tullo. Industry Braces for Nylon 6,6 Shortage. *C&EN Global Enterprise* **2018**, 96 (40), 22–23. https://doi.org/10.1021/cen-09640-feature3.

(142) Roose, P., Eller, K., Henkes, E., Rossbacher, R., & Höke, H. Amines, Aliphatic. *Ullmann's Encyclopedia of Industrial Chemistry* **2015**, 1–55. https://doi.org/10.1002/14356007.A02_001.PUB2

(143) Tobita, H.; Hamielec, A. E. Polymerization Processes, 2. Modeling of Processes and Reactors. *Ullmann's Encyclopedia of Industrial Chemistry* **2015**, 1–50. https://doi.org/10.1002/14356007.O21_O01.PUB2.

(144) Hoover, J. Ammonia Activation at a Metal. *Science* **2016**, 354 (6313), 707–708. https://doi.org/10.1126/science.aaj2332.

(145) Tolman, C. A.; McKinney, R. J.; Seidel, W. C.; Druliner, J. D.; Stevens, W. R. Homogeneous Nickel-Catalyzed Olefin Hydrocyanation. *Adv Catal* **1985**, 33 (C), 1–46. https://doi.org/10.1016/S0360-0564(08)60257-6.

(146) Bini, L.; Müller, C.; Vogt, D. Mechanistic Studies on Hydrocyanation Reactions. *ChemCatChem* **2010**, 2 (6), 590–608. https://doi.org/10.1002/CCTC.201000034.

(147) Bini, L.; Müller, C.; Vogt, D. Ligand Development in the Ni-Catalyzed Hydrocyanation of Alkenes. *Chem Commun* **2010**, 46 (44), 8325–8334. https://doi.org/10.1039/C0CC01452D.

(148) Pollak, P.; Romeder, G.; Hagedorn, F.; Gelbke, H. Nitriles. *Ullmann's Encyclopedia of Industrial Chemistr*y; Wiley, **2000**. https://doi.org/10.1002/14356007.a17_363.

(149) Lu, Q.; Liu, J.; Ma, L. Recent Advances in Selective Catalytic Hydrogenation of Nitriles to Primary Amines. *J Catal* **2021**, 404, 475–492. https://doi.org/10.1016/J.JCAT.2021.10.028.

(150) Bagal, D. B.; Bhanage, B. M. Recent Advances in Transition Metal-Catalyzed Hydrogenation of Nitriles. *Adv Synth Catal* **2015**, 357 (5), 883–900. https://doi.org/10.1002/ADSC.201400940.

(151) Franke, R.; Selent, D.; Börner, A. Applied Hydroformylation. *Chem Rev* **2012**, 112 (11), 5675–5732. https://doi.org/10.1021/CR3001803.

(152) Gross, T.; Seayad, A. M.; Ahmad, M.; Beller, M. Synthesis of Primary Amines: First Homogeneously Catalyzed Reductive Amination with Ammonia. *Org Lett* **2002**, 4 (12), 2055–2058. https://doi.org/10.1021/OL0200605.

(153) Hahn, G.; Kunnas, P.; de Jonge, N.; Kempe, R. General Synthesis of Primary Amines via Reductive Amination Employing a Reusable Nickel Catalyst. *Nat Catal* **2018** 2:1 2018, 2 (1), 71–77. https://doi.org/10.1038/s41929-018-0202-6.

(154) Senthamarai, T.; Murugesan, K.; Schneidewind, J.; Kalevaru, N. V; Baumann, W.; Neumann, H.; Kamer, P. C. J.; Beller, M.; Jagadeesh, R. V. Simple Ruthenium-Catalyzed Reductive Amination Enables the Synthesis of a Broad Range of Primary Amines. *Nat Commun **2018***, 9(1), 4123. https://doi.org/10.1038/s41467-018-06416-6

(155) Murugesan, K.; Wei, Z.; Chandrashekhar, V. G.; Jiao, H.; Beller, M.; Jagadeesh, R. V. General and Selective Synthesis of Primary Amines Using Ni-Based Homogeneous Catalysts. *Chem Sci* **2020**, 11 (17), 4332–4339. https://doi.org/10.1039/d0sc01084g.

(156) Pingen, D.; Schwaderer, J. B.; Walter, J.; Wen, J.; Murray, G.; Vogt, D.; Mecking, S. Diamines for Polymer Materials via Direct Amination of Lipid- and Lignocellulose-Based Alcohols with NH3. *ChemCatChem* **2018**, 10 (14), 3027–3033. https://doi.org/10.1002/cctc.201800365.

(157) Damljanović, I.; Vukićević, M.; Vukićević, R. D. A Simple Synthesis of Oximes. *Monatsh Chem* **2006**, 137 (3), 301–305. https://doi.org/10.1007/s00706-005-0427-3.

(158) Hinzmann, A.; Betke, T.; Asano, Y.; Gröger, H. Synthetic Processes toward Nitriles without the Use of Cyanide: A Biocatalytic Concept Based on Dehydration of Aldoximes in Water. *Chem Eur J* **2021**, 27 (17), 5313–5321. https://doi.org/10.1002/chem.202001647.

(159) Betke, T.; Maier, M.; Gruber-Wölfler, H.; Gröger, H. Biocatalytic Production of Adiponitrile and Related Aliphatic Linear α,ω-Dinitriles. *Nat Commun* **2018**, 9 (1), 1–9. https://doi.org/10.1038/s41467-018-07434-0.

(160) Plass, C.; Hinzmann, A.; Terhorst, M.; Brauer, W.; Oike, K.; Yavuzer, H.; Asano, Y.; Vorholt, A. J.; Betke, T.; Gröger, H. Approaching Bulk Chemical Nitriles from Alkenes: A Hydrogen Cyanide-Free Approach through a Combination of Hydroformylation and Biocatalysis. *ACS Catal* **2019**, 9 (6), 5198–5203. https://doi.org/10.1021/acscatal.8b05062.

(161) Hinzmann, A.; Druhmann, S. S.; Gröger, H. Synthesis of Bifunctional Molecules for the Production of Polymers Based on Unsaturated Fatty Acids as Bioderived Raw Materials. *Sust Chem* **2020**, Vol. 1, Pages 275-289 2020, 1 (3), 275–289. https://doi.org/10.3390/SUSCHEM1030018.

(162) Terhorst, M.; Plass, C.; Hinzmann, A.; Guntermann, A.; Jolmes, T.; Rösler, J.; Panke, D.; Gröger, H.; Vogt, D.; Vorholt, A. J.; Seidensticker, T. One-Pot Synthesis of Aldoximes from Alkenes via Rh-Catalysed Hydroformylation in an Aqueous Solvent System. *Green Chem* **2020**, 22 (22), 7974–7982. https://doi.org/10.1039/D0GC03141K.

(163) Ivankin, D. I.; Borisova, M. S.; Sokolov, D. N.; Luzina, O. A.; Tolstikova, T. G.; Salakhutdinov, N. F. Design, Synthesis, and Anti-Ulcer Activity of New 1-Thia-4,8-Diazaspiro[4,5]Decan-3-One Derivatives. *Pharm Chem J* **2022**, 55 (12), 1288–1292. https://doi.org/10.1007/S11094-022-02573-7/TABLES/1.

(164) Feuer, H.; Braunstein, D. M. The Reduction of Oximes, Oxime Ethers, and Oxime Esters with Diborane. A Novel Synthesis of Amines. *J Org Chem* **1969**, 34 (6), 1817–1821. https://doi.org/10.1021/JO01258A062.

(165) Ipaktschi, J. Reduktion von Oximen Mit Natriumboranat in Gegenwart von Übergangsmetallverbindungen. *Chem Ber* **1984**, 117 (2), 856–858. https://doi.org/10.1002/CBER.19841170237.

(166) Kumari, P.; Gautam, R.; Yadav, H.; Kushwaha, V.; Mishra, A.; Gupta, S.; Arora, V. Efficient Reduction of C–N Multiple Bonds Catalyzed by Magnetically Retrievable Magnetite Nanoparticles with Sodium Borohydride. *Catal Letters* **2016**, 146 (10), 2149–2156. https://doi.org/10.1007/s10562-016-1822-6.

(167) Bolotin, D. S.; Bokach, N. A.; Demakova, M. Y.; Kukushkin, V. Y. Metal-Involving Synthesis and Reactions of Oximes. *Chem Rev* **2017**, 117 (21), 13039–13122. https://doi.org/10.1021/ACS.CHEMREV.7B00264.

(168) Reeve, W.; Christian, J. A Comparison of Raney Nickel and Raney Cobalt Catalysts for the Hydrogenation of Oximes. *J Am Chem Soc* **1956**, 78 (4), 860–861. https://doi.org/10.1021/JA01585A042.

(169) Gebauer-Henke, E.; Leitner, W.; Prokofieva, A.; Vogt, H.; Muïler, T. E.; Müller, T. E. Controlling Selectivity in the Reaction Network of Aldoxime Hydrogenation to Primary Amines. *Catal Sci Technol* **2012**, 2 (12), 2539–2548. https://doi.org/10.1039/c2cy20356a.

(170) Bai-cheng, F.; Bao-hu, X.; Zhen-chao, Z.; Yu-hui, H.; Yan, J.; Qing-lin, Y. Production of Heterocyclic Primary Amines from Heterocyclic Aldehydes on Ni-Mo/ZrO2. *Chem Eng Technol* **2022**, 45 (6), 1027–1035. https://doi.org/10.1002/CEAT.202100581.

(171) Liu, Y.; Quan, Z.; He, S.; Zhao, Z.; Wang, J.; Wang, B. Heterogeneous Palladium-Based Catalyst Promoted Reduction of Oximes to Amines: Using H 2 at 1 Atm in H 2 O under Mild Conditions †. *React Chem Eng* **2019**, 4 (6), 1145–1152. https://doi.org/10.1039/C9RE00003H.

(172) Biermann, U.; Bornscheuer, U.; Meier, M. A. R.; Metzger, J. O.; Schäfer, H. J. Oils and Fats as Renewable Raw Materials in Chemistry. *Angew Chem Int Ed* **2011**, 50 (17), 3854–3871. https://doi.org/10.1002/anie.201002767.

(173) Thomas, A.; Matthäus, B.; Fiebig, H.-J. Fats and Fatty Oils. *Ullmann's Encyclopedia of Industrial Chemistry* **2015**, 1–84. https://doi.org/10.1002/14356007.A10_173.PUB2.

(174) Phosphorus (CAS Number 338800-13-8) : Strem Product Catalog. https://www.strem.com/catalog/v/15-0063/52/phosphorus_338800-13-8 (accessed 2022-07-25).

(175) Phosphorus (CAS Number 22031-12-5) : Strem Product Catalog. https://www.strem.com/catalog/v/15-7870/52/phosphorus_22031-12-5 (accessed 2022-07-25).

(176) Hapiot, F.; Leclercq, L.; Azaroual, N.; Fourmentin, S.; Tilloy, S.; Monflier, E. Rhodium-Catalyzed Hydroformylation Promoted by Modified Cyclodextrins:Current Scope and Future Developments. *Curr Org Synth* **2008**, 5 (2), 162–172. https://doi.org/10.2174/157017908784221585.

(178) Künnemann, K. U.; Schurm, L.; Lange, D.; Seidensticker, T.; Tilloy, S.; Monflier, E.; Vogt, D.; Dreimann, J. M. Continuous Hydroformylation of 1-Decene in an Aqueous Biphasic System Enabled by Methylated Cyclodextrins. *Green Chem* **2020**, 22 (12), 3809–3819. https://doi.org/10.1039/D0GC00820F.

9. Annex

9.1. List of abbreviations

Abbreviation	Full name	Comment
Ac	Acyl	
acac	Acetylacetonate	
aq.	Aqueous	
ATR	Attenuated total reflectance	Often ATR-IR; see IR
Boc	tert-Butyloxycarbonyl protecting group	
Bu	Butyl	
CD	Cyclodextrine	
Cy	Cyclohexyl	
DABCO	1,4-Diazabicyclo[2.2.2]octane	
DBU	1,8-Diazabicyclo[5.4.0]undec-7-en	
Dioxane	1,4-Dioxane	
DMC	Dichloromethane	
DMOP	3,5-dimethoxyphenyl	
DMSO	Dimethylsulfoxide	
dppe	1,2-Bis(diphenylphosphino)ethane	
E	Trans configured double bond	Also see Z
eq.	Equivalents	
Et	Ethyl	
FID	Flame ionization detector	
GC	Gas chromatography	
HPLC	High-performance liquid chromatography	Sometimes in the literature as “high pressure liquid chromatography”
HRMS	High resolution mass spectrometry	
IR	Infrared spectroscopy	
l/b-ratio	Linear to branched ratio	
MIBA	5-methoxy-2-iodophenylboronic acid	
MS	Mass spectrometry	
n	amount	
NHC	N-Heterocyclic carbene	
NMR	Nuclear magnetic resonance spectroscopy	
PA-12	Polyamide-12	Also PA-6 and others
PA-12,12	Polyamide-12,12	Also PA6,6 and others
Ph	Phenyl	
POP	2,8-Dimethyl-10*H*-phenoxaphosphine	
rpm	Revolutions per minute	
RT	Room temperature	
S	Selectivity	
t-Bu, ^{t}Bu	*tert-butyl*	
TCCA	trichloroisocyanuric acid	
Tf	Triflate; trifluoromethanesulfonate	

TMM	2-Methylidenepropane-1,3-diyl	
TOF_{20}	Turn over frequency	20 stands for TOF at 20 % conversion
wt%	Weight percent	Relative weight
X	Conversion	
xyl	Xylyl	
Y	Yield	
Z	Cis configured double bond	Also see E

9.2. List of chemicals

Table 24: List of chemicals used in this chapter.

Chemical	Purity [%]	Supplier
1,2-Bis(dicyclohexylphosphino)ethane	99	Aldrich
1,3-Dimesitylimidazol-2-ylidene	98	Acros
1,4-Dioxane	99 stabilized	abcr
2-Methyltetrahydrofuran	99	Merck
2,4,6-Trimethylaniline	97	Acros
3-Chlorpropionic acid	98	Acros
4-Nitrobenzoic acid	99+	Acros
Acetic acid	99+	Acros
Argon	99.9	Messer Industriegase GmbH
Benzoic acid	99	Acros s
Bis[1,2-bis(diphenylphosphino)ethane]-palladium	99	Aldrich
Buta-1,3-diene	99.3	GERLING Holz+Co
Carbon monoxide	98	Messer Industriegase GmbH
Cinnamic acid	99	Fisher Scientific
Cyclohexane	99	Hanke+Seidel
Cyclohexyldiphenylphosphine	98	Acros
Di(adamantan-1-yl) (butyl)phosphine	99	Acros
Dibuthylamine	98	abcr
Dicyclohexylphenylphosphine	95	Acros
Ethyl acetate	98	Hanke+Seidel
Formic acid	98	Acros
Isoprene	98	Acros
Morpholine	99+	Acros
m-Toluic acid	99	Acros
n-decane	99+	Merck
Nicotinic Acid	99+	Acros
N-Methylaniline	98	Aldrich
o-Chloro-benzoic acid	98	Acros
Palladium(II)-acetate	-	umicore
o-Toluic acid	98	Acros
Picolinic acid	98	Acros
Piperidine	99	Acros
Magnesium sulfate		Acros
p-Methoxy-benzoic acid	98	Acros
Morpholine	99+	Acros
p-Toluic acid	98	Acros
ß-Myrcene	90	Aldrich
Tetrahydrofuran	99+ stabilized	Acros
Toluene	99+	Acros
Tricyclohexylphosphine	97	Fisher Scientific
Tri-i-butylphosphine	98	abcr
Tri-n-butylphosphine	97	Aldrich
Triphenylphosphine	99	Alfa Aesar
Tri-tert-butylphosphine	95	abcr
Vinylacetic acid	97 stabilized	abcr
Xantphos	98	carbolution chemicals

Table 25: List of chemicals chapter 4.

Name	Purity / %	Brand
1,4-dioxane	99	Merck
1-Octene		TCI
1-Pentene	97	TCI
2,6-Bis(di-t-butylphosphinomethyl)pyridine	99	abcr
2-Ethylbutyraldehyde		TCI
2-Furaldehyde	98	Alfa Aesar
6-bromopicolinaldehyde oxime	99	Synthesized by Hansmann Group at TU Dortmund
Anisol	99	Carl Roth
Benzaldehyde	99.5	Alfa Aesar
Bis(2-diphenylphosphinoethyl)phenylphosphine	97	Abcr
Citronellal	93	Acros Organics
Cyclohexanone oxime	97	Alfa Aesar
DBU	98	Carl Roth
1,2-Bis(diphenylphosphino)ethane (dppe)	98	Thermo Scientific
Hexanal	98	Carl Roth
Hydroxylamine	50	Sigma Aldrich
Methyl 10-Undecenoate	96	TCI
Nonanal	97	Carl Roth
Pentanal	97	Merck
Pivalaldehyde	97	TCI
Potassium hydroxide	85.7	Carl Roth
Potassium tert butoxide	97	Thermo Scientific
$Ru(acac)_3$		TCI
Triphenylphosphine	99	abcr
Triphos	97	Alfa Aesar
Xantphos	98	